Solidification caused by under-cooling

Awatif Alhowaity

School of Mathematics,

University of East Anglia,

Norwich NR4 7TJ, England.

A thesis submitted to the University of East Anglia for degree of

Doctor of Philosophy

March 2018

Acknowledgements

First, I would like to express my gratitude to Allah (God), for providing me the opportunity and patience to complete my PhD study.

Second, I would like to express my special thank to my supervisors, Prof. Alexander Korobkin and Dr. Mark Cooker for their assistance, guidance, support, patience, respect, kindness and motivation. I am deeply grateful to their always available, generous encouragements, and suggestion over the past years. Thank you for giving your time and support.

In addition, I would like to thank my kind father (Salem) for his love and support. I do not have enough word to express my thanks to him. I wish to dedicate my work to my beloved late mother. Thanks also go to my beloved husband for his support, encouragement and patience during the duration of this PhD. My lovely kids (Hosam, Nourah, and Wisam) who were the source of spirit in every step of my PhD. Thank you for their patience.

Further, thanks go to my brothers, sisters, and friends for their help and support. My PhD work was funded by a Saudi Arabian Government scholarship, I am very grateful for the funding opportunity.

Finally, thanks to all staff and colleagues at the School of Mathematics in University of East Anglia for helping and supporting me.

Abstract

Many crude oils contain dissolved waxes that can cause significant problems, such as blockage of pipeline, because of the precipitation and deposition of wax particles during the production and transportation of the oil. The waxy oils are transported through very long pipelines from warm natural reservoirs to cooler conditions in the surrounding of the pipe. An important phenomenon occurring during the under-cooling of the pipeline is the formation of solid matter inside the pipe. The wax deposition is one of the most serious problems, potentially restricting flow and plugging the pipe. Wax deposits begin to form when the temperature is below the wax appearance temperature. We model a particle's growth in the oil pipe once the temperature falls below the wax appearance temperature. We determine the temperature distribution in the oil, formulate and solve a self-similar problem of wax particle growth from a single point. A corresponding initial boundary value problem is studied numerically by a time- stepping numerical algorithm. The numerical algorithm is used to compute the non-linear solution of an initial value problem of diffusion and transport of wax towards the particle. The numerical solution is compared with and validated against the self-similar solution derived for specific conditions. Then the boundary value problem is formulated for the general case. A coupled diffusion/ flow problem of a single wax particle is formulated. An asymptotic

analysis is used to describe the motion and growth of the wax particle. At the leading order, we consider a spherical wax particle and assume the velocity of the particle to be close to the local velocity of the flow. The flow relative to the wax particle is negligible in the leading order problem. In the first-order correction problem, the wax particle is treated as spherical initially, and the correction to the particle shape is caused by a small difference between the wax particle speed and the speed of the local flow. We draw conclusions and recommendation for further work at the end of this thesis.

Contents

Chapter 1

Introduction

This chapter contains four sections, beginning with the physical motivation, then a problem description, the context of a literature survey, and ends with a statement of the aim and structure of this thesis.

1.1 Physical motivation

Crude oils containing a quantity of waxes, are usually called waxy crude oils. Crude oil is transported from offshore oil fields to refineries in subsea production pipelines. The oil is extracted from offshore reservoirs from under the seabed and the reservoirs usually have a uniform temperature between $70°C - 150°C$, see [46]. However, during the transportation of oil through a subsea pipeline, the temperature of the oil may decrease below the wax appearance temperature, WAT. The wax appearance temperature is the temperature at which paraffin starts to crystallize in a solution [26]. Heat is lost from the

oil in the pipeline to the cold surrounding seawater at a temperature which can be as low as 10°C. As the temperature of the oil decreases due to the cold environment of the sea, the solubility of the wax also decreases. However, the wax molecules are dissolved at reservoir temperature and exist in the oil as liquid phase. At the wax appearance temperature, the wax molecules start to precipitate out of the solution and deposit on the wall of the pipe, or on small impurities (e.g. dust), or on surfaces of existing solid wax particles moving in the oil. Wax precipitation during the flow of waxy crude oil through a pipe causes the deposition of waxes on the pipe walls. Thus, wax deposition occurs only if the temperature of the oil is lower than the wax appearance temperature.

Wax deposition is a major problem in production pipelines. In the worst case, the production must be stopped to remove the plugged portion in the pipeline [46]. The wax deposits can be formed from the precipitation of dissolved wax molecules through the diffusion mechanism. Sigh et al. [71] reported that there are two steps for the wax deposition, firstly wax gel formation and then aging of deposited wax gel. The oil contains some water, sand, and gums, which are trapped during the deposition process. The trapped oil causes diffusion of wax molecules into the gel deposit. The diffusion transport process leads to both an initial gel deposit, and an increase in the amount of wax in a gel deposit. This in turn leads to a second step of wax deposition, which is aging of the deposited wax. Sigh et al. [70] found the deposition of wax on the pipe wall can be described by the following: gelation of waxy oil (formation of an incipient gel layer) on the cold surface, diffusion of waxes from the flow toward the gel layer, internal diffusion of these molecules inside the gel layer, and precipitation of these wax molecules in the deposit.

Let the temperature near the wall or a piece of dust be lower than the wax appearance temperature. This leads to a concentration gradient of dissolved wax (lower concentration near the particle than elsewhere in the fluid) and so molecular transport toward the wall or the dust surface through the diffusion process. The shape and size of wax particles will be different from those of the wax particles at the centre of the pipe, because the temperature near the pipe wall drops due to the cooler environment. The wax deposition can be due to different mechanisms such as molecular diffusion, Brownian diffusion, and shear dispersion [12]. In this thesis we only take into account the molecular diffusion as the main deposition mechanism. We suppose there are nuclei in the oil. A typical nucleus becomes the site of growth of wax, when the nucleus moves into a region where the oil temperature is below the wax appearance temperature. We study the deposition of waxes onto nucleus, while assuming the deposition thickness is small compared with the pipe radius. The rest of this introductory chapter discusses the problem, a review of technical literature, and ends with the aim and the structure of the thesis.

1.2 Description of the problem

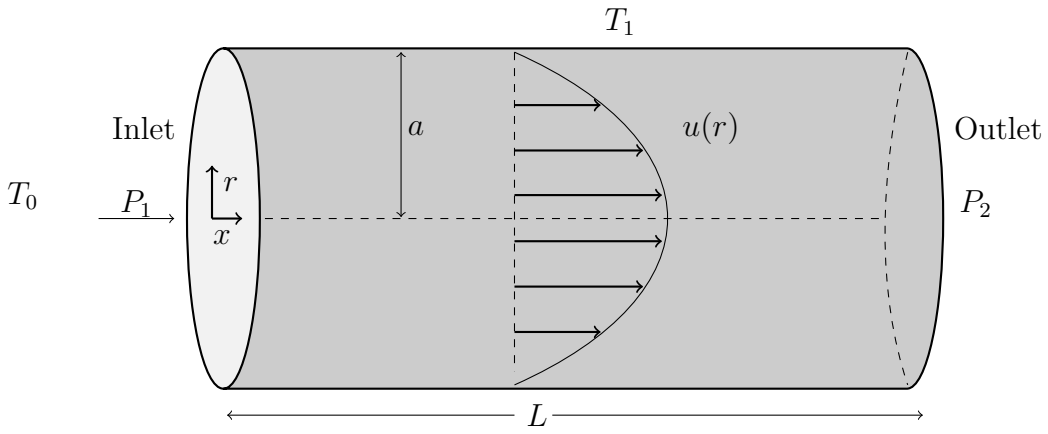

Figure 1.2.1: Sketch of a steady viscous flow in a stationary pipe of circular cross-section. The fluid temperature at the inlet is T_0 and the wall temperature is T_1.

The problem is described mathematically in the geometry of cylindrical production pipeline of crude oils. The inlet end of the pipe is beneath the sea bottom with, say, 60°C for the inlet oil temperature [13]. The pipe is surrounded by sea water at, say, 10°C so that the pipe wall also has the temperature 10°C. Once the oil leaves the reservoir and flows through the subsea pipeline, its temperature drops due to the cold environment of the sea. The temperature at which wax molecules start to solidify is known as the wax appearance temperature. The temperature of the oil is varying along the pipe and the oil temperature at the entrance of the pipe is greater than the wax appearance temperature. The waxy oils are transported through pipelines and an important phenomenon occurring during the under-cooling of the pipeline is the formation of solid matter inside the pipe.

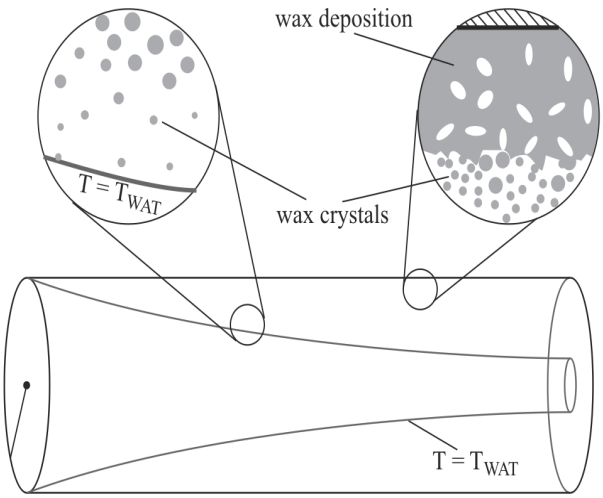

Figure 1.2.2: The deposition of wax in the pipe

In the past a main part of published research was focused on deposition of wax onto the inner wall of the pipe where the wall temperature is lower than the WAT, see figure 1.2.2. However, in this thesis, at a distance from the wall and far from the entrance to the pipe, where the temperature is below the wax appearance temperature, there are wax particles in the flow and we are most interested in this region and these particles. We will study how a wax particle grows in the fluid domain being sufficiently far from the wall, that is, far from the wall.

Initially there is a small impurity in the oil (e.g. dust), and the solid wax molecules start to build up on its surface when the temperature around this piece of dust becomes lower than the wax appearance temperature. This grows and becomes a wax particle. It grows due to a mass flux of wax molecules moving towards this wax particle. In this way wax particles become bigger and start to interact and contact each other, making a gel of particles. Such wax gel particle conglomerates contribute to the gel layer. The oil flow presses the gel layer to the wall and increases the deposition of wax on the wall of the

pipe. In this thesis, wax deposition is modelled in the laminar flow regime and the oil wax solution is saturated when the temperature is lowered below the wax appearance temperature, taking only the molecular diffusion into account. The concentration profile is the driving force of the diffusion of wax molecules toward the piece of dust that moves inside the pipe.

1.3 Literature Review

Wax deposition in production pipes which are draining oil from a subsea reservoir is a significant problem in the petroleum industry. The deposition of wax in waxy crude oil has been studied by several authors. The most important pioneering studies were done by Burger et al. [12], Bern et al. [10], Brown et al. [11], Creek et al. [22], and Hamouda et al. [40] on the wax deposition model. The possible mechanisms of wax deposition on a pipe wall are molecular diffusion, shear dispersion, brownian diffusion, and gravity settling.

Molecular diffusion. The wax molecules in the oil crystallize on the wall where the pipe wall temperature is below the wax wax appearance temperature (WAT). This leads to a concentration gradient of wax molecules near the pipe wall. According to Fick's diffusion law, the wax molecules in the oil flow migrate to the wall of the pipe are deposited on the wall. The rate of wax transport to the wall is given by Fick's law of diffusion:

$$\frac{dm}{dt} = \rho D A \frac{dC}{dr}, \tag{1.3.1}$$

where m is the mass of deposited wax, ρ is density of solid wax deposited, D is the diffusion coefficient, A is the area of deposition, $\frac{dC}{dr}$ is the radial concentration gradient of wax molecules in solution.

Shear dispersion. When the oil flows, there is a certain velocity gradient in the radial direction of the flow. Bern et al. [10] defines this as ".., the shearing of the fluid close to the pipe wall also induces a lateral movement of the particles known as shear dispersion."

Brownian diffusion. "The erratic random movement of microscopic particles in a fluid as a result of continuous bombardment of molecules of surrounding medium.", see [72].

Gravity settling. When a wax particle is precipitated from the oil it is more dense than the liquid oil. Over a long time the wax particles are deposited at the bottom of the pipe due to the effect of gravity.

Burger et al. [12] studied wax deposition mechanisms in the Trans-Alaska pipeline. They showed the deposition of wax on the pipe wall occurs as a result of molecular diffusion, shear dispersion, Brownian diffusion, and Gravity settling. In their experiments, deposition of wax in vertical and horizontal pipes was compared to assess the contribution of gravity settling. They found there was no significant influence of gravity settling on total deposition. The shear dispersion might redisperse settled solids in pipeline flow, therefore any effect of gravity settling on rate of wax deposition can be eliminated. They identified as possible mechanisms, molecular diffusion, shear dispersion, and Brownian diffusion. They found the contribution of Brownian diffusion is small compared with two other mechanisms. They concluded that the molecular diffusion is the main mechanism for transporting wax towards the wall of the pipe. There was a radial temperature gradient, when the oil is being cooled in the pipe. They showed that the solubility of wax in the oil is a decreasing function of temperature. They found that the size distribution of the precipitated wax particles increases linearly with decreasing temperature.

The temperature gradient produced a concentration gradient of dissolved wax in oil. This dissolved wax was transported towards the wall of the pipe by molecular diffusion. They wrote the equation (1.3.1) in terms of wax solubility coefficient of the oil, $\frac{dC}{dT}$, as

$$\frac{dm}{dt} = \rho D A \frac{dC}{dT}\frac{dT}{dr}, \tag{1.3.2}$$

where $\frac{dT}{dr}$ is the radial temperature gradient at the wall which can be determined from the solution of the energy equation.

Bern et al. [10] measured the wax deposition rates using their laboratory data, and used these rates to estimate the effect of wax deposition on realistic pipeline pressure drops. They concluded that the total deposition of wax results from a combination of molecular diffusion of dissolved wax and shear dispersion of previously precipitated solid waxes. They tested the shear dispersion mechanism and they found the shear dispersion becomes important when the precipitated wax content in the turbulent core is high. Increasing shear rate (flow rates) leads to more wax particles dispersing toward the wall, but the corresponding increase in wall shear stress may cause the looser held deposits to be stripped from the wall .

Brown et al. [11] discussed an experimental technique to measure wax deposition rates. They indicated that the wax deposition by shear dispersion is not significant, as confirmed by their field experience. This is due to no deposition being observed under conditions of zero heat flux.

Creek et al. [22] studied experimentally wax deposition using crude oil from the Gulf of Mexico. They studied the effect of temperature difference between the oil and the pipe wall. They found there was an increase in the wax deposition rate with increasing difference in temperature between the oil

and the pipe wall. They also reported that the deposition rate decreases with increasing flow velocity. The oil flow velocity can be so large that the flow becomes turbulent (non laminar). They also concluded that the oil fraction of the gel layer in turbulent flow was significantly lower than the oil fraction of the gel layer in laminar flow.

Hamouda et al. [40] investigated the effect of various combinations of flow characteristics on paraffin wax deposition rates. They present a three-dimensional model for the behaviour of oil in a Teesside pipeline, in various flow regimes. They concluded that molecular diffusion is the dominant mechanism, and the radial concentration gradient of the paraffin $\frac{dC}{dr}$, is the driving force for this molecular diffusion.

Many authors [11, 16, 22, 40, 70] have shown that Brownian diffusion and shear dispersion mechanisms are not significant, and that molecular diffusion is the dominant mechanism in wax deposition. They concluded that molecular diffusion toward the wall is the main mechanism for the transport of waxes from solution to the wall of the pipe.

In our study we neglect the gravity settling and the Brownian diffusion. Also we neglect the shear dispersion which is negligible because we study the growth of small wax particle far from the wall of the pipe, and the flow velocity around the wax particle is approximately uniform. The wax deposition in our study is modelled assuming the laminar flow regime and we take into account only the molecular diffusion mechanism.

Svendsen et al. [74] have developed a mathematical model for prediction of wax deposition in a horizontal pipeline, by using a combination of analytical and numerical modelling. They calculated the temperature distribution which depends on the velocity profile, $v(r) = v_{max}\left(1 - (\frac{r}{a})^{m+1}\right)$, where v_{max} is the

maximum velocity of the flow and a is the internal radius of the pipe, for the oil flow in terms of the radial coordinate r measured from the centreline. For a Newtonian fluid $m = 1$ and the flow is laminar. They solve the problem of plug flow, where $m = \infty$, and they ignored the heating and axial thermal diffusion term in the energy equation. The solution of this problem can then be expressed in terms of Bessel functions, as shown in [15]. In chapter 2 we find the solution of the energy equation when $m = 1$, for a parabolic velocity profile. The molecular diffusion has been assumed to be the dominant mechanism in the wax deposition [55]. The more complicated problem of modelling wax deposition in non-isothermal flow is still in an early stage of development [6]. The heat transfer is one of the main processes that come from conduction and convection which affect the deposition of wax in a pipeline. The radial component of the convective velocity in the region, which contains the wax deposition for the laminar flow, has been neglected in the past [10–12, 23, 55, 65, 67, 70, 74]. The radial velocity component is expected to be relatively small, compared with the axial velocity component. To the best of our knowledge, in most of the models in the literature the driving force for the radial diffusion is written in terms of the concentration gradient and then, using the chain rule, in terms of the temperature gradient [10, 12, 30, 34, 40, 47, 55]. In our model, the mass transfer coefficient $k_r(T)$ is a function of the local temperature. On the other hand, we consider the diffusion be driven by a concentration gradient, not by the temperature gradient. Hunt et al. [47] and Eaton et al. [28] experimentally studied the wax deposition with zero heat flux conditions, and they concluded that no wax deposition occurred at zero heat flux condition. Wardhaugh et al. [80] made an assumption related to the flow: if the temperature is below the wax appearance temperature, then the waxy oils are non-Newtonian fluids,

and if the temperature is above the wax appearance temperature, then waxy oils are Newtonian fluids.

Correa et al. [19] studied the deposition of solid matter on the pipe walls during the transport of oil. The solidification occurs on the wall when the external temperature is lower than the wax appearance temperature, and this leads to a deposit on the wall of the pipe. They modelled wax deposition onto a pipe wall in a turbulent flow of waxy crude oil, in a cylindrical pipeline, and they took into account the molecular diffusion. The diffusion of wax molecules towards the cold wall is caused by the concentration gradient. Their model relies on the physical properties of waxes. The derivative of wax solubility with respect to temperature is important because it determines the concentration of dissolved waxes in the radial direction, and the diffusivity of dissolved wax determines the rate at which waxes are driven towards the wall.

According to the molecular diffusion mechanism, the precipitation of wax out of solution into a deposit on the cold wall causes a radial concentration gradient and this precipitation reduces the concentration of wax near the pipe wall. The concentration gradient leads to a transport of wax molecules in the oil toward the wall. This concentration gradient is the driving force for wax deposition [46].

Fasano et al. [33] formulated a mathematical model of heat and mass transfer in non-isothermal solution. They took into account the process of segregation of solid wax and its deposition on the boundary. They considered the molecular diffusion as the main mechanism of wax deposition on the pipe wall. They showed that for some waxy crude oils the densities in both dissolved and segregated phases are equal to that of the solvent. The density of the mixture is constant in their study. Their model described the diffusive mass flow within

the solution toward the cold wall, which was induced by the thermal gradient.

Ramirez et al. [65] have developed a wax deposition model in pipelines. They modelled the heat transfer, and they found that the temperature decreases in the direction of the flow along the pipe. They found that the deposition of wax occurs due to the radial mass diffusion which is driven by a concentration gradient, induced by the temperature gradient. They found that the increase in the maximum of deposited layer thickness occurs when the temperature of the fluid reaches the wax appearance temperature at a specific axial location. They concluded that the Reynolds numbers and the mass Peclet number strongly influence the mass deposition rate. They showed a significant increase in the solid deposition with Reynolds number up to $Re \approx 100$, there is a steep increase in the solid deposition with Re number up to 100, where a more gradual increase is observed for higher Re number. They also found a decrease in the mass deposition when $Re > 2000$. The reason for this phenomenon comes from the fact that the shear forces acting on the deposit layer become large with high Re number, and at some point the shear force removes the wax deposit on the wall and decreases the rate of wax deposition. When they estimated the average molecular diffusion coefficient, they found there is an important connection between the mass Peclet number and the radial mass flux. They observed a substantial dependence of deposition mass layer-thickness on the value of average molecular diffusion coefficient.

Bautista et al. [9] studied the wax deposition on the internal surface of oil production pipelines and the influence of flow rate on the deposit thickness for a crude oil. They calculated the temperature distribution along the pipe and they found that the deposit thickness is increased when the wall temperature is decreased and the opposite effect takes place when the temperature

is increased. When the flow rate is low, they found that the temperature gradient tends to zero very quickly, the wax appearance temperature is reached faster and then the wax is deposited over a short length. They showed that increased flow rate reduced the maximum deposit thickness, and the deposited wax spreads over a long distance in the pipe with constant pipe wall temperature. Also they found that the maximum deposition of wax layer thickness increases or decreases depending on whether the temperature profile has a positive or a negative slope along the pipe wall.

Fasano et al. [31] formulated a mathematical model to describe the wax deposition in pipelines and the mechanisms of mass transport in saturated non-isothermal solution. They measured the wax solubility and diffusivity using an experimental device. The thermal gradient in a saturated solution produced a concentration gradient which forced the solute to diffuse. They modelled a one-dimensional problem with uniform initial concentration and uniform initial temperature. They found no mass flux occurs when the temperature of the solution is greater than the wax appearance temperature and the concentration is constant. They concluded that a small non-diffusive region starts growing at the cold wall while the rest of the layer remains unsaturated, and they showed there is a gel region between the unsaturated region and the deposit region. Then this gel region undergoes further changes over time, later becoming a deposit.

1.4 Model assumptions

1. The flow is laminar with the Reynolds number being low enough. Even if secondary circulation is present we assume that this is small compared with

velocity component in the direction of pipe axis. The flow is also steady (there is no time-dependence in the flow velocity) and we neglect pressure oscillations due to, for example, pumping.

2. Molecular diffusion is the most important mechanism for the growth of particles in the flow (away from the wall). Molecular diffusion dominates other mechanisms which might be considered as contributing to a particle's growth.

3. Brownian motion is the random motion of, for example, a smoke particle struck by air molecules: the molecular impacts are sometimes greater on one side than the other and the smoke particle moves in one direction, briefly; a very short time later the molecular impacts push the particle in another direction. The smoke particle dances randomly. The some occurs with small wax particles surrounded by oil molecules. This Brownian motion moves wax particles separating a set of them or sometimes bringing two wax particles together. We assume this affect provides a small contribution to particle growth.

4. Shear dispersion, Bern et al. [10] revealed that this is only important in turbulent flows with high Reynolds number, for a low Reynolds number flow regime shear dispersion is negligible.

5. Gravity is negligible, see Burger et al. [12].

6. Rotation of a wax particle is negligible, the viscous flow considered exerts a negligible a torque on a particle. (This changes if the flow field has a very large shear.)

7. The density of the oil (in liquid state) is assumed to be constant over the range of temperatures. The density of solid wax is also assumed constant and independent of temperature.

8. The temperature distribution in the pipe is not uniform. As a wax particle is advected by the oil along the pipe, the particle experiences a reduction in

temperature. We assume that the particle has the same temperature as the oil in its immediate neighbourhood. We expect there to be local changes in temperature due to the process of wax solidification (in the associated latent heat of solidification). But we assume that the heat exchanges are confined to a neighbourhood of the particle surface and bring about a negligible change in temperature.

1.5 Thesis goals and outline

Wax deposition is one of the major issues in the oil industry during production and transportation of crude oil from offshore to onshore through a pipe. The problems occur because as the oil moves along the pipe, the oil temperature is decreasing and then the solubility of the wax also decreases. As the temperature falls below the wax appearance temperature, the wax precipitates out of solution and forms solid wax particles, and these start to grow inside the pipe. In this thesis, we study the temperature profile within the pipe. We study an axisymmetric flow and temperature fields where the temperature is initially above the wax appearance temperature, and later the oil moves downstream to surroundings at a temperature lower than the wax appearance temperature, to induce diffusion of wax molecules onto solid nuclei.

We develop and investigate new mathematical models for spherical wax particle growth, formulating a corresponding free boundary problem. We solve the equations of the models both analytically and numerically. In particular, we compare a self-similar solution which is derived for a special case in terms of the mass transfer coefficient $k_r(t)$ with a numerical solution by our numerical algorithm. In this work, we use asymptotic analysis with a small parameter.

At the leading order, we consider a spherical particle and assume the speed of the wax particle is close to the local speed of the flow. So, the flow relative to the wax particle is negligible in the leading order problem. In the first-order correction we assume the wax particle is spherical initially, and that the correction to the particle shape is caused by a small difference in speed between the wax particle and the local flow. We formulate and study the coupled diffusion/ flow problem for a single particle without assuming that the particle shape is spherical.

To achieve these goals, in the following chapters, we have the following contents:

In chapter 2 we discuss the flow of the oil in a circular pipe. We study the temperature distribution with viscous heating, and we find that the viscous heating term does not significantly affect the temperature distribution. We conclude that we can evaluate the temperature distribution without the viscous heating term. The temperature decreases monotonically as a function of radial coordinate, from the centreline of the pipe toward the wall. We also find how the centreline temperature decreases along the length of the pipe.

In chapter 3 we study the growth of a spherical wax particle moving together with the waxy crude oil while it grows in time. We model one spherical wax particle which is far from other particles. This wax particle is small and it moves together with the flow, the relative velocity of the wax particle with respect to the flow is very small. Hence we neglect the convective term relative to the diffusion term in the convective-diffusion equation. The growth of the wax particle is due to diffusion of wax molecules towards the surface of the particle. We derive boundary conditions for the mass flux and the consequent particle growth. We investigate the self-similar solution and we find the

concentration distribution of a single wax particle.

In chapter 4 we present the numerical part of this thesis. We study the initial boundary value problem numerically, by developing a time-stepping numerical algorithm. In order to validate this algorithm, we compare the numerical results with the self-similar solution of chapter 3, where the mass transfer coefficient $k_r(t)$ is a special function of time. Then the boundary value problem is formulated for a constant mass transfer coefficient k_r. We found the solution for the leading order spherically symmetric problem with constant mass transfer coefficient.

In chapter 5 the coupled diffusion/ flow problem of a single wax particle is formulated. The flow is uniform and the shape of the particle is non-spherical. However, we assume the wax particle is spherical initially. This coupled problem is studied in the spherical coordinate system as the three-dimensional problem of wax particle growth. Then we restrict ourselves to an axisymmetric case. We use asymptotic analysis to determine the motion of the wax particle and the growth of the wax particle. The leading order solution corresponds to a spherical wax particle without flow around it. In the first order correction we find that the particle stays spherical. However, the deposition at the wax particle is non-uniform.

In chapter 6 we present the conclusions of the study and make suggestions for future work.

Chapter 2

Temperature distribution in oil flow in a pipe

In this chapter, the temperature distribution in a circular pipe is obtained when a viscous incompressible fluid is flowing through the pipe. In section 2.1, we find the velocity distribution of the flow, and in section 2.2, we find the temperature distribution in a production pipe. In 2.2.1, we analyse the energy equation and show that the viscous heating term does not affect significantly the temperature distribution. So, we neglect the viscous heating term in the energy equation and we solve this equation in 2.2.2. Venkatesan et al. [37] reported on the crude oil transport through subsea pipelines, which is a complex mixture consisting of paraffins, aromatis, etc. The solubility of waxes in crude oil decreases dramatically with decreasing temperature. At the offshore reservoir temperature ($70 - 150°\mathrm{C}$) the solubility of waxes is sufficiently high to keep the wax fully dissolved in the oil. As the oil leaves the reservoir and flows through the pipe, its temperature drops due to the cold environment of

the sea, and the ambient temperature can be about 4°C. Our analysis is general with T_1 being the temperature outside the pipe. In our study we choose the pipe wall temperature T_1 to be 10°C, but this ambient temperature can be any value in our analysis less than the temperature of the oil at the entrance and also less than the WAT ($T_1 < T_{WAT}$). The wax precipitates out due to the decreased solubility and then wax deposition on the cold pipe wall can occur. Alyejina et al. [3] show that the radial temperature gradient and wax crystallisation occur near the cooled walls of the pipe, where the oil temperature is below the wax appearance temperature. Then, the solid wax appears in the oil. The solubility of the wax in the oil decreases with the decreasing temperature. Hence the wax molecules precipitate out of solution, form a solid and deposit on the cold pipe walls.

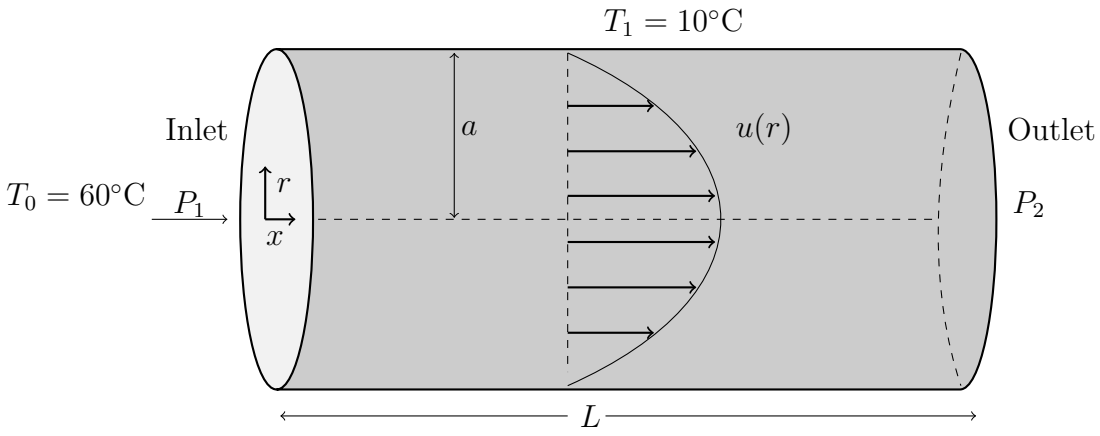

Figure 2.0.1: Sketch of a steady viscous flow in a stationary pipe of circular cross-section. The fluid temperature at the inlet is T_0 and the wall temperature is T_1.

Figure 2.0.1 shows the geometry of the flow through a circular pipe in the positive x direction, where a is the radius of the pipe, L is the length of part

of the pipe, at the ends of which the pressures are P_1 and P_2, respectively.

2.1 Velocity distribution of the oil flow in a circular production pipe

For completeness of the thesis and to make it self-contained we start our analysis from very basic equations and concepts of hydrodynamics and thermodynamics. This also helps us to introduce and explain the main quantities and notations to be used throughout our study.

We consider a laminar steady flow of a viscous fluid of constant density ρ and dynamic viscosity μ in a circular pipe. The flow is described in a cylindrical polar coordinate system r, θ and x. The pipe has circular cross-section with radius a and length L. The pressures at the inlet and outlet are P_1 and P_2, respectively. Laminar flow is a flow, in which all the fluid particles move in layers such as one layer of fluid slides smoothly over an adjacent layer [56]. Fluid flow is said to be steady if at every geometric point of the flow domain, all the properties (pressure, density, specific heat, velocity, thermal conductivity, temperature, etc.) do not change with time [52]. Mathematically, we can write

$$\frac{\partial(\text{properties of the fluid})}{\partial t} = 0.$$

We start from the continuity equation in cylindrical polar coordinates, see [73],

$$\frac{\partial \rho}{\partial t} + \frac{1}{r}\frac{\partial(\rho r u_r)}{\partial r} + \frac{1}{r}\frac{\partial(\rho u_\theta)}{\partial \theta} + \frac{\partial(\rho u_x)}{\partial x} = 0. \tag{2.1.1}$$

As the density ρ is constant for incompressible fluid, the continuity equation (2.1.1) becomes

$$\frac{1}{r}\frac{\partial(r u_r)}{\partial r} + \frac{1}{r}\frac{\partial u_\theta}{\partial \theta} + \frac{\partial u_x}{\partial x} = 0, \tag{2.1.2}$$

where u_r, u_θ, and u_x are the velocity components in the r, θ, and x directions respectively.

Now, we consider the Navier-Stokes equations of the flow in cylindrical coordinates (r, θ, x), see [49],

$$\begin{aligned}
&\rho\left[\frac{\partial u_r}{\partial t}+u_r\frac{\partial u_r}{\partial r}+\frac{u_\theta}{r}\frac{\partial u_r}{\partial \theta}+u_x\frac{\partial u_r}{\partial x}-\frac{u_\theta^2}{r}\right]= \\
&\qquad -\frac{\partial P}{\partial r}+\mu\left[\frac{1}{r}\frac{\partial}{\partial r}\left(\frac{r\partial u_r}{\partial r}\right)-\frac{u_r}{r^2}+\frac{1}{r^2}\frac{\partial^2 u_r}{\partial \theta^2}+\frac{\partial^2 u_r}{\partial x^2}-\frac{2}{r^2}\frac{\partial u_\theta}{\partial \theta}\right], \\
&\rho\left[\frac{\partial u_\theta}{\partial t}+u_r\frac{\partial u_\theta}{\partial r}+\frac{u_\theta}{r}\frac{\partial u_\theta}{\partial \theta}+u_x\frac{\partial u_\theta}{\partial x}+\frac{u_r u_\theta}{r}\right]= \\
&\qquad -\frac{1}{r}\frac{\partial P}{\partial \theta}+\mu\left[\frac{1}{r}\frac{\partial}{\partial r}\left(\frac{r\partial u_\theta}{\partial r}\right)-\frac{u_\theta}{r^2}+\frac{1}{r^2}\frac{\partial^2 u_\theta}{\partial \theta^2}+\frac{\partial^2 u_\theta}{\partial x^2}+\frac{2}{r^2}\frac{\partial u_r}{\partial \theta}\right], \\
&\rho\left[\frac{\partial u_x}{\partial t}+u_r\frac{\partial u_x}{\partial r}+\frac{u_\theta}{r}\frac{\partial u_x}{\partial \theta}+u_x\frac{\partial u_x}{\partial x}\right]= \\
&\qquad -\frac{\partial P}{\partial x}+\mu\left[\frac{1}{r}\frac{\partial}{\partial r}\left(\frac{r\partial u_x}{\partial r}\right)+\frac{1}{r^2}\frac{\partial^2 u_x}{\partial \theta^2}+\frac{\partial^2 u_x}{\partial x^2}\right],
\end{aligned} \tag{2.1.3}$$

where $P = P(r, \theta, x)$ is the hydrodynamic pressure.

In our problem we assume that the flow is in the positive x-direction and also we consider a steady flow. So, only one component of the flow velocity is non-zero, $u_x \neq 0$ and $u_r = u_\theta = 0$. Due to axial symmetry of the flow the axial velocity u_x is independent of θ, so that $u_x = u_x(r, x)$. The continuity equation reduces to the following,

$$\frac{\partial u_x}{\partial x} = 0. \tag{2.1.4}$$

Therefore, the continuity equation implies that u_x is independent of x. So the

non-zero velocity component is a function of r only,

$$u_x = u(r).$$

With $u_r = 0$, $u_\theta = 0$ and $u_x = u(r)$ the Navier-Stokes equations (2.1.3) reduce to the following three equations

$$\frac{\partial P}{\partial r} = 0, \tag{2.1.5}$$

$$\frac{\partial P}{\partial \theta} = 0, \tag{2.1.6}$$

and

$$\frac{\partial P}{\partial x} = \mu \frac{1}{r} \frac{d}{dr} \left(\frac{r du}{dr} \right). \tag{2.1.7}$$

In equation (2.1.7), the right hand side is a function of r but equations (2.1.5) and (2.1.6) show that the pressure P is independent of r and θ. Thus P is function of x only.

This implies that the pressure $P(x)$ changes linearly between the inlet and outlet (in the direction of the flow), which can be written as

$$\frac{\partial P}{\partial x} = \frac{P_2 - P_1}{L} = \frac{\Delta P}{L}. \tag{2.1.8}$$

Note that the liquid flow is in the positive x-direction. Hence $P_2 < P_1$ and $\Delta P < 0$, and $\frac{\Delta P}{L}$ is the pressure gradient.

Now, using (2.1.8) and (2.1.7) we find

$$\frac{d}{dr} \left(\frac{r du}{dr} \right) = \frac{r \Delta P}{\mu L}. \tag{2.1.9}$$

Integrating (2.1.9) with respect to r we find

$$r \frac{du}{dr} = \frac{1}{\mu} \frac{\Delta P}{L} \frac{r^2}{2} + c_1, \tag{2.1.10}$$

where c_1 is a constant of integration.

Next we divide both sides of (2.1.10) by r and integrate the result once again:

$$u(r) = \frac{1}{\mu}\frac{\Delta P}{L}\frac{r^2}{4} + c_1 \log(r) + c_2. \tag{2.1.11}$$

The constants c_1 and c_2 in (2.1.11) are obtained by using the regularity condition and the wall boundary condition. The first condition requires that the velocity of the flow, $u(r)$, is finite at every point of the flow. However, the second term in (2.1.11) predicts unbounded velocity at $r = 0$ if $c_1 \neq 0$. The velocity of the flow is finite if and only if $c_1 = 0$. Equation (2.1.11) yields

$$u(r) = \frac{1}{\mu}\frac{\Delta P}{L}\frac{r^2}{4} + c_2. \tag{2.1.12}$$

The boundary condition on the wall of the pipe, the so-called no-slip boundary condition, $u = 0$ where $r = a$, gives:

$$c_2 = \frac{-1}{\mu}\frac{\Delta P}{L}\frac{a^2}{4}.$$

By substituting the obtained constant c_2 in (2.1.12), we find

$$\begin{aligned} u(r) &= \frac{1}{\mu}\frac{\Delta P}{L}\frac{r^2}{4} - \frac{1}{\mu}\frac{\Delta P}{L}\frac{a^2}{4} \\ &= \frac{1}{4\mu}\frac{\Delta P}{L}(r^2 - a^2). \end{aligned} \tag{2.1.13}$$

The expression obtained for u can be presented in the form

$$u(r) = \frac{-a^2}{4\mu}\frac{\Delta P}{L}\left(1 - \left(\frac{r}{a}\right)^2\right), \tag{2.1.14}$$

where $\Delta P < 0$. Equation (2.1.14) describes the axial velocity distribution. The velocity (2.1.14) has a parabolic profile (see figure 2.0.1).

The maximum velocity u_{max} is achieved at $r = 0$,

$$u_{max} = \frac{-a^2}{4\mu}\frac{\Delta P}{L}. \tag{2.1.15}$$

By using (2.1.15), equation (2.1.14) can be presented as

$$u(r) = u_{max}(1 - \frac{r^2}{a^2}). \tag{2.1.16}$$

The equation (2.1.16) is used in the next section to find the temperature distribution in an offshore production oil pipeline. Production pipeline has radius a which is about, say, 25 cm. The maximum velocity u_{max} is in the range (1 m/s - 6 m/s). The dynamic viscosity μ depends on the temperature and varies from $3.8 \cdot 10^{-3}$ kg $\cdot$ m$^{-1}\cdot$s^{-1} at 12°C to $1.3 \cdot 10^{-3}$ kg $\cdot$ m$^{-1}\cdot$s^{-1} at 60°C. The oil density ρ also varies with temperature from 824 kg/m^3 at 15°C to 806 kg/m^3 at 40°C [41]. In the following analysis we take $a = 20$ cm as a reference radius. Also, $u_{max} = 1$ m/s is taken as a reference flow velocity, [75]. We take $\mu_{oil} = 2 \cdot 10^{-3}$ kg $\cdot$ m$^{-1}\cdot$s^{-1} and neglect dependence of the dynamic viscosity on the temperature. We take $\rho_{oil} = 806$ kg/m^3. We assume the flow velocity is independent of temperature and its variation along the pipe.

2.2 Temperature distribution in a production pipe

Many authors have studied the temperature distribution in a pipe of circular cross-section, see [7, 29, 48, 51, 53, 58, 61, 62, 69, 78, 79]. The heat transfer in a duct flow of a Newtonian fluid was first studied by Greatz in 1883 for a slug flow and later in 1885 for a Poiseuille flow [81].

Min et al [59] presented a solution for Graetz problem with axial diffusion and flow heating effects in a semi-infinite domain with a given inlet condition. The solution was presented in terms of eigenfunctions of a spectral problem by using the separation variables method.

The temperature distribution in an oil pipeline determines the location where precipitation of wax particles starts, [63]. If the oil temperature falls below the wax appearance temperature, the wax may precipitate out of the solution. Deposition can occur on the walls, or onto dust particles inside the flow. The second case is the one we focus on in the next chapter.

2.2.1 Problem description

The aim of our analysis is to determine the temperature distribution $T(r, x)$ in a flow. Consider a laminar steady incompressible flow inside the pipe of radius a and length L sketched in figure 2.0.1. The fluid properties are assumed constants. Let T_0 be the temperature of the fluid entering the pipe at $x = 0$ and let T_1 be the temperature of the walls [sea water temperature]. In the cylindrical coordinates system (r, θ, x), the steady thermal transport equation is, [49]

$$\rho c_v u(r) \frac{\partial T}{\partial x} = k \left(\frac{\partial^2 T}{\partial r^2} + \frac{1}{r} \frac{\partial T}{\partial r} + \frac{\partial^2 T}{\partial x^2} \right) + \Phi(r, \theta, x), \tag{2.2.1}$$

where c_v is the specific heat capacity of the oil, $c_v = 1950$ J/(kg $\cdot$ K), K stands for Kelvin as the unit of the temperature, k is the oil thermal conductivity, $k = 0.261$ J/(s $\cdot$ m $\cdot$ K) [50]. The axial velocity of the flow $u(r)$ is given by (2.1.16), and $T = T(x, r)$ is the temperature distribution to be determined. The symbol Φ denotes the viscous heating function, which in terms of the velocity components is [49]

$$\Phi = 2\mu[(\frac{\partial u_r}{\partial r})^2 + (\frac{1}{r}\frac{\partial u_\theta}{\partial \theta} + \frac{u_r}{r})^2 + (\frac{\partial u_x}{\partial x})^2 + \frac{1}{2}(\frac{\partial u_\theta}{\partial r} - \frac{u_\theta}{r} + \frac{1}{r}\frac{\partial u_r}{\partial \theta})^2 + \frac{1}{2}(\frac{1}{r}\frac{\partial u_x}{\partial \theta} + \frac{\partial u_\theta}{\partial x})^2 + \frac{1}{2}(\frac{\partial u_r}{\partial x} + \frac{\partial u_x}{\partial r})^2].$$

With $u_r = 0$, $u_\theta = 0$ and u_x independent of θ, $u_x = u(r)$, the equation (2.2.1) without external heat sources reduces to :

$$\rho c_v u(r)\frac{\partial T}{\partial x} = k\left(\frac{\partial^2 T}{\partial r^2} + \frac{1}{r}\frac{\partial T}{\partial r} + \frac{\partial^2 T}{\partial x^2}\right) + \mu\left(\frac{\partial u}{\partial r}\right)^2. \tag{2.2.2}$$

The boundary condition for equation (2.2.2) is $T = T_1$, see (2.2.12)-(2.2.13) prescribed at the wall of the pipe, $r = a$. Part of the pipe is beneath the sea bottom with the inlet oil temperature, say, $T_0 = 60°\text{C}$ and the part of the pipe is surrounded by sea water at temperature, say, $T_1 = 10°\text{C}$. We specify in this study the wax appearance temperature as, $T_{WAT} = 33°\text{C}$. The wax appearance temperature is the temperature at which the first wax particle appears because the wax begins to precipitate from the oil when the temperature is at or below the WAT.

To estimate the contribution of the viscous heating term in (2.2.2), we consider the solution of equation (2.2.2) far from the entrance, where the temperature is independent of x :$\frac{\partial T}{\partial x} = 0$. Then equation (2.2.2) becomes

$$k\left(\frac{\partial^2 T}{\partial r^2} + \frac{1}{r}\frac{\partial T}{\partial r}\right) = -\mu\left(\frac{\partial u}{\partial r}\right)^2. \tag{2.2.3}$$

Using (2.1.16) in (2.2.3) yields

$$k\left(\frac{\partial^2 T}{\partial r^2} + \frac{1}{r}\frac{\partial T}{\partial r}\right) = -\frac{4\mu u_{max}^2 r^2}{a^4}$$

and

$$\frac{d}{dr}\left(r\frac{dT}{dr}\right) = \frac{-4\mu u_{max}^2 r^3}{ka^4}. \tag{2.2.4}$$

Integrating (2.2.4) twice with respect to r gives:

$$T(r) = \frac{-\mu u_{max}^2 r^4}{4ka^4} + c_1 \log(r) + c_2. \tag{2.2.5}$$

Now, we need two conditions to determine the constants of integration. They are

1) The temperature T is finite in the flow region, $0 \leq r \leq a$.

2) $T = T_1$ at $r = a$.

The first condition yields that the temperature (2.2.5) can not contain the log term because it is singular at $r = 0$. So we set $c_1 = 0$. Then (2.2.5) becomes

$$T(r) = \frac{-\mu u_{max}^2 r^4}{4ka^4} + c_2. \tag{2.2.6}$$

Substituting (2.2.6) into the second condition gives

$$\frac{-\mu u_{max}^2}{4k} + c_2 = T_1. \tag{2.2.7}$$

Then

$$c_2 = \frac{\mu u_{max}^2}{4k} + T_1. \tag{2.2.8}$$

Equations (2.2.6) and (2.2.8) provide

$$T(r) = T_1 + \frac{\mu u_{max}^2}{4k}\left(1 - \frac{r^4}{a^4}\right), \qquad (0 \leq r \leq a). \tag{2.2.9}$$

This is the temperature distribution in the Poiseuille flow with constant temperature T_1 at the wall, $r = a$. Note that the temperature $T(r)$ increases with increasing distance from the wall. Therefore, (2.2.9) shows that the viscous heating increases the temperature in the flow. The maximum increase of the temperature is achieved at the axis of the pipe, $r = 0$, where it takes the value $T_1 + \frac{\mu u_{max}^2}{4k}$. For our reference values, we find that the temperature difference between the centre and wall is

$$T(0) - T_1 = \frac{\mu u_{max}^2}{4k} = \frac{2 \times 10^{-3}\text{kg}/(\text{m} \cdot \text{s}) \times (1\text{m}/\text{s})^2}{4 \times 0.261\text{J}/(\text{s} \cdot \text{m} \cdot \text{K})} \approx 0.0019\text{K}. \tag{2.2.10}$$

We have seen that $T(0) - T_1$ in equation (2.2.10) is independent of the pipe radius a, and is rather small. The temperature profile (2.2.9) is shown in figure 2.2.1. Then $T(r) - T_1$ is small compared with T_1 and can be neglected. So, the calculation of the temperature $T(x, r)$ by (2.2.1) can be achieved with good accuracy with $\Phi = 0$.

We have found that the maximum temperature difference due to the viscous heating term is very small compared with the wall temperature. This means the viscous heating does not affect significantly the temperature distribution in the pipe.

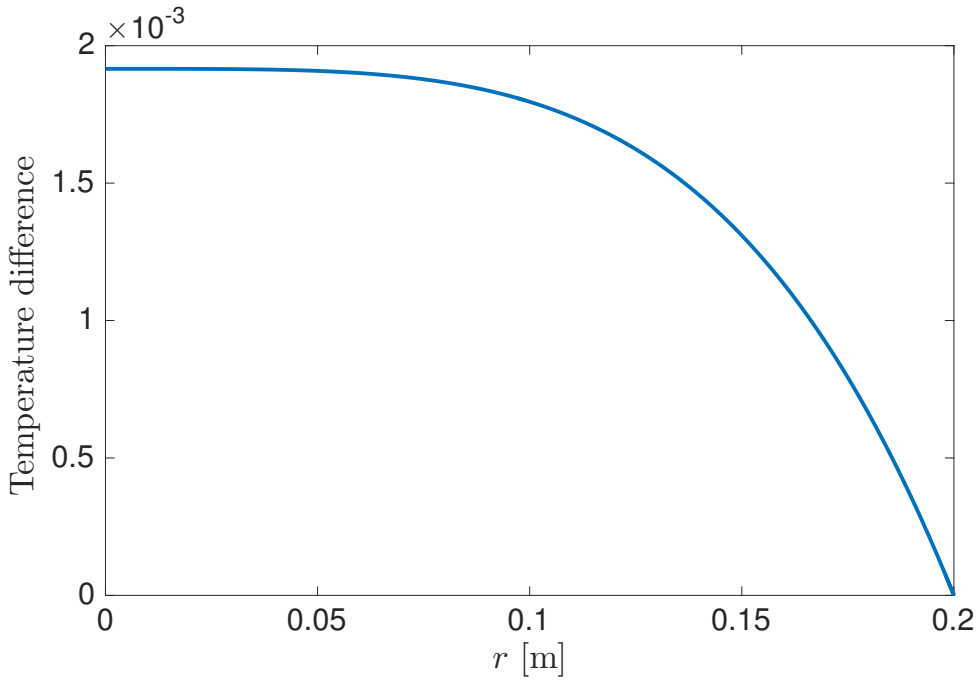

Figure 2.2.1: Plot showing the temperature difference, $T(r) - T_1$, as a function of r: $0 \leq r \leq 0.2$ for a pipe of radius $a = 0.2$.

2.2.2 Temperature distribution without viscous heating

It was shown in section 2.2.1 that the viscous heating term $\Phi(x, r)$ in equation (2.2.1) does not affect significantly the temperature distribution. So in this section we neglect Φ in (2.2.2). In this section, the so-called Graetz problem is formulated and solved using the separation variables method and the Kummer equation. Here, we consider equation (2.2.2) without the viscous heating term, but with T dependent on r and x,

$$\rho c_v u(r) \frac{\partial T}{\partial x} = k \left(\frac{\partial^2 T}{\partial r^2} + \frac{1}{r} \frac{\partial T}{\partial r} + \frac{\partial^2 T}{\partial x^2} \right). \tag{2.2.11}$$

The boundary conditions for (2.2.11) are:

$$T(0, r) = T_0, \qquad \text{where} \qquad x = 0, \qquad 0 \leq r \leq a, \tag{2.2.12}$$

$$T(x, a) = T_1, \qquad \text{where} \qquad x > 0, \qquad r = a. \tag{2.2.13}$$

To write the energy equation (2.2.11) in a more convenient form, we introduce the following dimensionless variables,

$$\widetilde{r} = \frac{r}{a}, \qquad \widetilde{x} = \frac{x}{X}, \qquad \widetilde{\theta}(\widetilde{x}, \widetilde{r}) = \frac{T - T_1}{T_0 - T_1}, \tag{2.2.14}$$

where $\widetilde{r}$, $\widetilde{x}$ and $\widetilde{\theta}(\widetilde{x}, \widetilde{r})$ are dimensionless, and a is the radius of the pipe, X is the length scale of thermal effects along the pipe to be specified below, T_0 is the temperature of the oil entering the pipe, and T_1 is the temperature of the walls of the pipe. By using the chain rule, we find

$$\begin{cases} \frac{\partial T}{\partial x} = \frac{\partial T}{\partial \widetilde{x}} \frac{\partial \widetilde{x}}{\partial x} = (T_0 - T_1) \frac{1}{X} \frac{\partial \widetilde{\theta}}{\partial \widetilde{x}} \\ \\ \frac{\partial^2 T}{\partial x^2} = (T_0 - T_1) \frac{1}{X^2} \frac{\partial^2 \widetilde{\theta}}{\partial \widetilde{x^2}} \\ \\ \frac{\partial T}{\partial r} = (T_0 - T_1) \frac{\partial T}{\partial \widetilde{r}} \frac{\partial \widetilde{r}}{\partial r} = (T_0 - T_1) \frac{1}{a} \frac{\partial \widetilde{\theta}}{\partial \widetilde{r}} \\ \\ \frac{\partial^2 T}{\partial r^2} = (T_0 - T_1) \frac{1}{a^2} \frac{\partial^2 \widetilde{\theta}}{\partial \widetilde{r^2}} \end{cases} \tag{2.2.15}$$

In terms of these variables the equation for the dimensionless temperature become:

$$\frac{a^2}{k} \rho c_v u \frac{1}{X} \frac{\partial \widetilde{\theta}}{\partial \widetilde{x}} = \frac{\partial^2 \widetilde{\theta}}{\partial \widetilde{r^2}} + \frac{1}{\widetilde{r}} \frac{\partial \widetilde{\theta}}{\partial \widetilde{r}} + \frac{a^2}{X^2} \frac{\partial^2 \widetilde{\theta}}{\partial \widetilde{x^2}}, \qquad (0 \leq \widetilde{r} \leq 1, 0 < \widetilde{x} < \infty), \tag{2.2.16}$$

where u is the axial velocity of the flow given by (2.1.16). Then equation (2.2.16) becomes

$$\frac{a^2}{kX} \rho c_v u_{max} (1 - \widetilde{r}^2) \frac{\partial \widetilde{\theta}}{\partial \widetilde{x}} = \frac{\partial^2 \widetilde{\theta}}{\partial \widetilde{r^2}} + \frac{1}{\widetilde{r}} \frac{\partial \widetilde{\theta}}{\partial \widetilde{r}} + \frac{a^2}{X^2} \frac{\partial^2 \widetilde{\theta}}{\partial \widetilde{x^2}}, \qquad (0 \leq \widetilde{r} \leq 1, 0 < \widetilde{x} < \infty), \tag{2.2.17}$$

where the length scale X along the pipe is to be determined in such a way that all coefficients in the energy equation are less than or equal to one in the dimensionless variables. We choose $X = \frac{a^2}{k} \rho c_v u_{max}$ and then equation (2.2.17), becomes

$$(1 - \widetilde{r}^2) \frac{\partial \widetilde{\theta}}{\partial \widetilde{x}} = \frac{\partial^2 \widetilde{\theta}}{\partial \widetilde{r^2}} + \frac{1}{\widetilde{r}} \frac{\partial \widetilde{\theta}}{\partial \widetilde{r}} + \frac{a^2}{X^2} \frac{\partial^2 \widetilde{\theta}}{\partial \widetilde{x^2}}, \qquad (0 \leq \widetilde{r} \leq 1, 0 < \widetilde{x} < \infty). \tag{2.2.18}$$

The dimensionless boundary conditions at the inlet $\widetilde{x} = 0$, and at the wall $\widetilde{r} = 1$, for equation (2.2.18), are:

$$\widetilde{\theta}(0, \widetilde{r}) = 1 \qquad \text{where} \qquad \widetilde{x} = 0, \qquad 0 \leq \widetilde{r} \leq 1, \tag{2.2.19}$$

$$\widetilde{\theta}(\widetilde{x},1)=0 \qquad \text{where} \qquad \widetilde{x}>0, \qquad \widetilde{r}=1. \tag{2.2.20}$$

The dimensional temperature is given by

$$T(x,r)=T_1+(T_0-T_1)\widetilde{\theta}\,(\widetilde{x},\widetilde{r})\,. \tag{2.2.21}$$

We obtain thermal transport equation in the dimensionless variables (tilde is dropped below),

$$(1-r^2)\theta_x=\theta_{rr}+\frac{1}{r}\theta_r+\epsilon^2\theta_{xx}, \qquad (0\le r\le 1, 0<x<\infty) \tag{2.2.22}$$

where

$$\epsilon=\frac{a}{X}=\frac{a}{\frac{a^2\rho c_v u_{max}}{k}}=\frac{k}{a\rho c_v u_{max}}=\frac{1}{P_e}. \tag{2.2.23}$$

The Peclet number is defined as $P_e=\frac{a\rho c_v u_{max}}{k}$ which is the product of the Reynolds number and Prandtl number, see [27], and $P_e>>1$ in our problem. So, $\frac{1}{P_e}<<1$ and ϵ is a small parameter of the problem.

In our reference case we find :

$$\begin{aligned} X=\frac{a^2}{k}\rho c_v u_{max} &\approx \frac{(0.2m)^2\times 806(\mathrm{kg/m^3})\times 1950(\mathrm{J/(kg\cdot K)})\times 1(\mathrm{m/s})}{0.261(\mathrm{J/s\cdot m\cdot K})} \\ &\approx 2\times 10^5\mathrm{m}, \end{aligned} \tag{2.2.24}$$

and then we find

$$\epsilon=\frac{a}{X}=\frac{0.2\mathrm{m}}{2\times 10^5\mathrm{m}}=10^{-6}. \tag{2.2.25}$$

From the calculation above we find the length scale of the thermal effects is about 200 km. The value of ϵ in equation (2.2.25) is very small. Thus, the axial diffusion term in equation (2.2.22), $\epsilon^2\theta_{xx}$, can be neglected relative to the radial diffusion. So, we obtain the following approximate equation at leading order as $\epsilon\longrightarrow 0$,

$$(1-r^2)\theta_x = \theta_{rr} + \frac{1}{r}\theta_r, \qquad (0 \le r \le 1, 0 < x < \infty). \tag{2.2.26}$$

Equation (2.2.26) is of parabolic type with x being a time-like variable. For the parabolic equation (2.2.26), the solution $\theta(x,r)$ at $x = x_*$ depends on $\theta(x,r)$, where $x < x_*$, but is independent of the temperature downstream, $x > x_*$, where x_* stand for the downstream axis.

The dimensionless boundary conditions (2.2.19) and (2.2.20) provide (tildes are dropped)

$$\theta(0,r) = 1 \qquad \text{where} \qquad x = 0, \qquad 0 < r < 1, \tag{2.2.27}$$

$$\theta(x,1) = 0 \qquad \text{where} \qquad x > 0, \qquad r = 1. \tag{2.2.28}$$

We consider the solution of equation (2.2.26) when the wall of the pipe is kept at a constant temperature, see (2.2.28). The boundary condition (2.2.27) provides the initial condition for the parabolic equation (2.2.26).

Equation (2.2.26) is a linear equation where x and r are independent variables. We use the method of separation of variables by assuming the solution in the form

$$\theta(x,r) = g(x)f(r). \tag{2.2.29}$$

Substituting (2.2.29) into (2.2.26) and separating the variables yields

$$\frac{g'(x)}{g(x)} = \frac{1}{r(1-r^2)}\left[r\frac{f''(r)}{f(r)} + \frac{f'(r)}{f(r)}\right] = -\beta^2, \tag{2.2.30}$$

where β is a positive real constant to guarantee that $T(x,r)$ decays as $x \longrightarrow +\infty$. Then we have two separate equations:

$$\frac{dg}{dx} + \beta^2 g(x) = 0, \qquad (x > 0) \tag{2.2.31}$$

and

$$f''(r) + \frac{1}{r}f'(r) + \beta^2(1-r^2)f(r) = 0 \qquad (0 < r < 1). \tag{2.2.32}$$

The boundary condition (2.2.28) gives the condition

$$f(1) = 0, \tag{2.2.33}$$

for equation (2.2.32). The nontrivial, $f(r) \not\equiv 0$, and regular solution of spectral problem (2.2.32) and (2.2.33) exist only for some values of the spectral parameter $\beta = \beta_m$, where we choose β_m to be real and positive numbers with $\beta_{m+1} > \beta_m$ and $m \geq 0$. Equation (2.2.32) is a linear ordinary differential equation for $f(r)$. In order to solve it, we introduce a new unknown function $W(Z)$ and a new independent variable Z by, see [81],

$$Z = \beta r^2, \qquad W(Z) = e^{\frac{Z}{2}} f(r). \tag{2.2.34}$$

Then equation (2.2.32) is transformed to

$$Z\frac{d^2W}{dZ^2} + (1-Z)\frac{dW}{dZ} - \left(\frac{1}{2} - \frac{\beta}{4}\right) W = 0. \tag{2.2.35}$$

Equation (2.2.35) is known as Kummer's equation. It has two linearly independent solutions, one of them is singular at $Z = 0$. The regular solution of equation (2.2.35) is

$$W(Z) = CM\left(\frac{1}{2} - \frac{\beta}{4}, 1, Z\right),$$

where C is an arbitrary constant and the function $M(a, b, z)$ is introduced in [1] as the following series,

$$\begin{aligned} M(a,b,Z) =& 1 + \frac{a}{b}Z + \frac{a(a+1)Z^2}{b(b+1)n!} + \cdots + \frac{a(a+1)\cdots(a+n+1)Z^n}{b(b+1)\cdots(b+n-1)n!} + \ldots \\ =& 1 + \sum_{k=1}^{\infty} \frac{(a)_k}{(k!)^2} Z^k, \end{aligned} \tag{2.2.36}$$

where

$$a = \frac{1}{2} - \frac{\beta}{4}, \qquad b = 1, \qquad (a)_k = a(a+1)(a+2)\cdots(a+k-1), \qquad (a)_0 = 1,$$

$$k \geq 1.$$

The boundary condition (2.2.33) leads to the following equation for the spectral parameter β,

$$M\left(\frac{1}{2} - \frac{\beta}{4}, 1, \beta\right) = 0, \tag{2.2.37}$$

where

$$M\left(\frac{1}{2} - \frac{\beta}{4}, 1, \beta\right) \approx 1 + \sum_{k=1}^{K} \frac{(\frac{2-\beta}{4})_k}{(k!)^2}\beta^k. \tag{2.2.38}$$

The level of truncation K in equation (2.2.38) was determined numerically in [81], as $K = 40$, see also [41,68]. Corresponding to each root β_m of (2.2.37), there is the eigenfunction $f_m(r)$ given by

$$f_m(r) = e^{\frac{-\beta_m r^2}{2}} W(\beta_m r^2). \tag{2.2.39}$$

In the following we use the result from [81], that the eigenfunctions $f_m(r)$ are orthogonal with the weight function $r(1-r^2)$ over the interval $r \in [0,1]$, see Appendix A for statement about orthogonal. The corresponding solution of equation (2.2.31) is

$$g(x) = Ae^{-\beta_m^2 x}. \tag{2.2.40}$$

The method of separation variables yields an infinite series solution for the dimensionless temperature

$$\theta(x,r) = \sum_{m=0}^{\infty} A_m e^{-\beta_m^2 x} f_m(r). \tag{2.2.41}$$

This series satisfies equation (2.2.26), the wall condition (2.2.28), and decays at $x \to +\infty$.

The inlet condition (2.2.27) provides the equation for the coefficients A_m,

$$1 = \theta(0, r) = \sum_{m=0}^{\infty} A_m f_m(r), \tag{2.2.42}$$

which should be satisfied for any $r \in [0, 1]$.

To obtain the coefficients A_m, we multiply both sides of equation (2.2.42) by $r(1 - r^2)f_n(r)$ and integrate in r from 0 to 1, with account for orthogonality condition,

$$\int_0^1 r(1 - r^2) f_n(r) f_m(r) dr = 0 \qquad (n \neq m). \tag{2.2.43}$$

We have

$$\int_0^1 r(1 - r^2) f_n(r) dr = A_n \int_0^1 r(1 - r^2) f_n^2(r) dr. \tag{2.2.44}$$

Then equation (2.2.44) gives the constants A_m as

$$A_m = \frac{\int_0^1 r(1 - r^2) f_m(r) dr}{\int_0^1 r(1 - r^2) f_m^2(r) dr}. \tag{2.2.45}$$

Substituting equations (2.2.36) and (2.2.39) into (2.2.45), we obtain

$$A_m = \frac{\int_0^1 r(1 - r^2) e^{\frac{-\beta_m r^2}{2}} \left(1 + \sum_{k=1}^{K} \frac{(a_m)_k}{(k!)^2} \beta_m^k r^{2k}\right) dr}{\int_0^1 r(1 - r^2) e^{-\beta_m r^2} \left(1 + \sum_{k=1}^{K} \frac{(a_m)_k}{(k!)^2} \beta_m^k r^{2k}\right)^2 dr}. \tag{2.2.46}$$

The first ten eigenvalues β_n and coefficients A_n are shown in the Table 2.1, taken from [81]. However, we checked these roots by equation (2.2.37) using accurate Matlab computations and we find the first 15 roots of β and the coefficients A as shown in Table 2.2. As m increases, β_m values differ in the 6^{th} significant digit, and A_m differ by about one percent, between the two tables.

m	β_m	A_m
0	2.7043644	+1.476435
1	6.6790315	-0.806124
2	10.6733795	+0.588761
3	14.6710785	-0.475850
4	18.6698719	+0.405019
5	22.6691438	-0.355757
6	26.6686716	+0.319169
7	30.6684241	-0.290745
8	34.6686899	+0.267952
9	38.6704098	-0.249322

Table 2.1: Eigenvalues of Graetz problem, these numerical values are taken from [81].

Consequently equations (2.2.34), (2.2.36), (2.2.41), yield the dimensionless temperature in the form

$$\theta(x,r) = \sum_{m=0}^{\infty} A_m e^{-\beta_m(\beta_m x + \frac{1}{2}r^2)} \left(1 + \sum_{k=1}^{K} \frac{(a_m)_k}{(k!)^2} \beta_m^k r^{2k}\right), \tag{2.2.47}$$

where the values of β_m and A_m are given in the Table 2.1.

The number of terms m in the series (2.2.47) is limited in calculations here to the first fifteen terms. The dimensionless temperature (2.2.47) is shown in figure 2.2.2. From the figure 2.2.2 we see a decreasing temperature for $x > 0$ and we arrive at a flat distribution when x is large enough. The surrounding sea water absorb the thermal energy as the oil moves in the positive x direction. At the centre of the pipe $r = 0$ the temperature decreases more slowly toward

zero as x increases, where the temperature near the wall, $r \approx 1$, drops quickly toward the wall temperature with increasing x. Figure 2.2.3 shows the dimensional temperature distributions as functions of r at several position along the pipe. We see the temperature is varying along the pipe, and as x increases the temperature decreases. The temperature decreases monotonically as a function of the radial coordinate. Finally, the dimensional temperatures everywhere inside the pipe decrease towards 10°C as x increases. For $x = 1km$, the wax appearance temperature is achieved only close to the wall. This means that at the distance $1km$ from the entrance to the pipe, the wax molecules precipitate out of the solution only close to the wall where the temperature is below the wax appearance temperature. The dimensionless temperature (2.2.47) at $r = 0$, $T(x, 0)$, as a function of the dimensionless distance x from the pipe entrance is shown in figure 2.2.4. It is seen that the temperature quickly decays as x increases. Figure 2.2.5 shows the dimensionless temperature (2.2.47) as a function of r when $x = 0.01$ for different numbers of terms in the series solution. The figure shows the rapid convergence of the solution as number of terms increases.

Figure 2.2.6 shows temperature contours, yellow region indicate high temperature and blue region indicate lower temperature. In Figure 2.2.6 we see at $x = 0$, $r = a$, the contours of constant temperature meet at this point. This occurs because of discontinuity in boundary conditions at this point: T_1 on pipe and T_0 at entrance.

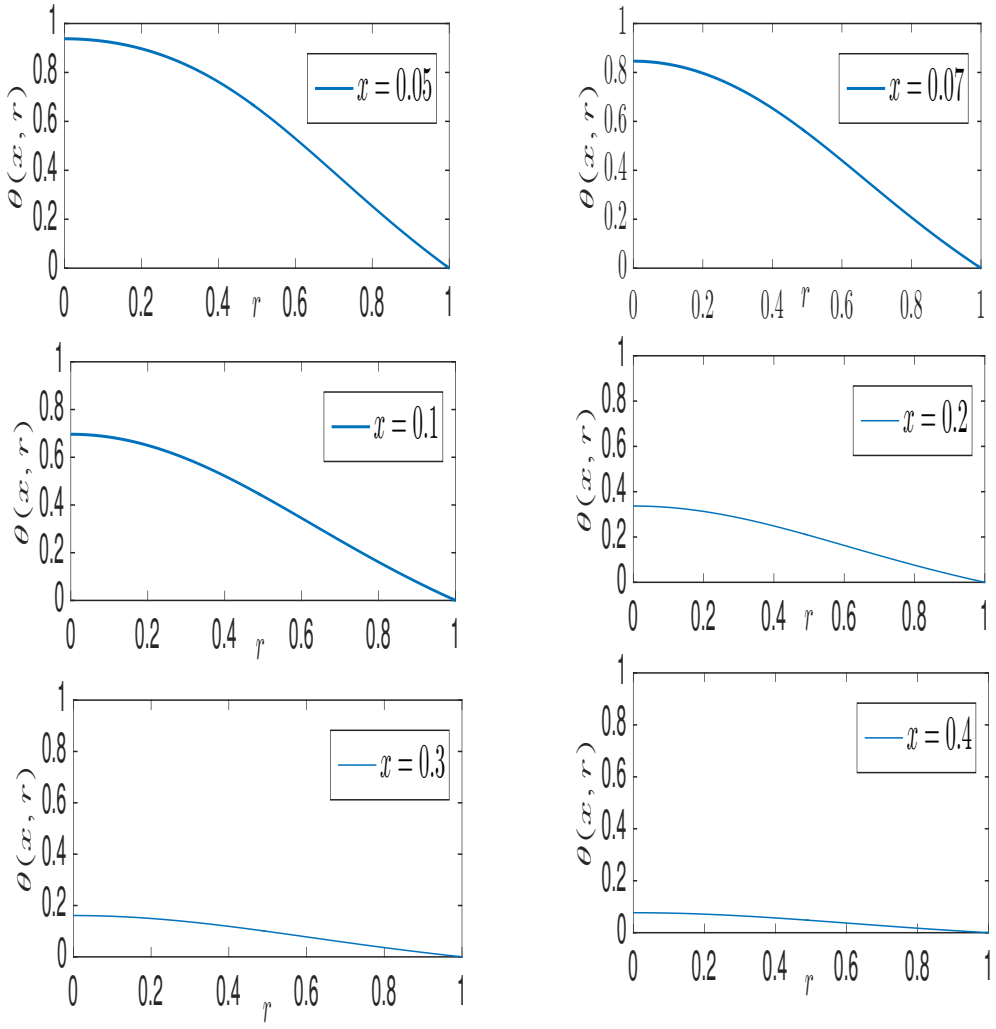

Figure 2.2.2: The dimensionless temperature distributions $T(r, x)$ as functions of r, $0 \leq r \leq 1$, for different distances x of the pipe.

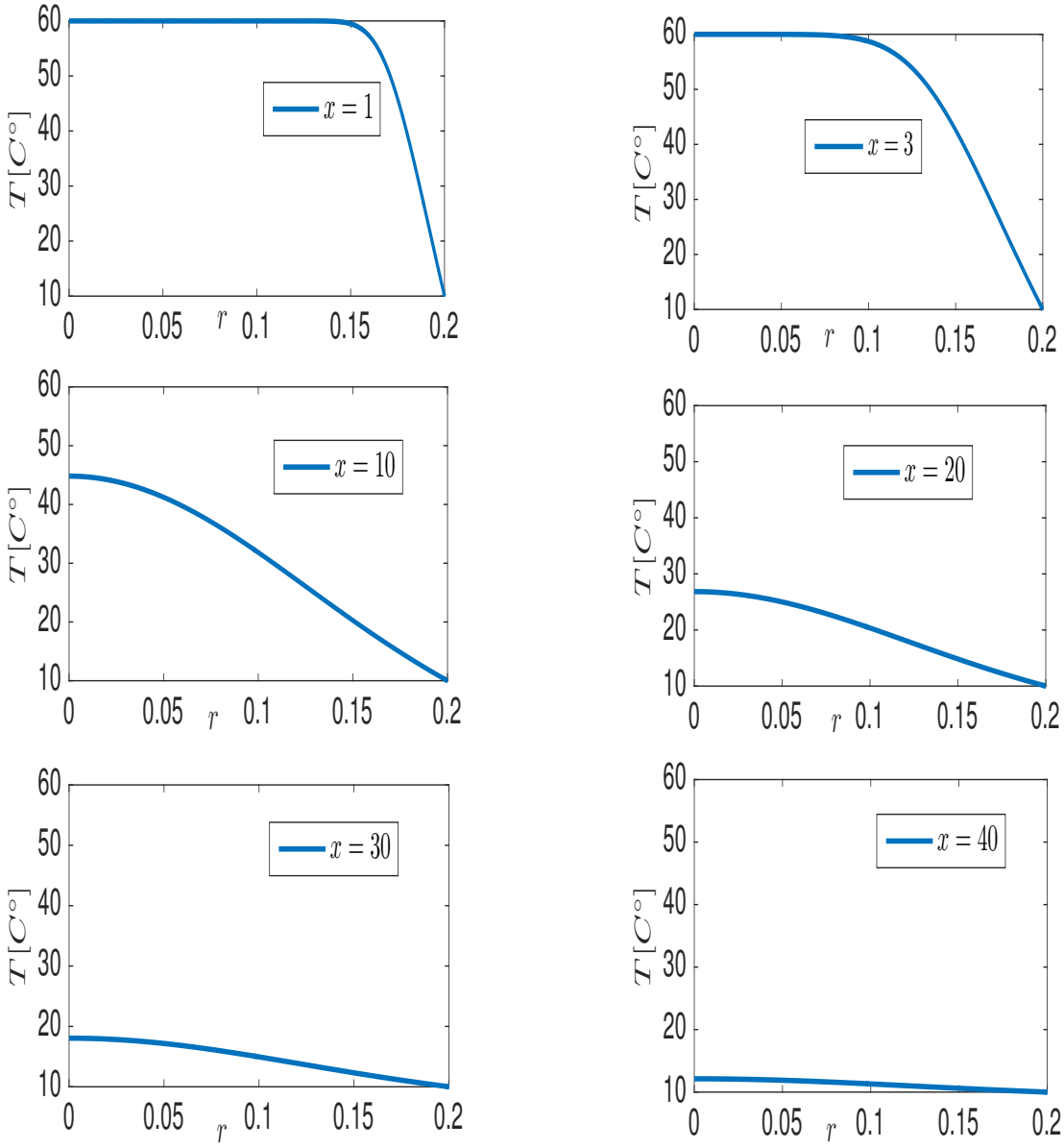

Figure 2.2.3: The dimensional temperature distributions T as functions of r, $0 \leq r \leq 0.2$ [m], for different distances x[km] from the entrance to the pipe.

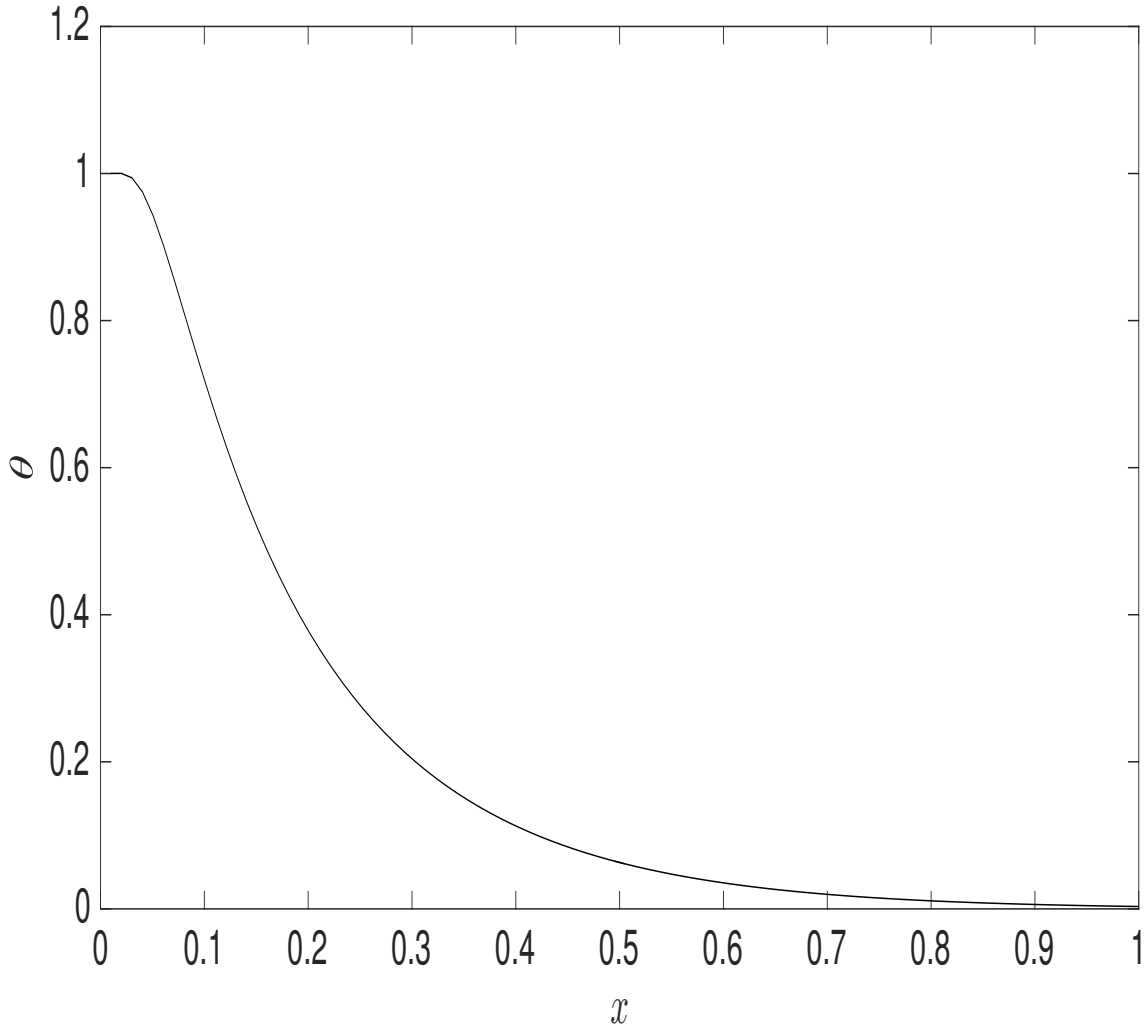

Figure 2.2.4: The dimensionless temperature (2.2.47) at the axis of the pipe, $r = 0$, as a function of distance x from the entrance to the oil pipe.

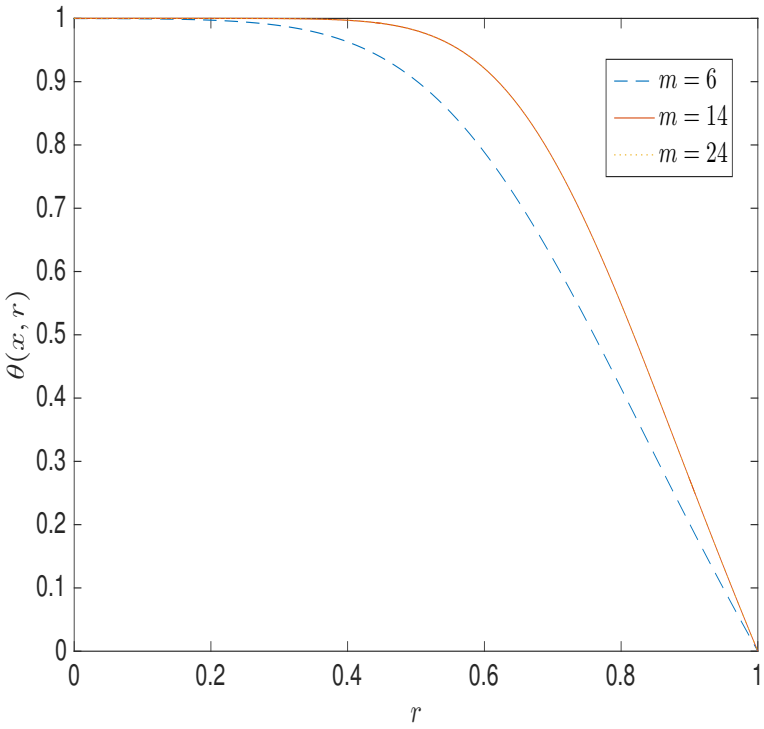

Figure 2.2.5: The dimensionless temperature when $x = 0.01$, as a function of r, each curve plotted for different value of m, where m is the number of terms in the series (2.2.47).

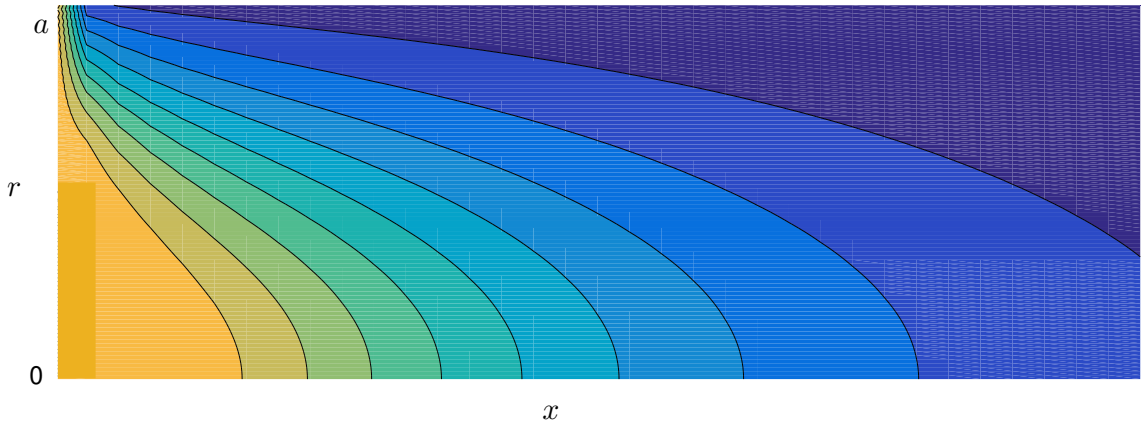

Figure 2.2.6: Contour temperature, yellow region indicate high temperature and blue region indicate lower temperature.

m	β_m	A_m
0	2.704364420	1.479465155
1	6.679031449	-0.8097330056
2	10.67337954	0.5924034190
3	14.67107846	-0.4791944207
4	18.66987186	0.4080620926
5	22.66914336	-0.3585345121
6	26.66866200	0.3217268881
7	30.66832334	-0.2931085984
8	34.66807382	0.2701069718
9	38.66788335	-0.2511437176
10	42.66773381	0.2351923287
11	46.66761370	-0.2215539004
12	50.66751540	0.2097347031
13	54.66743365	-0.1993751973
14	58.66736475	0.1902068142

Table 2.2: Numerical values of β_m and A_m.

Chapter 3

Spherically symmetric growth of a single wax particle

Some types of crude oil contain dissolved waxes that can be precipitated out of solution and become deposited on the internal walls of oil pipes. The wax begins to precipitate out of solution at or below a so-called wax appearance temperature (WAT) which is the temperature at which the first solid wax particle appears in the solution. Many authors have studied the wax deposition onto the wall of a pipe, see [5, 18, 44, 77]. The deposition causes many problems for the oil industry, restricting flow and possibly leading to blocking the pipe. Correa et al. [19] modelled the wax deposition in the turbulent flow of waxy crude oil in a cylindrical pipeline. They assumed the transport of waxes towards the wall is essentially due to molecular diffusion. A mathematical formulation of the spherically symmetric mass transfer problem was presented in [35]. It focused on the particle growth by precipitation from a solution onto a solid particle. In the leading order problem, the convective term in the dif-

fusion equation is neglected and the radius of the particle did not change with time. The diffusion equation in a time-independent domain with stationary particle surface is solved.

To our knowledge there are many models focused on the deposition of wax molecules on the wall of the pipe, but there are very few models focused on what happens to the wax particles before they are deposited on the pipe wall. In this chapter, we are interested in knowing what happens before a wax particle arrives at the wall and sticks to it. We will estimate how a wax particle grows from a microscopic dust particle in the oil. Many particles stuck together make a gel. By definition, a gel or (a semi-solid) is a mixture which has a structure consisting of particles of wax, between which there is a liquid oil phase. Gelification is a process of gel growth, and this occurs at temperatures below the wax appearance temperature, which depends on concentration of wax in the solution [32]. As the wax particles are pressed together in time by hydrodynamic forces, the gel is transformed into a solid wax phase. In this chapter, we consider a single wax particle growth. We deal with a self-similar solution of a single wax particle problem in a viscous flow. The diffusion equation will give the concentration of wax molecules around the wax particle as a function of distance and time.

In this chapter we will derive an analytical solution of diffusion equation for a special dependence of the mass transfer coefficient on time. A reason for deriving an analytical solution for artificial mass transfer coefficient in the boundary condition on the wax particle surface is to validate the numerical algorithm in chapter 4. In section 3.1, we give a description of a single spherical wax particle problem. In section, 3.2, we introduce the boundary conditions and finalize the formulation of the dimensional problem. In section 3.3, we

investigate the self-similar solution for the coupled problem $C = C(r,t)$ and $R = R(t)$, and we find the distribution of the concentration in the fluid. Finally, in section 3.4, we compute the speed of the particle growth.

3.1 Growth of a single spherical particle in an unbounded solution

We consider the motion and growth of a small solid spherical particle in the oil flowing in the pipe. Hot oil enters the pipe from underground. In offshore oil fields, it comes from beneath the sea bottom and flows along the pipe. The pipe is surrounded by seawater, the temperature of which is below the temperature of the oil at the entrance to the production pipe. A crude oil is a mixture of oil and wax molecules. We introduce a small impurity (e.g. dust) of initial radius R_0 at the entrance of the pipe at a distance H from the wall. Initially there is a small particle such as piece of dust that forms the nucleus of the later growing wax particle. The spherical wax particle moves with the flowing oil. At the beginning the wax particle does not increase its radius because the temperature at the entrance of the pipe is too high for the wax to precipitate out of the oil. At a distance from the entrance, where the temperature is below the wax appearance temperature, the wax dissolved in the oil comes to the wax particle and makes it bigger. The wax particle has radius $R(t)$ at time $t \geq 0$. Initially $R(0) = R_0$. The radius of the wax particle is increasing with time, hence, $\frac{dR(t)}{dt}$ is positive. The mass flux of wax molecules in the oil away from the surface of the wax particle is given by Fick's first law which relates the diffusive mass flux $\vec{J}$ to the concentration gradient,

see [14, 21]

$$\vec{J} = -\rho_{wl} D \nabla C, \tag{3.1.1}$$

where ∇C is the gradient of the wax concentration $C(x, y, z, t)$, $D \geq 0$ is the diffusivity of wax, D is assumed constant, and ρ_{wl} is the density of solid wax. The definition of concentration C is $C = \frac{V_{wax}}{V_{wax}+V_{oil}}$ where V_{wax} is the volume of wax and $V_{wax} + V_{oil}$ is the total volume of an infinitesimal portion of the oil and wax mixture. So, the concentration is the volume concentration, which is non-dimensional and $0 \leq C \leq 1$. The mass concentration of the wax is $\frac{\rho_{ws} V_{wax}}{\rho_{ws} V_{wax}+\rho_{oil} V_{oil}}$. Equation (3.1.1) describes the fact that the diffusion of wax particles occurs from regions of higher concentration towards regions of lower concentration.

The conservation of wax mass in every region of the fluid domain, along with the divergence theorem for mass flux (3.1.1) imply that, see [57],

$$\rho_{wl} \frac{DC}{Dt} = -\nabla \cdot \vec{J}. \tag{3.1.2}$$

Here the operator $\frac{D()}{Dt}$ is called the material derivative,

$$\frac{D()}{Dt} = \frac{\partial()}{\partial t} + (\vec{u} \cdot \nabla)\,(), \tag{3.1.3}$$

where $\vec{u}$ is the fluid velocity relative to the wax particle.

Combining Fick's first law (3.1.1) with the mass conservation law (3.1.2) we arrive at the equation which describes how wax molecules diffuse in the fluid domain outside the wax particle surface,

$$\rho_{ws} \frac{DC}{Dt} = -\nabla(-\rho_{ws} D \nabla C).$$

For constant diffusivity D, the convective-diffusion equation reads,

$$\frac{DC}{Dt} = D \nabla^2 C. \tag{3.1.4}$$

If the wax particle is spherical or almost spherical, it is convenient to use the spherical coordinate system. The diffusion equation (3.1.4) in the spherical coordinate system (r, θ, ϕ) , see figure 3.1.1, with the origin at the centre of the spherical wax particle, has the form

$$\frac{DC}{Dt} = D\left[\frac{1}{r^2}\frac{\partial}{\partial r}\left(r^2\frac{\partial C}{\partial r}\right) + \frac{1}{r^2\sin\theta}\frac{\partial}{\partial\theta}\left(\sin\theta\frac{\partial C}{\partial\theta}\right) + \frac{1}{r^2\sin^2\theta}\frac{\partial^2 C}{\partial\phi^2}\right], \quad (3.1.5)$$

where $C = C(r, \theta, \phi, t)$ is the volume concentration of wax in the oil, t is time. If the wax particle is small, the relative velocity of the wax particle with respect to the flow is negligibly small. So, we can neglect the convective terms, $(\vec{u}\cdot\nabla)\,C$, with respect to the diffusion term in (3.1.3). Hence the material derivative (3.1.3) becomes $\frac{DC}{Dt} \approx \frac{\partial C}{\partial t}$, at the leading order for small wax particles.

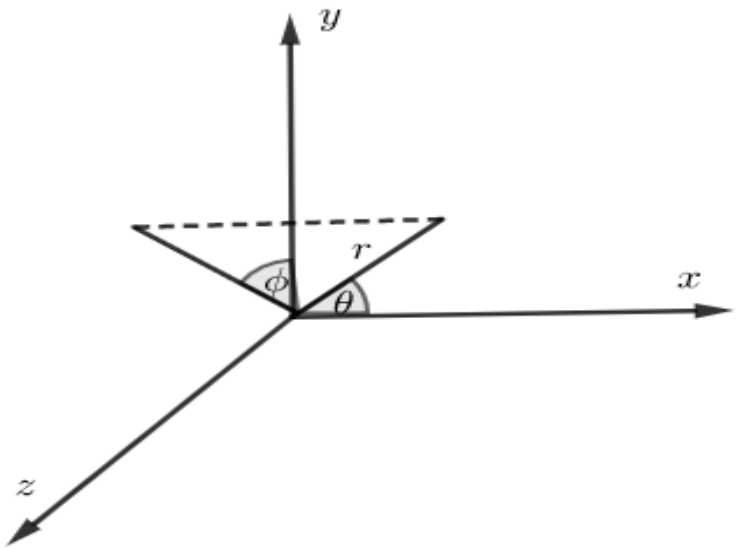

Figure 3.1.1: Spherical coordinate system.

3.2 Modelling of the growth of a spherical wax particle

Here, we model the growth of a single spherical wax particle. The radius of the wax particle is increasing due to a flux of wax molecules moving towards the wax particle, and sticking to its surface. Let a wax particle which is introduced at the entrance to the pipe, be placed at a certain distance from the wall. Its radius is small and there is negligible motion of fluid relative to it. The wax particle maintains its distance from the wall because of laminar flow. The wax particle follows a straight path along one of the straight streamlines of the oil flow. Dawson et al. [24] introduced the boundary condition at the surface of a salt crystal, which relates the mass flux towards the crystal surface to the value of the salt concentration on the surface,

$$-D\frac{\partial C}{\partial n} = k_r(C - C_*), \tag{3.2.1}$$

where $\vec{n}$ is the unit normal directed into the salt crystal from its surface, k_r is the mass transfer coefficient, which has dimension of velocity m/s, and C_* is the solubility of the salt in water. We use this boundary condition to describe the growth of the wax particle. In [24], the authors assumed the coefficient k_r to be constant, but in our case we generalize the boundary condition by assuming k_r to be a function of temperature. We also assume that the wax particle is spherical. Hence, on the surface of the growing wax particle, condition (3.2.1) gives

$$D\frac{\partial C}{\partial r} = k_r\{T_{WAT} - T\}(C - C_*), \tag{3.2.2}$$

where the local radial coordinate r increases out of the particle into the fluid, C

is the concentration at the particle surface boundary, $r = R(t)$, $k_r\{T_{WAT} - T\}$ is a function of temperature and $T = T(x(t), r_p)$ is the temperature distribution in the pipe, where $(x(t), r_p)$ is the location of the particle in the pipe, $x(t)$ is the distance the wax particle travelled from the entrance to the pipe and r_p is the distance of the particle trajectory for the pipe axis, as discussed in chapter 2. Here r_p= constant and $x(t) \approx u(r_p)t$, where $u(r_p)$ is the flow velocity and t is time. So overall, $T = T(t)$. The coefficient k_r is assumed to be a positive function of temperature, $k_r\{T_{WAT} - T\}$. We expect the temperature T to decrease in time, because the particle travels from a hot part towards a cold part of the pipe. Hence, following the wax particle along the pipe, we may assume the temperature to be a given function of time. So, $k_r\{T_{WAT} - T\} = k_r(t)$ and $k_r \geq 0$. Note that $k_r = 0$ where $T > T_{WAT}$, and $k_r > 0$ where $T < T_{WAT}$.

For a spherical particle the concentration gradient on its surface is,

$$\left(\frac{\partial C}{\partial r}\right)_{r=R(t)} = \begin{cases} \frac{k_r(t)}{D}(C - C_*) & \text{if } C(R,t) > C_*, \\ \\ 0 & \text{if } C(R,t) < C_*, \end{cases} \tag{3.2.3}$$

as it follows from (3.2.2).

Summarizing the condition above, we conclude that a wax particle begins to grow if the temperature around the wax particle is below the wax appearance temperature, and also if the concentration on the surface exceeds the solubility concentration C_*. We assume in the following that $C_0 > C_*$, where C_0 is the wax concentration far from the wax particle, $r \longrightarrow \infty$. The rate of increase of the particle mass, $m = m(t)$, is equal to the inward-direction radial mass flux at the surface of the wax particle multiplied by the surface area of the particle and the wax density. All together this gives

$$\frac{dm}{dt} = 4\pi R^2 \rho_{ws} D \left(\frac{\partial C}{\partial r} \right)_{r=R(t)}, \tag{3.2.4}$$

where $\frac{dm}{dt}$ $(\frac{\text{kg}}{\text{s}})$ is the mass rate of wax transfer from the oil, ρ_{ws} $(\frac{\text{kg}}{\text{m}^3})$ is the constant density of solid wax, and the diffusivity D has dimension $(\frac{\text{m}^2}{\text{s}})$.

The mass of a spherical wax particle of radius R and constant density ρ_{ws} is

$$m = \frac{4}{3}\pi R^3 \rho_{ws}. \tag{3.2.5}$$

Differentiating (3.2.5) with respect to time,

$$\frac{dm}{dt} = 4\pi R^2 \rho_{ws} \frac{dR}{dt}, \tag{3.2.6}$$

and combining (3.2.4) and (3.2.6), we obtain the final form of the boundary condition on the surface of the wax particle:

$$\frac{dR}{dt} = D \left(\frac{\partial C}{\partial r} \right)_{r=R(t)}. \tag{3.2.7}$$

The time-dependent, spherically symmetric problem can be summarize as follows:

Field equation for the wax concentration in the oil, $C = C(r,t)$,

$$\frac{\partial C}{\partial t} = \frac{D}{r^2} \frac{\partial}{\partial r} \left(r^2 \frac{\partial C}{\partial r} \right), \qquad r > R(t), \qquad t > 0. \tag{3.2.8}$$

Initial conditions in the oil

$$C(r,0) = C_0, \qquad r > R(0). \tag{3.2.9}$$

and for the wax particle

$$R(0) = R_0.$$

The concentration at infinity is C_0 and the concentration around the particle is different from C_0 because the particle accumulates wax molecules from the

solution. If we integrate the $-(C - C_0)$ outside the particle, it should be directly proportional to the finite mass of the wax which joins the particle,

$$I = \int_0^{2\pi} \int_0^{\pi} \int_{R_0}^{\infty} (C_0 - C) r^2 \sin\theta dr d\theta d\phi. \tag{3.2.10}$$

The integral is finite if $(C - C_0)r^2$ decays quicker than $\frac{1}{r}$ as $r \longrightarrow \infty$. This gives that

$$(C(r,t) - C_0)\, r^3 \longrightarrow 0 \qquad \text{as} \qquad r \longrightarrow \infty$$

Boundary and far-field conditions:

$$\begin{cases} D\frac{\partial C}{\partial r} = k_r(t)(C - C_*), & r = R(t), \qquad t > 0 \\ \\ (C(r,t) - C_0)\, r^3 \longrightarrow \quad 0 \quad & \text{as } r \longrightarrow \infty, \qquad t > 0 \end{cases} \tag{3.2.11}$$

The mass balance:

$$\frac{dR}{dt} = D\frac{\partial C}{\partial r}, \qquad r = R(t), \qquad t > 0. \tag{3.2.12}$$

We assume in the following that $k_r(t) = Dk_1\zeta(t)$, where k_1 is a given coefficient and $\zeta(t)$ is a known function of time.

3.3 Self-similar solution of the problem

We look for a self-similar solution of the coupled problem (3.2.8)-(3.2.12) with respect to $C = C(r,t)$ and $R = R(t)$. The spherically symmetric diffusion equation (3.2.8) admits a self-similar solution in the form $C = f(\xi)$, where $\xi = \frac{r}{\sqrt{Dt}}$ is a dimensionless similarity variable. We assume the radius of the wax particle growing as $R(t) = \lambda\sqrt{Dt}$, where λ is a positive constant coefficient to be determined. On the wax particle surface, $r = R(t)$, we have

$$\xi = \frac{R(t)}{\sqrt{Dt}} = \frac{\lambda\sqrt{Dt}}{\sqrt{Dt}} = \lambda.$$

So the moving boundary of the growing wax particle in (r,t) space is now a fixed boundary in ξ space. The dimensions in this problem are:
The concentration $[C]=1$, the radial coordinate $[r]=\mathrm{m}$, the time $[t]=\mathrm{s}$ and the diffusion coefficient $[D]=\mathrm{m}^2/\mathrm{s}$. Therefore, ξ is non-dimensional and the function $f(\xi)$ satisfies the following equation obtained from (3.2.8)

$$f''(\xi)+\left(\frac{2}{\xi}+\frac{\xi}{2}\right)f'(\xi)=0, \qquad \xi>\lambda. \tag{3.3.1}$$

By substituting $C=f(\frac{r}{\sqrt{Dt}})$ into (3.2.11) we obtain

$$\frac{f'(\lambda)}{\sqrt{Dt}}=k_1\zeta(t)(f(\lambda)-C_*) \tag{3.3.2}$$

Equation (3.3.2) gives that a self-similar solution exists only if $\zeta(t)=\frac{1}{\sqrt{t}}$ for $t>0$. With such a function $\zeta(t)$, equation (3.3.2) becomes

$$f'(\lambda)=k_1\sqrt{D}\,(f(\lambda)-C_*)\,. \tag{3.3.3}$$

Then the condition (3.2.12) gives

$$f'(\lambda)=\frac{1}{2}\lambda. \tag{3.3.4}$$

The problem with respect to $f(\xi)$ and λ is formulated as:

$$\begin{cases} f''(\xi)+\left(\frac{2}{\xi}+\frac{\xi}{2}\right)f'(\xi)=0, \qquad \xi>\lambda, \\ \\ f'(\lambda)=k_1\sqrt{D}\,(f(\lambda)-C_*)\,, \\ \\ f'(\lambda)=\frac{1}{2}\lambda, \\ \\ f(\xi)\longrightarrow C_0 \qquad \text{as} \qquad \xi\longrightarrow\infty. \end{cases} \tag{3.3.5}$$

Now we want to figure out what is the dimension of the coefficient k_1. We have that $k_r(t) = Dk_1\zeta(t)$ and $\zeta(t) = \frac{1}{\sqrt{t}}$, where the mass transfer coefficient k_r has the unit $[\frac{\mathrm{m}}{\mathrm{s}}]$ see (3.2.1), the diffusion coefficient has a unit $[\frac{\mathrm{m}^2}{\mathrm{s}}]$, and the function $\zeta(t)$ has the unit $[\frac{1}{\sqrt{\mathrm{s}}}]$. So, k_1 is a coefficient has a unit $[\frac{\sqrt{\mathrm{s}}}{\mathrm{m}}]$. Therefore, in equation $(3.3.5)_2$, $k_1\sqrt{D}$ is nondimensional. We denote $k_1\sqrt{D} = \epsilon$, where ϵ is a non-dimensional parameter.

A general solution of the second order ordinary differential equation $(3.3.5)_1$ is

$$f(\xi) = A + Bf_2(\xi), \tag{3.3.6}$$

where A and B are arbitrary constants. Putting $f_2'(\xi) = u(\xi)$, we find that $u(\xi)$ must satisfy the first-order ordinary differential equation

$$u'(\xi) + \left(\frac{2}{\xi} + \frac{\xi}{2}\right) u(\xi) = 0. \tag{3.3.7}$$

This equation is solved by separating the variables ξ and u:

$$\frac{du}{u} + \left(\frac{2}{\xi} + \frac{\xi}{2}\right) d\xi = 0. \tag{3.3.8}$$

Integrating both sides of (3.3.8) yields

$$\ln u + 2\ln\xi + \frac{\xi^2}{4} = c, \tag{3.3.9}$$

where c is a constant of integration. We obtain

$$\ln u\xi^2 + \frac{\xi^2}{4} = c,$$

and

$$u\xi^2 = e^{c-\frac{\xi^2}{4}}. \tag{3.3.10}$$

Dividing both sides of equation (3.3.10) by ξ^2, we have

$$u(\xi) = \frac{c_2}{\xi^2} e^{-\frac{\xi^2}{4}}. \tag{3.3.11}$$

We see that $u(\xi) \longrightarrow 0$ as $\xi \longrightarrow \infty$. The constant c_2 is set to 1 because $f_2(\xi)$ is a particular solution of the ODE $(3.3.5)_1$. Then we integrate both sides of $f_2'(\xi) = u(\xi)$ to find $f_2(\xi)$, where we require that $f_2(\xi) \to 0$ as $\xi \to \infty$,

$$f_2(\xi) = -\int_{\xi}^{\infty} u(\xi_0) d\xi_0. \tag{3.3.12}$$

Equations (3.3.11) and (3.3.12), give

$$f_2(\xi) = -\int_{\xi}^{\infty} \xi_0^{-2} e^{-\frac{\xi_0^2}{4}} d\xi_0. \tag{3.3.13}$$

Substituting (3.3.13) into equation (3.3.6), we find a general solution of the second order ODE $(3.3.5)_1$:

$$f(\xi) = A - B \int_{\xi}^{\infty} \xi_0^{-2} e^{-\frac{\xi_0^2}{4}} d\xi_0. \tag{3.3.14}$$

The far-field condition $(3.3.5)_4$, $f(\xi) \longrightarrow C_0$, as $\xi \longrightarrow \infty$, gives $A = C_0$.
Then equation (3.3.14) becomes

$$f(\xi) = C_0 - B \int_{\xi}^{\infty} \xi_0^{-2} e^{-\frac{\xi_0^2}{4}} d\xi_0. \tag{3.3.15}$$

The constant B is determined by the boundary condition $(3.3.5)_2$. Differentiating (3.3.6) with respect ξ, and setting $\xi = \lambda$, we find

$$f'(\lambda) = Bu(\lambda). \tag{3.3.16}$$

Substituting (3.3.16) into equation $(3.3.5)_2$, we have

$$Bu(\lambda) = \epsilon(f(\lambda) - C_*). \tag{3.3.17}$$

Substituting $f(\lambda)$ from equation (3.3.15) and $u(\lambda)$ from equation (3.3.11) into equation (3.3.17), we have

$$B\frac{1}{\lambda^2}e^{-\frac{\lambda^2}{4}} = \epsilon\left(C_0 - B\int_\lambda^\infty \xi_0^{-2}e^{-\frac{\xi_0^2}{4}}d\xi_0 - C_*\right). \tag{3.3.18}$$

Simplifying (3.3.18) we obtain

$$B\left(\frac{1}{\lambda^2}e^{-\frac{\lambda^2}{4}} + \epsilon\int_\lambda^\infty \xi_0^{-2}e^{-\frac{\xi_0^2}{4}}d\xi_0\right) = \epsilon(C_0 - C_*). \tag{3.3.19}$$

We substitute $f'(\lambda)$ from equation (3.3.16) into the boundary condition $(3.3.5)_3$,

$$\lambda = 2B\frac{1}{\lambda^2}e^{-\frac{\lambda^2}{4}}, \tag{3.3.20}$$

where B is defined by equation (3.3.19),

$$B = \frac{\epsilon(C_0 - C_*)}{\frac{1}{\lambda^2}e^{-\frac{\lambda^2}{4}} + \epsilon\int_\lambda^\infty \xi_0^{-2}e^{-\frac{\xi_0^2}{4}}d\xi_0}. \tag{3.3.21}$$

Then (3.3.20) provides the equation with respect to the coefficient λ,

$$\lambda = \frac{2\epsilon(C_0 - C_*)}{1 + \epsilon\lambda^2 e^{\frac{\lambda^2}{4}}\int_\lambda^\infty \xi_0^{-2}e^{-\frac{\xi_0^2}{4}}d\xi_0}. \tag{3.3.22}$$

Equation (3.3.22) can be written in term of $\epsilon(\lambda)$:

$$\epsilon\left(\lambda^3 e^{\frac{\lambda^2}{4}}\int_\lambda^\infty \xi_0^{-2}e^{-\frac{\xi_0^2}{4}}d\xi_0 - 2(C_0 - C_*)\right) = -\lambda, \tag{3.3.23}$$

where $\lambda > 0$, $\epsilon > 0$, and $C_0 > C_*$. Then

$$\epsilon = \frac{\lambda}{2(C_0 - C_*) - \lambda^3 e^{\frac{\lambda^2}{4}}\int_\lambda^\infty \xi_0^{-2}e^{-\frac{\xi_0^2}{4}}d\xi_0} \tag{3.3.24}$$

and

$$\lambda = 2\epsilon(C_0 - C_*) - \lambda^3\epsilon e^{\frac{\lambda^2}{4}}\int_\lambda^\infty \xi_0^{-2}e^{-\frac{\xi_0^2}{4}}d\xi_0. \tag{3.3.25}$$

Integrating by parts the integral in the right-hand side of (3.3.25), we find

$$\lambda = 2\epsilon(C_0 - C_*) - \lambda^3\epsilon e^{\frac{\lambda^2}{4}}\left[\frac{e^{\frac{-\lambda^2}{4}}}{\lambda} - \frac{1}{2}\int_\lambda^\infty e^{\frac{-\xi_0^2}{4}}d\xi_0\right]. \tag{3.3.26}$$

Using the substitution $u = \frac{\xi_0}{2} \Rightarrow d\xi_0 = 2du$ into (3.3.26), we obtain

$$\lambda = 2\epsilon(C_0 - C_*) - \lambda^3 \epsilon e^{\frac{\lambda^2}{4}} \left[\frac{e^{\frac{-\lambda^2}{4}}}{\lambda} - \frac{\sqrt{\pi}}{2} \left(1 - \text{erf}\left(\frac{\lambda}{2}\right)\right)\right], \tag{3.3.27}$$

where $\text{erfc}(\frac{\lambda}{2}) = 1 - \text{erf}(\frac{\lambda}{2})$.

Rearranging this equation, we finally obtain the following equation for λ

$$\lambda = 2\epsilon(C_0 - C_*) - \lambda^2\epsilon + \frac{\sqrt{\pi}}{2}\epsilon\lambda^3 e^{\frac{\lambda^2}{4}} \text{erfc}\left(\frac{\lambda}{2}\right), \tag{3.3.28}$$

where $\text{erfc}(\frac{\lambda}{2})$ is the complementary error function defined by $\text{erfc}(\frac{\lambda}{2}) = \frac{2}{\sqrt{\pi}} \int_{\frac{\lambda}{2}}^{\infty} e^{-\xi^2} d\xi$ and $\text{erf}(\frac{\lambda}{2}) = \frac{2}{\sqrt{\pi}} \int_0^{\frac{\lambda}{2}} e^{-\xi^2} d\xi$, see [83].

Equation (3.3.20), provides the coefficient B as a function of λ,

$$B = \frac{1}{2}\lambda^3 e^{\frac{\lambda^2}{4}}. \tag{3.3.29}$$

Substituting equation (3.3.29) into (3.3.15), we obtain the solution $f(\xi)$

$$f(\xi) = C_0 - \frac{\lambda^3 e^{\frac{\lambda^2}{4}}}{2} \int_{\xi}^{\infty} \xi_0^{-2} e^{-\frac{\xi_0^2}{4}} d\xi_0 \qquad \xi > \lambda. \tag{3.3.30}$$

Then, we find the concentration distribution for self-similar solution, where $C = f(\xi)$,

$$C = C_0 - \frac{\lambda^3 e^{\frac{\lambda^2}{4}}}{2} \int_{\xi}^{\infty} \xi_0^{-2} e^{-\frac{\xi_0^2}{4}} d\xi_0 \qquad \xi > \lambda. \tag{3.3.31}$$

Integrating by parts, we obtain

$$C(\xi) = C_0 - \frac{\lambda^3 e^{-\frac{\xi^2}{4}} e^{\frac{\lambda^2}{4}}}{2\xi} + \frac{\lambda^3\sqrt{\pi} e^{\frac{\lambda^2}{4}}}{4} \text{erfc}\left(\frac{\xi}{2}\right), \tag{3.3.32}$$

where $\xi = \frac{r}{\sqrt{Dt}}$ and $R(t) = \lambda\sqrt{Dt}$. Substituting ξ into (3.3.32), we find the concentration as a function of r and t,

$$C(r,t) = C_0 - \frac{\lambda^3 e^{-\frac{r^2}{4Dt}} e^{\frac{\lambda^2}{4}} \sqrt{Dt}}{2r} + \frac{\lambda^3\sqrt{\pi} e^{\frac{\lambda^2}{4}}}{4} \text{erfc}\left(\frac{r}{2\sqrt{Dt}}\right). \tag{3.3.33}$$

Equation (3.3.33) describes the concentration distribution in the fluid outside the surface of the wax particle.

The concentration on the surface of the wax particle, $r = R(t) = \lambda\sqrt{Dt}$, is

$$C(\lambda) = C_0 - \frac{\lambda^2}{2} + \frac{\lambda^3\sqrt{\pi}e^{\frac{\lambda^2}{4}}}{4}\text{erfc}\left(\frac{\lambda}{2}\right). \tag{3.3.34}$$

3.4 Computing the root λ of equation (3.3.28)

Equation (3.3.28) can be written as

$$-\epsilon\frac{\sqrt{\pi}}{2}\lambda^3 e^{\frac{\lambda^2}{4}}\text{erfc}\left(\frac{\lambda}{2}\right) + \lambda + \epsilon\lambda^2 = 2\epsilon(C_0 - C_*). \tag{3.4.1}$$

Equation (3.4.1) cannot be solved analytically, so we approach the problem by using a graphical method. We seek a solution $\lambda > 0$. The first term in the left-hand side of this equation is negative, the second and third terms are positive, and the right-hand side is positive. We investigate two possibilities asymptotically, assuming only that $2\epsilon(C_0 - C_*) > 0$.

(i) If λ is large then we can approximate the left-hand side in (3.4.1) by using the asymptotic expansion of the complementary error function $\text{erfc}(x) = 1 - \text{erf}(x)$, as $x \longrightarrow \infty$, see [1]. The complementary error function is defined by

$$\text{erfc}(x) = \frac{2}{\sqrt{\pi}}\int_x^\infty e^{-\xi^2}d\xi.$$

The asymptotic expansion of the complementary error function as $x \longrightarrow \infty$ can be written as

$$\begin{aligned}\text{erfc}(x) \approx \frac{e^{-x^2}}{\sqrt{\pi}x}\Bigg(1 - \frac{1}{2x^2} + \frac{1\cdot 3}{(2x^2)^2} - \frac{1\cdot 3\cdot 5}{(2x^2)^3} - \frac{1\cdot 3\cdot 5\cdot 7}{(2x^2)^6} - \frac{1\cdot 3\cdot 5\cdot 7\cdot 9}{(2x^2)^5} \\ + \frac{1\cdot 3\cdot 5\cdot 7\cdot 9\cdot 11}{(2x^2)^6} + \cdots + \frac{(-1)^n(2n-1)!!}{(2x^2)^n} + \cdots\Bigg),\end{aligned} \tag{3.4.2}$$

where $(2n-1)!!$ is a double factorial: the product of all odd numbers up to $2n-1$.

For large λ, we have

$$\operatorname{erfc}\left(\frac{\lambda}{2}\right) \approx \frac{e^{\frac{-\lambda^2}{4}}}{\sqrt{\pi}\frac{\lambda}{2}}\left(1-\frac{2}{\lambda^2}+\frac{12}{\lambda^4}-\frac{120}{\lambda^6}+\frac{1680}{\lambda^8}-\frac{30240}{\lambda^{10}}+O\left(\frac{1}{\lambda^{12}}\right)\right). \tag{3.4.3}$$

Inserting (3.4.3) into (3.4.1), we obtain

$$2\epsilon-\frac{12\epsilon}{\lambda^2}+\frac{120\epsilon}{\lambda^4}-\frac{1680\epsilon}{\lambda^6}+\frac{30240\epsilon}{\lambda^8}+\lambda+O\left(\frac{1}{\lambda^{10}}\right)=2\epsilon(C_0-C_*). \tag{3.4.4}$$

Divided both sides of (3.4.4) by ϵ, then we have

$$2-\frac{12}{\lambda^2}+O\left(\frac{1}{\lambda^4}\right)+\frac{\lambda}{\epsilon}=2(C_0-C_*), \tag{3.4.5}$$

For $\lambda >> 1$, both the second and third terms in the left-hand side of (3.4.5) are very small and can be neglected,

$$\lambda \approx \epsilon\left(-2+2(C_0-C_*)\right). \tag{3.4.6}$$

Here C_0 is the wax concentration far from the wax particle, C_* is the solubility of the wax, $0 < C_* < C_0 < 1$. In (3.4.6), $C_0 - C_* - 1 < 0$ because $C_0 < 1 < 1 + C_*$. Therefore the right-hand side in (3.4.6) is negative for any positive ϵ. But we assumed that λ is positive and large and we arrived at a contradiction because the left-hand side and the right-hand side have opposite sign. This means that there is no solution of (3.4.1), which is large and tends to infinity as $\epsilon \longrightarrow \infty$. However we can conclude that the left-hand side of (3.4.1) behaves as $\lambda + 2\epsilon + O(\frac{1}{\lambda^2})$, see (3.4.4) as $\lambda \longrightarrow \infty$. So, we consider another possibility with λ being small.

(ii) If λ is small, $\lambda << 1$, then we can approximate the left-hand side in (3.4.1) by using the following inequalities from Abramowitz and Stegun, see [1] for $x \geq 0$:

$$\frac{1}{x+\sqrt{x^2+2}} < e^{x^2}\int_x^\infty e^{-t^2}dt \le \frac{1}{x+\sqrt{x^2+\frac{4}{\pi}}}, x \ge 0. \tag{3.4.7}$$

Multipling (3.4.7) by $\frac{2}{\sqrt{\pi}}$ and dividing by e^{x^2}, we find

$$\frac{2}{\sqrt{\pi}}\frac{e^{-x^2}}{x+\sqrt{x^2+2}} < \operatorname{erfc}(x) \le \frac{2}{\sqrt{\pi}}\frac{e^{-x^2}}{x+\sqrt{x^2+\frac{4}{\pi}}}. \tag{3.4.8}$$

For $x = \frac{\lambda}{2}$, the inequalities above give tight bounds,

$$\frac{2}{\sqrt{\pi}}\frac{e^{-\frac{\lambda^2}{4}}}{\frac{\lambda}{2}+\sqrt{\frac{\lambda^2}{4}+2}} < \operatorname{erfc}\left(\frac{\lambda}{2}\right) \le \frac{2}{\sqrt{\pi}}\frac{e^{-\frac{\lambda^2}{4}}}{\frac{\lambda}{2}+\sqrt{\frac{\lambda^2}{4}+\frac{4}{\pi}}}, \tag{3.4.9}$$

To obtain the same expression as in the left-hand side of (3.4.1), we multiply the inequality (3.4.9) by $-\epsilon\frac{\sqrt{\pi}}{2}\lambda^3 e^{\frac{\lambda^2}{4}}$ and add $\lambda+\epsilon\lambda^2$. We obtain bounds on the left-hand side of (3.4.1)

$$\begin{aligned} -\frac{\lambda^3\epsilon}{\frac{\lambda}{2}+\sqrt{\frac{\lambda^2}{4}+2}} + \lambda + \lambda^2\epsilon &> -\frac{\sqrt{\pi}\epsilon}{2}\lambda^3 e^{\frac{\lambda^2}{4}}\operatorname{erfc}\left(\frac{\lambda}{2}\right) + \lambda + \lambda^2\epsilon \\ &\ge -\frac{\lambda^3\epsilon}{\frac{\lambda}{2}+\sqrt{\frac{\lambda^2}{4}+\frac{4}{\pi}}} + \lambda + \lambda^2\epsilon, \frac{\lambda}{2} \ge 0. \end{aligned} \tag{3.4.10}$$

Inequality (3.4.10) shows the left-hand side of (3.4.1) is bounded and these bounds are very tight for small λ, later we will show it in Figure 3.4.2. Also (3.4.10) is valid for positive ϵ. Using these inequalities we estimate the value of λ.

The asymptotic behaviour of λ defined by equation (3.3.28) for small $C_0 - C_*$ has the form

$$\lambda = (C_0 - C_*)\lambda_0 + (C_0 - C_*)^2\lambda_1 + O\left((C_0 - C_*)^3\right), \tag{3.4.11}$$

where λ_0 and λ_1 are to be determined. Substituting (3.4.11) into (3.3.28) and equating the terms of the same order in $(C_0 - C_*)$, we find

$$\lambda_0 = 2\epsilon, \qquad \lambda_1 = -\epsilon\lambda_0^2 \Rightarrow \lambda_1 = -4\epsilon^3. \tag{3.4.12}$$

Then the asymptotic behaviour of λ for fixed ϵ and small $C_0 - C_*$ becomes

$$\lambda = 2\epsilon(C_0 - C_*) - 4\epsilon^3(C_0 - C_*)^2 + O\left((C_0 - C_*)^3\right). \tag{3.4.13}$$

Figure 3.4.1 illustrates the left-hand side of equation (3.4.1) which was computed by MATLAB for different values for ϵ. We can see the left-hand side of equation (3.4.1) is positive for $\lambda > 0$ and any value of positive ϵ. The function on the left-hand side of (3.4.1) is a monotonically increasing function of λ for the conditions of the figure. This means that the coefficient λ, as a solution of (3.4.1), is positive and, therefore, the radius of the wax particle is always increasing with time. In the following calculations, the value of C_0 is taken from [66] and C_* is chosen such that $0 < C_* < C_0 < 1$ so we choose $C_* = 0.01$, see Table 3.1. Also we estimated the value of dimensionless parameter $\epsilon = k_1\sqrt{D}$, we know the value of the diffusion coefficient D but we choose the value of k_1. Figure 3.4.2 illustrates the inequalities (3.4.10) and shows both left-hand side and right-hand side of (3.4.1). We can see that the bounds in (3.4.10) are tight for small λ, and that the left-hand side in (3.4.1) increasing monotonically. We see in figure 3.4.3 that the root λ is very small, $\lambda = 0.01438$, for $\epsilon = 0.08$ and $C_0 - C_* = 0.09$. Figure 3.4.4 illustrates the asymptotic behaviour of λ given by equation (3.4.13) as a function of $C_0 - C_*$ for fixed values of $\epsilon = 0.08$. We can see that the two-term asymptotic formula (3.4.13) gives $\lambda = 0.014$ for $(C_0 - C_*) = 0.09$ and $\epsilon = 0.08$. In figure 3.4.5 we find $\lambda = 0.15996$ for $\epsilon = 0.8$ and $(C_0 - C_*) = 0.09$. In figure 3.4.6 we plot the concentration as a function of the distance from the surface of the wax particle, see equation (3.3.33). We see that the concentration outside the wax particle is lower than $C = 0.1$ where $r \geq R(t)$ and the concentration at the surface of

the wax particle is lower than the concentration at infinity. We see in figure 3.4.6 a positive gradient $\frac{\partial C}{\partial r} > 0$, this means that diffusion transports wax from the surroundings toward the wax particle. The wax molecules are transported from a higher concentration to lower concentration. We see that in 3.4.6 the concentration increases in the far field. Also, we can see the radius of the wax particle is growing with time, as time increases the radius increases. Figure 3.4.7 shows that the concentration on the surface of the wax particle decreases with the increase of the growth speed λ. If the wax particle is growing faster, then it is accumulated more wax molecules from the solution reducing $C(\lambda)$. The values of the parameters used in the calculations are given in Table 3.1.

Param.	Description	Value	Reference
C_0	initial concentration	0.1	[66]
C_*	solubility concentration	0.01	chosen
k_r	the mass transfer coefficient	$4.5{\cdot}10^{-6}(\frac{m}{s})$	[24]
ϵ	$k_1\sqrt{D}$	0.08	chosen
D	diffusion coefficient	10^{-6}	[20]

Table 3.1: Estimates of values of the model's parameters

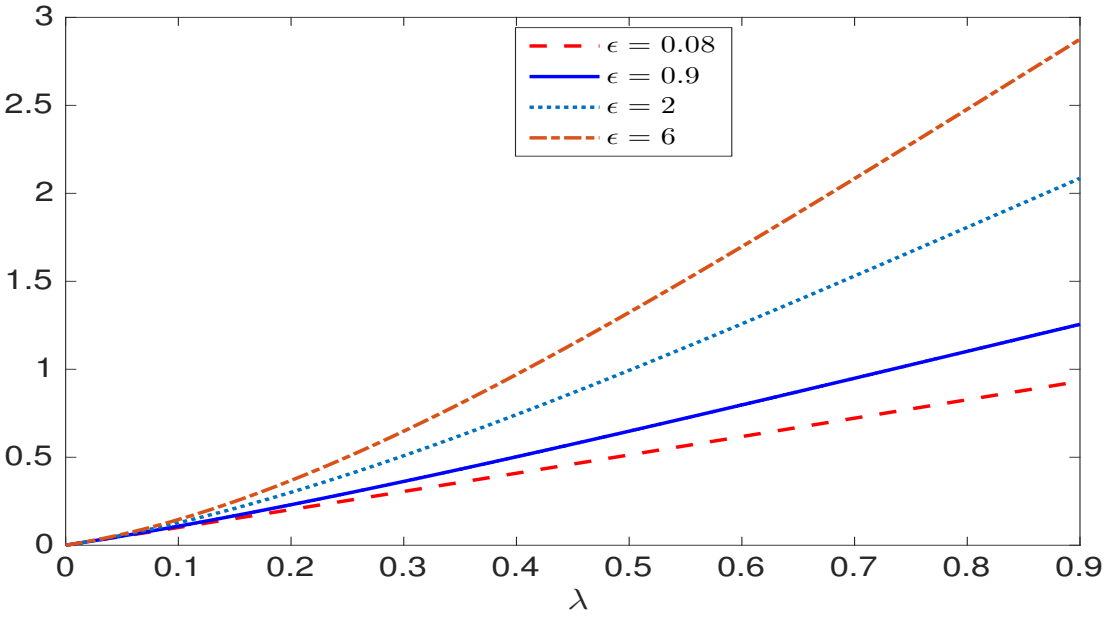

Figure 3.4.1: The left hand side of equation (3.4.1) for different values of ϵ.

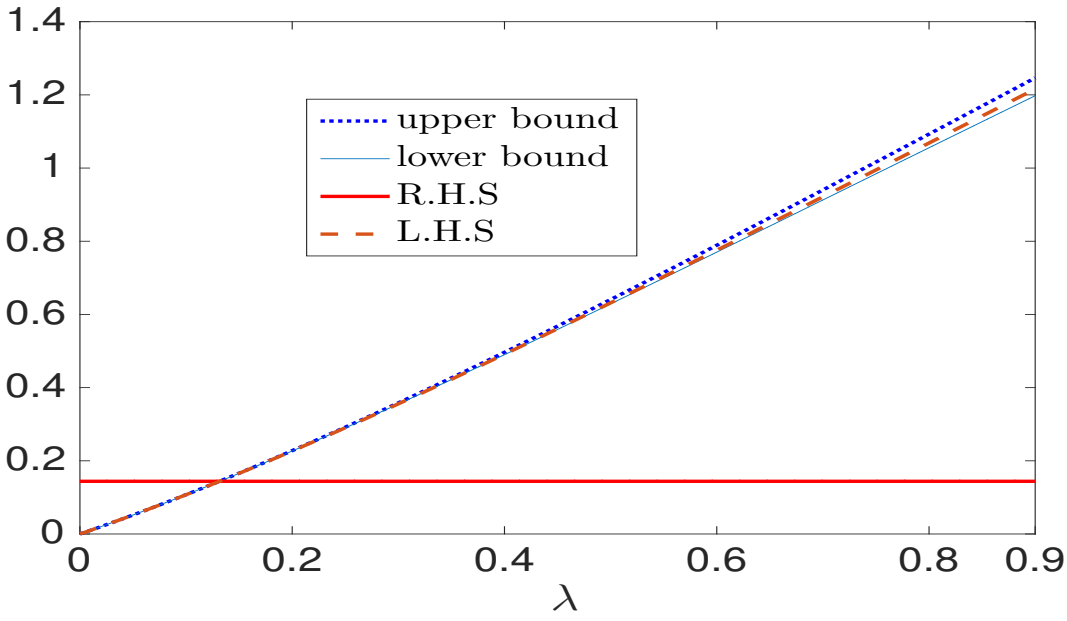

Figure 3.4.2: Plot of the left-hand side (3.4.1), right-hand side (3.4.1), and the two bounds described in the inequalities (3.4.10), where $\epsilon = 0.9$ and $C_0 - C_* = 0.09$.

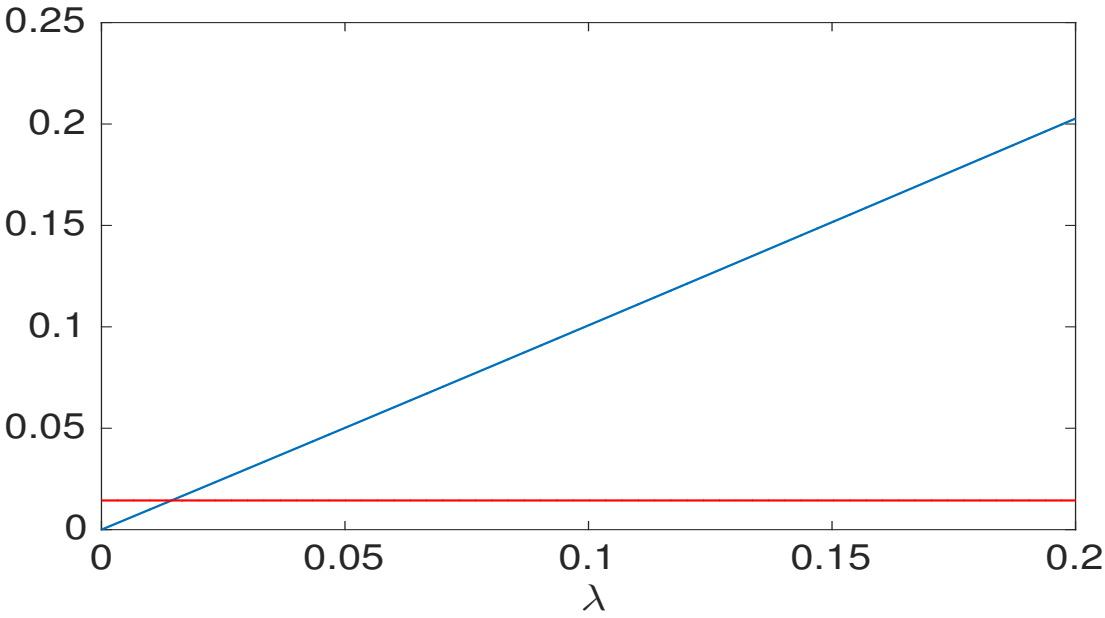

Figure 3.4.3: Plot of the two sides of equation (3.4.1) to determine graphically the root λ, ($\epsilon = 0.08$ and $C_0 - C_* = 0.09$). The left-hand side is shown by blue and the right-hand side by red lines.

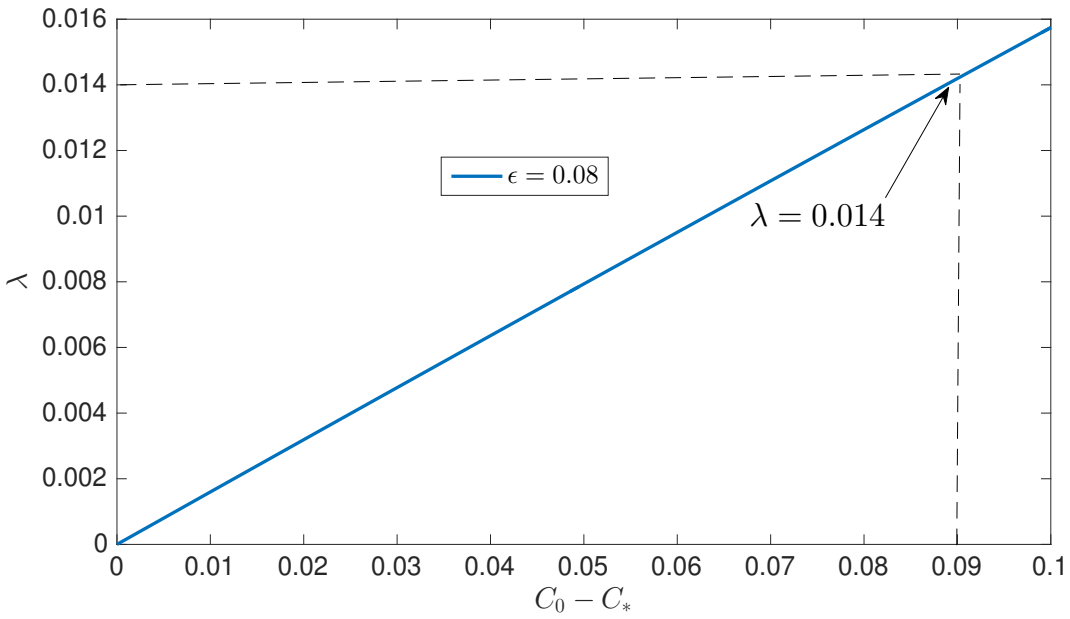

Figure 3.4.4: The asymptotic behaviour of λ as a function of $C_0 - C_*$.

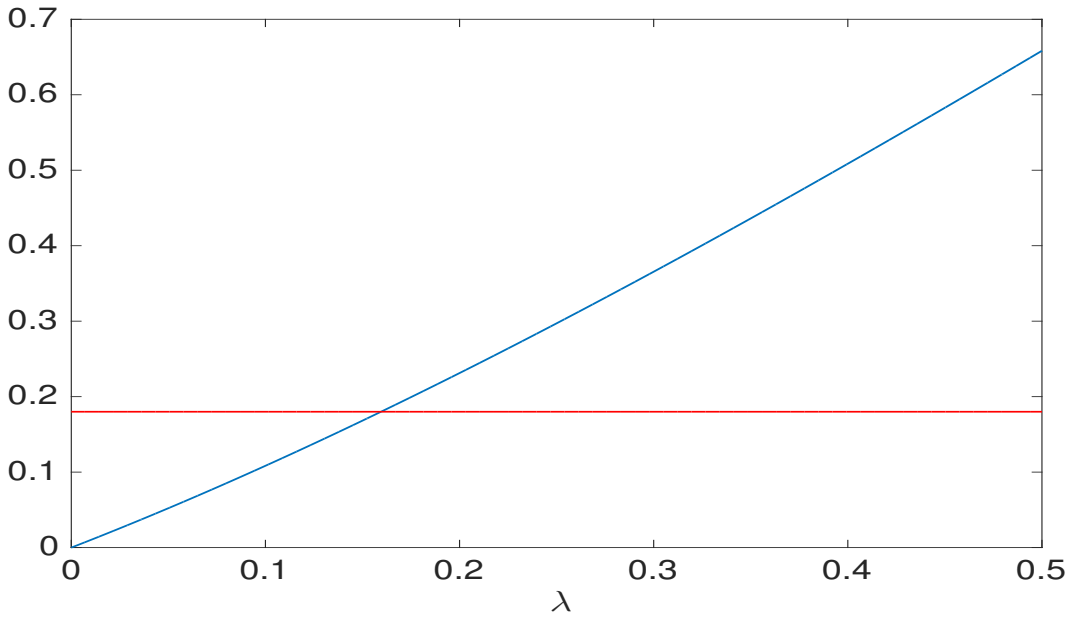

Figure 3.4.5: Plot of the two sides of equation (3.4.1) to determine graphically the root λ, ($\epsilon = 0.8$ and $C_0 - C_* = 0.09$). The left-hand side is shown by blue and the right-hand side by red lines.

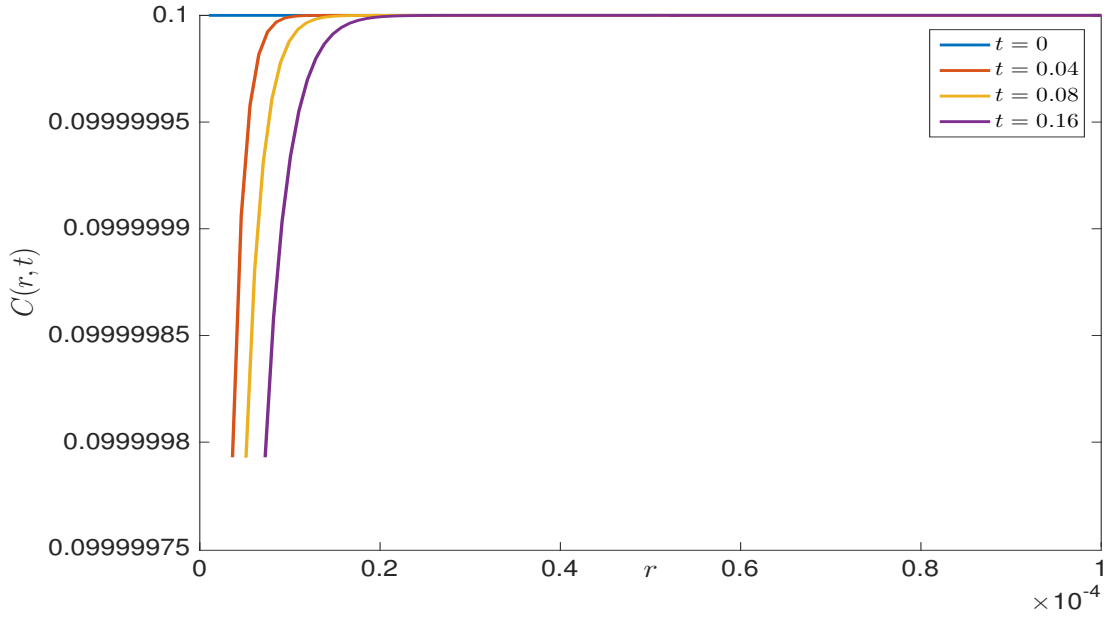

Figure 3.4.6: The concentration $C(r,t)$ as a function of distance from the surface of the wax particle, where $r > R(t)$ and $\lambda = 0.01$. Each curve is plotted for a given value of t.

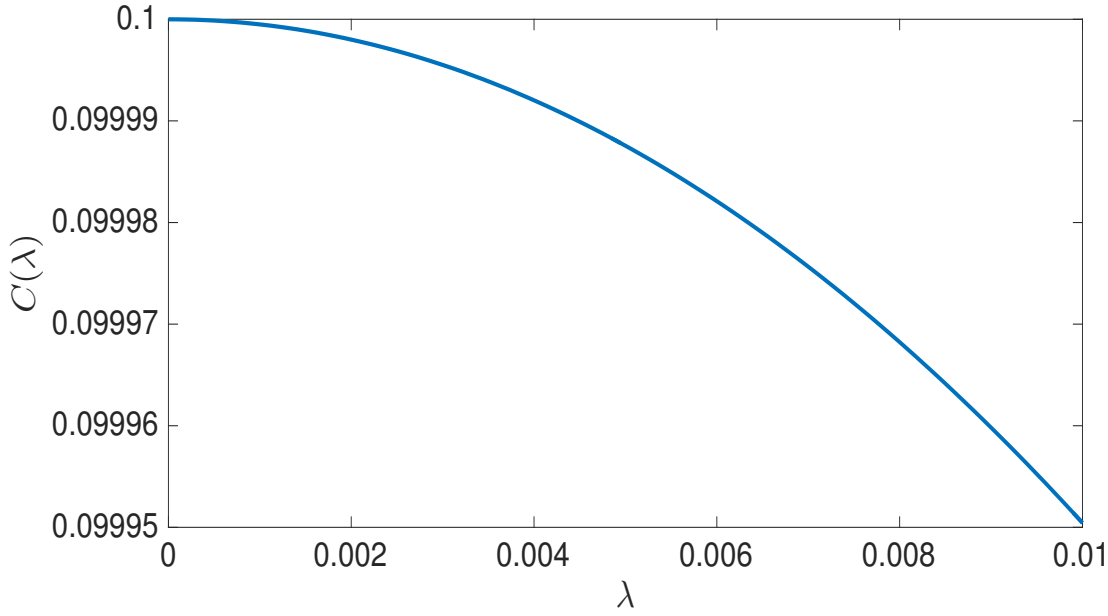

Figure 3.4.7: The concentration on the surface of the wax particle given by (3.3.34).

Chapter 4

Numerical investigation of spherical wax particle

In this chapter, we study numerically the initial boundary value problem (3.2.8)-(3.2.12) formulated in chapter 3 for spherical growth of a wax particle. The problem is summarized in section 4.1. In section 4.2, we introduce the non-dimensional variables and simplify the problem by introducing a new unknown function. In section 4.3, we find an integral representation of the solution of this problem through the initial and boundary values of the unknown concentration by using a Green's function. The boundary condition on the surface of the growing spherical wax particle provides an integral equation for the wax concentration on the particle surface. This integral equation should be solved together with the differential equation for the radius of the growing wax particle. In section 4.4, we discretise the integral boundary equation by developing a time stepping numerical algorithm. Piecewise linear functions are used to approximate the nonlinear solution [39]. In section 4.5, we explain how

the ordinary differential equation for the radius of the wax particle is solved by using a Modified Euler Method. In section 4.6, we compare the self-similar solution from chapter 3, with the numerical results of this chapter in order to validate the numerical algorithm. In section 4.7, we study the boundary value problem of one wax particle with constant mass transfer coefficient. The results of this chapter are obtained using analytical and numerical methods. These results help us to gain a better understanding of the growth of one spherical wax particle.

4.1 Problem description

In this section, we summarize the initial boundary value problem (3.2.8)-(3.2.12) derived in chapter 3, where it was solved analytically for particular mass transfer coefficient as a function of time. In the present chapter, we develop a numerical method for any mass transfer coefficient that change with temperature and validate it by comparing the numerical results with our self-similar solution from chapter 3. Also we develop a numerical method for constant mass transfer coefficient k_r as shown in section 4.8.

The spherically symmetric dimensional problem of a wax particle growth is formulated as

$$
\begin{cases}
\frac{\partial C}{\partial t} = \frac{D}{r^2}\frac{\partial}{\partial r}\left(r^2\frac{\partial C}{\partial r}\right) \qquad (r \geq R(t), t > 0), \\
C(r,0) = C_s(r) \qquad (r \geq R(0)), \\
(C(r,t) - C_0)\, r^3 \longrightarrow 0 \qquad (\text{as } r \longrightarrow \infty), \\
\frac{\partial C}{\partial r} = k_1\zeta(t)(C - C_*) \qquad (r = R(t)), \\
\frac{dR}{dt} = D\frac{\partial C}{\partial r} \qquad (r = R(t)), \\
R(0) = R_0 \qquad (t = 0).
\end{cases}
\tag{4.1.1}
$$

where $C(r,t)$ is the concentration of the wax in the oil, t is the time, r is the radial distance from the centre of the wax particle, and k_1 is a constant coefficient in the formula for the mass transfer coefficient $k_r(t) = Dk_1\zeta(t)$. The initial concentration, $C_s(r)$, satisfies the far-field condition, $C_s(r) \longrightarrow C_0$ as $r \longrightarrow \infty$, and it is not necessarily uniform. The solubility C_* is assumed constant in this study.

4.2 Non-dimensional variables

In order to reduce the number of parameters and to make the formulation of the problem simpler, we introduce dimensionless variables. Let us introduce a characteristic length and time to be $\sqrt{Dt_0}$ and t_0, respectively, where t_0 is a timescale which will be specified later. The dimensionless variables and functions (denoted by over bars) are introduced by

$$\bar{r} = \frac{r}{\sqrt{Dt_0}}, \qquad \bar{t} = \frac{t}{t_0}, \qquad \bar{R}(\bar{t}) = \frac{R(t)}{\sqrt{Dt_0}}, \qquad \bar{C}(\bar{r},\bar{t}) = \frac{C(r,t)-C_0}{(C_0-C_*)},$$

$$\bar{\zeta}(\bar{t}) = \sqrt{t_0}\zeta(t),$$

where $\bar{\zeta}(\bar{t})$ which defined in chapter 3, is a non-dimensional function of the dimensionless time $\bar{t}$. We use these non-dimensional variables to obtain:

$$\begin{cases} \frac{\partial \bar{C}}{\partial \bar{t}} = \frac{1}{\bar{r}^2}\frac{\partial}{\partial \bar{r}}\left(\bar{r}^2\frac{\partial \bar{C}}{\partial \bar{r}}\right) \qquad (\bar{r} \geq \bar{R}(\bar{t})\bar{t} > 0), \\ \bar{C}(\bar{r},0) = \frac{C_s(\bar{r})-C_0}{C_0-C_*} \qquad (\bar{r} \geq \bar{R}(0)), \\ \bar{r}^3\bar{C}(\bar{r},\bar{t}) \longrightarrow 0 \qquad (\text{as } \bar{r} \longrightarrow \infty), \\ \frac{\partial \bar{C}}{\partial \bar{r}} = \epsilon\bar{\zeta}(\bar{t})(\bar{C}+1) \qquad (\bar{r} = \bar{R}(\bar{t})), \\ \frac{d\bar{R}}{d\bar{t}} = (C_0-C_*)\frac{\partial \bar{C}}{\partial \bar{r}} \qquad (\bar{r} = \bar{R}(\bar{t})), \\ \bar{R}(0) = \frac{R_0}{\sqrt{Dt_0}}. \end{cases} \tag{4.2.1}$$

where $\epsilon = k_1\sqrt{D}$, see chapter 3. The equation for $\bar{C}(\bar{r},\bar{t})$ in the problem (4.2.1) can be simplify by introducing new unknown function $u(\bar{r},\bar{t}) = \bar{r}\bar{C}(\bar{r},\bar{t})$. Then the problem becomes (over bars are dropped below)

$$
\begin{cases}
u_t = u_{rr} \qquad (r \geq R(t), t \geq 0), \\
u(r,0) = u_0(r), \\
r^2 u(r,t) \longrightarrow 0 \qquad (\text{as } r \longrightarrow \infty), \\
u_r = \frac{u}{R(t)}\left[1 + \epsilon\zeta(t)R(t)\right] + \epsilon\zeta(t)R(t) \qquad (r = R(t)), \\
\frac{dR}{dt} = \epsilon(C_0 - C_*)\zeta(t)\left(\frac{u}{R(t)} + 1\right) \qquad (r = R(t)), \\
R(0) = \frac{R_0}{\sqrt{Dt_0}}.
\end{cases}
\tag{4.2.2}
$$

where $u_0(r) = \frac{r(C_s(r)-C_0)}{C_0-C_*}$. The dimensionless parameters in this set of equations are ϵ, $C_0 - C_*$, and the non-dimensional initial radius of the wax particle, $\frac{R_0}{\sqrt{Dt_0}}$; the dimensionless function to be specified are $\zeta(t)$ and $u_0(r)$. The equation governing the new unknown function $u(r,t)$ in the flow domain is the one-dimensional diffusion equation. The boundary, $r = R(t)$, of the flow region is unknown in advance and should be determined as part of the solution. Equation $(4.2.2)_3$ implies that $u(r,t)$ tends to zero faster than $\frac{1}{r^2}$ as $r \longrightarrow \infty$, which follows from equation (3.2.10).

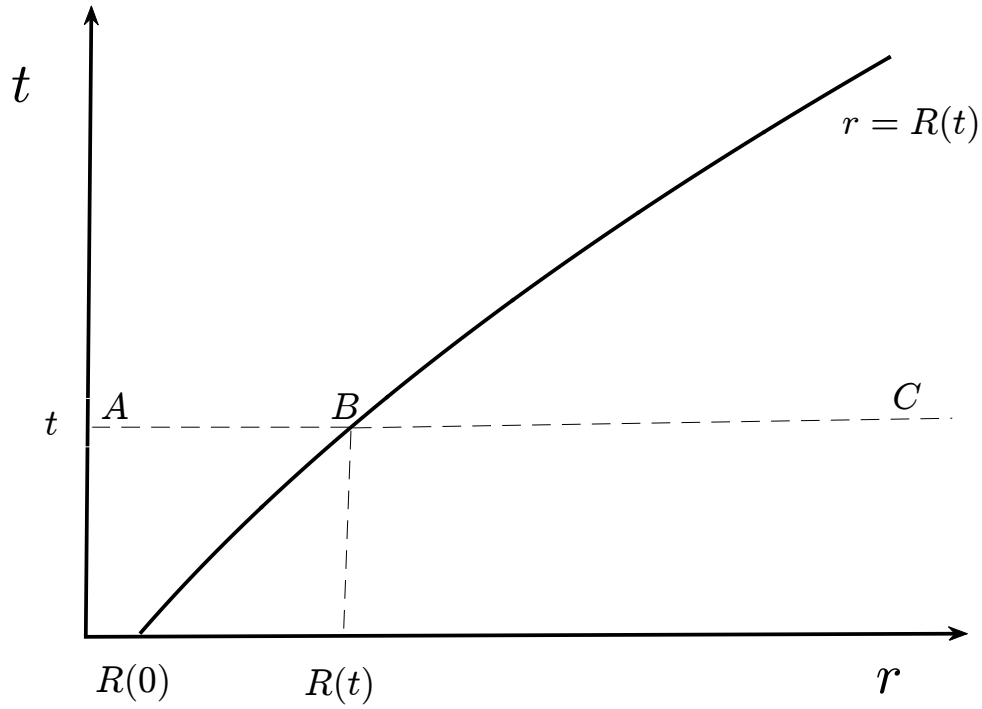

Figure 4.2.1: The horizontal line t=constant, contains segment AB which corresponds to the solid wax (inside wax particle), B which is on the boundary of the wax particle, and BC which is the instantaneous fluid domain.

4.3 Integral equation on the particle boundary

In this section we reduce the problem (4.2.2) to a boundary integral equation using a Green's function of the one-dimensional diffusion equation. The Green function $G(r,t;r',t')$, where r' and t' are parameters, is defined as the solution of the following initial problem, [17]

$$\begin{cases} G_t = G_{rr}, \qquad (-\infty < r < +\infty, \qquad t > t'), \\ \\ G(r,t';r',t') = \delta(r-r'), \qquad (-\infty < r < +\infty, \qquad t = t'), \\ \\ G \longrightarrow 0, \qquad (r \longrightarrow \infty). \end{cases} \tag{4.3.1}$$

Here $\delta(r)$ is the Dirac delta function. The Green function is the solution of the problem (4.3.1) for $0 \leq t' < t$, see [8]. This solution has the form,

$$G(r,t;r',t') = \frac{1}{2\sqrt{\pi(t-t')}} e^{-\frac{(r-r')^2}{4(t-t')}}. \tag{4.3.2}$$

Note that $r > R(t) > R(0) \geq 0$ in equation (4.2.2), see figure 4.2.1, but r varies from $-\infty$ to $+\infty$ in (4.3.1). The variable r in (4.2.2) is the radial coordinate which should be positive. However, the field equation $(4.2.2)_1$ is the one-dimensional diffusion equation in contrast to equation $(4.2.1)_1$ which is for spherically symmetric diffusion.

We shall solve the dimensionless problem for $u = u(r,t)$ and $R = R(t)$ with two given dimensionless constants ϵ and $\epsilon(C_0 - C_*)$, and the given non-dimensional function $\zeta(t)$ in the boundary conditions. We write equation $(4.2.2)_1$ in the variables r', t'. Now $u = u(r',t')$ where $r' > R(t')$, $t' > 0$, and

$$\frac{\partial u}{\partial t'} = \frac{\partial^2 u}{\partial r'^2}. \tag{4.3.3}$$

We multiply both sides of (4.3.3) by $G(r,t;r',t')$ and integrate both sides of the result over the region indicated in Figure 4.3.1. To do this we integrate with respect to r' from the surface $r' = R(t')$ to infinity, and then we integrate both sides with respect to t' from the initial instant $t' = 0$ to $t' = t$,

$$\int_0^t \int_{R(t')}^{\infty} u_{t'}(r,' t')G(r,t;r',t')dr'dt' = \int_0^t \int_{R(t')}^{\infty} u_{r'r'}(r',t')G(r,t;r',t')dr'dt'. \tag{4.3.4}$$

The radius $R(t)$ is assumed monotonically increasing, $R'(t) > 0$. Then the order of integration in the double integral on the left hand side of equation (4.3.4) can be changed by considering the diagram in Figure 4.3.1,

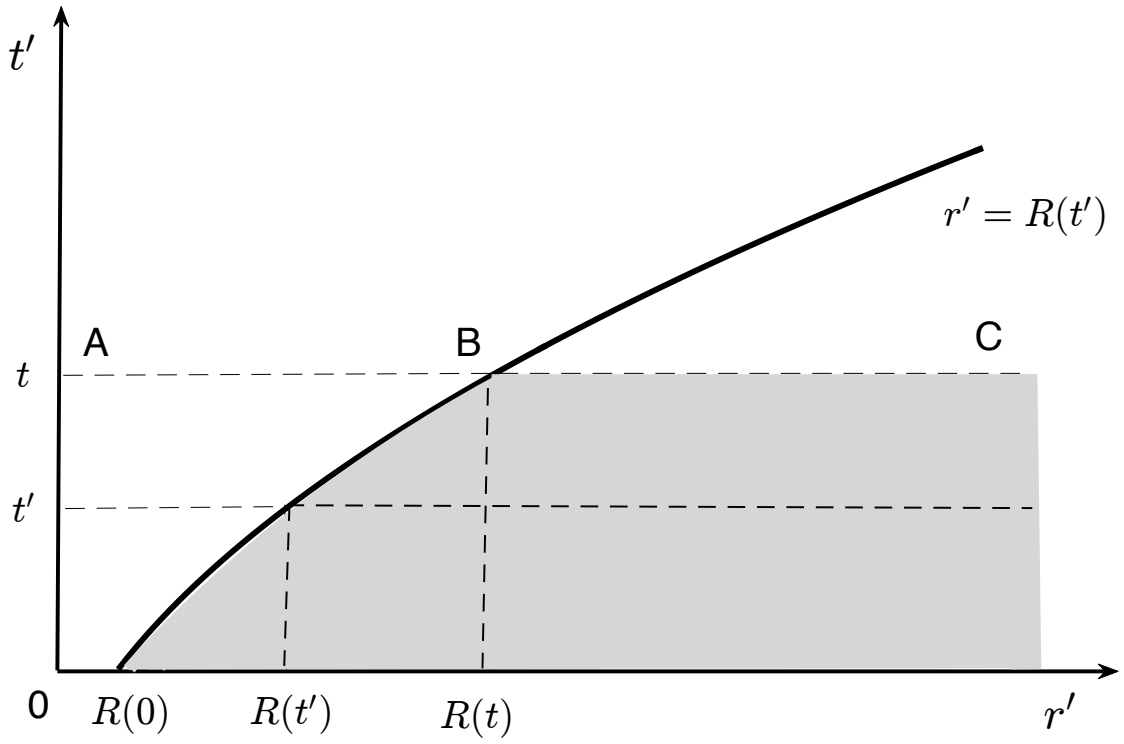

Figure 4.3.1: The curve $r' = R(t')$ separates solid wax, to the left, from the fluid domain to the right. The region of integration in equation (4.3.4) is shown in grey.

which gives

$$\int_0^t \int_{R(t')}^{\infty} u_{t'}(r',t')G(r,t;r',t')dr'dt' = \int_{R(0)}^{R(t)} dr' \int_0^{t(r')} u_{t'}(r',t')G(r,t;r',t')dt' + \int_{R(t)}^{\infty} dr' \int_0^t u_{t'}(r',t')G(r,t;r',t')dt', \tag{4.3.5}$$

where $t(r')$ is a monotone increasing function defined by the equation $R(t(r')) \equiv r'$. The inner integrals in (4.3.5) are integrated by parts, giving

$$\begin{aligned}
&\int_0^t \int_{R(t')}^{\infty} u_{t'}(r',t')G(r,t;r',t')dr'dt' \\
&= \int_{R(0)}^{R(t)} \left[u(r',t')G(r,t;r',t') \mid_0^{t(r')} - \int_0^{t(r')} u(r',t')G_{t'}(r,t;r',t')dt' \right] dr' \\
&+ \int_{R(t)}^{\infty} \left[u(r',t')G(r,t;r',t') \mid_0^{t} - \int_0^{t} u(r',t')G_{t'}(r,t;r',t')dt' \right] dr' \\
&= \int_{R(0)}^{R(t)} \Big[u(r',t(r'))G(r,t;r',t(r')) - u(r',0)G(r,t;r',0) \\
&- \int_0^{t(r')} u(r',t')G_{t'}(r,t;r',t')dt' \Big] dr' + \int_{R(t)}^{\infty} \Big[u(r',t)G(r,t;r',t) - u(r',0)G(r,t;r',0) \\
&- \int_0^{t} u(r',t')G_{t'}(r,t;r',t')dt' \Big] dr'.
\end{aligned} \tag{4.3.6}$$

To continue transformation of the integrals above, we should calculate $G_{t'}(r,t;r',t')$ by using (4.3.1). It is convenient to introduce new variables $\xi = r - r'$ and $\tau = t - t'$. Then $G(r,t;r',t') = G_O(\xi,\tau)$, where

$$\begin{cases} G_{O\tau} = G_{O\xi\xi}, \qquad (-\infty < \xi < +\infty), \\ \\ G(\xi,0) = \delta(\xi) \qquad (\tau = 0). \end{cases} \tag{4.3.7}$$

Differentiating $G(r,t;r',t') = G_O(\xi,\tau)$ with respect to t', we have

$$\frac{\partial G}{\partial t'} = \frac{\partial G_O}{\partial \tau}\frac{\partial \tau}{\partial t'} = -\frac{\partial G_O}{\partial \tau}, \tag{4.3.8}$$

and differentiating $G(r,t;r',t') = G_O(\xi,\tau)$ twice with respect to r', gives

$$\frac{\partial^2 G}{\partial r'^2} = \frac{\partial^2 G_O}{\partial \xi^2}. \tag{4.3.9}$$

By using the equation $G_{O\tau} = G_{O\xi\xi}$, we find

$$\frac{\partial G}{\partial t'} = -\frac{\partial G_O}{\partial \tau} = -\frac{\partial^2 G_O}{\partial \xi^2} = -\frac{\partial^2 G}{\partial r'^2}. \tag{4.3.10}$$

By using equation (4.3.10) we can calculate the following integrals,

$$\int_0^{t(r')} u(r',t')G_{t'}(r,t;r',t')dt' = -\int_0^{t(r')} u(r',t')G_{r'r'}(r,t;r',t')dt'. \tag{4.3.11}$$

and

$$\int_0^{t} u(r',t')G_{t'}(r,t;r',t')dt' = -\int_0^{t} u(r',t')G_{r'r'}(r,t;r',t')dt'. \tag{4.3.12}$$

Substituting equations (4.3.11) and (4.3.12) into (4.3.6), we obtain

$$\begin{aligned}
&\int_0^t \int_{R(t')}^{\infty} u_{t'}(r',t')G(r,t;r',t')dr'dt' = \int_{R(0)}^{R(t)} u(r',t(r'))G(r,t;r',t(r'))dr' \\
&- \int_{R(0)}^{\infty} u(r',0)G(r,t;r',0)dr' + \int_{R(t)}^{\infty} u(r',t)\delta(r-r')dr' \\
&+ \left(\int_{R(0)}^{R(t)} \int_0^{t(r')} + \int_{R(t)}^{\infty} \int_0^{t}\right) u(r',t')G_{r'r'}(r,t;r',t')dt'dr'.
\end{aligned} \tag{4.3.13}$$

In the first integral on the right hand side of equation (4.3.13), we make the substitution $r' = R(t')$ and use $dr' = \frac{dR}{dt}(t')dt'$, $t(R(t')) \equiv t'$, then

$$\int_{R(0)}^{R(t)} u(r',t(r'))G(r,t;r',t(r'))dr' = \int_0^t u(R(t'),t')G(r,t;R(t'),t')\frac{dR}{dt}(t')dt', \tag{4.3.14}$$

which is the integral along the trajectory of the particle's radius in the (r,t) plane. In the second integral on the right hand side of equation (4.3.13), $u(r',0)$ is given by the initial data as $u_0(r')$, then this integral reads

$$\int_{R(0)}^{\infty} u(r',0)G(r,t;r',0)dr' = \int_{R(0)}^{\infty} u_0(r')G(r,t;r',0)dr'. \tag{4.3.15}$$

By the property of the delta function, the third integral in (4.3.13) reads as, see [8],

$$\int_{R(t)}^{\infty} u(r',t)\delta(r-r')dr' = \begin{cases} u(r,t) & \text{where} \quad r > R(t), \\ \\ \frac{1}{2}u(R(t),t) & \text{where} \quad r = R(t). \end{cases} \tag{4.3.16}$$

The integral above is equal to $u(r,t)$ in the fluid region, where $r > R(t)$, and equal to $\frac{1}{2}u(R(t),t)$ on the surface of the wax particle where $r = R(t)$. The value of the integral can be written as $\omega u(r,t)$, where $\omega = 1$ for $r > R(t)$ and $\omega = \frac{1}{2}$, where $r = R(t)$. To show (4.3.16), we consider the function $\delta_n(x)$ which approximates the delta function $\delta(x)$ as $n \to \infty$. The function $\delta_n(x)$ is defined by

$$\delta_n(x) = \begin{cases} 0 & |x| > \frac{1}{n}, \\ \\ \frac{n}{2} & |x| < \frac{1}{n}. \end{cases} \tag{4.3.17}$$

The function $\delta_n(x)$ is such that

$$\int_{-\infty}^{\infty} \delta_n(x)dx = 1$$

and $\delta_n(x) \to 0$ for any $|x| > 0$ and $n \to \infty$. For any function $f(x)$ continuous in a neighbourhood of the origin, see [43, 45], we have

$$\lim_{n\to\infty} \int_{-\infty}^{+\infty} f(x)\delta_n(x)dx = \lim_{n\to\infty} \int_{-\frac{1}{n}}^{+\frac{1}{n}} \frac{n}{2} f(x)dx = \frac{n}{2} \lim_{n\to\infty} \int_{-1}^{1} f\left(\frac{\xi}{n}\right) d\left(\frac{\xi}{n}\right)$$
$$= \frac{1}{2} \lim_{n\to\infty} \int_{-1}^{1} f\left(\frac{\xi}{n}\right) d\xi = \frac{1}{2} \lim_{n\to\infty} \int_{-1}^{1} \left[f(0) + f'(0)\frac{\xi}{n} + O\left(\left(\frac{\xi}{n}\right)^2\right)\right] d\xi = f(0). \tag{4.3.18}$$

Correspondingly,

$$\lim_{n\to\infty}\int_0^{+\infty} f(x)\delta_n(x)dx = \lim_{n\to\infty}\int_0^{+\frac{1}{n}} \frac{n}{2}f(x)dx = \frac{1}{2}\lim_{n\to\infty}\int_0^1 f\left(\frac{\xi}{n}\right)d\xi$$
$$= \frac{1}{2}\lim_{n\to\infty}\int_0^1 \left[f(0) + f'(0)\frac{\xi}{n} + O\left(\left(\frac{\xi}{n}\right)^2\right)\right]d\xi = \frac{1}{2}f(0). \tag{4.3.19}$$

The double integral in equation (4.3.13), (see the diagram 4.3.1) can be written as

$$\int_0^t \left[\int_{R(t')}^{\infty} u(r',t')G_{r'r'}(r,t;r',t')dr'\right]dt'.$$

Integrating the inner integral twice by parts yields

$$\begin{aligned}
&\int_0^t \left[\int_{R(t')}^{\infty} u(r',t')G_{r'r'}(r,t;r',t')dr'\right]dt' \\
&= \int_0^t \left[u(r',t')G_{r'}(r,t;r',t')\ |_{r'=R(t')}^{r'=\infty} - \int_{R(t')}^{\infty} u_{r'}(r',t')G_{r'}(r,t;r',t')dr'\right]dt' \\
&= \int_0^t \Big[-u(R(t'),t')G_{r'}(r,t;R(t'),t') - u_{r'}(r',t')G(r,t;r',t')\ |_{r'=R(t')}^{r'=\infty} \\
&+ \int_{R(t')}^{\infty} u_{r'r'}(r',t')G(r,t;r',t')dr'\Big]dt'.
\end{aligned} \tag{4.3.20}$$

Therefore,

$$\begin{aligned}
&\int_0^t \int_{R(t')}^{\infty} u(r',t')G_{r'r'}(r,t;r',t')dr'dt' \\
&= -\int_0^t u(R(t'),t')G_{r'}(r,t;R(t'),t')dt' + \int_0^t u_{r'}(R(t'),t')G(r,t;R(t'),t')dt' \\
&+ \int_0^t \int_{R(t')}^{\infty} u_{r'r'}(r',t')G(r,t;r',t')dr'dt'.
\end{aligned} \tag{4.3.21}$$

Substituting (4.3.21) and (4.3.14)-(4.3.16) into (4.3.13), we obtain

$$
\begin{aligned}
&\int_0^t \int_{R(t')}^{\infty} u_{t'}(r',t')G(r,t;r',t')dr'dt' \\
&= \int_0^t u(R(t'),t')G(r,t;R(t'),t')\frac{dR}{dt}(t')dt' - \int_{R(0)}^{\infty} u_0(r')G(r,t;r',0)dr' \\
&\quad + \omega u(r,t) - \int_0^t u(R(t'),t')G_{r'}(r,t;R(t'),t')dt' \\
&\quad + \int_0^t u_{r'}(R(t'),t')G(r,t;R(t'),t')dt' \\
&\quad + \int_0^t \int_{R(t')}^{\infty} u_{r'r'}(r',t')G(r,t;r',t')dr'dt'.
\end{aligned}
\tag{4.3.22}
$$

Now we substitute (4.3.22) into (4.3.4), and notice that the double integrals with $u_{r'r'}$ in the equation cancel each other and the result is:

$$
\begin{aligned}
&\int_0^t u(R(t'),t')G(R(t'),t)\frac{dR}{dt}(t')dt' - \int_{R(0)}^{\infty} u_0(r')G(r,t;r',0)dr' + \omega u(r,t) \\
&- \int_0^t u(R(t'),t')G_{r'}(r,t;R(t'),t')dt' + \int_0^t u_{r'}(R(t'),t')G(r,t;R(t'),t')dt' = 0.
\end{aligned}
\tag{4.3.23}
$$

We can view the result as a representation of the solution $u(r,t)$ in the fluid, where $r > R(t)$, and on the boundary, where $r = R(t)$, through the boundary values of the solution $u(R(t),t)$, its normal derivative, $u_r(R(t),t)$ and its initial value, $u_0(r)$:

$$
\begin{aligned}
\omega u(r,t) = &\int_{R(0)}^{\infty} u_0(r')G(r,t;r',0)dr' \\
&+ \int_0^t u(R(t'),t')\left[G_{r'}(r,t;R(t'),t') - \frac{dR}{dt}(t')G(r,t;R(t'),t)\right]dt' \\
&- \int_0^t u_{r'}(R(t'),t')G(r,t;R(t'),t')dt'.
\end{aligned}
\tag{4.3.24}
$$

The Green function and its r'-derivative in the integrals with respect to t' are regular and bounded if $r > R(t)$. The derived representation (4.3.24) of $u(r,t)$

provides the solution in the fluid region, $r > R(t)$, $t > 0$ in terms of given initial data $u(r,0)$ and boundary data $u(R(t),t)$ and $u_r(R(t),t)$. On the boundary, $r = R(t)$, and $t > 0$, where $\omega = \frac{1}{2}$, (4.3.24) gives an integral equation for $u(R(t),t)$

$$\begin{aligned}\frac{1}{2}u(R(t),t) &= \int_{R(0)}^{\infty} u_0(r')G(R(t),t;r',0)dr' \\ &+ \int_0^t u(R(t'),t')\left[G_{r'}(R(t),t;R(t'),t') - \frac{dR}{dt}(t')G(R(t),t;R(t'),t)\right]dt' \\ &- \int_0^t u_{r'}(R(t'),t')G(R(t),t;R(t'),t')dt'.\end{aligned} \tag{4.3.25}$$

Rearranging the integrals

$$\begin{aligned}u(R(t),t) &= 2\int_{R(0)}^{\infty} u_0(r')G(R(t),t;r',0)dr' \\ &+ 2\int_0^t \Big[u(R(t'),t')G_{r'}(R(t),t;R(t'),t') - u_{r'}(R(t'),t')G(R(t),t;R(t'),t') \\ &- u(R(t'),t')G(R(t),t;R(t'),t')\frac{dR}{dt}(t')\Big]dt'.\end{aligned} \tag{4.3.26}$$

Now we will find the derivative of the Green function with respect to r' which appear in (4.3.26).

The r'-derivative of the Green function (4.3.2) is:

$$G_{r'}(r,t;r',t') = \frac{r-r'}{4\sqrt{\pi}(t-t')^{\frac{3}{2}}}e^{-\frac{(r-r')^2}{4(t-t')}}. \tag{4.3.27}$$

We can rewrite $G_{r'}(r,t;r',t')$ by using (4.3.2) as:

$$G_{r'}(r,t;r',t') = \frac{1}{2}G(r,t;r',t')\frac{r-r'}{t-t'}. \tag{4.3.28}$$

The Green function and its derivative on the boundary, $r = R(t)$, are:

$$G(R(t),t;R(t'),t') = \frac{1}{2\sqrt{\pi(t-t')}}e^{-\frac{(R(t)-R(t'))^2}{4(t-t')}}. \tag{4.3.29}$$

and

$$G_{r'}(R(t),t;R(t'),t') = \frac{1}{2}G\left(R(t),t;R(t'),t'\right)\frac{R(t)-R(t')}{t-t'}. \tag{4.3.30}$$

The function (4.3.29) is singular as $t' \longrightarrow t$. To find the behaviour of the Green function as $t' \longrightarrow t$, we use the Taylor expansion, [76]

$$R(t') = R(t) + \frac{dR}{dt}(t)(t'-t) + O[(t'-t)^2].$$

Then the exponential in (4.3.29) becomes

$$\exp\left[-\frac{(R(t)-R(t'))^2}{4(t-t')}\right] = \exp\left[-\left(\frac{dR}{dt}\right)^2\frac{1}{4}(t-t') + O(t-t')^2\right].$$

As $t' \longrightarrow t$, we find

$$\exp\left[-\frac{(R(t)-R(t'))^2}{4(t-t')}\right] = 1 + O(t-t'). \tag{4.3.31}$$

Therefore, when $t' \longrightarrow t$, the Green function (4.3.29) behaves as

$$G(R(t),t;R(t'),t') \sim \frac{1}{2\sqrt{\pi(t-t')}}. \tag{4.3.32}$$

However, this singularity is integrable. Substituting equations (4.3.29) and (4.3.30) into (4.3.26), we find the boundary integral equation:

$$\begin{aligned}\frac{1}{2}u(R(t),t) = &\int_{R(0)}^{\infty} u_0(r')\frac{1}{2\sqrt{\pi t}}e^{-\frac{(R(t)-r')^2}{4t}}dr' \\ &+ \frac{1}{\sqrt{\pi}}\int_0^t\Bigg[u(R(t'),t')\frac{R(t)-R(t')}{2(t-t')} - u_{r'}\left(R(t'),t'\right) \\ &- u(R(t'),t')\frac{dR}{dt}(t')\Bigg]\frac{1}{2\sqrt{t-t'}}e^{-\frac{(R(t)-R(t'))^2}{4(t-t')}}dt'.\end{aligned} \tag{4.3.33}$$

The integral above can be written as

$$\begin{aligned}\frac{1}{2}u(R(t),t) = &\int_{R(0)}^{\infty} u_0(r')G(R(t),t;r',0)dr' \\ &+ \frac{1}{\sqrt{\pi}}\int_0^t\Bigg[u(R(t'),t')\frac{R(t)-R(t')}{2(t-t')} - u_{r'}\left(R(t'),t'\right) \\ &- u(R(t'),t')\frac{dR}{dt}(t')\Bigg]\frac{1}{2\sqrt{t-t'}}e^{-\frac{(R(t)-R(t'))^2}{4(t-t')}}dt'.\end{aligned} \tag{4.3.34}$$

The second integral is singular as $t' \to t$, so we use (4.3.31) to avoid the singularity in the exponential. If we use L'Hopital's Rule to calculate the ratio $\frac{R(t')-R(t)}{t'-t}$ as $t' \to t$,

$$\lim_{(t' \to t)} \frac{R(t') - R(t)}{t' - t} = \frac{dR}{dt}(t),$$

then the integrand in the second integral when $t' \to t$ behaves as

$$\left[-\frac{1}{2} u(R(t), t) \frac{dR}{dt}(t) - u_r \left(R(t), t \right) \right] \frac{1}{2\sqrt{t - t'}}, \tag{4.3.35}$$

where $\frac{1}{2\sqrt{t-t'}}$ is integrable and therefore, the integral tends to zero as $t \to 0$. Let us show that the limits of left-hand side, which is equal to the boundary value of the function $u(r, t)$, and right-hand side, which is equal to the initial value of $u(r, t)$ calculated on the boundary, in (4.3.34) as $t \to 0$ are equal. We find

$$\frac{1}{2} u(R_0, 0) = \int_{R(0)}^{\infty} u_0(r') G(R_0, 0; r', 0) dr' + 0, \tag{4.3.36}$$

where $G(R_0, 0; r', 0) = \delta(R_0 - r')$ from $(4.3.1)_2$. Hence (4.3.36) provides

$$\frac{1}{2} u(R_0, 0) = \int_{R(0)}^{\infty} u_0(r') \delta(R_0 - r') dr'. \tag{4.3.37}$$

Substituting (4.3.16) into (4.3.37) where $r = R_0$ is the lower limit of integration, we obtain

$$\frac{1}{2} u(R_0, 0) = \frac{1}{2} u_0(R_0). \tag{4.3.38}$$

We conclude that the boundary value of the solution at $t = 0$, $u(R_0, 0)$, and the initial value at the surface of the wax particle, $u_0(R_0)$, are equal to each other.

In the fluid, $r > R(t)$ and $t > 0$, we have $\omega = 1$. Then (4.3.24) gives the solution of the diffusion equation by using the Green function

$$u(r,t) = \frac{1}{2\sqrt{\pi}} \int_{R(0)}^{\infty} u_0(r') \frac{1}{\sqrt{t}} e^{-\frac{(r-r')^2}{4t}} dr' + \frac{1}{2\sqrt{\pi}} \int_0^t \Bigg[u(R(t'),t') \frac{r - R(t')}{2(t-t')} - u_{r'}(R(t'),t') - u(R(t'),t') \frac{dR}{dt}(t') \Bigg] \frac{1}{\sqrt{t-t'}} e^{-\frac{(r-R(t'))^2}{4(t-t')}} dt'. \tag{4.3.39}$$

Substituting the boundary conditions $(4.2.2)_4$ and $(4.2.2)_5$ into the integrals of (4.3.39), we find

$$u(r,t) = \int_{R(0)}^{\infty} u_0(r') \frac{1}{2\sqrt{\pi t}} e^{-\frac{(r-r')^2}{4t}} dr' + \frac{1}{2\sqrt{\pi}} \int_0^t \Bigg[u(R(t'),t') \frac{r - R(t')}{2(t-t')} - \left(\epsilon\zeta(t') + \frac{1}{R(t')} \right) u(R(t'),t') - \epsilon\zeta(t') R(t') - g\zeta(t') \left(\frac{u(R(t'),t')}{R(t')} + 1 \right) u(R(t'),t') \Bigg] \frac{1}{\sqrt{t-t'}} e^{-\frac{(r-R(t'))^2}{4(t-t')}} dt', \tag{4.3.40}$$

where the constant $g = \epsilon(C_0 - C_*)$.

The boundary integral equation (4.3.33) can be written in terms of three unknown functions, $U(t) = u(R(t),t)$, $S(t) = u_r(R(t),t)$ and the radius $R(t)$:

$$U(t) = \frac{1}{\sqrt{\pi t}} \int_{R(0)}^{\infty} u_0(r') e^{-\frac{(R(t)-r')^2}{4t}} dr' + \frac{1}{\sqrt{\pi}} \int_0^t \left[U(t') \frac{R(t) - R(t')}{2(t-t')} - S(t') - U(t') \frac{dR}{dt}(t') \right] \frac{1}{\sqrt{t-t'}} e^{-\frac{(R(t)-R(t'))^2}{4(t-t')}} dt', \tag{4.3.41}$$

where $S(t)$ is related to $U(t)$ and $R(t)$ by $(4.2.2)_4$.

We derived the formula (4.3.40) for $u(r,t)$ in the fluid, where $r > R(t)$, and the integral equation (4.3.41) for $U(t)$ at the boundary of the fluid region, where $r = R(t)$. In the next section 4.4, we solve the integral equation (4.3.41) numerically.

4.4 Discretization

The original problem has been reduced to the integral equation (4.3.41) and the differential equation $(4.2.2)_5$ for the two unknown functions, $u(r,t)$ and $R(t)$. These equations should be solved simultaneously. We solve equation (4.3.41) for $U(t)$ numerically by developing a time-stepping numerical method. First, we discretize t into equal increments of size $\triangle t > 0$,

$$t = 0, \qquad \triangle t, \qquad 2 \triangle t, \qquad 3 \triangle t, \ldots, (n-1) \triangle t. \tag{4.4.1}$$

The discretisation of the time starts from the initial time instant, $t = 0$. The time steps are numbered by index j, where $j = 1$ for $t_1 = 0$,

$$t_2 = \triangle t, \qquad t_3 = 2 \triangle t, \ldots, t_n = (n-1) \triangle t. \tag{4.4.2}$$

The discretized instants in time are defined as $t_j = (j-1) \triangle t$ for $1 \leq j \leq n$, and the time step size $\triangle t$ is related to n by $\triangle t = \frac{t_n - t_1}{n-1}$, where n is the number of discrete instants in the closed time-interval $[t_1, t_n]$, $t_1 = 0$.

The equation (4.3.41) is written then at $t = t_n$,

$$\begin{aligned} U_n = & \frac{1}{\sqrt{\pi t_n}} \int_{R(0)}^{\infty} u_0(r') e^{-\frac{(R_n - r')^2}{4t_n}} dr' \\ & + \frac{1}{\sqrt{\pi}} \int_0^{t_n} \left[U(t') \frac{R_n - R(t')}{2(t_n - t')} - S(t') - U(t') \frac{dR}{dt}(t') \right] \frac{1}{\sqrt{t_n - t'}} e^{-\frac{(R_n - R(t'))^2}{4(t_n - t')}} dt', \end{aligned} \tag{4.4.3}$$

where $U_n = U(t_n)$ and $R_n = R(t_n)$.

In the second integral on the right hand side of equation (4.4.3), we observe that when $t' \longrightarrow t_n$, the ratio $\frac{R(t) - R(t')}{t - t'}$ should be calculated by L'Hopital's Rule:

$$\lim_{(t' \to t)} \frac{R(t') - R(t)}{t' - t} = \frac{dR}{dt}(t). \tag{4.4.4}$$

Then the expression in (4.4.3) in the square brackets is equal to

$$-\frac{1}{2}U(t_n)\frac{dR}{dt}(t_n) - S(t_n) \qquad \text{as} \qquad t' \to t_n. \tag{4.4.5}$$

Also, we should use (4.3.31) to avoid singularity in the exponential when $t' \longrightarrow t_n$.

Substituting the boundary conditions $(4.2.2)_4$ and $(4.2.2)_5$ into the boundary integral equation (4.4.3), we have

$$\begin{aligned} U_n =& \frac{1}{\sqrt{\pi t_n}} \int_{R(0)}^{\infty} u_0(r') e^{-\frac{(R_n - r')^2}{4t_n}} dr' \\ &+ \frac{1}{\sqrt{\pi}} \int_0^{t_n} \left[U(t') \frac{R_n - R(t')}{2(t_n - t')} - g\zeta(t') \left(\frac{U(t')}{R(t')} + 1 \right) U(t') - \left(\frac{1}{R(t')} + \epsilon\zeta(t') \right) U(t') \right. \\ &\left. - \epsilon\zeta(t') R(t') \right] e^{-\frac{(R_n - R(t'))^2}{4(t_n - t')}} \frac{dt'}{\sqrt{t_n - t'}}, \end{aligned} \tag{4.4.6}$$

where $g = \epsilon(C_0 - C_*)$.

We use the following piecewise linear approximations to $U(t')$, $R(t')$, $\delta(t')$, and $e^{-\frac{(R_n - R(t'))^2}{4(t_n - t')}}$ inside an integral, $t_j < t' < t_{j+1}$:

$$U(t') = U(t_j) + [U(t_{j+1}) - U(t_j)] \frac{t' - t_j}{t_{j+1} - t_j}, \tag{4.4.7}$$

$$R(t') = R(t_j) + [R(t_{j+1}) - R(t_j)] \frac{t' - t_j}{t_{j+1} - t_j}, \tag{4.4.8}$$

$$\zeta(t') = \delta(t_j) + [\zeta(t_{j+1}) - \zeta(t_j)] \frac{t' - t_j}{t_{j+1} - t_j}, \tag{4.4.9}$$

and

$$e^{-\frac{(R_n - R(t'))^2}{4(t_n - t')}} = e^{-\frac{(R_n - R(t_j))^2}{4(t_n - t_j)}} + \left[e^{-\frac{(R_n - R(t_{j+1}))^2}{4(t_n - t_{j+1})}} - e^{-\frac{(R_n - R(j))^2}{4(t_n - t_j)}} \right] \frac{t' - t_j}{t_{j+1} - t_j}, \tag{4.4.10}$$

where $1 \le j \le n-1$, $t_1 = 0$ and

$$t' = t_j + \xi(t_{j+1} - t_j), \qquad 0 \le \xi \le 1.$$

We substitute equations (4.4.7)-(4.4.10) into equation (4.4.6) and represent the interval $(0, t_n)$ as the sum of intervals over j from 1 to $n-1$,

$$\int_0^{t_n} = \int_{t_{n-1}}^{t_n} + \sum_{j=1}^{n-2} \int_{t_j}^{t_{j+1}}.$$

We use (4.4.5) and (4.3.31) at the last panel for $t' = t_n$ to avoid the singularity. Then the discretized equation (4.4.6) can be approximated by

$$\begin{aligned}
U_n = F(t_n) + \frac{1}{\sqrt{\pi}} \int_0^1 \Bigg[& -\frac{g}{2}[\zeta_{n-1} + \xi(\zeta_n - \zeta_{n-1})] \frac{[U_{n-1} + \xi(U_n - U_{n-1})]^2}{[R_{n-1} + \xi(R_n - R_{n-1})]} \\
& - \frac{g}{2}[\zeta_{n-1} + \xi(\zeta_n - \zeta_{n-1})][U_n + \xi(U_n - U_{n-1})] - \frac{[U_{n-1} + \xi(U_n - U_{n-1})]}{[R_{n-1} + \xi(R_n - R_{n-1})]} \\
& - \epsilon[\zeta_{n-1} + \xi(\zeta_n - \zeta_{n-1})][U_{n-1} + \xi(U_n - U_{n-1})] - \epsilon[\zeta_{n-1} + \xi(\zeta_n - \zeta_{n-1})] \\
& [R_{n-1} + \xi(R_n - R_{n-1})] \Bigg] \frac{(t_n - t_{n-1})^{\frac{1}{2}} d\xi}{\sqrt{1-\xi}} \\
& + \frac{1}{\sqrt{\pi}} \sum_{j=1}^{n-2} \int_0^1 \Bigg[[U_j + \xi(U_{j+1} - U_j)] \frac{R_n - \Big[R_j + \xi(R_{j+1} - R_j)\Big]}{2(t_n - t_j - \xi(t_{j+1} - t_j)} \\
& - g[\delta_j + \xi(\zeta_{j+1} - \zeta_j)] \frac{[U_j + \xi(U_{j+1} - U_j)]^2}{[R_j + \xi(R_{j+1} - R_j)]} \\
& - g[\zeta_j + \xi(\zeta_{j+1} - \zeta_j)][U_j + \xi(U_{j+1} - U_j)] - \frac{[U_j + \xi(U_{j+1} - U_j)]}{[R_j + \xi(R_{j+1} - R_j)]} \\
& - \epsilon[\zeta_j + \xi(\zeta_{j+1} - \zeta_j)][U_j + \xi(U_{j+1} - U_j)] - \epsilon[\zeta_j + \xi(\zeta_{j+1} - \zeta_j)] \\
& [R_j + \xi(R_{j+1} - R_j)] \Bigg] \left(e^{-\frac{(R_n - R_j)^2}{4(t_n - t_j)}} + \xi \left[e^{-\frac{(R_n - R_{j+1})^2}{4(t_n - t_{j+1})}} - e^{-\frac{(R_n - R_j)^2}{4(t_n - t_j)}} \right] \right) \\
& \frac{t_{j+1} - t_j}{\sqrt{t_n - t_j - \xi(t_{j+1} - t_j)}} d\xi,
\end{aligned} \tag{4.4.11}$$

$$F(t_n) = \frac{1}{\sqrt{\pi t}} \int_{R(0)}^{\infty} u_0(r') e^{-\frac{(R_n - r')^2}{4t}} dr'.$$

In equation (4.4.11) we have U_n in both the left and right hand sides. We move all terms to the left-hand side and collect terms with U_n and U_n^2, then we have

$$
\begin{aligned}
&U_n\Bigg(1-\frac{(t_n-t_{n-1})^{\frac{1}{2}}}{\sqrt{\pi}}\int_0^1\Bigg[\Big(-\frac{g}{2}-\epsilon\Big)\xi[\zeta_{n-1}+\xi(\zeta_n-\zeta_{n-1})]\\
&-\frac{\xi}{[R_{n-1}+\xi(R_n-R_{n-1})]}-\frac{g}{2}\Big(2\xi U_{n-1}-2\xi^2U_{n-1}\Big)\\
&\frac{[\zeta_{n-1}+\xi(\zeta_n-\zeta_{n-1})]}{[R_{n-1}+\xi(R_n-R_{n-1})]}\Bigg]\frac{d\xi}{\sqrt{(1-\xi)}}\Bigg)+U_n^2\Bigg[\frac{g}{2\sqrt{\pi}}(t_n-t_{n-1})^{\frac{1}{2}}\\
&\int_0^1\xi^2\frac{[\zeta_{n-1}+\xi(\zeta_n-\zeta_{n-1})]}{[R_{n-1}+\xi(R_n-R_{n-1})]}\frac{d\xi}{\sqrt{(1-\xi)}}\Bigg]-U_{n-1}\Bigg[\frac{(t_n-t_{n-1})^{\frac{1}{2}}}{\sqrt{\pi}}\int_0^1\Bigg[\Big(-\frac{g}{2}-\epsilon\Big)\\
&(1-\xi)[\zeta_{n-1}+\xi(\zeta_n-\zeta_{n-1})]-\frac{(1-\xi)}{[R_{n-1}+\xi(R_n-R_{n-1})]}\frac{d\xi}{\sqrt{(1-\xi)}}\Bigg]\Bigg]\\
&+U_{n-1}^2\Bigg[\frac{g}{2\sqrt{\pi}}(t_n-t_{n-1})^{\frac{1}{2}}\int_0^1\Big(1-2\xi+\xi^2\Big)\frac{[\zeta_{n-1}+\xi(\zeta_n-\zeta_{n-1})]}{[R_{n-1}+\xi(R_n-R_{n-1})]}\frac{d\xi}{\sqrt{(1-\xi)}}\Bigg]\\
&+\frac{\epsilon}{\sqrt{\pi}}(t_n-t_{n-1})^{\frac{1}{2}}\int_0^1\Bigg[[\zeta_{n-1}+\xi(\zeta_n-\zeta_{n-1})][R_{n-1}+\xi(R_n-R_{n-1})]\frac{d\xi}{\sqrt{(1-\xi)}}\Bigg]\\
&-\frac{1}{\sqrt{\pi}}\sum_{j=1}^{n-2}\int_0^1(\text{all terms})\Bigg(e^{-\frac{(R_n-R_j)^2}{4(t_n-t_j)}}+\xi\Bigg[e^{-\frac{(R_n-R_{j+1})^2}{4(t_n-t_{j+1})}}-e^{-\frac{(R_n-R_j)^2}{4(t_n-t_j)}}\Bigg]\Bigg)\\
&\frac{t_{j+1}-t_j}{\sqrt{t_n-t_j-\xi(t_{j+1}-t_j)}}d\xi-F(t_n)=0,
\end{aligned}
\tag{4.4.12}
$$

where " all terms" means all of the preceding terms $\sum_{j=1}^{n-2}$ in (4.4.11).

Equation (4.4.12) is a quadratic equation for U_n. If we consider this as

$$aU_n^2+bU_n+c=0$$

Then the value for a, b, and c are:

$$
\begin{aligned}
a&=\frac{g}{2\sqrt{\pi}}(t_n-t_{n-1})^{\frac{1}{2}}\int_0^1\xi^2\frac{[\zeta_{n-1}+\xi(\zeta_n-\zeta_{n-1})]}{[R_{n-1}+\xi(R_n-R_{n-1})]}\frac{d\xi}{\sqrt{(1-\xi)}},\\
b=&1-\frac{(t_n-t_{n-1})^{\frac{1}{2}}}{\sqrt{\pi}}\int_0^1\Bigg[\Big(-\frac{g}{2}-\epsilon\Big)\xi[\zeta_{n-1}+\xi(\zeta_n-\zeta_{n-1})]\\
&-\frac{\xi}{[R_{n-1}+\xi(R_n-R_{n-1})]}-gU_{n-1}\xi\Big(1-\xi\Big)\frac{[\zeta_{n-1}+\xi(\zeta_n-\zeta_{n-1})]}{[R_{n-1}+\xi(R_n-R_{n-1})]}\Bigg]\\
&\frac{d\xi}{\sqrt{(1-\xi)}},
\end{aligned}
\tag{4.4.13}
$$

$$
\begin{aligned}
c = &\frac{(t_n - t_{n-1})^{\frac{1}{2}}}{\sqrt{\pi}} \int_0^1 \Bigg[U_{n-1} \left(\frac{g}{2} + \epsilon \right) (1-\xi)[\zeta_{n-1} + \xi(\zeta_n - \zeta_{n-1})] \\
&+ U_{n-1} \frac{(1-\xi)}{[R_{n-1} + \xi(R_n - R_{n-1})]} + U_{n-1}^2 \frac{g}{2} \Bigg(1 - 2\xi + \xi^2 \Bigg) \\
&\frac{[\zeta_{n-1} + \xi(\zeta_n - \zeta_{n-1})]}{[R_{n-1} + \xi(R_n - R_{n-1})]} + \epsilon[\zeta_{n-1} + \xi(\zeta_n - \zeta_{n-1})][R_{n-1} + \xi(R_n - R_{n-1})] \Bigg] \frac{d\xi}{\sqrt{(1-\xi)}} \\
&- \frac{1}{\sqrt{\pi}} \sum_{j=1}^{n-2} \int_0^1 (\text{all terms}) \left(e^{-\frac{(R_n - R_j)^2}{4(t_n - t_j)}} + \xi \left[e^{-\frac{(R_n - R_{j+1})^2}{4(t_n - t_{j+1})}} - e^{-\frac{(R_n - R_j)^2}{4(t_n - t_j)}} \right] \right) \\
&\frac{(t_{j+1} - t_j)\, d\xi}{\sqrt{t_n - t_j - \xi(t_{j+1} - t_j)}} - F(t_n).
\end{aligned}
\tag{4.4.14}
$$

The integrands in a, b, and the first term of c are singular as $\xi \to 1$. Note that the integrands in the series for c from $j = 1$ to $j = n-2$ are not singular. Owing to the presence of singularities $\sqrt{1-\xi}$ in the integrands of (4.4.12), we approximate the integrals in a, b and c by using the substitution $\tau = \sqrt{1-\xi}$, then $\xi = 1 - \tau^2$, and

$$
\frac{1}{[R_{n-1} + \xi(R_n - R_{n-1})]} = \frac{1}{[R_n - \tau^2(R_n - R_{n-1})]} = \frac{1}{R_n[1 - \beta\tau^2]}, \tag{4.4.15}
$$

where $\beta = \frac{R_n - R_{n-1}}{R_n}$. Next we expand equation (4.4.15) for small β,

$$
\frac{1}{[R_{n-1} + \xi(R_n - R_{n-1})]} = \frac{1}{R_n}[1 + \beta\tau^2 + O(\beta^2)]. \tag{4.4.16}
$$

We rewrite a, b, and part of c after using the substitution $\xi = 1 - \tau^2$ and (4.4.16) as

$$
a = \frac{\sqrt{t_n - t_{n-1}}}{\sqrt{\pi}} \int_0^1 g(1-\tau^2)^2 \frac{[\zeta_n - \tau^2(\zeta_n - \zeta_{n-1})]}{R_n}[1 + \beta\tau^2] d\tau, \tag{4.4.17}
$$

$$
\begin{aligned}
b = &1 + \frac{2\sqrt{t_n - t_{n-1}}}{\sqrt{\pi}} \int_0^1 \Bigg[\left(\frac{g}{2} + \epsilon \right) (1-\tau^2)[\zeta_n - \tau^2(\zeta_n - \zeta_{n-1})] \\
&+ \frac{1}{R_n}(1-\tau^2)[1 + \beta\tau^2] + g U_{n-1} \tau^2 (1-\tau^2) \frac{[\zeta_n - \tau^2(\zeta_n - \zeta_{n-1})]}{R_{n-1}} (1 + \beta\tau^2) \Bigg] d\tau,
\end{aligned}
\tag{4.4.18}
$$

$$
\begin{aligned}
c = & \frac{2\sqrt{t_n - t_{n-1}}}{\sqrt{\pi}} \int_0^1 \Bigg[U_{n-1} u^2 \Bigg((\frac{g}{2} + \epsilon)[\zeta_n - \tau^2(\zeta_n - \zeta_{n-1})] \\
& + \frac{1}{R_n}[1 + \beta\tau^2] \Bigg) + \frac{g}{2} U_{n-1}^2 \tau^4 \frac{[\zeta_n - \tau^2(\zeta_n - \zeta_{n-1})]}{R_n}[1 + \beta\tau^2] \\
& + \epsilon[\zeta_n - \tau^2(\zeta_n - \zeta_{n-1})][R_n - \tau^2(R_n - R_{n-1})] \Bigg] d\tau \\
& - \frac{1}{\sqrt{\pi}} \sum_{j=1}^{n-2} \int_0^1 [\text{all terms}] \left(e^{-\frac{(R_n - R_j)^2}{4(t_n - t_j)}} + \xi \left[e^{-\frac{(R_n - R_{j+1})^2}{4(t_n - t_{j+1})}} - e^{-\frac{(R_n - R_j)^2}{4(t_n - t_j)}} \right] \right) \\
& \frac{(t_{j+1} - t_j)\, d\xi}{\sqrt{t_n - t_j - \xi(t_{j+1} - t_j)}} - F(t_n).
\end{aligned}
\tag{4.4.19}
$$

Now the integrals (4.4.17)-(4.4.19) are non-singular and they can be evaluated by Matlab. The values of U_n, which are related to the wax concentration on the particle surface at $t = t_n$, are given by:

$$
U_n = \frac{-b \pm \sqrt{b^2 - 4ac}}{2a}, \tag{4.4.20}
$$

where a, b, and c are given in (4.4.17)-(4.4.19). We have two solutions for U_n in (4.4.20). We start with certain value of U_1 and for small Δt we select the solution, which is closer to the solution U_{n-1} at the previous time step, the solution is $U_n^+ = \frac{-b+\sqrt{b^2-4ac}}{2a}$. Also, by looking for the coefficient a, b, and c which are given in (4.4.17)-(4.4.19), we find that a, b, and c behave as $a \sim O(\sqrt{\Delta t})$, $b \sim 1 + O(\sqrt{\Delta t})$, and $c \sim O(1)$, then using the formula

$$
U_n^- = \frac{-b - \sqrt{b^2 - 4ac}}{2a} = O\left((\Delta t)^{-\frac{1}{2}} \right),
$$

which is not good because if we decrease Δt, then $U_n^- \to \infty$. The step of integration has to be small to approaching the exact solution. So the other root $U_n^+ = \frac{-b+\sqrt{b^2-4ac}}{2a}$ is the relevant solution.

The concentration in the fluid is given by equation (4.3.40). We find that the integrand in the second integral is not singular, when $t' \longrightarrow t$, because the

power of the exponential function tends to $-\infty$ for $r > R(t')$. Then $e^{-\infty} = 0$ and the integrand tends to zero as $t' \to t$.

The integral $\int_0^{t_n}$ in (4.3.40) is evaluated by using the trapezidal rule. The trapezoidal rule is a numerical method that approximates the value of a definite integral. We consider our definite integral (4.3.40) as

$$\begin{aligned} \int_0^{t_n} f(t')dt' &= \frac{\Delta t}{2}\Big[f_1 + 2f_2 + \cdots + 2f_{n-1} + f_n\Big], \\ \int_0^{t_n} f(t')dt' &= \Delta t\Big[\frac{1}{2}(f_n + f_1) + \sum_{j=2}^{n-1} f_j\Big], \end{aligned} \tag{4.4.21}$$

where $f_n = 0$ for the last panel as we discussed above and then (4.3.40) can be written as

$$\begin{aligned} u(r_m, t_n) = \int_{R(0)}^{\infty} u_0(r')\frac{1}{2\sqrt{\pi t_n}}e^{-\frac{(r_m - r')^2}{4t}}dr' + \Delta t\Bigg\{\frac{1}{2\sqrt{\pi}}\Bigg[u_1\frac{r_m - R_1}{2(t_n - t_1)} \\ - u_1\left(\frac{1}{R_1} + \epsilon\zeta_1\right) - \epsilon\zeta_1 R_1 - g u_1\zeta_1\left(\frac{u_1}{R_1} + 1\right)\Bigg]\frac{1}{\sqrt{t_n - t_1}}e^{-\frac{(r-R_1)^2}{4(t_n - t_1)}} \\ + \sum_{j=2}^{n-1}\frac{1}{2\sqrt{\pi}}\Bigg[u_j\frac{r - R_j}{2(t_n - t_j)} - u_j\left(\frac{1}{R_j} + \epsilon\zeta_j\right) - \epsilon\zeta_j R_j \\ - g u_j\zeta_j\left(\frac{u_j}{R_j} + 1\right)\Bigg]\frac{1}{\sqrt{t_n - t_j}}e^{-\frac{(r-R_j)^2}{4(t_n - t_j)}}\Bigg\}, \end{aligned} \tag{4.4.22}$$

where $t_1 = 0$.

4.5 Numerical Solution of Ordinary Differential Equation $(4.2.2)_5$

To solve numerically the ordinary differential equation $(4.2.2)_5$,

$$\frac{dR}{dt} = F(R, t),$$

where the right-hand side is a function of both R and t, we use the Modified Euler Method,

$$R_{j+1} = R_j + \frac{\triangle t}{2}\left[F(R_j, t_j) + F(\tilde{R}_j, t_j)\right], \tag{4.5.1}$$

where $j = 1, 2, \ldots, n-1$ and $\tilde{R}_j$ is obtained by using the Euler method, [4],

$$\tilde{R}_j = R_j + \triangle t F(R_j, t_j).$$

Then equation $(4.2.2)_5$ becomes

$$\begin{aligned} R_{j+1} =& R_j + \frac{\triangle t}{2}\left[\epsilon(C_0 - C_*)\zeta_j\left(\frac{U_j}{R_j} + 1\right)\right. \\ &\left. + \epsilon(C_0 - C_*)\zeta_j\left(\frac{U_j}{R_j + \triangle t\epsilon(C_0 - C_*)\zeta_j\left(\frac{U_j}{R_j} + 1\right)} + 1\right)\right]. \end{aligned} \tag{4.5.2}$$

By taking the last time step when $j = n - 1$, equation (4.5.2) becomes

$$\begin{aligned} R_n =& R_{n-1} + \frac{\triangle t}{2}\left[\epsilon(C_0 - C_*)\zeta_{n-1}\left(\frac{U_{n-1}}{R_{n-1}} + 1\right)\right. \\ &\left. + \epsilon(C_0 - C_*)\zeta_{n-1}\left(\frac{U_{n-1}}{R_{n-1} + \triangle t\epsilon(C_0 - C_*)\zeta_{n-1}\left(\frac{U_{n-1}}{R_{n-1}} + 1\right)} + 1\right)\right], \end{aligned} \tag{4.5.3}$$

where R_{n-1}, ζ_{n-1}, and U_{n-1} are known from the previous time step.

4.6 Comparison between the self-similar solution and the numerical solution

Next we validate the numerical algorithm of the initial boundary value problem for $C(r,t)$ and $R(t)$. We return to the original notations in the dimensional variables. We consider the problem with $\zeta(t) = \frac{1}{\sqrt{t}}$ and we use the self-similar solution as discussed in chapter 3, where $0 < t < t_0$, where t_0 is arbitrary. For

$t > t_0$ the problem is solved numerically with corresponding initial condition at $t = t_0$. We introduce a new variable $\tilde{t} = t - t_0$, see Figure 4.6.1, where the constant $t_0 > 0$ is the duration of the initial stage during which we use the self-similar solution, t_0 is considered as the time scale of the problem. The function $\zeta(t)$ can be written in term of the new variable $\tilde{t}$ as $\zeta(\tilde{t} + t_0) = \frac{1}{\sqrt{\tilde{t}+t_0}} = a(\tilde{t})$, where $\tilde{t} \geq 0$ is the numerical time and $a(\tilde{t})$ is a given function. The self-similar solution is also valid for $t > t_0$. In order to validate the numerical algorithm, we solve the problem (4.1.1) with t changed to $\tilde{t}$ and $\zeta(t)$ changed to $a(\tilde{t})$ numerically for $\tilde{t} > 0$ with an appropriate matching conditions at $\tilde{t} = 0$. This numerical solution should be close to the self-similar solution of chapter 3 with the difference between the numerical and self-similar solution being a measure of accuracy of the numerical algorithm.

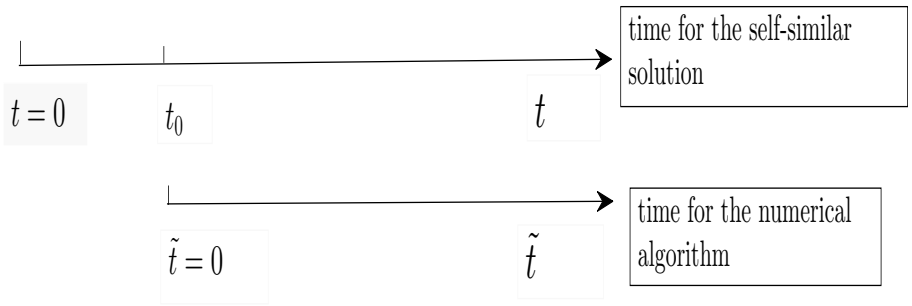

Figure 4.6.1: The self-similar solution time and the numerical time.

The dimensional problem for $\tilde{t} > 0$ is:

$$
\begin{cases}
\frac{\partial C}{\partial \tilde{t}} = \frac{D}{r^2}\frac{\partial}{\partial r}\left(r^2\frac{\partial C}{\partial r}\right) & r \geq R(\tilde{t}), \tilde{t} > 0, \\
C(r,0) = f(\frac{r}{\sqrt{Dt_0}}) & r \geq R(0), \\
C(r,\tilde{t}) \longrightarrow C_0 & \text{as } r \longrightarrow \infty, \\
\frac{\partial C}{\partial r} = k_1 a(\tilde{t})(C - C_*) & \text{on } r = R(\tilde{t}), \\
\frac{dR}{d\tilde{t}} = D\frac{\partial C}{\partial r} & \text{on } r = R(\tilde{t}), \\
R(\tilde{t}=0) = \lambda\sqrt{Dt_0}, &
\end{cases}
\tag{4.6.1}
$$

where $C(r,\tilde{t})$ denotes the wax concentration in the oil, the time $\tilde{t} = t - t_0$, r is the radial distance from the centre of the wax particle, and k_1, C_0 are constant coefficients, the function $f(\xi)$ in the initial condition $(4.6.1)_2$ is given by the self-similar solution (3.3.30). We use here the non-dimensional variables introduce in section 4.2 to obtain:

$$
\begin{cases}
\frac{\partial \bar{C}}{\partial \bar{t}} = \frac{1}{\bar{r}^2}\frac{\partial}{\partial \bar{r}}\left(\bar{r}^2\frac{\partial \bar{C}}{\partial \bar{r}}\right) & \bar{r} \geq \bar{R}(\bar{t}), \bar{t} > 0, \\
\bar{C}(\bar{r}, 0) = f(\bar{r}) & \bar{r} \geq \bar{R}(0), \\
\bar{C}(\bar{r}, \bar{t}) \longrightarrow 0 & \text{as } \bar{r} \longrightarrow \infty, \\
\frac{\partial \bar{C}}{\partial \bar{r}} = \epsilon \bar{a}(\bar{t})(\bar{C} + 1) & \text{on } \bar{r} = \bar{R}(\bar{t}), \\
\frac{d\bar{R}}{d\bar{t}} = (C_0 - C_*)\frac{\partial \bar{C}}{\partial \bar{r}} & \text{on } \bar{r} = \bar{R}(\bar{t}), \\
\bar{R}(0) = \lambda,
\end{cases}
\tag{4.6.2}
$$

where $\epsilon = k_1\sqrt{D}$. The self-similar solution of (4.6.2) was obtained in chapter 3. This solution is given by equation (3.3.32), which is the concentration as a function of distance from the surface of the wax particle, $C = f(\xi)$, where $\xi = \frac{r}{\sqrt{Dt}}$. By using the non-dimensional variables of section 4.2 and changing the time t to the non-dimensional numerical time $t = t_0 + t_0\bar{t}$, we find

$$
\bar{C} = \bar{f}(\xi) = \bar{f}\left(\frac{r}{\sqrt{Dt}}\right) = \bar{f}\left(\frac{\bar{r}\sqrt{Dt_0}}{\sqrt{D(t_0 + t_0\bar{t})}}\right) = \bar{f}\left(\frac{\bar{r}}{\sqrt{\bar{t}+1}}\right) \tag{4.6.3}
$$

From chapter 3, we have:

$$
\bar{f}\left(\frac{\bar{r}}{\sqrt{\bar{t}+1}}\right) = \frac{-\lambda^3 e^{\frac{\lambda^2}{4}}}{2(C_0 - C_*)}\left[\frac{e^{-\frac{\bar{r}^2}{4(\bar{t}+1)}}\sqrt{\bar{t}+1}}{\bar{r}} - \frac{\sqrt{\pi}}{2}\text{erfc}\left(\frac{\bar{r}}{2\sqrt{\bar{t}+1}}\right)\right].
$$

Initially $\bar{t} = 0$ and then equation (4.6.3) leads to the initial condition for the numerical solution,

$$
\bar{C}(\bar{r}, 0) = \bar{f}(\bar{r}), \tag{4.6.5}
$$

where

$$\bar{f}(\bar{r}) = \frac{-\lambda^3 e^{\frac{\lambda^2}{4}}}{2(C_0 - C_*)} \left[\frac{e^{-\frac{r^2}{4}}}{r} - \frac{\sqrt{\pi}}{2} \text{erfc}\left(\frac{r}{2}\right) \right]$$

The functions $\bar{a}(\bar{t})$ and $\bar{R}(\bar{t})$ have the following non-dimensional forms,

$$\bar{a}(\bar{t}) = \frac{1}{\sqrt{\bar{t}+1}}, \qquad \text{and} \qquad \bar{R}(\bar{t}) = \lambda\sqrt{\bar{t}+1}.$$

We simplify the problem (4.6.2) by letting $u(\bar{r},\bar{t}) = \bar{r}\bar{C}(\bar{r},\bar{t})$ and substituting it into equation $(4.6.2)_1 - (4.6.2)_5$, then the problem becomes (drop the bars)

$$\begin{cases} u_t = u_{rr} \qquad r \geq R(t), t \geq 0, \\ \\ u(r,0) = rf(r) = u_0(r), \\ \\ u(r,t) \longrightarrow 0 \qquad \text{as } r \longrightarrow \infty, \\ \\ u_r = \frac{u}{R(t)}\left[1 + \epsilon a(t) R(t)\right] + \epsilon a(t) R(t) \qquad \text{on } \ r = R(t), \\ \\ \frac{dR}{dt} = \epsilon(C_0 - C_*) a(t) \left(\frac{u}{R(t)} + 1\right) \qquad \text{on } r = R(t), \\ \\ R(0) = \lambda, \end{cases} \tag{4.6.6}$$

where $u_0(r)$ comes from the self-similar solution. In this section we compare the self-similar solution (3.3.30) with the numerical solution of the problem (4.6.6) by the method of section 4.4 and 4.5.

Now we rewrite the boundary integral equation (4.4.6) after substituting $a(t)$ as:

$$\begin{aligned} U_n =& F(t_n) + \frac{1}{2\sqrt{\pi}} \int_0^{t_n} \left[U(t') \frac{R_n - R(t')}{2(t_n - t')} - g a(t') \left(\frac{U(t')}{R(t')} + 1 \right) U(t') \right. \\ & \left. - \left(\frac{1}{R(t')} + \epsilon a(t') \right) U(t') - \epsilon a(t') R(t') \right] e^{-\frac{(R_n - R(t'))^2}{4(t_n - t')}} \frac{dt'}{\sqrt{t_n - t'}}, \end{aligned} \tag{4.6.7}$$

where

$$F(t_n) = \frac{-\lambda^3 e^{\frac{\lambda^2}{4}}}{2\sqrt{\pi t}(C_0 - C_*)} \int_{R(0)}^{\infty} \left[e^{-\frac{r'^2}{4}} - r' \frac{\sqrt{\pi}}{2} \text{erfc}\left(\frac{r'}{2}\right) \right] e^{-\frac{(R_n - r')^2}{4t_n}} dr'. \quad (4.6.8)$$

The integral above cannot be evaluated in terms of elementary functions. We approximate the integrand using a piecewise linear approximation. By making a piecewise linear approximation to $e^{-\frac{r'^2}{4}}$, $\text{erfc}\left(\frac{r'}{2}\right)$, and $e^{-\frac{(R_n - r')^2}{4t_n}}$ inside the integral, $r_j < r' < r_{j+1}$:

$$e^{-\frac{r'^2}{4}} = e^{-\frac{r_j^2}{4}} + \left[e^{-\frac{r_{j+1}^2}{4}} - e^{-\frac{r_j^2}{4}} \right] \frac{r' - r_j}{r_{j+1} - r_j}, \quad (4.6.9)$$

$$\text{erfc}\left(\frac{r'}{2}\right) = \text{erfc}\left(\frac{r_j}{2}\right) + \left[\text{erfc}\left(\frac{r_{j+1}}{2}\right) - \text{erfc}\left(\frac{r_j}{2}\right) \right] \frac{r' - r_j}{r_{j+1} - r_j}, \quad (4.6.10)$$

$$e^{-\frac{(R_n - r')^2}{4t_n}} = e^{-\frac{(R_n - r_j)^2}{4t_n}} + \left[e^{-\frac{(R_n - r_{j+1})^2}{4t_n}} - e^{-\frac{(R_n - r_j)^2}{4t_n}} \right] \frac{r' - r_j}{r_{j+1} - r_j}, \quad (4.6.11)$$

where r' defined as

$$r' = r_j + \xi(r_{j+1} - r_j), \qquad 0 \le \xi \le 1.$$

We substitute equations (4.6.9)-(4.6.11) into (4.6.8) and we sum up the intervals over j from 1 until the result does not change any more, see Figure 4.6.2. Then equation (4.6.8) written as

$$\begin{aligned} F(t_n) = & \frac{-\lambda^3 e^{\frac{\lambda^2}{4}}}{2\sqrt{\pi t}(C_0 - C_*)} \sum_{j=1}^{m} \int_0^1 \left[e^{-\frac{r_j^2}{4}} + \xi \left(e^{-\frac{r_{j+1}^2}{4}} - e^{-\frac{r_j^2}{4}} \right) \right. \\ & - \frac{\sqrt{\pi}}{2} [r_j + \xi(r_{j+1} - r_j)] \left(\text{erfc}\left(\frac{r_j}{2}\right) + \xi \left[\text{erfc}\left(\frac{r_{j+1}}{2}\right) - \text{erfc}\left(\frac{r_j}{2}\right) \right] \right) \\ & \left. \left(e^{-\frac{(R_n - r_j)^2}{4t_n}} + \xi \left[e^{-\frac{(R_n - r_{j+1})^2}{4t_n}} - e^{-\frac{(R_n - r_j)^2}{4t_n}} \right] \right) \right] (r_{j+1} - r_j) d\xi. \end{aligned} \quad (4.6.12)$$

The boundary integral equation (4.6.7) is solved numerically by the method of section 4.4.

The concentration on the boundary $U(t)$ at $r = R(t) = \lambda\sqrt{t+1}$, from the self-similar solution is:

$$U(t) = \frac{-\lambda^3 e^{\frac{\lambda^2}{4}}}{2(C_0 - C_*)} \left[e^{-\frac{\lambda^2}{4}} \sqrt{t+1} - \lambda \frac{\sqrt{\pi}}{2} \text{erfc}\left(\frac{\lambda}{2}\right) \right]. \quad (4.6.13)$$

Also, we rewrite equation (4.3.40) in the fluid after substituting $u_0(r)$ from the self-similar solution as

$$\begin{aligned} u(r,t) =& \frac{-\lambda^3 e^{\frac{\lambda^2}{4}}}{4(C_0 - C_*)\sqrt{\pi t}} \int_{R(0)}^{\infty} \left[e^{-\frac{r'^2}{4}} - r' \frac{\sqrt{\pi}}{2} \text{erfc}\left(\frac{r'}{2}\right) \right] e^{-\frac{(r-r')^2}{4t}} dr' \\ &+ \frac{1}{2\sqrt{\pi}} \int_0^t \left[U(t') \frac{r - R(t')}{2(t-t')} - \frac{U(t')}{R(t')} \left[1 + \epsilon a(t') R(t') \right] - \epsilon a(t') R(t') \right. \\ &\left. - gU(t') a(t') \left(\frac{U(t')}{R(t')} + 1 \right) \right] \frac{1}{\sqrt{t-t'}} e^{-\frac{(r-R(t'))^2}{4(t-t')}} dt'. \end{aligned} \tag{4.6.14}$$

The first integral in (4.6.14) is evaluated numerically. The function in the square brackets,

$$M(r') = e^{-\frac{r'^2}{4}} - r' \frac{\sqrt{\pi}}{2} \text{erfc}\left(\frac{r'}{2}\right), \tag{4.6.15}$$

is plotted in Figure 4.6.2. We can see that the function quickly decreases from 1 to $O(10^{-4})$ as r' increases from 0 to 4.

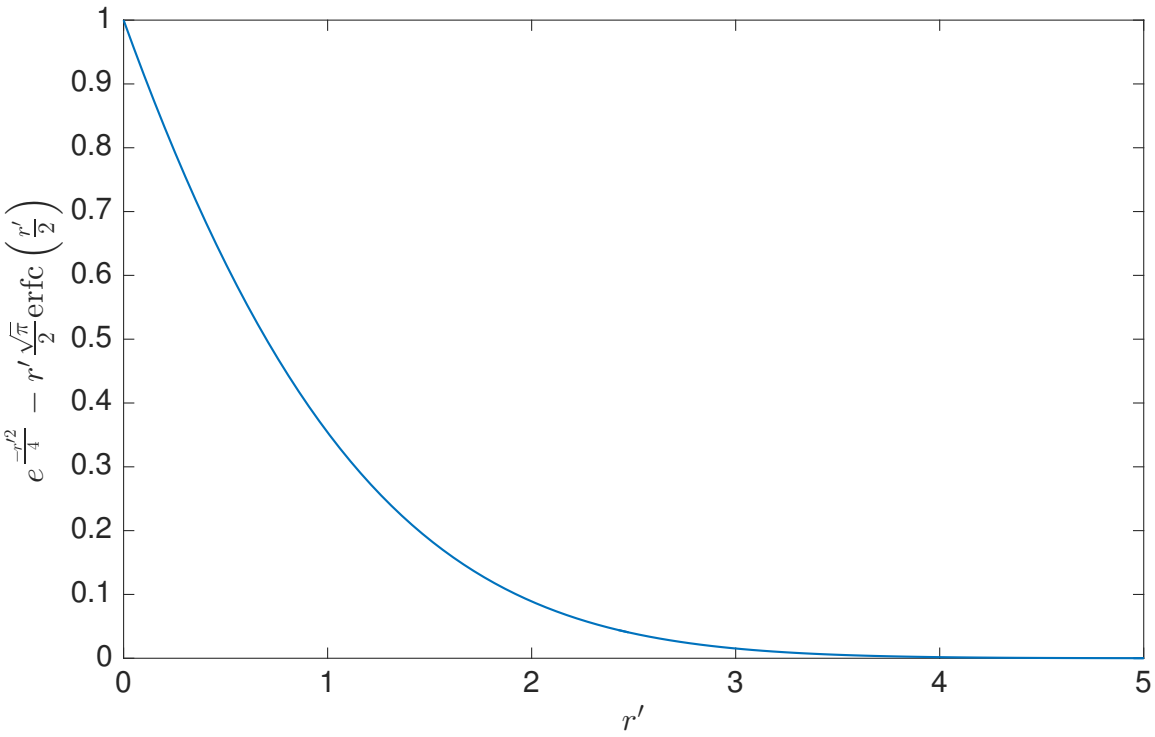

Figure 4.6.2: The function $M(r')$ given by (4.6.15).

We write the first term in (4.6.14) as

$$F(r,t) = \frac{-\lambda^3 e^{\frac{\lambda^2}{4}}}{4(C_0 - C_*)\sqrt{\pi t}} \int_{R(0)}^{\infty} \left[e^{-\frac{r'^2}{4}} - r' \frac{\sqrt{\pi}}{2} \text{erfc}\left(\frac{r'}{2}\right) \right] e^{-\frac{(r-r')^2}{4t}} dr'. \tag{4.6.16}$$

We use a substitution to avoid the numerically extreme behaviour of the exponential in the integrand, as r' increases. We introduce a new variable of integration σ which is related to r' by the equation $\sigma = -\frac{(r-r')}{2\sqrt{t}}$. Then $r' = r + 2\sqrt{t}\sigma$ and $dr' = 2\sqrt{t}d\sigma$. The function $M(r')$ decreases as shown in Figure 4.6.2, so we truncate the upper limit in (4.6.16) of its argument to 5. Then the function $F(r,t)$ in (4.6.16) after truncating the upper limit in r' to 5 and using σ, reads

$$F(r,t) = \frac{-\lambda^3 e^{\frac{\lambda^2}{4}}}{2(C_0 - C_*)\sqrt{\pi}} \int_{\frac{R(0)-r}{2\sqrt{t}}}^{\frac{5-r}{2\sqrt{t}}} M(r + 2\sqrt{t}\sigma) e^{-\sigma^2} d\sigma. \tag{4.6.17}$$

The integral in (4.6.17) has no closed form expression and it is evaluated by using the trapezoidal rule.

We have equation (4.4.22) which is for the concentration as a function of time and the distance from the surface of the wax particle. We know that $u(r,t) = r\bar{C}(r,t)$ and then the concentration in the fluid is

$$C(r,t) = C_0 + (C_0 - C_*)\bar{C}(\bar{r},\bar{t}),$$

where $\bar{C} = \frac{u(r,t)}{r}$, then we can write

$$C(r,t) = C_0 + (C_0 - C_*)\frac{u(r,t)}{r}. \tag{4.6.18}$$

Substituting equation (4.4.22) into (4.6.18), where $\delta(t) = a(t)$, we obtain the concentration in the fluid as discussed in (4.4.22)

$$C(r_m,t_n) = C_0 + (C_0 - C_*)\frac{F(r_m,t_n)}{r_m} + \Delta t\frac{(C_0 - C_*)}{r_m}\Bigg\{\frac{1}{2\sqrt{\pi}}\Bigg[U_1\frac{r_m - R_1}{2(t_n - t_1)}$$
$$- U_1\left(\frac{1}{R_1} + \epsilon a_1\right) - \epsilon a_1 R_1 - gU_1 a_1\left(\frac{U_1}{R_1} + 1\right)\Bigg]\frac{1}{\sqrt{t_n - t_1}}e^{-\frac{(r_m - R_1)^2}{4(t_n - t_1)}}$$
$$+ \sum_{j=2}^{n-1}\frac{1}{2\sqrt{\pi}}\Bigg[U_j\frac{r_m - R_j}{2(t_n - t_j)} - U_j\left(\frac{1}{R_j} + \epsilon a_j\right) - \epsilon a_j R_j$$
$$- gU_j a_j\left(\frac{U_j}{R_j} + 1\right)\Bigg]\frac{1}{\sqrt{t_n - t_j}}e^{-\frac{(r_m - R_j)^2}{4(t_n - t_j)}}\Bigg\} \tag{4.6.19}$$

where U_n is computed from equation (4.6.7).

In chapter 3 we derived the concentration in the fluid,

$$C(r,t) = C_0 - \frac{\lambda^3 e^{-\frac{r^2}{4\sqrt{t+1}}}e^{\frac{\lambda^2}{4}}\sqrt{t+1}}{2r} + \frac{\lambda^3\sqrt{\pi}e^{\frac{\lambda^2}{4}}}{4}\text{erfc}\left(\frac{r}{2\sqrt{t+1}}\right). \tag{4.6.20}$$

To validate the numerical algorithm for the concentration $C(r,t)$, we compare (4.6.19) with the analytical expression for the concentration from the self-similar solution (4.6.20).

4.7 Numerical results

In this section we compute numerically the wax concentration on the boundary of the wax particle, $r = R(t)$, the concentration in the fluid, $r > R(t)$, and the wax particle radius. We compare these numerical results with the analytical results from the previous chapter. The initial conditions of the numerical solution come from the self-similar solution of the previous chapter. In this computation, the values of C_0, C_*, and k_1 are taken from Table 3.1. The main steps of the numerical algorithm for predicting the growth of spherical wax particle, concentration on the boundary, and the concentration on the oil are the following:

1- Specify the initial data of the problem;

2- Select time step of integration Δt;

3- By using the values of $U(t)$ and $R(t)$ at previous time steps, calculate simultaneously the concentration on the boundary, $U(t + \Delta t)$, and the growth of the wax particle radius, $R(t + \Delta t)$, at current time step;

4- Calculate the concentration in the fluid at discrete values of the radial coordinate, r, for the current time step.

5- Return to 3 for next time step.

Computations are performed by our own code as it is explained above. Here we summarise the numerical algorithm in brief. We use a Green function to obtain the boundary integral equation (4.4.6). The boundary integral equation on the moving surface of the wax particle, $r = R(t)$, is solved numerically by a time-stepping numerical method. First we discretize the time into equal steps, $\Delta t > 0$. We have a singularity in (4.4.6) when $t' \to t_n$, we use equa-

tions (4.4.5) and (4.3.31) to avoid this singularity. The forcing term in (4.4.6) is evaluated numerically by approximating the integrand by piecewise linear functions. Equation (4.4.6) is reduced to a quadratic equation with coefficients a, b, and c, the solution of which is computed by Matlab. The ordinary differential equation for the radius $R(t)$ is solved using modified Euler method as discussed in section 4.5 and equation (4.5.3) is solved using Matlab. Figures 4.7.1 and 4.7.2 show the comparison between the numerical solution of equation (4.6.7) and the exact solution (4.6.13) for $U(t)$ as a function of time. The time step in computation is chosen as $\Delta t = 10^{-4}$. It is seen that the numerical solution and the exact solution are indistinguishable. In Figure 4.7.2 the time interval is longer.

Figures 4.7.3 and 4.7.4 show the comparison between the numerical solution (4.5.3) and the exact solution for the radius $R(t) = \lambda\sqrt{t+1}$. We see in Figures 4.7.3 and 4.7.4 that the wax particle absorbs particles from the solution and then the radius of the wax particle grows as the time increases. In Figure 4.7.3 the time interval is $[0, 0.1]$ and in Figure 4.7.4 the time interval is longer, $0 < t < 10$.

The wax concentration in the fluid, where $r > R(t)$, is given by equation (4.3.40). We evaluate this equation by using the trapezoidal rule as shown in equation (4.4.22). Figures 4.7.5, 4.7.6, and 4.7.7, show the comparison between the numerical, equation (4.6.19), and exact, equation (4.6.20), wax concentrations $C(r, t)$ as functions of the distance from the surface of the wax particle. We can see that the concentration at the surface of the wax particle is lower than the concentration at infinity. The wax molecules are absorbed by the surface of the wax particle. This leads to a reduced concentration of the wax molecules near the surface of the wax particle. The reduced concentration

gives rise to the mass flux of wax molecules towards the growing wax particle. Figure 4.7.8 shows the comparison between the numerical result for equation (4.6.19), and the exact result from equation (4.6.20), wax concentrations $C(r,t)$ as functions of the distance from the surface of the wax particle when $t = 5$.

Figures 4.7.9 and 4.7.10 show the difference in the numerical and analytical results for larger time step. Our numerical solution is an approximate solution and it becomes closer to the analytical solution with decrease of the time step. But we can not expect that our piecewise linear approximations of unknown functions and the trapezoidal rule provide a good approximation to the analytical solution if we take a longer time step as shown in Figures 4.7.9 and 4.7.10. So, our approximation is accurate for small enough time step and is rough for relatively large time step.

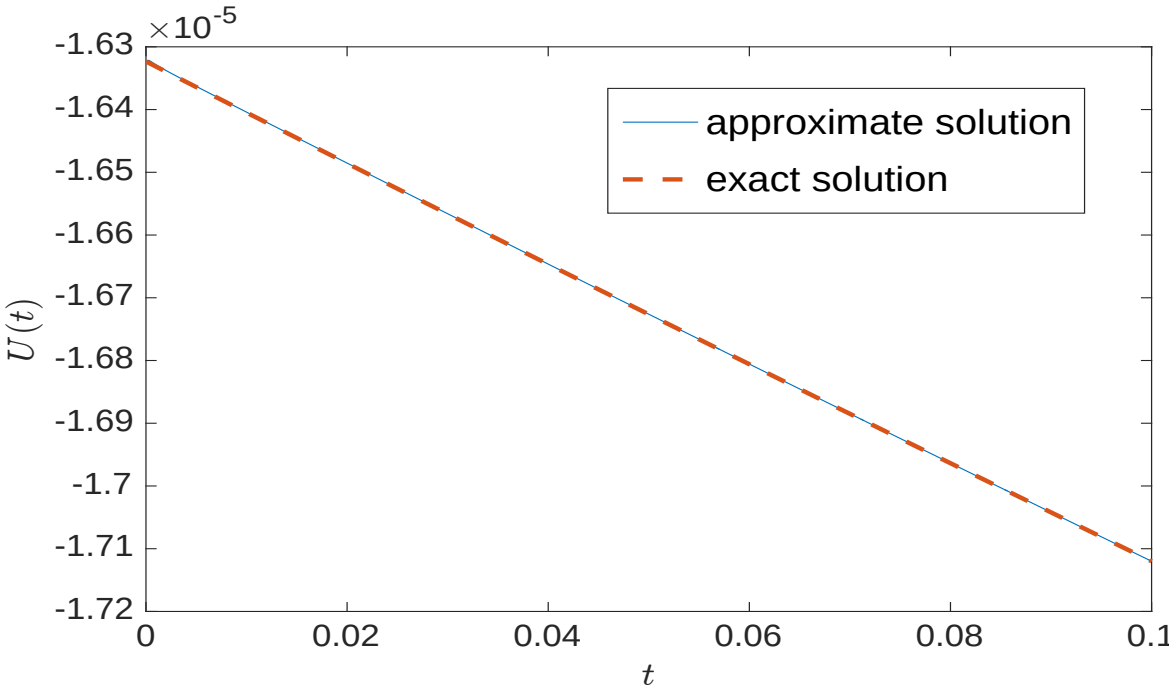

Figure 4.7.1: Comparison between the exact solution (4.6.13) and the numerical solution (4.4.12) for the function $U(t)$, where $\lambda = 0.01$. For this computation $\Delta t = 10^{-4}$.

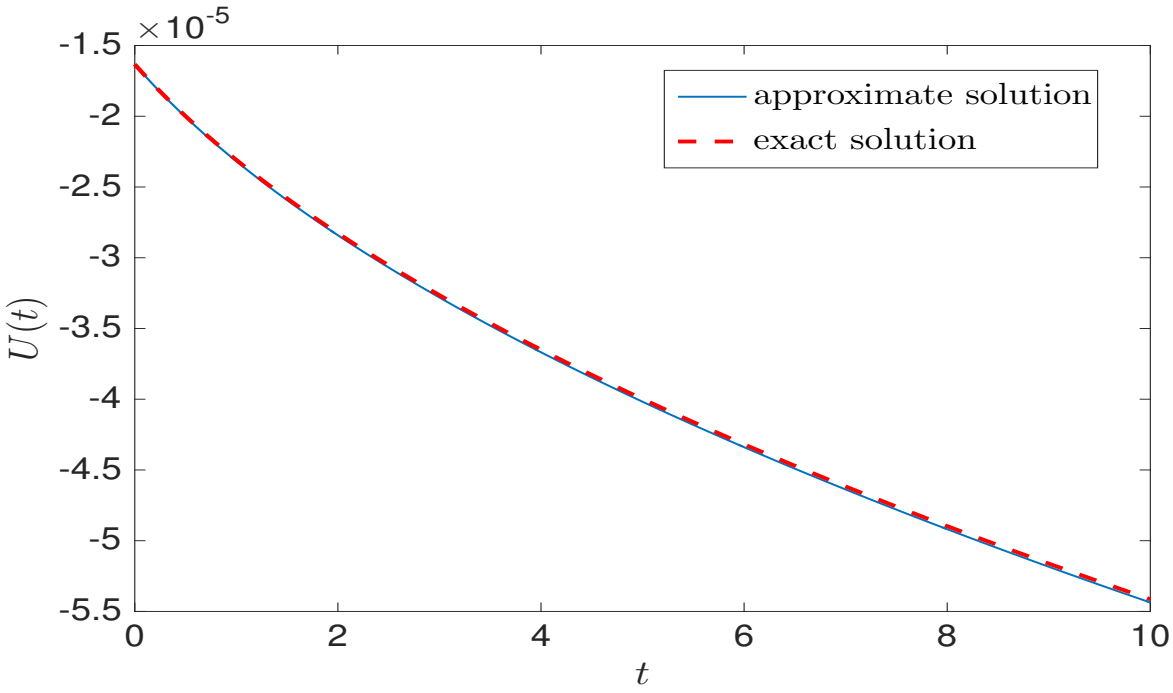

Figure 4.7.2: Comparison between the exact solution (4.6.13) and the numerical solution (4.4.20) for the function $U(t)$, where $\lambda = 0.1$.

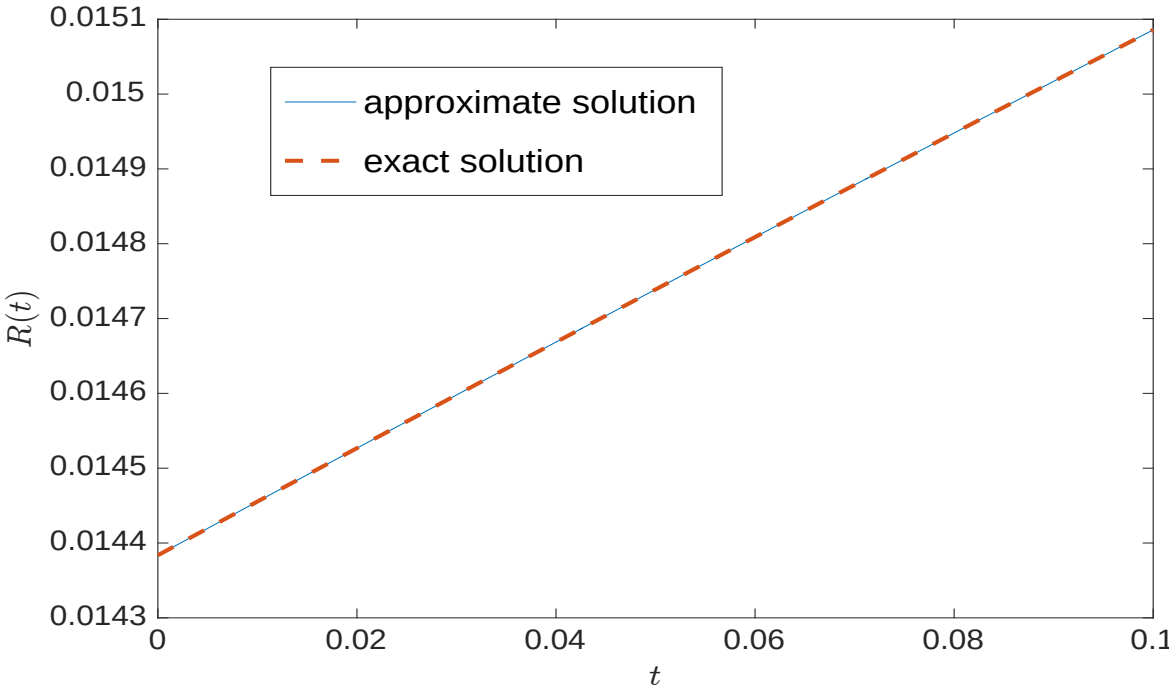

Figure 4.7.3: Comparison between the exact solution $R(t) = \lambda\sqrt{t+1}$ and the numerical solution (4.5.3) for the wax particle radius as a function of dimensionless time. For this computation $\Delta t = 10^{-4}$.

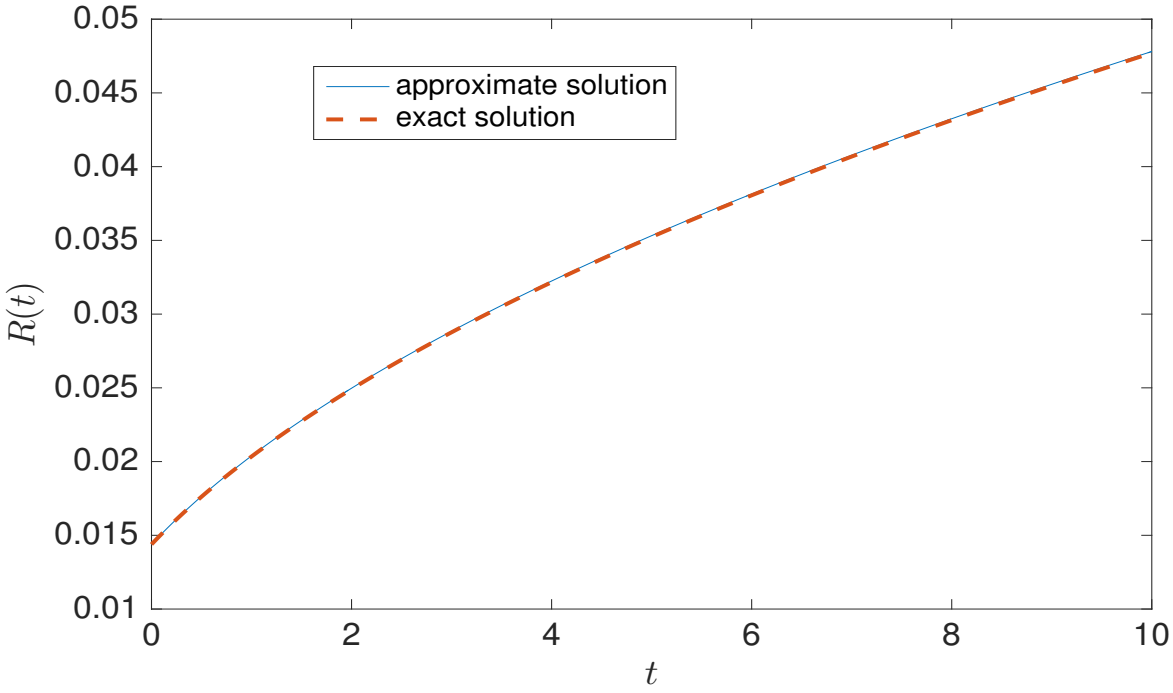

Figure 4.7.4: Comparison between the exact solution $R(t) = \lambda\sqrt{t+1}$ (dashed curve) and the numerical solution (4.5.3) (solid curve) for the wax particle radius as a function of dimensionless time.

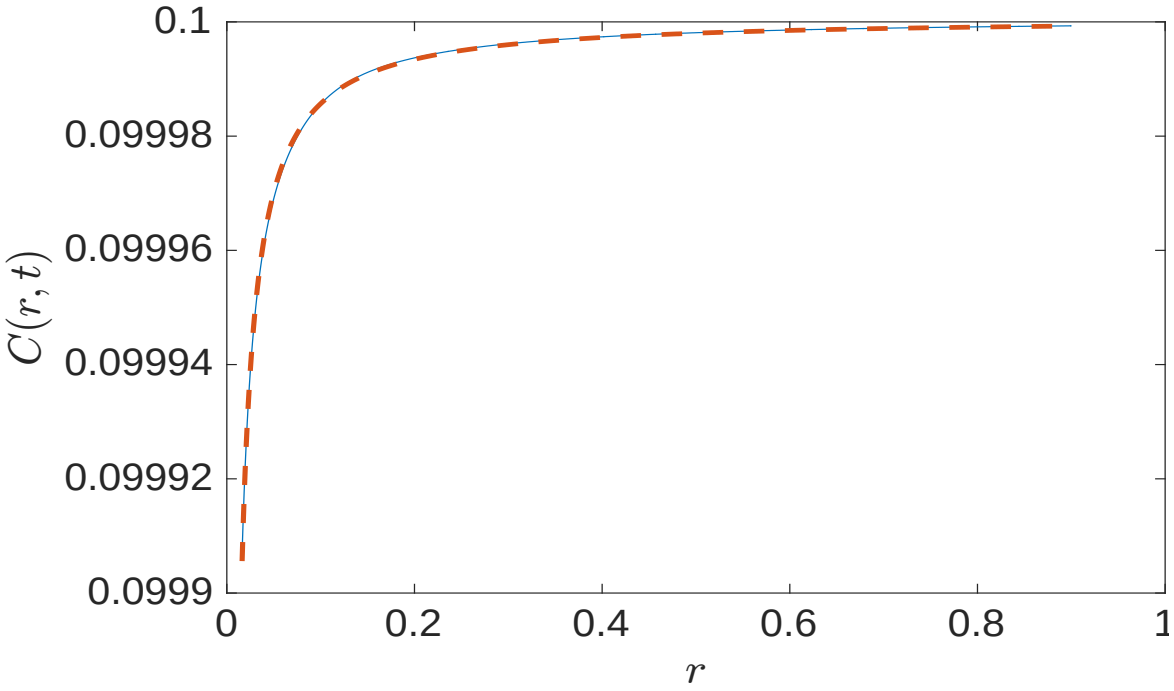

Figure 4.7.5: Comparison between the exact solution (4.6.20) for the concentration in the fluid $C(r,t)$ and the numerical solution (4.6.19) at $t = 0.1$. In this computation the time step is $\Delta t = 10^{-4}$.

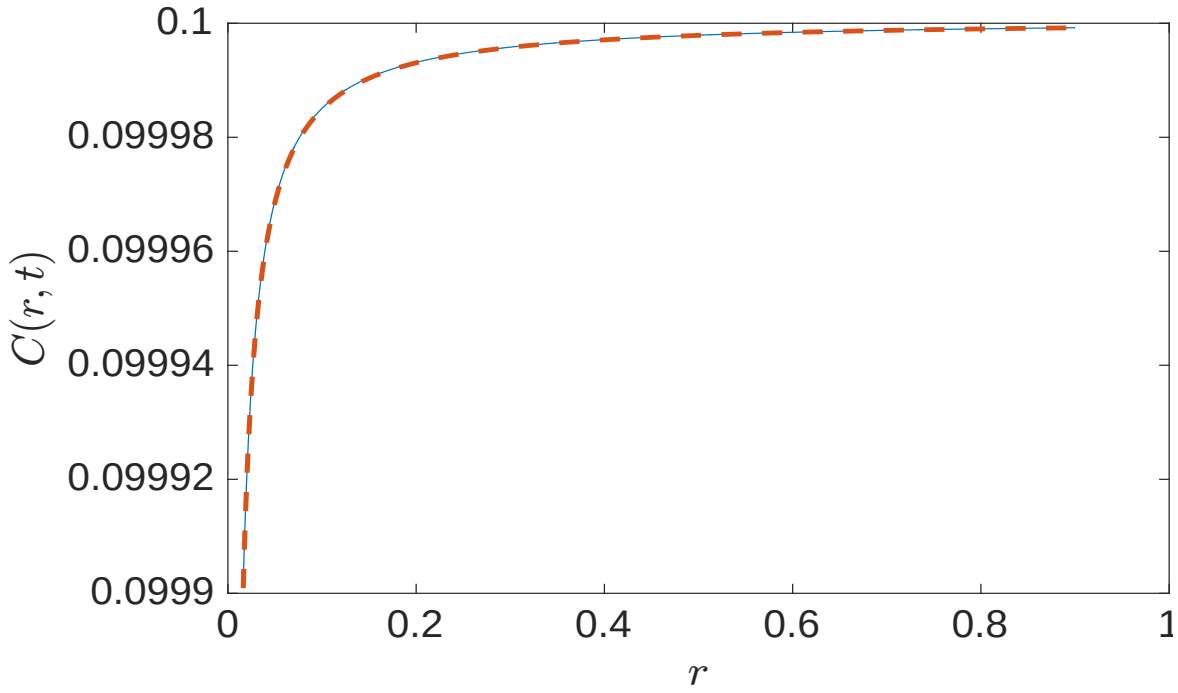

Figure 4.7.6: The same as in Figure 4.7.5 but for $t = 0.2$.

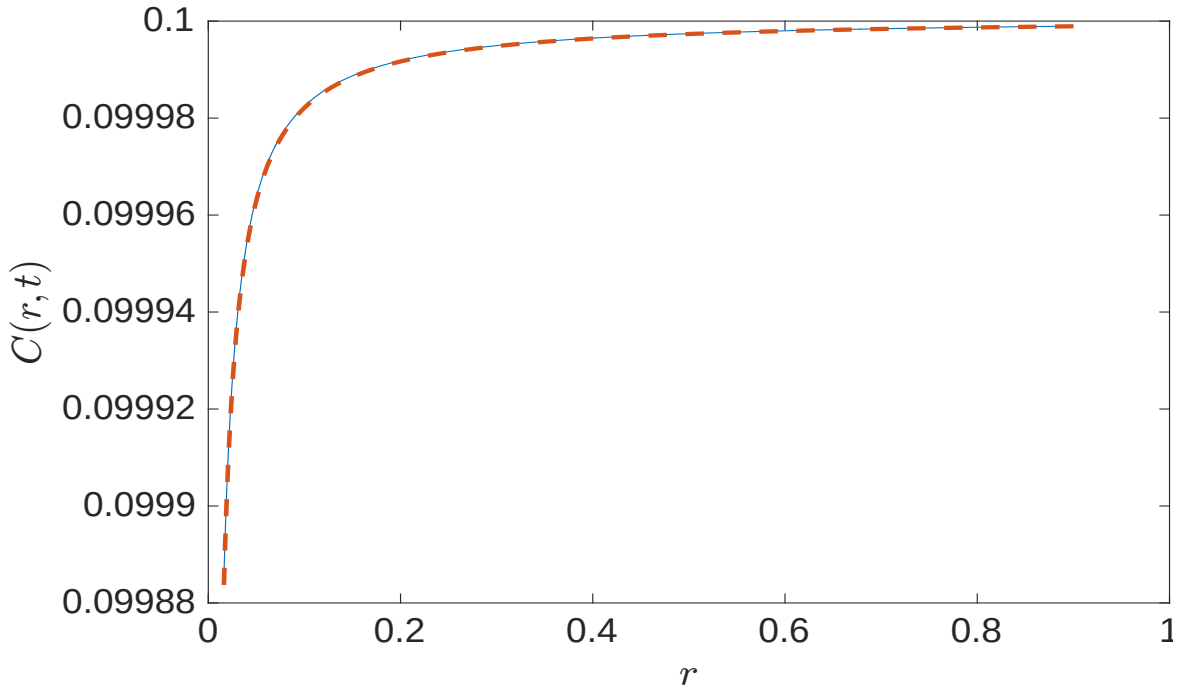

Figure 4.7.7: The same as in Figure 4.7.5 but for $t = 0.7$.

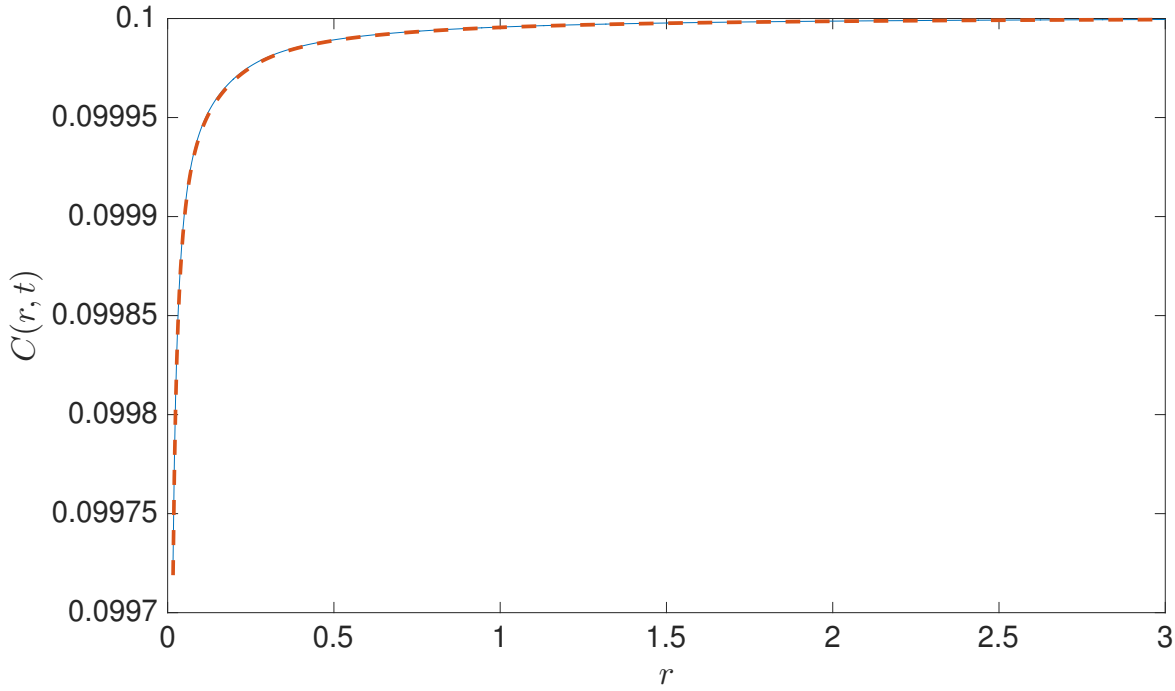

Figure 4.7.8: Comparison between the exact solution (4.6.20) for the concentration in the fluid $C(r,t)$ and the numerical solution (4.6.19) at $t = 5$.

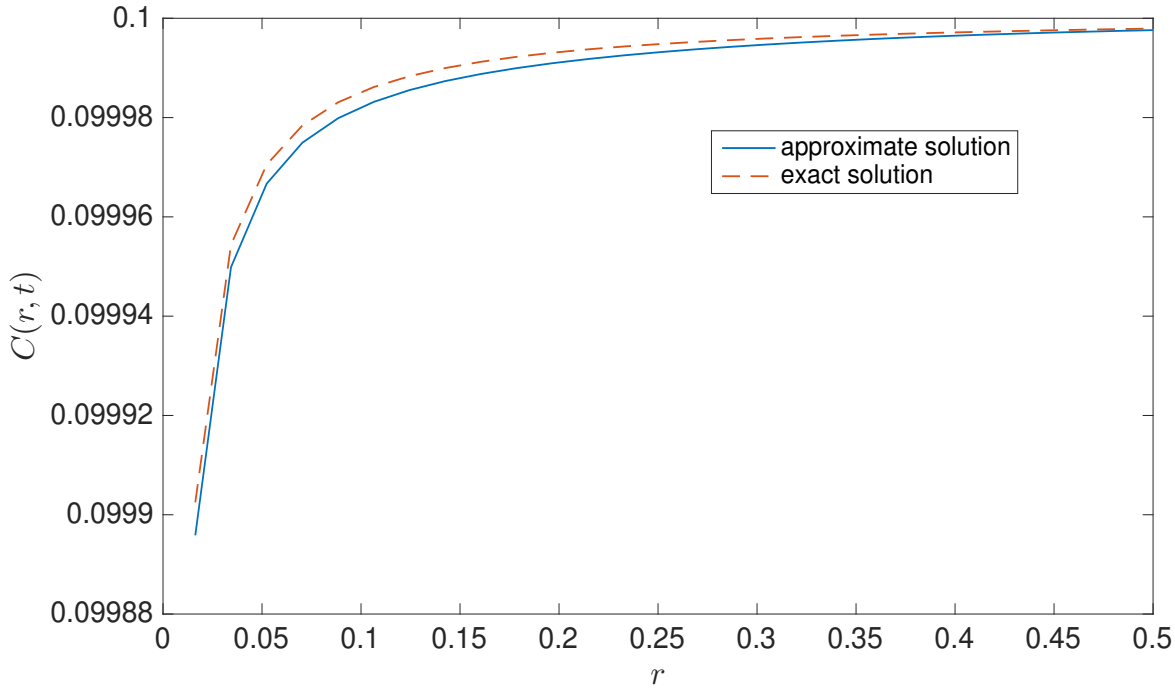

Figure 4.7.9: The same as in Figure 4.7.5 but for $t = 0.17$ and $\Delta t = 0.2$.

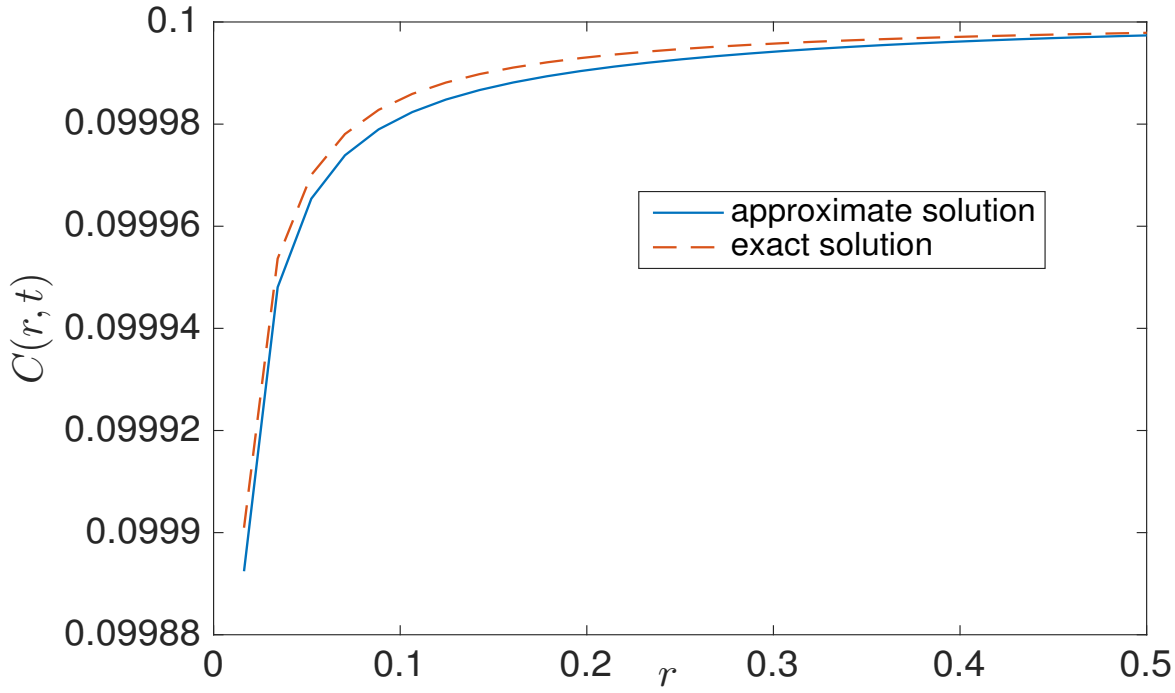

Figure 4.7.10: The same as in Figure 4.7.5 but for $t = 0.21$ and $\Delta t = 0.2$.

4.8 Problem for a single spherical wax particle with constant mass transfer coefficient

In this section we consider the initial boundary value problem of a wax particle (3.2.8)-(3.2.12), see chapter 3, with constant mass transfer coefficient k_r. The problem in chapter 3 was considered for a special dependence with respect to time of the mass transfer coefficient, $k_r(t) = Dk_1\zeta(t)$. In this section, we consider the problem with constant mass transfer coefficient by using new scaled variables. The dimensional problem is:

$$\begin{cases} \frac{\partial C}{\partial t} = \frac{D}{r^2}\frac{\partial}{\partial r}\left(r^2\frac{\partial C}{\partial r}\right) & r \geq R(t), t > 0, \\ C(r,0) = C_0 & r \geq R(0), \\ C(r,t) \longrightarrow C_0 & \text{as } r \longrightarrow \infty, \\ D\frac{\partial C}{\partial r} = k_r(C - C_*) & \text{on } r = R(t), \\ \frac{dR}{dt} = D\frac{\partial C}{\partial r} & \text{on } r = R(t), \\ R(t=0) = R_0. \end{cases} \tag{4.8.1}$$

We write the problem (4.8.1) using the following non-dimensional variables:

$$\hat{r} = \frac{r}{R_0}, \qquad \hat{t} = \frac{t}{T}, \qquad \hat{R}(\hat{t}) = \frac{R(t)}{R_0}, \qquad \hat{C}(\hat{r},\hat{t}) = \frac{C(r,t) - C_0}{(C_0 - C_*)},$$

where $T = \frac{R_0^2}{D}$ is the timescale. Note that the dimensionless variables in this

section are different from the dimensionless variables in section 4.2 because section 4.2 was intended to compare the numerical solution with the self-similar solution of chapter 3. Now we consider another case. In this section, the mass transfer coefficient k_r is constant. Using the non-dimensional variables above, we can write the problem (after dropping hats) as:

$$\begin{cases} \frac{\partial C}{\partial t} = \frac{1}{r^2}\frac{\partial}{\partial r}\left(r^2\frac{\partial C}{\partial r}\right) \qquad r \geq R(t), t > 0 \\ \\ C(r,0) = 0 \qquad r \geq R(0), \\ \\ C(r,t) \longrightarrow 0 \qquad \text{as} \qquad r \longrightarrow \infty, \\ \\ \frac{\partial C}{\partial r} = k_r\left[C+1\right] \qquad \text{on } r = R(t), \\ \\ \frac{dR}{dt} = (C_0 - C_*)\frac{\partial C}{\partial r} \qquad \text{on } r = R(t), \\ \\ R(0) = 1 \qquad \text{when } t = 0, \end{cases} \tag{4.8.2}$$

where $\hat{k_r} = \frac{k_r R_0}{D}$. We simplify the problem (4.8.2) by using $u(r,t) = rC(r,t)$

$$
\begin{cases}
u_t = u_{rr} \qquad r \geq R(t), t \geq 0, \\
u(r,0) = 0, \\
u(r,t) \longrightarrow 0 \qquad \text{as} \qquad r \longrightarrow \infty, \\
u_r = \frac{u}{R(t)}\left[1 + k_r R(t)\right] + k_r R(t) \qquad \text{on} \quad r = R(t), \\
\frac{dR}{dt} = k_r(C_0 - C_*)\left(\frac{u}{R(t)} + 1\right) \qquad \text{on } r = R(t), \\
R(0) = 1.
\end{cases} \tag{4.8.3}
$$

The same numerical algorithm as that described in section 4.4 is used. We use equation (4.4.3) with $u_0(r) = 0$, then we have the following boundary-integral equation

$$
U_n = \frac{1}{\sqrt{\pi}} \int_0^{t_n} \left[U(t') \frac{R_n - R(t')}{2(t_n - t')} - S(t') - U(t') \frac{dR}{dt}(t') \right] \frac{1}{\sqrt{t_n - t'}} e^{-\frac{(R_n - R(t'))^2}{4(t_n - t')}} dt', \tag{4.8.4}
$$

where $S(t') = u_r(R(t'), t')$ and $U(t') = u(R(t'), t')$.

We substitute the boundary conditions $(4.8.3)_4$ and $(4.8.3)_5$ into the integral equation (4.8.4), to obtain

$$
\begin{aligned}
U_n = \frac{1}{\sqrt{\pi}} \int_0^{t_n} \Bigg[& U(t') \frac{R_n - R(t')}{2(t_n - t')} - g\left(\frac{U(t')}{R(t')} + 1\right) U(t') - \left(\frac{1}{R(t')} + k_r\right) U(t') \\
& - k_r R(t') \Bigg] \frac{1}{\sqrt{t_n - t'}} e^{-\frac{(R_n - R(t'))^2}{4(t_n - t')}} dt',
\end{aligned} \tag{4.8.5}
$$

where $g = k_r(C_0 - C_*)$.

Also, we can apply the same numerical treatment as above for the radius $R(t)$. We use the discretized evolution equation (4.5.3) with constant coefficients k_r,

C_0, and C_*:

$$R_n = R_{n-1} + \frac{\triangle t}{2}\left[k_r(C_0 - C_*)\left(\frac{U_{n-1}}{R_{n-1}} + 1\right) + k_r(C_0 - C_*)\left(\frac{U_{n-1}}{R_{n-1} + \triangle t k_r(C_0 - C_*)\left(\frac{U_{n-1}}{R_{n-1}} + 1\right)} + 1\right)\right]. \tag{4.8.6}$$

We apply the same numerical treatment as before for the concentration $C(r,t)$ in the fluid

$$C(r,t) = C_0 + (C_0 - C_*)\frac{u(r,t)}{r}. \tag{4.8.7}$$

We plot below several quantities: the function $U(t)$ from equation (4.8.5), the concentration $C(r,t)$ from equation (4.8.7), and the radius $R(t)$ from equation (4.8.6) for constant values of k_r, C_0, and C_* as indicated in the figure captions.

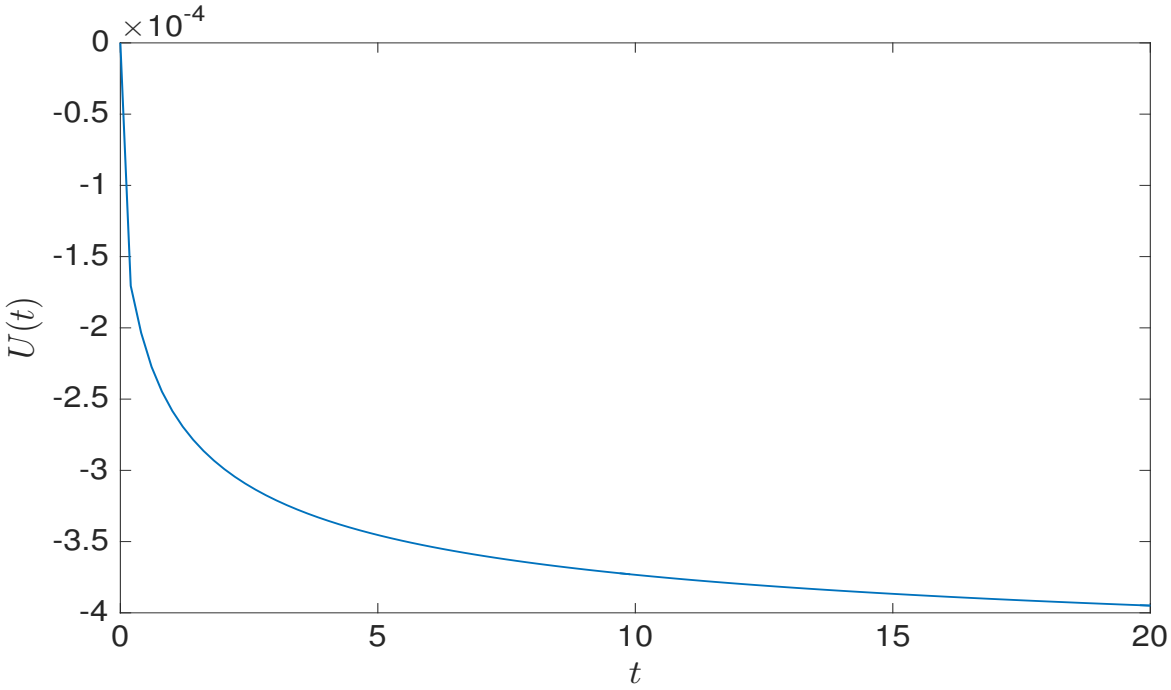

Figure 4.8.1: The function $U(t)$ for $k_r = 4.5 \times 10^{-4}$, $C_0 = 0.1$, and $C_* = 0.01$ as a function of the non-dimensional time t.

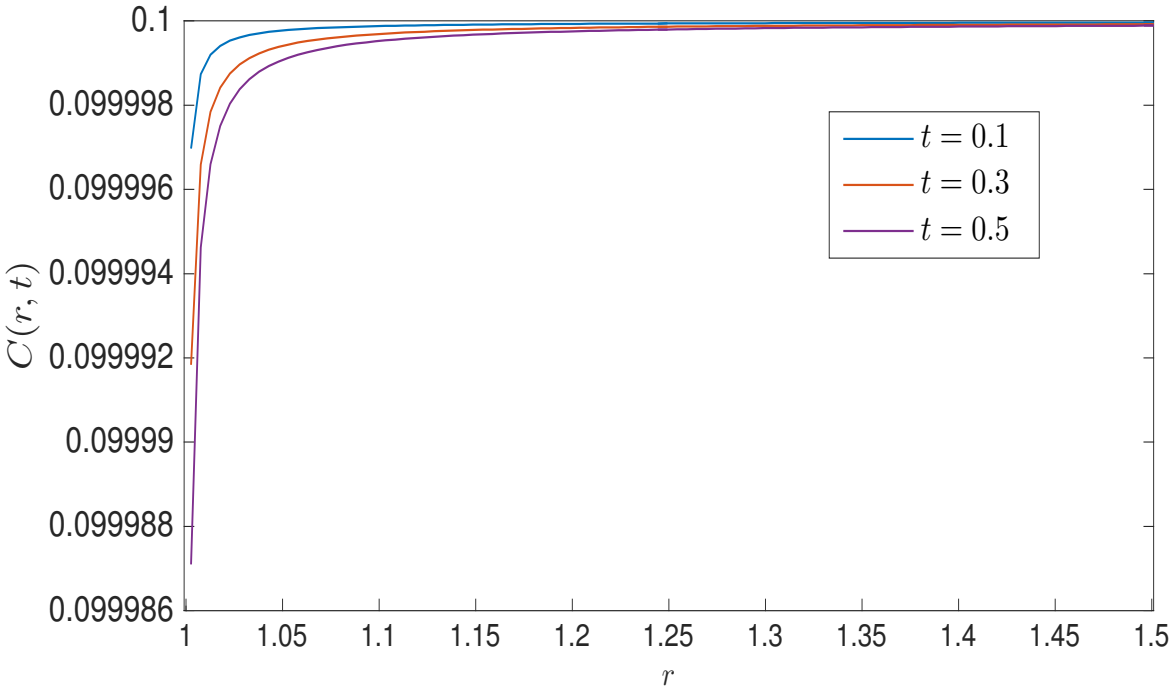

Figure 4.8.2: The wax concentrations $C(r,t)$ in the fluid domain as functions of the non-dimensional radial coordinate r calculated for $k_r = 4.5 \times 10^{-4}$, $C_0 = 0.1$, and $C_* = 0.01$ at different time instants.

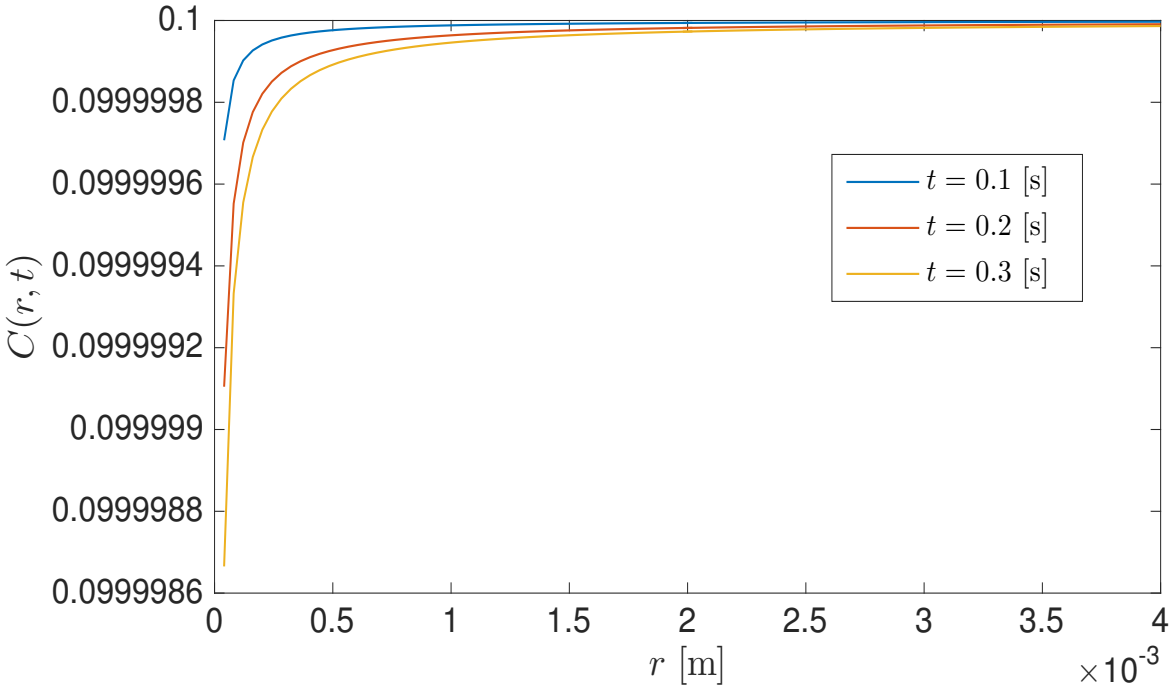

Figure 4.8.3: The wax concentrations $C(r,t)$ in the fluid domain as functions of the dimensional radial coordinate calculated for dimensional mass transfer, $k_r = 4.5 \times 10^{-6}$m/s, $C_0 = 0.1$, and $C_* = 0.01$ at different time instants.

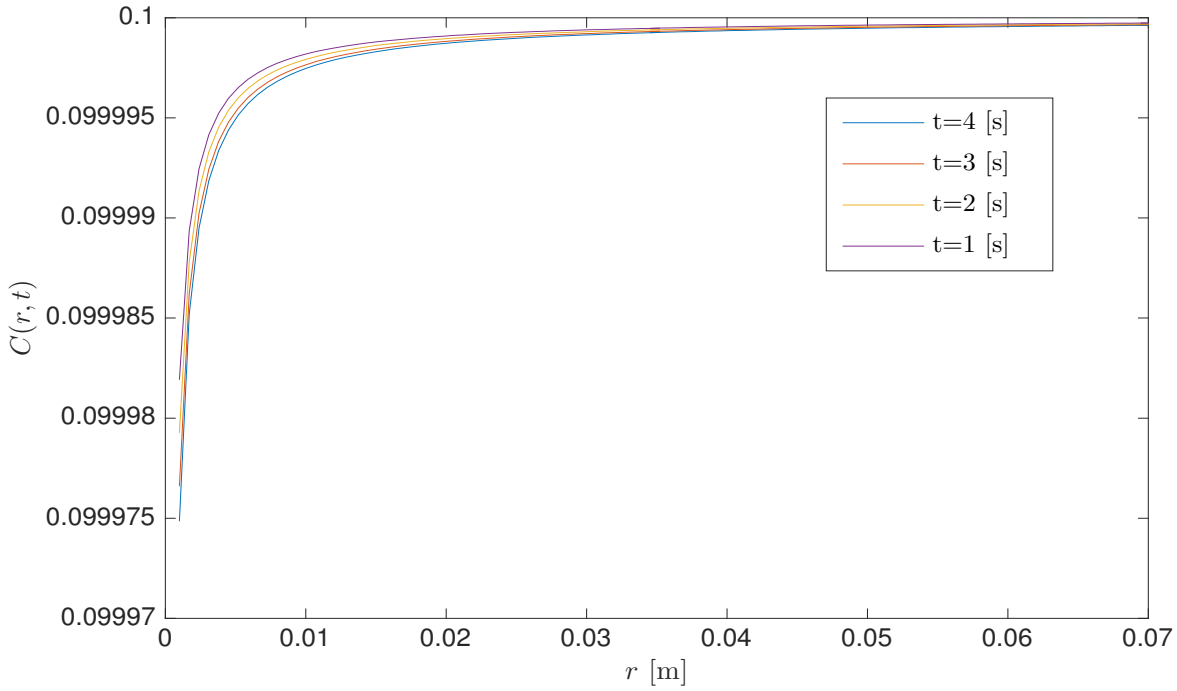

Figure 4.8.4: The wax concentrations $C(r,t)$ in the fluid domain as functions of the dimensional radial coordinate calculated for dimensional mass transfer, $k_r = 4.5 \times 10^{-6}$m/s, $C_0 = 0.1$, and $C_* = 0.01$ at different time instants.

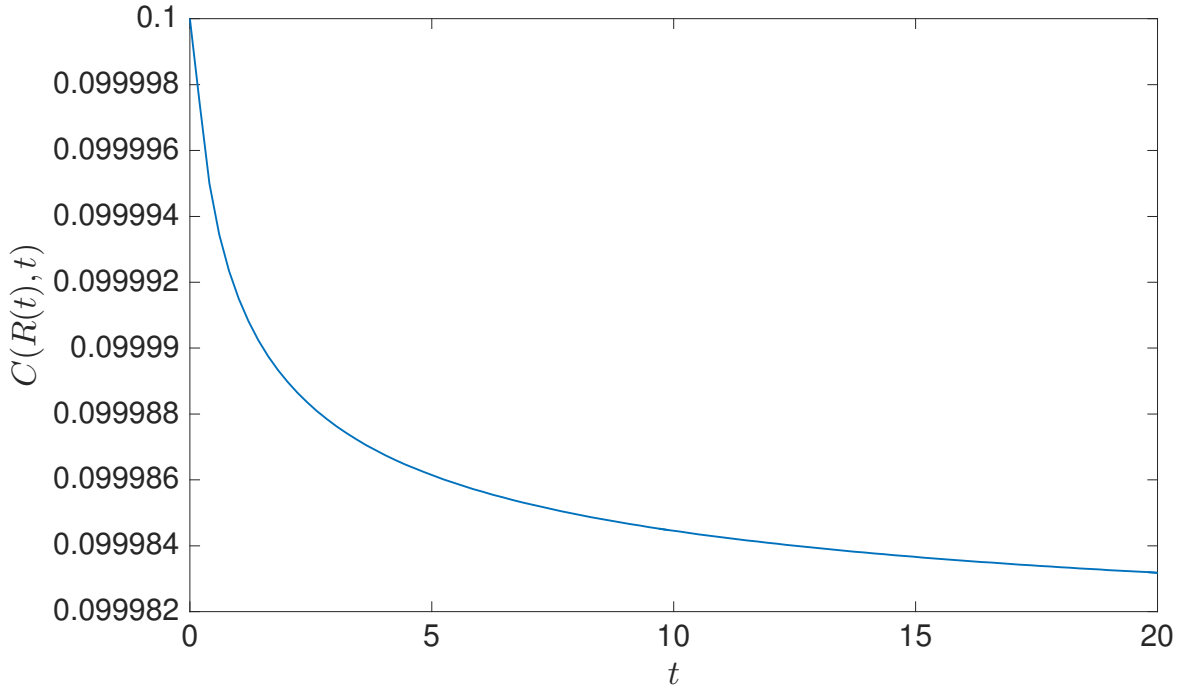

Figure 4.8.5: The concentration on the surface of the wax particle as a function of the non-dimensional time for $k_r = 4.5 \times 10^{-4}$.

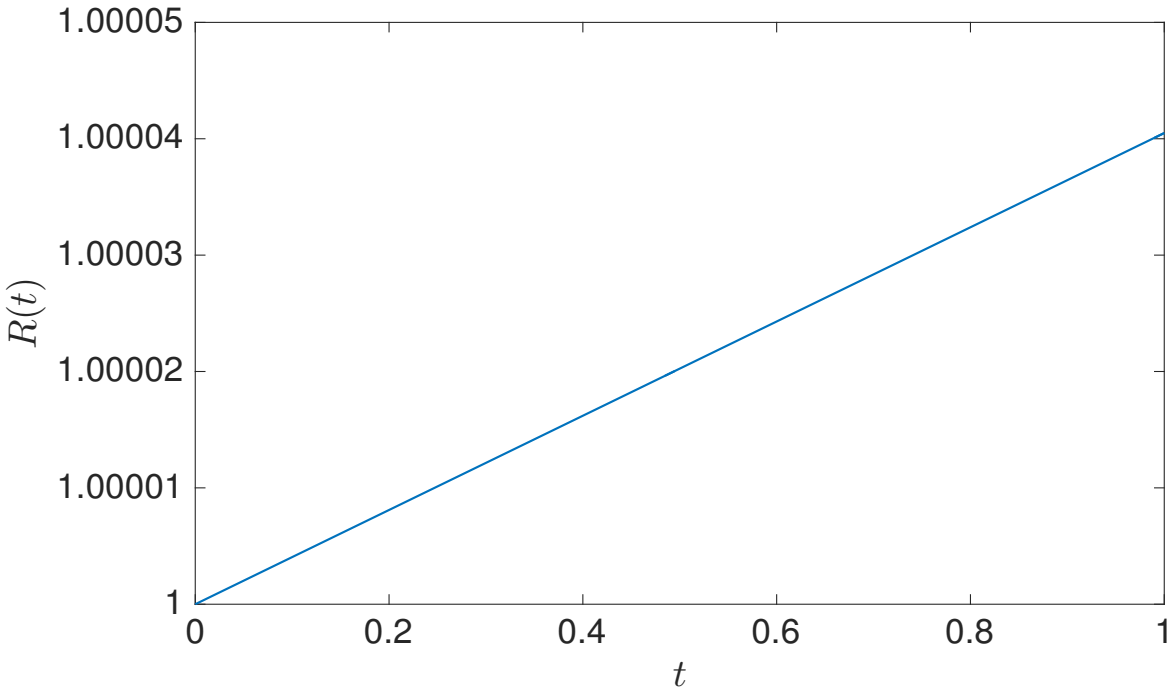

Figure 4.8.6: The radius $R(t)$ of the growing wax particle for $k_r = 4.5 \times 10^{-4}$, $C_0 = 0.1$, and $C_* = 0.01$.

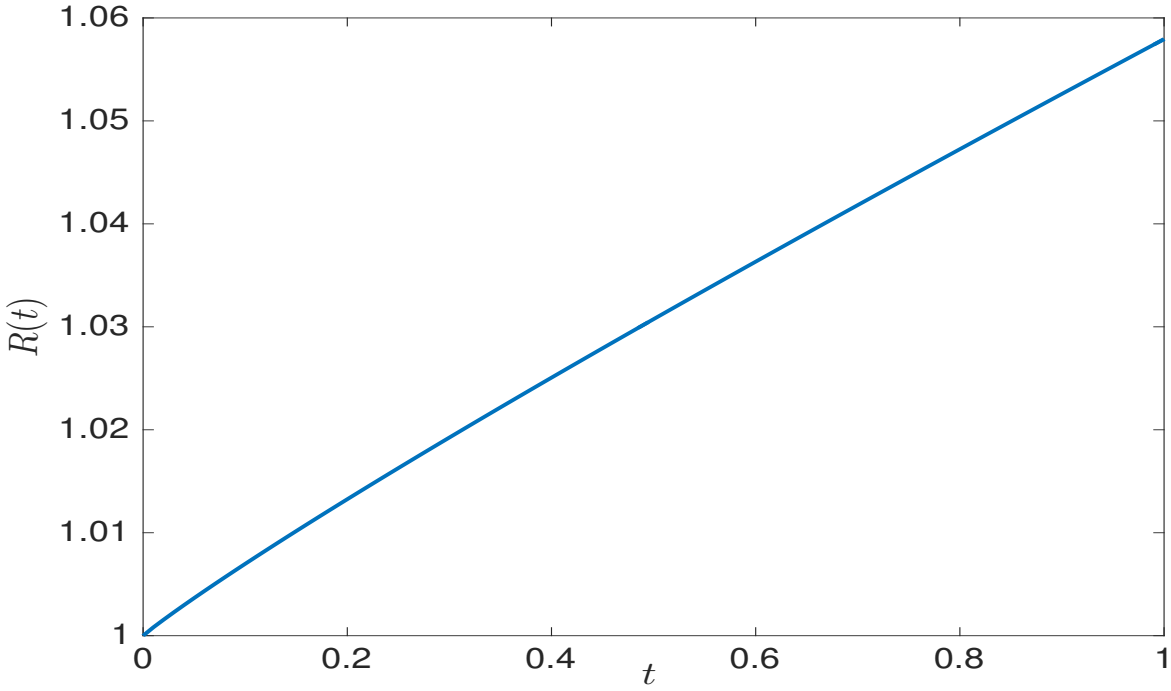

Figure 4.8.7: The radius $R(t)$ of the growing wax particle for $k_r = 0.9$, $C_0 = 0.1$, and $C_* = 0.01$.

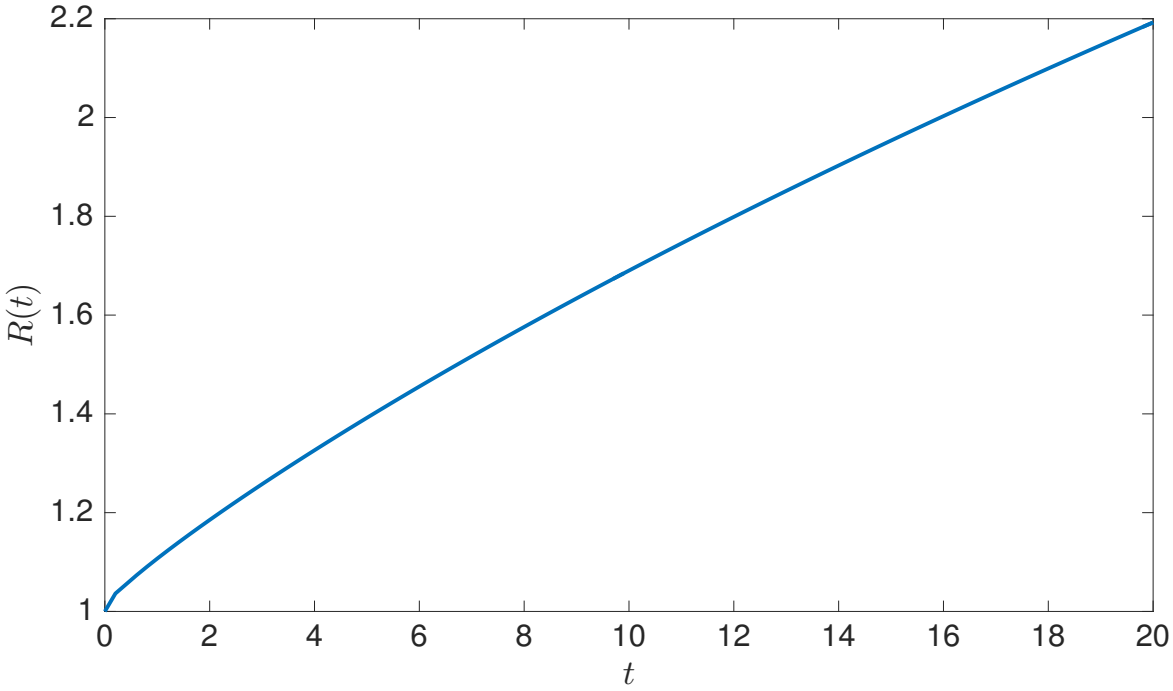

Figure 4.8.8: The radius $R(t)$ of the growing wax particle for $k_r = 2$, $C_0 = 0.1$, and $C_* = 0.01$.

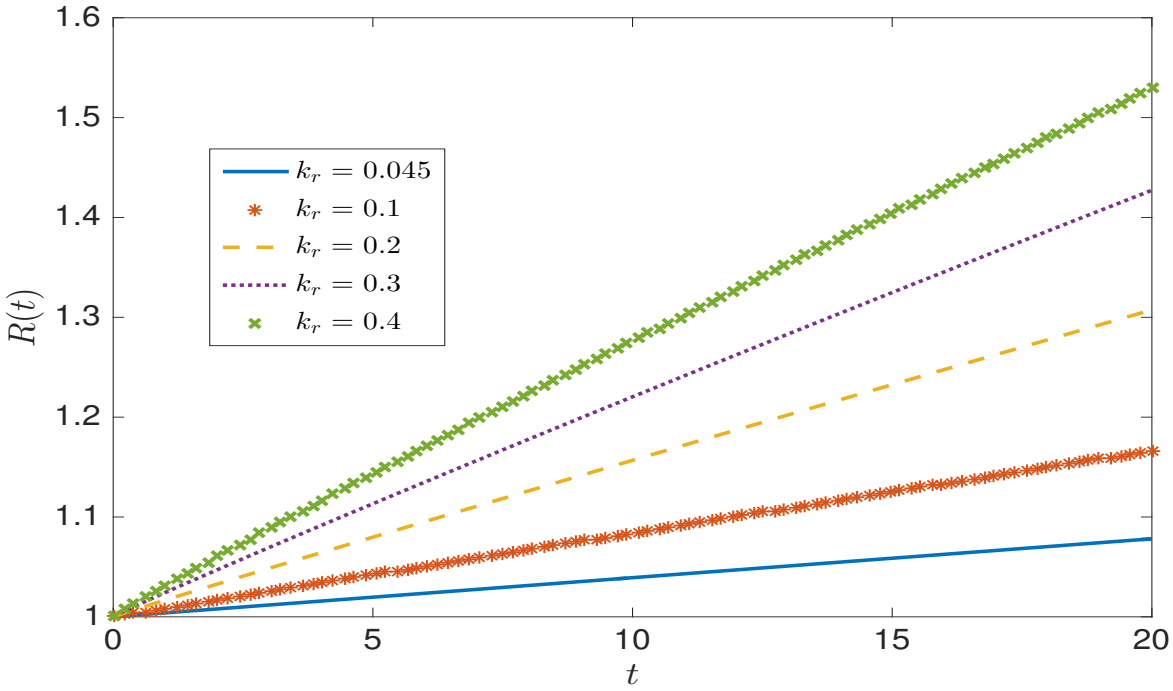

Figure 4.8.9: The radius $R(t)$ as a function of time for different values of the dimensionless mass transfer coefficient k_r.

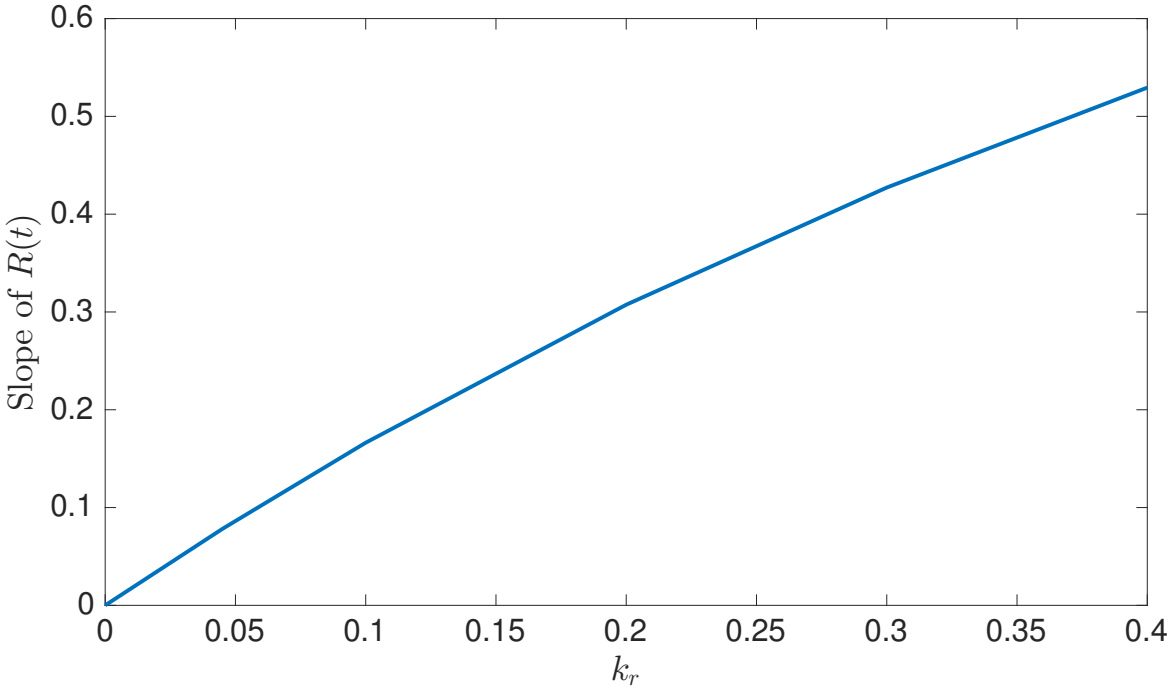

Figure 4.8.10: The average rate of change of $R(t)$.

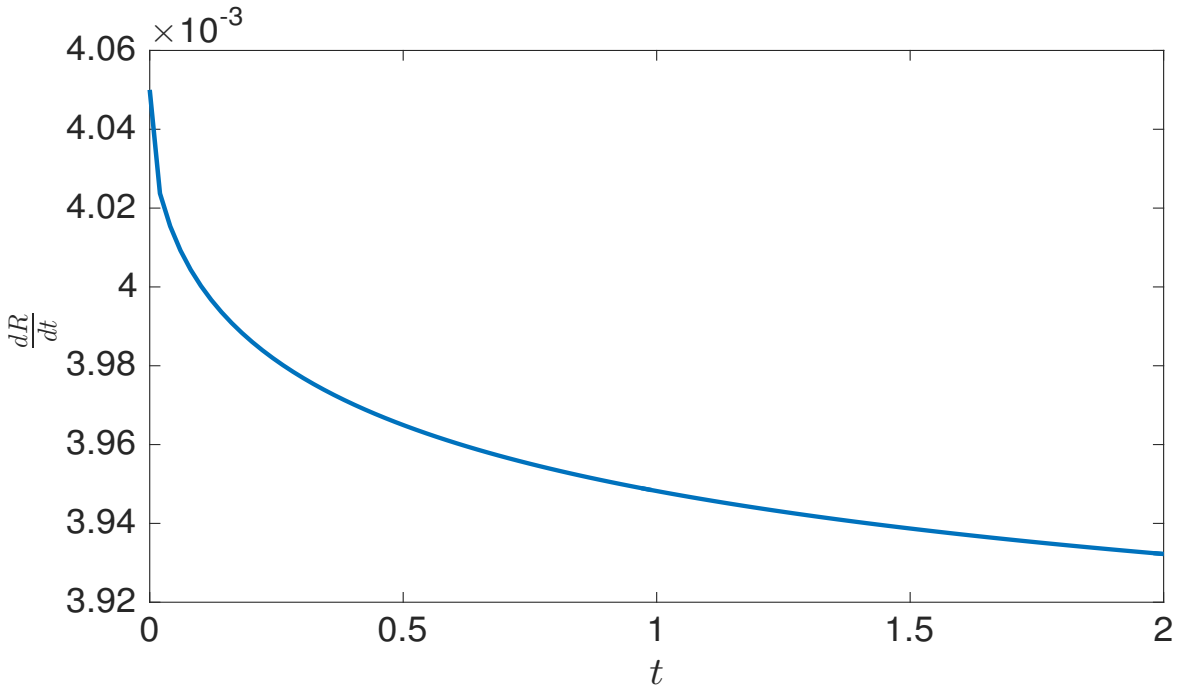

Figure 4.8.11: The dimensionless rate of change of $R(t)$ as a function of time, where $k_r = 4.5 \times 10^{-2}$.

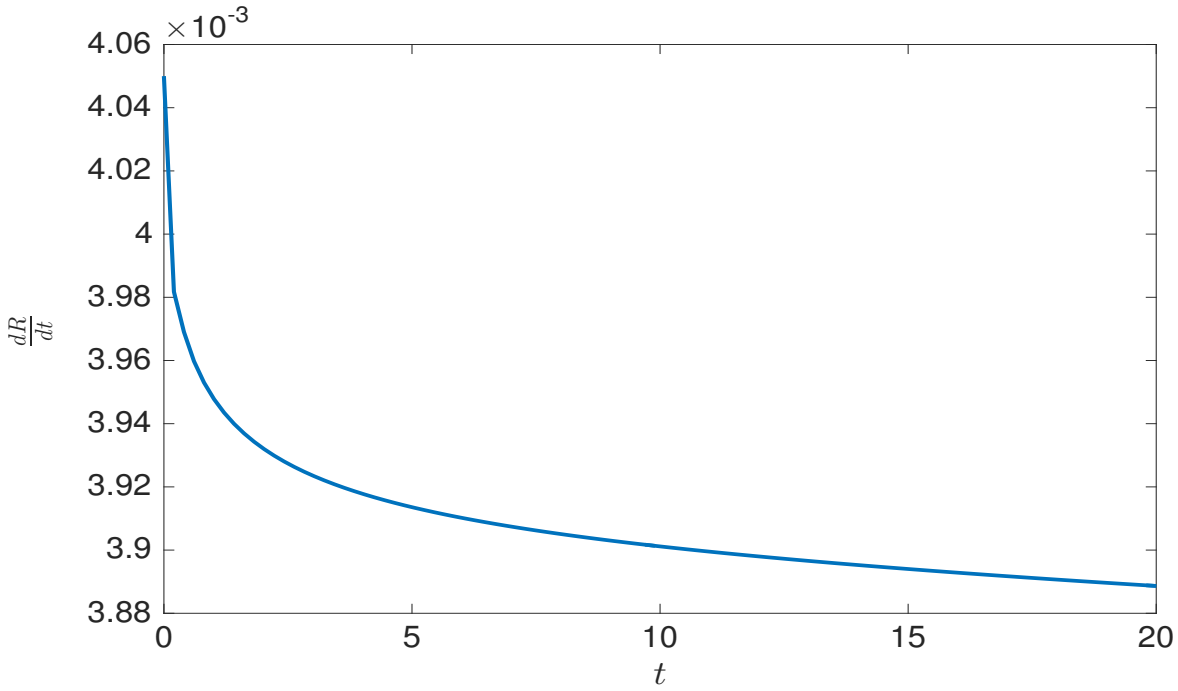

Figure 4.8.12: The dimensional radius $R(t)$ as a function of dimensional time, where $k_r = 10^{-4}$ [m/s].

Figure 4.8.1 shows that the function $U(t)$ for the constant coefficients, k_r, C_0, and C_* decreases in time in order for the wax particle to grow. Figure 4.8.2 illustrates the concentration distribution $C(r,t)$ as a function of distance from the surface of the wax particle with constant mass transfer coefficient. Each curve in Figure 4.8.2 is plotted for a given value of time. As time passes, the concentration at the surface of the particle decreases. Also, $C(r,t)$ departs from its far-field value more and more over a wider range of distance, as t increases. In Figure 4.8.3 the concentration around the particle is shown in the dimensional variables and for smaller value of k_r. It is seen that at $t = 0.3$ s the concentration is visibly decreased on the surface of the wax particle. The radius of the wax particle increased three times by $t = 0.3$ s. At this time the particle radius is 0.3 mm. We can see at $t = 0.3$ s the concentration is visibly decreased over a distance of about 6 particle radii from the particle surface. It is over this distance that the neighbouring particles start to disturb each other from this time onward. Also, we can see that the difference between the concentration at $r = 1.8$ mm and the far-field concentration is of order 10^{-7}. Figure 4.8.5 illustrates the concentration on the surface of the wax particle as a function of time. The concentration decreases in time, which means that the concentration on the surface of the wax particle is lower than the far-field concentration.

Figure 4.8.6 shows the wax particle radius for $k_r = 4.5 \times 10^{-4}$. We see that $R(t)$ increases by only 0.04% per unit time, which is explained by small value of k_r. Figure 4.8.7 shows the growth of the wax particle radius by 6% per unit time when the mass transfer coefficient is $k_r = 0.9$. Figure 4.8.8 shows the radius of the wax particle increases as a function of longer time. We can see that the wax particle radius $R(t)$ is growing faster with larger value of the mass

transfer coefficient. This means the wax molecules close to the wax particle surface are quickly stuck to the surface of the wax particle if the mass transfer coefficient is large. Since the value of mass transfer coefficient could not be approximated from literature, in the following we investigate the dependence of the radius $R(t)$ on the value of the mass transfer coefficient k_r. Figure 4.8.9 shows the radius $R(t)$ as a function of time for different values of k_r. We see the radius of the wax particle grows more quickly with increase of k_r and that $R(t)$ is close to a linear increase as t increases. Also, in Figure 4.8.10 we calculate average speed of the radius growth, the slope of $R(t)$, $\frac{R(1)-R(0)}{1-0}$, as a function of k_r. We can see that the rate of increase of $R(t)$ is directly proportional to the mass transfer coefficient k_r. Figure 4.8.11 shows the dimensionless rate of increase of the radius $R(t)$ as a function of time for $k_r = 4.5 \times 10^{-2}$. We can see it starts from 4×10^{-3} and it changes just slightly with time. Figure 4.8.12 shows that for larger time, the rate of change of radius does not change significantly. Figure 4.8.12 illustrates the dimensional radius $R(t)$ for a wax particle which starts to grow from 0.5 mm initial radius.

The mass transfer coefficient k_r is assumed to be a positive function of temperature $k_r\{T_{WAT} - T\}$. If the temperature drops, more wax molecules appear in the solution, and the mass transfer coefficient increases monotonically, if we decrease the temperature. We assume that k_r increases linear with decreasing temperature as shown in figure 4.8.13. The particle moves together with the flow but the temperature around the particle changes in time, $T = T(x(t), r_p)$ is the temperature distribution in the pipe, where $(x(t), r_p)$ is the location of the particle in the pipe, $x(t)$ is the distance the wax particle travelled from the entrance to the pipe and r_p is the distance of the particle trajectory form the pipe axis. Here r_p= constant and $x(t) \approx u(r_p)t$, where

$u(r_p) = u_{max}(1-r_p^2/a^2)$ is the flow velocity and t is time as discussed in chapter 2. So overall, $T = T(t)$. The coefficient k_r is assumed to be a positive function of temperature, $k_r\{T_{WAT} - T\}$. We expect the temperature $T(t)$ to decrease in time, because the particle travels from a hot entrance towards a colder part of the pipe. Hence, following the wax particle along the pipe, we may assume the temperature to be a given function of time. So, $k_r\{T_{WAT} - T\} = k_r(t)$. Figure 4.8.14 shows the temperature at the location of the particle which enters the pipe at distance 5cm from the wall as a function of time. We can see at $t = 0$ the temperature is very high and as the time goes on the temperature drops. Figure 4.8.15 shows the corresponding mass transfer coefficient as a function of time. Figure 4.8.16 shows the radius of the wax particle $R(t)$ where the mass transfer coefficient $k_r(t)$ is from figure 4.8.15. Figure 4.8.17 shows the concentration in the fluid $C(r, t)$ where the mass transfer depend on time.

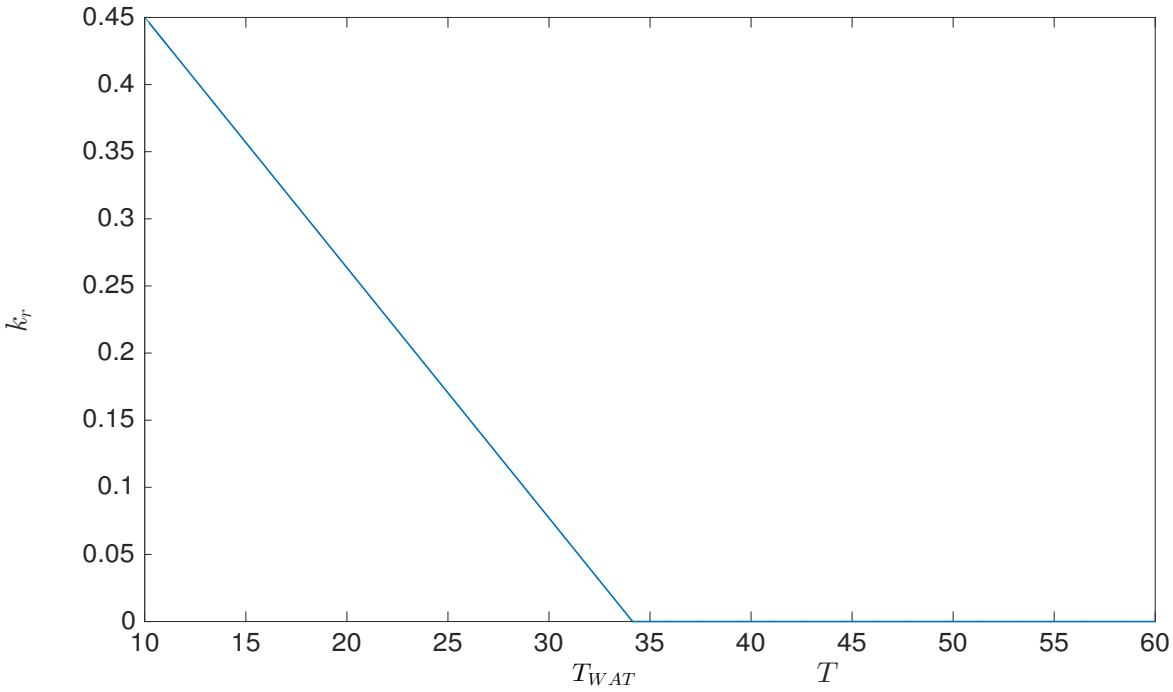

Figure 4.8.13: The mass transfer as a function of temperature.

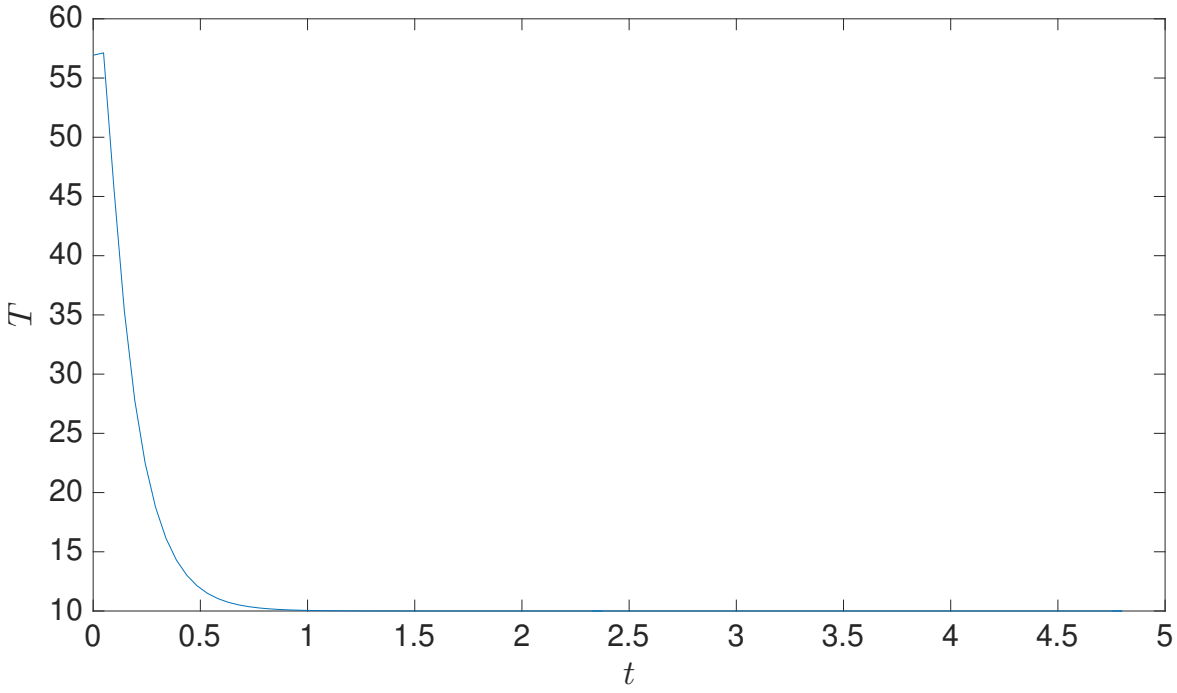

Figure 4.8.14: Temperature at the place of the particle as a function of time .

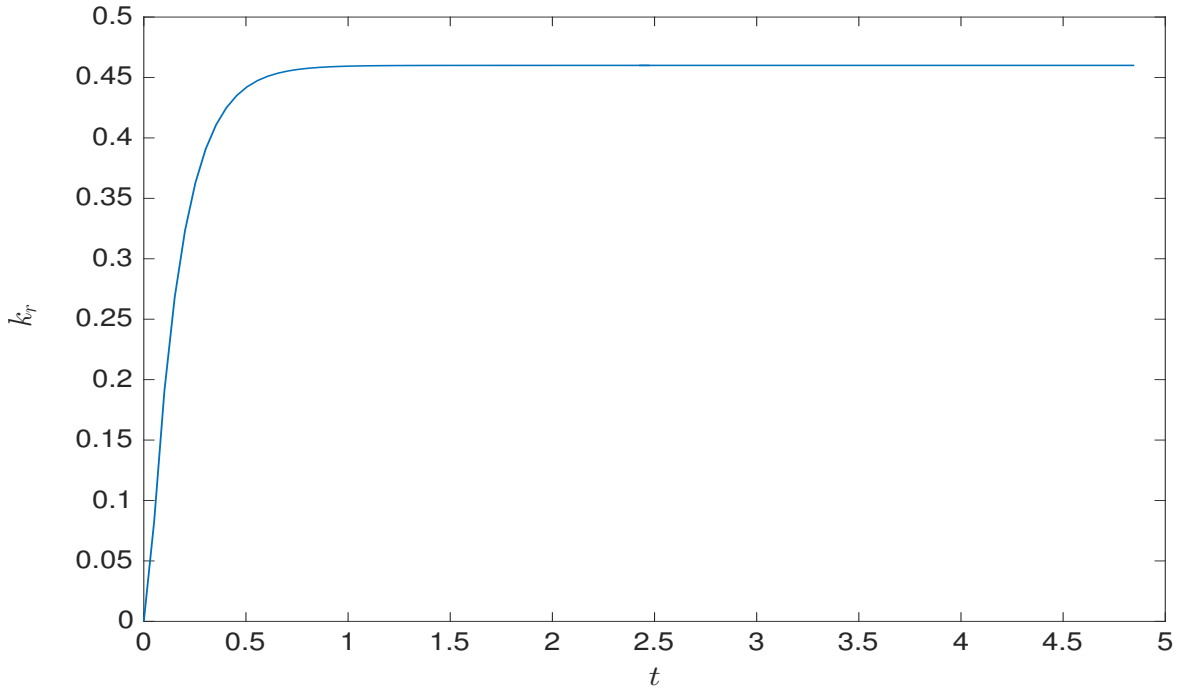

Figure 4.8.15: The mass transfer $k_r(t)$ as a function of time.

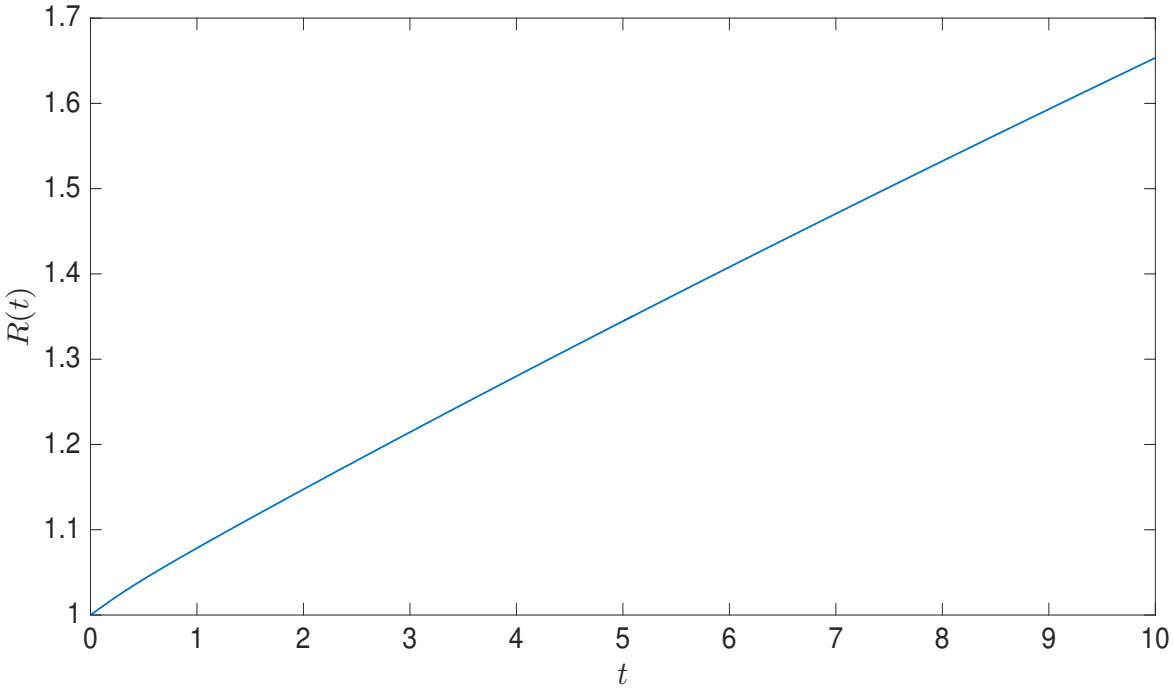

Figure 4.8.16: The function $R(t)$ as a function of the non-dimensional time t, when the mass transfer $k_r(t)$ depend on time.

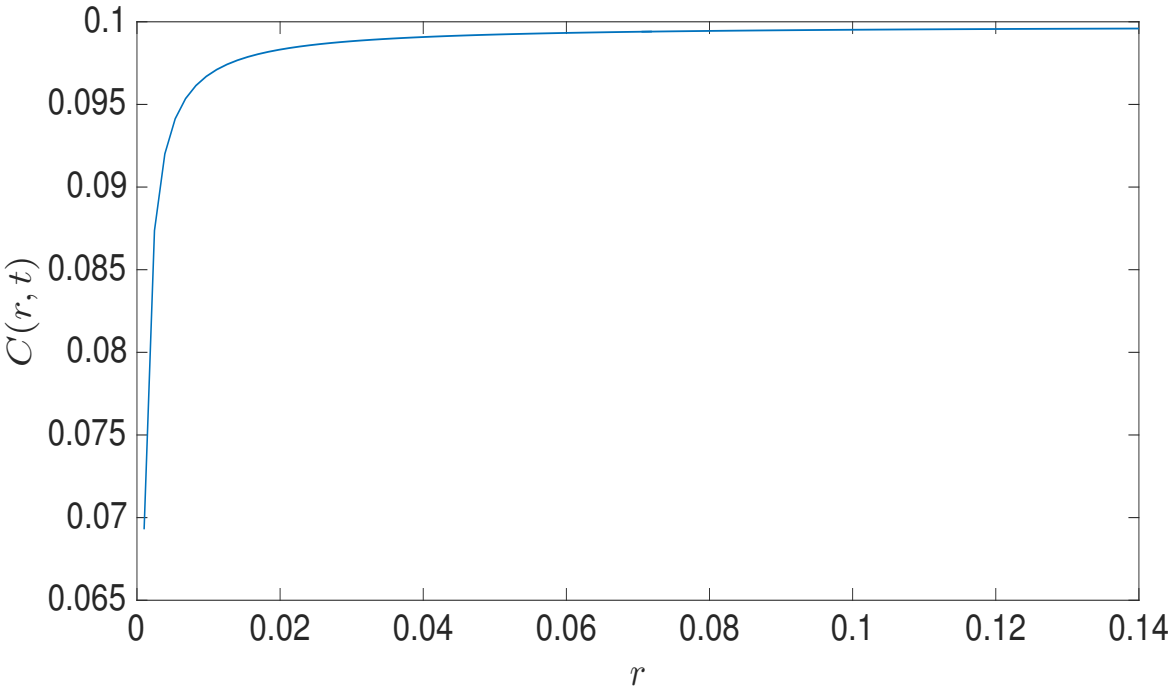

Figure 4.8.17: The wax concentrations $C(r,t)$ in the fluid domain as functions of the dimensional radial coordinate calculated for mass transfer $k_r(t)$ is function of time.

Chapter 5

Growth of wax particles in a laminar flow

5.1 Introduction

In this chapter, we consider wax particles moving together with the oil in a pipe. The wax particles are changing their size and shapes due to diffusion of wax molecules from the oil towards the particles and interaction between the particles. The motions of small particles, including wax particles, in oil pipe lines is a fundamental industrial problem. The motions of the wax particles and their evolutions in time depend on the ambient flow, temperature and characteristics of the particles, as well as their interaction between each other. In section 5.2, we formulate the coupled diffusion/flow problem for a single particle in a uniform flow without assuming that the shape of the particle is spherical. However, we assume that the particle is spherical initially. For a small wax particle moving far from the pipe wall, the flow shear can be

neglected at the scale of the particle size. We can assume that the speed of the wax particle is close to the local speed of the flow. That is the flow relative to the wax particle can be neglected at the leading order. Then the wax particle remains spherical at leading order and its radius can be calculated by using the technique developed in chapter 4. We are concerned here with the first-order correction of the particle shape caused by a small difference between the wax particle speed and speed of the local flow. On the other hand, the motion of the wax particle can be affected by this shape correction. This coupled problem is formulated and studied in the spherical coordinates. The coordinate system moves together with the wax particle.

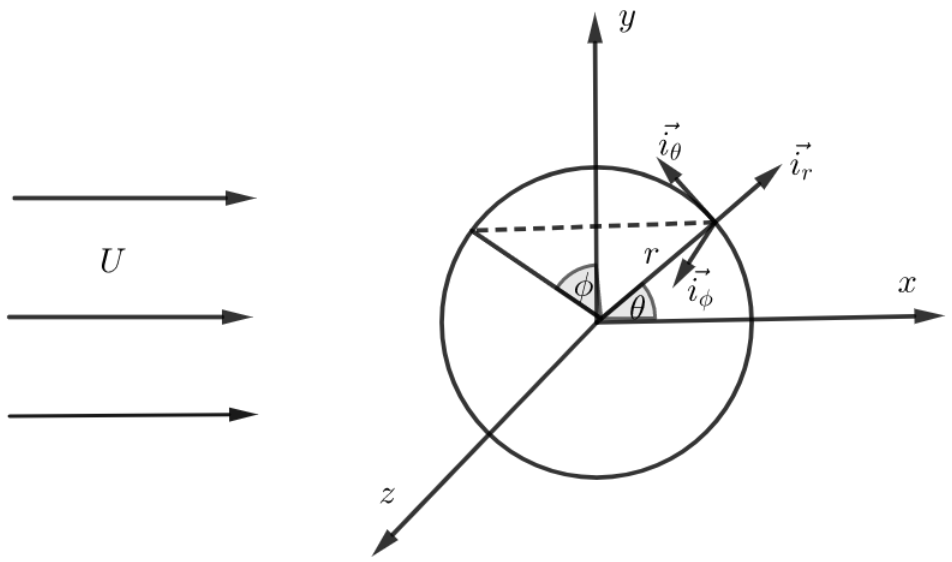

Figure 5.1.1: Spherical coordinates system. The ranges of the variables are $0 \leqslant r, 0 \leqslant \theta \leqslant \pi$, and $0 \leqslant \phi < 2\pi$, where U is the velocity of the flow.

In the coordinate system moving together with the particle, the diffusion of wax molecules toward the surface of the wax particle is described by the convective diffusion equation [64]:

$$\frac{\mathrm{D}C}{\mathrm{D}t} = D\nabla^2 C, \tag{5.1.1}$$

where $C = C(r, \theta, \phi, t)$ is the volume concentration of dissolved wax in the oil, $0 \leq C \leq 1$, t is time, D is the diffusivity of wax in oil, r, θ, ϕ are the polar coordinates with the origin at the centre of mass of the wax particle, see Figure 5.1.1, and $\mathrm{D}C/\mathrm{D}t$ is the material derivative. Equation (5.1.1) should be solved in the unbounded region of the fluid around the wax particle subject to the appropriate initial and boundary conditions. We consider a single wax particle assuming that other wax particles and the pipe wall are far away and do not affect the flow and the concentration of wax in the fluid around the wax particle of interest. If the wax particle is initially spherical and it moves at the speed of the flow, then the wax particle stays spherical for all times with its radius $R(t)$ governed by the radial diffusion and the mass transfer coefficient k_r, see equation (3.2.1). Indeed, without a relative flow and without other wax molecules nearby, which change the concentration field, there is no reason for non-spherical growth of the particle. The wax particle growth departs from spherically symmetric expansion if any one of the following occurs:

1- Initial velocity of a spherical wax particle inserted in the flow is different from the local velocity of the flow.

2- The initial shape of the particle is not spherical.

3- There are several particles close to each other.

For example, if we have two wax particles and the distance between them is relatively large then these particles do not feel each other because the concentration approaches the far-field value at short distances from the surfaces of each particle. We need to estimate the distance starting from which interaction between particles can be neglected with a good accuracy. If the wax particles

are close to each other, then the wax concentration around each particle is three-dimensional, in general, and convective terms in the diffusion equation (5.1.1) could be important.

In this chapter we restrict ourselves to axisymmetric problems in which the particle shapes only slightly deviate from spherical ones. Then the axisymmetric flow around the wax particle only slightly deviates from the uniform flow, which is due to a relative motion of the wax particle, its shape or the presence of other particles. The equations describing the motion and growth of the wax particle are solved by asymptotic methods with the leading-order solution corresponding to the spherical particle without a relative flow around it.

5.2 Formulation of the three-dimensional problem of a wax particle growth in the spherical local coordinates

Consider a wax particle moving through a viscous incompressible fluid. The spherical coordinates r, θ, ϕ, moving together with the centre of mass of the wax particle are convenient in problems with dominant variation of the concentration field in the radial direction, where r is the radial distance from the origin, θ is the polar angle from the axis of symmetry and ϕ is the azimuthal angle, see Figure 5.1.1, $0 \leqslant \theta \leqslant \pi$ and $0 \leqslant \phi < 2\pi$. The wax particle is growing with time. In the three-dimensional formulation, the surface of the wax particle is described by the equation

$$S(r, \theta, \phi, t) = r - R(\theta, \phi, t) = 0, \tag{5.2.1}$$

where $R(\theta, \phi, t)$ is the distance of a point on the wax particle surface from the centre of mass of the wax particle. The function $R(\theta, \phi, t)$ is to be determined as part of the solution. Note that motions of molecules along the wax particle surface are not allowed in our analysis. The particle surface is displaced only in the normal direction due to the particle growth. The initial shape of the wax particle is given,

$$R(\theta, \phi, 0) = R_0(\theta, \phi), \tag{5.2.2}$$

where $R_0(\theta, \phi)$ is a given function.

The unit outer normal vector $\vec{n}$ to the wax particle surface is given by, see [82],

$$\vec{n} = \frac{\nabla S}{|\nabla S|}, \tag{5.2.3}$$

where $S(r, \theta, \phi, t)$ is defined by (5.2.1) and the normal is directed outwards the particle.

Equations (5.2.1) and (5.2.3) provide

$$\vec{n} = \frac{\vec{i_r} - \frac{1}{R(\theta,\phi,t)}\left(\frac{\partial R}{\partial \theta}\right)\vec{i_\theta} - \frac{1}{R(\theta,\phi,t)\sin\theta}\left(\frac{\partial R}{\partial \phi}\right)\vec{i_\phi}}{\sqrt{1 + \frac{1}{R^2(\theta,\phi,t)}\left(\frac{\partial R}{\partial \theta}\right)^2 + \frac{1}{R^2(\theta,\phi,t)\sin^2\theta}\left(\frac{\partial R}{\partial \phi}\right)^2}}, \tag{5.2.4}$$

where $(\vec{i_r}, \vec{i_\theta}, \vec{i_\phi})$ are the unit vectors, see Figure 5.1.1.

The speed of the surface $S(r, \theta, \phi, t) = 0$ in the direction of outer normal $\vec{n}$ is equal to

$$V_r = -\frac{\frac{\partial S}{\partial t}}{|\nabla S|}. \tag{5.2.5}$$

The normal component of the velocity of the flow, $\vec{u} \cdot \vec{n}$, on the deformable surface (5.2.1) is obtained by using the mass conservation law, see [38], where

$\vec{u}$ is the fluid velocity in the moving coordinate system, see section 5.1. As in [38], we consider a general case where the wax density of the solid particle, ρ_{ws}, can be different from the wax density in the oil, ρ_{wl}. Then the mass flux from the oil to the surface of the wax particle is $-\rho_{wl}(\vec{u}-V_r\vec{n})\cdot\vec{n}$, and the mass flux from the surface to the solid wax is $\rho_{ws}V_r$. The fluxes are calculated with respect to the moving surface of the wax particle, see Figure 5.2.1, $\vec{u}\cdot\vec{n}-V_r$ is the normal component of the flow velocity with respect to the moving surface, in the direction of the outer normal $\vec{n}$. So, $-(\vec{u}\cdot\vec{n}-V_r)\,\rho_{wl}$ is the mass flux towards the surface of the wax particle and the mass flux from the surface of the wax particle towards the inner part of the wax particle is $\rho_{ws}V_r$.

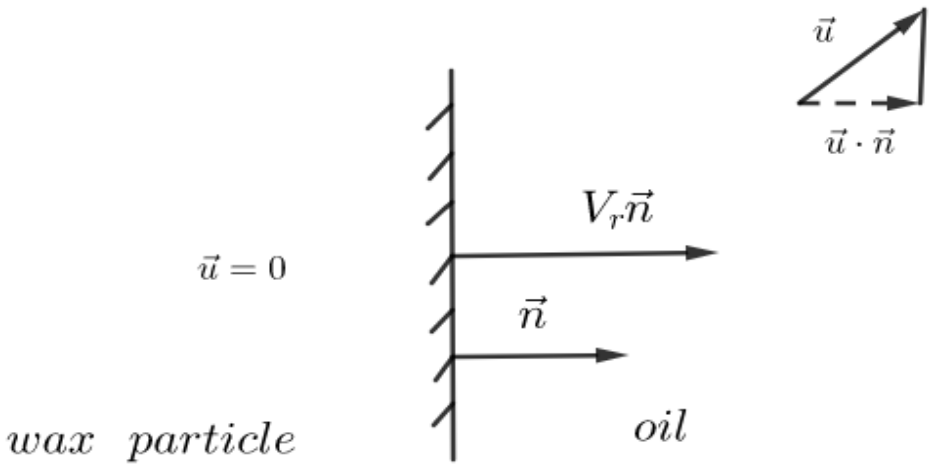

Figure 5.2.1: The moving surface of the wax particle.

The mass conservation law provides that the mass fluxes are equal,

$$-\rho_{wl}(\vec{u}-V_r\vec{n})\cdot\vec{n}=\rho_{ws}V_r,$$

and we obtain

$$\vec{u}\cdot\vec{n}=\left(1-\frac{\rho_{ws}}{\rho_{wl}}\right)V_r. \tag{5.2.6}$$

In present analysis, we assume $\rho_{ws} = \rho_{wl}$. Then equation (5.2.6) leads to the boundary condition for the flow around a wax particle,

$$\vec{u} \cdot \vec{n} = 0 \qquad (r = R(\theta, \phi, t)), \tag{5.2.7}$$

which is the boundary condition for the normal velocity of the fluid on the wax particle surface. The no-slip condition is written as, see [54]

$$\vec{u} - (\vec{u} \cdot \vec{n})\, \vec{n} = 0. \tag{5.2.8}$$

This condition implies that the tangential velocity of the flow is zero on the wax particle surface.

To determine the velocity field of the flow around the particle we use the Navier-Stokes equations of the motion for an incompressible viscous fluid, see [2],

$$\rho \left(\frac{\partial \vec{u}}{\partial t} + (\vec{u} \cdot \nabla)\vec{u} \right) = -\nabla P + \mu \nabla^2 \vec{u} - \rho \frac{\partial \vec{u}_p}{\partial t}, \tag{5.2.9}$$

together with the continuity equation,

$$\nabla \cdot \vec{u} = 0, \tag{5.2.10}$$

where $\vec{u}$ is the fluid velocity with respect to the wax particle, ρ is the constant oil density, P is the hydrodynamic pressure, μ is the constant dynamic viscosity, and $\vec{u}_p(t)$ is the velocity of the wax particle in the global coordinate system. The velocity of the flow in the global coordinate system, where the pipe is at rest, is $\vec{u}(\vec{x}, t) + \vec{u}_p(t)$. Far from the wax particle, $r \longrightarrow \infty$, the flow is uniform,

$$\vec{u}(\vec{x}, t) \longrightarrow (U, 0, 0) - \vec{u}_p(t), \tag{5.2.11}$$

where U is the flow velocity in the pipe at the level of the wax particle motion along the pipe. In the following, we restrict ourselves to the motion of the wax particle only along the pipe, $\vec{u}_p(t) = (u_p(t), 0, 0)$, assuming the flow velocity U constant. Here $\vec{u}_p(t)$ only slightly deviates from U.

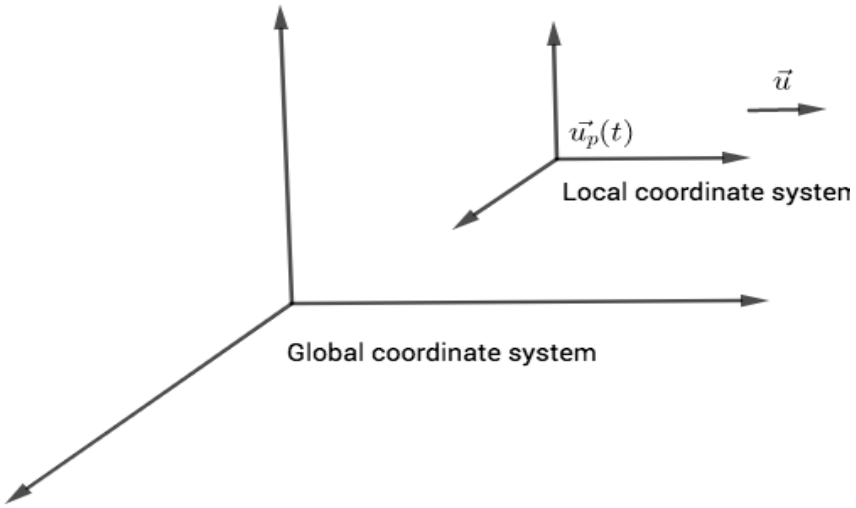

Figure 5.2.2: The global coordinate system for the pipe and local coordinate system for the particle, where $\vec{u_p}(t)$ is the absolute velocity for the particle in the global coordinate system and $\vec{u}$ is the velocity of the flow in the moving coordinate system.

The speed of the wax particle, $u_p(t)$, is governed by Newton's second law:

$$\frac{d}{dt}\left[m(t)u_p(t)\right] = F_x(t), \qquad u_p(0) = u_{p0}, \tag{5.2.12}$$

where $F_x(t)$ is the x-component of the hydrodynamic force acting on the wax particle and $m(t)$ is the time-dependent mass of the wax particle. The total force $\vec{F}(t)$ acting on the wax particle in the flow is given by

$$\vec{F}(t) = \int_0^{2\pi} d\phi \int_0^{\pi} \left(T \cdot \vec{n}\right)|_{r=R(\theta,\phi,t)} R^2(\theta,\phi,t)\sin\theta |\nabla\left(r - R(\theta,\phi,t)\right)| d\theta, \tag{5.2.13}$$

where T is the stress tensor, see [2],

$$T = -PI + 2\mu E, \qquad E = \frac{1}{2}\left(\nabla\vec{u} + \nabla\vec{u}^T\right), \tag{5.2.14}$$

I is the unit matrix and E is the rate-of-strain tensor.

In summary, the flow around the wax particle, $r > R(\theta, \phi, t)$, is governed by equations (5.2.9) and (5.2.10) in the moving coordinate system subject to the boundary conditions (5.2.7) and (5.2.8) and the far-field condition (5.2.11). The particle speed $u_p(t)$ is governed by equation (5.2.12), where the hydrodynamic force is given by (5.2.13) and (5.2.14). In this formulation, we assume that the shape function $R(\theta, \phi, t)$ and the mass of the particle $m(t)$ are given.

The concentration of wax, $C = C(r, \theta, \phi, t)$, in the flow around the particle, $r > R(\theta, \phi, t)$, is governed by the convective diffusion equation (5.1.1), see [14], which has the form

$$\frac{\mathrm{D}C}{\mathrm{D}t} = D\left[\frac{1}{r^2}\frac{\partial}{\partial r}\left(r^2\frac{\partial C}{\partial r}\right) + \frac{1}{r^2\sin\theta}\frac{\partial}{\partial\theta}\left(\sin\theta\frac{\partial C}{\partial\theta}\right) + \frac{1}{r^2\sin^2\theta}\frac{\partial^2 C}{\partial\phi^2}\right], \tag{5.2.15}$$

in the spherical coordinates, where

$$\frac{\mathrm{D}C}{\mathrm{D}t} = \frac{\partial C}{\partial t} + u_r\frac{\partial C}{\partial r} + \frac{u_\theta}{r}\frac{\partial C}{\partial\theta} + \frac{u_\phi}{r\sin\theta}\frac{\partial C}{\partial\phi}, \tag{5.2.16}$$

and u_r, u_θ and u_ϕ are the fluid velocity components in r, θ and ϕ directions, respectively, $\vec{u} = u_r\vec{i}_r + u_\theta\vec{i}_\theta + u_\phi\vec{i}_\phi$ in the spherical coordinates, see (5.2.9). Initially, before the particle has been inserted in the flow, $t < 0$, the wax concentration in the flow is assumed uniform,

$$C(r, \theta, \phi, 0) = C_0. \tag{5.2.17}$$

The concentration remains uniform far from the particle,

$$C(r,\theta,\phi,t) \longrightarrow C_0, \qquad (r \longrightarrow \infty, t > 0), \tag{5.2.18}$$

for all times. The boundary condition for the concentration on the time-dependent surface of the particle was formulated in terms of the mass flux by Dawson et al. [24], we discussed this condition in chapter 3 for spherical case. To derive this condition in $3D$ case, we recall that the diffusive mass flux $\vec{J}(r,\theta,\phi,t)$ of wax molecules within a medium is given by Fick's first law [21] through the concentration gradient,

$$\vec{J}(r,\theta,\phi,t) = -\rho_{wl} D \nabla C, \tag{5.2.19}$$

where ρ_{wl} is the density of the solid wax in the oil. The gradient of the concentration, ∇C, is given by

$$\nabla C = \frac{\partial C}{\partial r}\vec{i}_r + \frac{1}{r}\frac{\partial C}{\partial \theta}\vec{i}_\theta + \frac{1}{r\sin\theta}\frac{\partial C}{\partial \phi}\vec{i}_\phi. \tag{5.2.20}$$

The mass flux into the particle, evaluated on the surface of the particle, is $-\vec{J}\cdot\vec{n}$ where $\vec{n}$ is the unit outward normal vector. The mass flux, $-\vec{J}\cdot\vec{n}$, is equal to the mass of wax deposited to unit surface area per unit time. The dimension of mass flux is [kg/(m^{2}s)]. The boundary condition on the surface of the growing particle relates the mass flux in the direction along the outward normal to the surface, $-\vec{J}\cdot\vec{n}$, to the level of supersaturation on the particle surface, $C(R(r,\theta,\phi,t),\theta,\phi,t) - C_*(T)$, where $C_*(T)$ is the solubility of the wax in oil at temperature T. This boundary condition on the wax particle surface for the mass flux was suggested in [24] and [25], in the form

$$\rho_{wl} D \nabla C \cdot \vec{n} = \rho_{wl} k_r (C - C_*).$$

Here the left hand side is the mass flux towards the surface and the coefficient of proportionality in the right hand side is made of two parts: the density of wax which is diffused, ρ_{wl}, and mass transfer coefficient, k_r. Then we obtain

$$D\nabla C \cdot \vec{n} = k_r(C - C_*) \qquad (r = R(\theta, \phi, t)). \tag{5.2.21}$$

The mass transfer coefficient k_r, see [24], has dimension of velocity, m/s. The scalar product on the left hand side of equation (5.2.21) is evaluated by using equations (5.2.20) and (5.2.4).

The equation describing the dynamics of the particle growth is obtained by equating the mass dm deposited on an element dA of the particle surface per time Δt, $dm = -(\vec{J} \cdot \vec{n})dAdt$, to the increase of the local mass of the particle, $\rho_{wl} V_r dAdt$. By using equations (5.2.19) and (5.2.5), we obtain the deposited mass onto the element dA of the particle surface during the time interval dt,

$$dm = \rho_{wl} D \frac{\partial C}{\partial n} dAdt = \rho_{wl} \cdot \frac{-\frac{\partial S}{\partial t}}{|\nabla S|} dAdt. \tag{5.2.22}$$

Equation (5.2.22) provides

$$D\nabla C \cdot \vec{n} = \frac{-\frac{\partial S}{\partial t}}{|\nabla S|}, \tag{5.2.23}$$

where $|\nabla S| \cdot \vec{n} = \nabla S$, see equation (5.2.3), and $\frac{\partial S}{\partial t} = -\frac{\partial R}{\partial t}$, see equation (5.2.1). Then equation (5.2.23) leads to the following equation for the dynamics of the wax particle surface,

$$\frac{\partial R}{\partial t} = D(\nabla C \cdot \nabla S). \tag{5.2.24}$$

The mass of the wax particle, $m(t)$, in equation (5.2.12) is equal to the wax density, ρ_{ws}, multiplied by the particle volume. For a known function $R(\theta, \phi, t)$ in (5.2.1), we have

$$m(t) = \frac{1}{3} \rho_{ws} \int_0^{2\pi} d\phi \int_0^{\pi} R^3(\theta, \phi, t) \sin\theta d\theta, \tag{5.2.25}$$

see [36].

The three-dimensional coupled problem of a growing particle moving together with a uniform flow has been formulated above. Next we restrict ourselves to axisymmetric deformations of the particle, where the concentration C, the velocity field $\vec{u}$, the pressure P and the shape function R do not depend on the azimuthal coordinate ϕ.

5.3 Axisymmetric problem of a wax particle growth

The particle moves together with the flow from the entrance to the pipe along one stream line. At arbitrary fixed distance from the wall, we study the growth of an axisymmetric particle along the pipe. In this section, the problem is formulated for the axisymmetric case. For incompressible axisymmetric flow in spherical coordinate system (r, θ, ϕ) the solution is independent of ϕ. Consequently we write the surface of the particle (5.2.1) in axisymmetric form, independent of ϕ as:

$$S(r, \theta, t) = r - R(\theta, t) = 0. \tag{5.3.1}$$

The initial shape of the particle is spherical,

$$R(\theta, 0) = R_0. \tag{5.3.2}$$

The unit outward normal vector to the surface (5.3.1) is

$$\vec{n} = \frac{\vec{i_r} - \frac{1}{R(\theta,t)} \left(\frac{\partial R}{\partial \theta}\right) \vec{i_\theta}}{\sqrt{1 + \frac{1}{R^2(\theta,t)} \left(\frac{\partial R}{\partial \theta}\right)^2}}. \tag{5.3.3}$$

The normal component of velocity of the fluid on the wax particle surface is zero

$$\vec{u} \cdot \vec{n} = 0, \tag{5.3.4}$$

where $\vec{u} = u_r \vec{i_r} + u_\theta \vec{i_\theta}$, see (5.2.6).

The no-slip condition (5.2.8) reads

$$\vec{u} \cdot \vec{\tau} = 0, \tag{5.3.5}$$

on the particle surface, where

$$\vec{\tau} = \frac{\frac{1}{R(\theta,t)} \left(\frac{\partial R}{\partial \theta}\right) \vec{i_r} + \vec{i_\theta}}{\sqrt{1 + \frac{1}{R^2(\theta,t)} \left(\frac{\partial R}{\partial \theta}\right)^2}}$$

is the tangent vector to the surface (5.3.1). It is clear that $\vec{n} \cdot \vec{\tau} = 0$. Then (5.3.5) yields

$$u_r \cdot \frac{\partial R}{\partial \theta} + u_\theta \cdot R = 0 \qquad (r = R(\theta, t)). \tag{5.3.6}$$

An axisymmetric flow of an incompressible fluid is described by a stream function $\psi(r, \theta, t)$ which gives the flow velocity components, see [2],

$$u_r = \frac{1}{r^2 \sin\theta} \frac{\partial \psi(r,\theta,t)}{\partial \theta}, \qquad u_\theta = -\frac{1}{r \sin\theta} \frac{\partial \psi(r,\theta,t)}{\partial r}. \tag{5.3.7}$$

The components (5.3.7) satisfy the continuity equation (5.2.10) written in the spherical coordinates,

$$\nabla \cdot \vec{u} = \frac{1}{r^2} \frac{\partial}{\partial r}(r^2 u_r) + \frac{1}{r \sin\theta} \frac{\partial}{\partial \theta} (u_\theta \sin\theta) = 0, \tag{5.3.8}$$

for any function $\psi(r, \theta, t)$. The vorticity, $\vec{\omega}(r, \theta, t) = \nabla \times \vec{u}$, of an axisymmetric flow is $\vec{\omega}(r, \theta, t) = \omega(r, \theta, t)\vec{i_\phi}$, where, see [2],

$$\omega = \frac{1}{r} \left[\frac{\partial (r u_\theta)}{\partial r} - \frac{\partial u_r}{\partial \theta} \right] = -\frac{1}{r \sin\theta} \left(\frac{\partial^2 \psi}{\partial r^2} + \frac{\sin\theta}{r^2} \frac{\partial}{\partial \theta} \left(\frac{1}{\sin\theta} \frac{\partial \psi}{\partial \theta} \right) \right). \tag{5.3.9}$$

The Navier-Stokes equation (5.2.9) provides the following equation for vorticity $\vec{\omega}$, see [2],

$$\frac{\partial \vec{\omega}}{\partial t} + (\vec{u} \cdot \nabla)\vec{\omega} = (\vec{\omega} \cdot \nabla)\vec{u} + \nu \nabla^2 \vec{\omega}. \tag{5.3.10}$$

For axisymmetric flow the first term on the right-hand side of equation (5.3.10) is

$$(\vec{\omega} \cdot \nabla)\vec{u} = \left(\omega_r \frac{\partial}{\partial r} + \frac{\omega_\theta}{r}\frac{\partial}{\partial \theta} + \frac{\omega_\phi}{r \sin\theta}\frac{\partial}{\partial \phi}\right)\left(u_r \vec{i_r} + u_\theta \vec{i_\theta}\right), \tag{5.3.11}$$

where $\omega_r = \omega_\theta \equiv 0$ and $(\vec{\omega} \cdot \nabla)\vec{u} = \frac{\omega_\phi}{r \sin\theta}(u_r \sin\theta \vec{i_\phi} + u_\theta \cos\theta \vec{i_\phi})$.

Equation (5.3.10) leads to equation

$$\begin{gathered} \frac{\partial \omega}{\partial t} + u_r \frac{\partial}{\partial r} + \frac{u_\theta}{r}\frac{\partial \omega}{\partial \theta} - \left(\frac{u_r}{r} + \frac{u_\theta \cos\theta}{r \sin\theta}\right)\omega = \\ \nu\left[\frac{1}{r^2}\frac{\partial}{\partial r}\left(r^2 \frac{\partial \omega}{\partial r}\right) + \frac{1}{r^2 \sin\theta}\frac{\partial}{\partial \theta}\left(\sin\theta \frac{\partial \omega}{\partial \theta}\right) - \frac{\omega}{r^2}\frac{1}{\sin^2\theta}\right], \end{gathered} \tag{5.3.12}$$

for the scalar function $\omega(r, \theta, t)$.

The no-slip condition (5.3.6) and (5.3.7) give

$$\frac{1}{\sin\theta}\left(\frac{1}{R^2}\frac{\partial R}{\partial \theta}\frac{\partial \psi}{\partial \theta} - \frac{\partial \psi}{\partial r}\right) = 0.$$

On the other hand, the velocity component tangent to the wax particle surface is

$$\begin{aligned} \frac{\partial \psi}{\partial n} = \nabla\psi \cdot \vec{n} &= \left(\frac{\partial \psi}{\partial r}\vec{i_r} + \frac{1}{r}\frac{\partial \psi}{\partial \theta}\vec{i_\theta}\right) \cdot \frac{\vec{i_r} - \frac{1}{R(\theta,t)}\left(\frac{\partial R}{\partial \theta}\right)\vec{i_\theta}}{\sqrt{1 + \frac{1}{R^2(\theta,t)}\left(\frac{\partial R}{\partial \theta}\right)^2}} \\ &= \left(\frac{\partial \psi}{\partial r} - \frac{1}{R^2}\frac{\partial R}{\partial \theta}\frac{\partial \psi}{\partial \theta}\right)\frac{1}{\sqrt{1 + \frac{1}{R^2}\left(\frac{\partial R}{\partial \theta}\right)^2}}. \end{aligned}$$

Therefore, because of the no-slip condition, we have

$$\frac{\partial \psi}{\partial n} = \left(\frac{\partial \psi}{\partial r} - \frac{1}{R^2}\frac{\partial R}{\partial \theta}\frac{\partial \psi}{\partial \theta}\right)\frac{1}{\sqrt{1 + \frac{1}{R^2}\left(\frac{\partial R}{\partial \theta}\right)^2}} = 0. \tag{5.3.13}$$

Condition (5.3.4) gives

$$u_r - \frac{1}{R}\frac{\partial R}{\partial \theta}u_\theta = 0. \tag{5.3.14}$$

Substituting equations (5.3.7) into (5.3.14), we have

$$\frac{1}{R^2\sin\theta}\frac{\partial\psi}{\partial\theta}+\frac{\partial R}{\partial\theta}\frac{1}{R^2\sin\theta}\frac{\partial\psi}{\partial r}=0,$$

and rearrangement gives

$$\frac{\partial R}{\partial\theta}\frac{\partial\psi}{\partial r}+\frac{\partial\psi}{\partial\theta}=0, \tag{5.3.15}$$

where

$$\frac{\partial R}{\partial\theta}\frac{\partial\psi}{\partial r}+\frac{\partial\psi}{\partial\theta}=\frac{\partial\left[\psi(R(\theta,t),\theta,t)\right]}{\partial\theta}.$$

The stream-line $\theta=0$, where $r>R(0,t)$ is the symmetry line of the flow, which goes to infinity. We take $\psi=0$ on this line. Then the condition (5.3.15) can be integrated along the boundary and a boundary conditions on the particle surface read

$$\psi=0, \tag{5.3.16}$$

and

$$\frac{\partial\psi}{\partial n}=0 \qquad (r=R(\theta,t),0\leqslant\theta\leqslant\pi)\,. \tag{5.3.17}$$

The hydrodynamic part of the axisymmetric coupled problem consists of equations (5.3.7), (5.3.9) and (5.3.12), boundary conditions (5.3.16)-(5.3.17) and the far-field condition (5.2.11).

The vector force acting on the wax particle follows from (5.2.13) and for an axisymmetric flow is given by

$$\vec{F}(t)=2\pi\int_0^{\pi}(T\cdot\vec{n})\,|_{r=R(\theta,t)}R^2(\theta,t)\sin\theta\sqrt{1+\frac{1}{R^2}\left(\frac{\partial R}{\partial\theta}\right)^2}\,d\theta, \tag{5.3.18}$$

where the stress tensor T of the axisymmetric flow is, see [2],

$$T=\begin{pmatrix}T_{rr} & T_{r\theta}\\ T_{\theta r} & T_{\theta\theta}\end{pmatrix}, \tag{5.3.19}$$

where

$$T_{rr} = -P + 2\mu \frac{\partial u_r}{\partial r}, \qquad T_{\theta\theta} = -P + 2\mu \left(\frac{1}{r} \frac{\partial u_\theta}{\partial \theta} \right),$$

$$T_{r\theta} = T_{\theta r} = \mu \left(r \frac{\partial}{\partial r} \left(\frac{u_\theta}{r} \right) + \frac{1}{r} \frac{\partial u_r}{\partial \theta} \right).$$

Then the product $T \cdot \vec{n}$ on the surface of the wax particle, which is needed for evaluation of the hydrodynamic force (5.3.18), reads

$$T \cdot \vec{n} = \begin{pmatrix} T_{rr} & T_{r\theta} \\ T_{\theta r} & T_{\theta\theta} \end{pmatrix} \left(\vec{i_r} - \frac{1}{R} \frac{\partial R}{\partial \theta} \vec{i_\theta} \right) \frac{1}{\sqrt{1 + \frac{1}{R^2} (\frac{\partial R}{\partial \theta})^2}}$$

$$= \left[\left(T_{rr} - \frac{1}{R} \frac{\partial R}{\partial \theta} T_{r\theta} \right) \vec{i_r} + \left(T_{\theta r} - \frac{1}{R} \frac{\partial R}{\partial \theta} T_{\theta\theta} \right) \vec{i_\theta} \right] \frac{1}{\sqrt{1 + \frac{1}{R^2} (\frac{\partial R}{\partial \theta})^2}}. \quad (5.3.20)$$

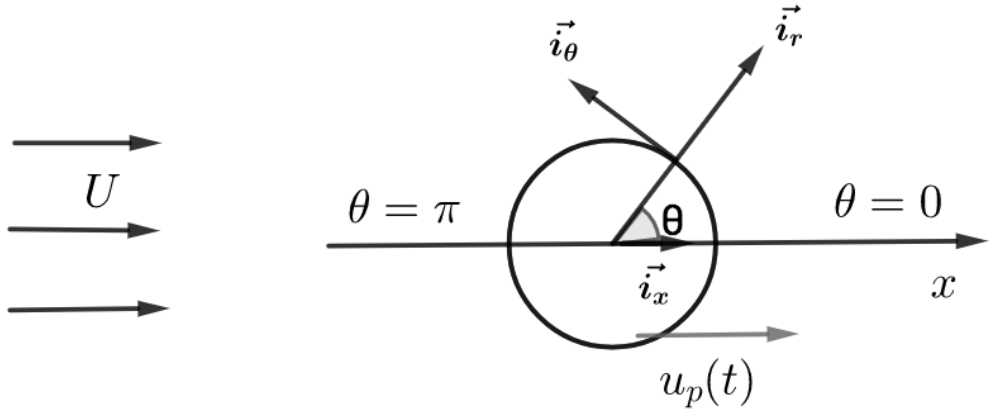

Figure 5.3.1: Uniform flow past an axisymmetric wax particle, $0 \leqslant \theta \leqslant \pi$, U is the velocity of the flow and $u_p(t)$ is the velocity of the wax particle.

It is clear that only the x-component of the hydrodynamic force, $F_x = \vec{F}(t) \cdot \vec{i_x}$, is non-zero in an axisymmetric flow. Here, see Figure 5.3.1,

$$\vec{i_r} \cdot \vec{i_x} = \cos\theta, \qquad \vec{i_\theta} \cdot \vec{i_x} = -\sin\theta,$$

and then

$$\vec{i_x} \cdot T \cdot \vec{n} = \left[\left(T_{rr} - \frac{1}{R}\frac{\partial R}{\partial \theta} T_{r\theta} \right) \cos\theta + \left(\frac{1}{R}\frac{\partial R}{\partial \theta} T_{\theta\theta} - T_{\theta r} \right) \sin\theta \right] \frac{1}{\sqrt{1 + \frac{1}{R^2}(\frac{\partial R}{\partial \theta})^2}}$$

$$= \left[T_{rr}\cos\theta - T_{r\theta}\left(\frac{1}{R}\frac{\partial R}{\partial \theta}\cos\theta + \sin\theta \right) + \frac{1}{R}\frac{\partial R}{\partial \theta} T_{\theta\theta}\sin\theta \right] \frac{1}{\sqrt{1 + \frac{1}{R^2}(\frac{\partial R}{\partial \theta})^2}}. \tag{5.3.21}$$

Equations (5.3.18) and (5.3.21) yield the force in the equation (5.2.12) for the particle speed $u_p(t)$.

Diffusion of the wax molecules toward the wax particle is described by the equations (5.2.15) and (5.2.16), initial (5.2.17) and far-field (5.2.18) conditions and the condition (5.2.21) on the surface of the particle. These equations have the following forms in the axisymmetric case:

$$\frac{\partial C}{\partial t} + u_r \frac{\partial C}{\partial r} + \frac{u_\theta}{r}\frac{\partial C}{\partial \theta} = D\left[\frac{1}{r^2}\frac{\partial}{\partial r}\left(r^2 \frac{\partial C}{\partial r} \right) + \frac{1}{r^2 \sin\theta}\frac{\partial}{\partial \theta}\left(\sin\theta \frac{\partial C}{\partial \theta} \right) \right]$$
$$(r > R(\theta, t), t > 0), \tag{5.3.22}$$

$$C(r, \theta, 0) = C_0 \qquad \text{at} \qquad t = 0, \tag{5.3.23}$$

$$C(r, \theta, t) \longrightarrow C_0 \qquad \text{as} \qquad r \longrightarrow \infty, t > 0, \tag{5.3.24}$$

$$\frac{\partial C}{\partial r} - \frac{1}{R^2}\frac{\partial R}{\partial \theta}\frac{\partial C}{\partial \theta} = \frac{k_r}{D}(C - C_*)\sqrt{1 + \frac{1}{R^2}\left(\frac{\partial R}{\partial \theta} \right)^2} \qquad \text{on} \qquad r = R(\theta, t). \tag{5.3.25}$$

Finally, equation (5.2.24), which describes the evolution of the wax particle shape, takes the form

$$\frac{\partial R}{\partial t} = D\left(\frac{\partial C}{\partial r} - \frac{1}{R^2}\frac{\partial R}{\partial \theta}\frac{\partial C}{\partial \theta} \right) \qquad \text{on} \qquad r = R(\theta, t), t > 0, \tag{5.3.26}$$

$$R(\theta, 0) = R_0 \qquad \text{when} \qquad t = 0. \tag{5.3.27}$$

Equation (5.2.25) in the axisymmetric case reads

$$m(t) = \frac{2\pi}{3}\rho_{ws}\int_0^{\pi} R^3(\theta,t)\sin\theta d\theta. \tag{5.3.28}$$

5.4 Non-Dimensionalized problem

To write the convective diffusion equation (5.3.22), the boundary conditions (5.3.25) and (5.3.26), Navier-Stokes equation (5.2.9)-(5.2.10), in a more clear form, we non-dimensionalize the variable of the length dimension with the initial particle radius R_0, velocity of the oil relative to the wax particle with $U_* = U - u_p(0)$, and pressure with $\frac{\rho\nu U_*}{R_0}$. Diffusion is considered as a dominant effect in this problem with the time scale $\frac{R_0^2}{D}$. Convective is assumed small compared with the diffusion, $\frac{U_* R_0}{D} = \epsilon$ and $\epsilon << 1$. Also we assume that the kinematic viscosity of the oil ν is much bigger than the diffusion coefficient D, $\epsilon_1 = \frac{D}{\nu}$, $\epsilon_1 << 1$. The dimensionless variables are denoted by hats:

$$\hat{r} = \frac{r}{R_0}, \qquad \hat{t} = \frac{Dt}{R_0^2}, \qquad \hat{C}(\hat{r},\theta,\hat{t}) = \frac{C(r,\theta,t) - C_0}{(C_0 - C_*)},$$

$$\hat{u}(\hat{t}) = \frac{u(t)}{U_*}, \qquad \hat{R}(\theta,\hat{t}) = \frac{R(\theta,t)}{R_0}, \qquad \hat{\nabla} = R_0\nabla, \qquad \hat{P} = \frac{PR_0}{\rho\nu U_*}.$$

Scales of other unknown functions will be introduced later. Hats are dropped below.

The diffusion part of the problem, which is described by equations (5.3.22)-(5.3.25), in the dimensionless variables is

$$\begin{aligned} &\frac{\partial C}{\partial t} + \epsilon\left[u_r(r,\theta,t)\frac{\partial C}{\partial r} + \frac{u_\theta(r,\theta,t)}{r}\frac{\partial C}{\partial \theta}\right] \\ &= \frac{1}{r^2}\left[\frac{\partial}{\partial r}\left(r^2\frac{\partial C}{\partial r}\right) + \frac{1}{\sin\theta}\frac{\partial}{\partial\theta}\left(\sin\theta\frac{\partial C}{\partial\theta}\right)\right] \qquad (r > R(\theta,t), t > 0), \end{aligned} \tag{5.4.1}$$

$$C(r,\theta,0) = 0 \qquad (t=0), \tag{5.4.2}$$

$$C(r,\theta,t) \longrightarrow 0 \qquad (r \longrightarrow \infty), \tag{5.4.3}$$

$$\frac{\partial C}{\partial r} - \frac{1}{R^2}\frac{\partial R}{\partial \theta}\frac{\partial C}{\partial \theta} = \hat{k_r}(C+1)\sqrt{1+\frac{1}{R^2}\left(\frac{\partial R}{\partial \theta}\right)^2} \qquad (r = R(\theta,t), t \geq 0), \tag{5.4.4}$$

where $\hat{k_r} = \frac{R_0 k_r}{D}$. We assume that the non-dimensional parameter $\hat{k_r}$ is of order $O(1)$ in the dimensionless variable.

The kinematic condition on the particle surface is given by equations (5.3.26) and (5.3.27) which read in the dimensionless variables,

$$\frac{\partial R}{\partial t} = (C_0 - C_*)\left(\frac{\partial C}{\partial r} - \frac{1}{R^2}\frac{\partial R}{\partial \theta}\frac{\partial C}{\partial \theta}\right) \qquad (r = R(\theta,t)), \tag{5.4.5}$$

$$R(\theta,0) = 1 \qquad (t=0), \tag{5.4.6}$$

where $C_0 - C_*$ is assumed to be $O(1)$.

The hydrodynamic part of the problem, equations (5.3.7)-(5.3.12), yields the scale $R_0^2 U_*$ for ψ and the scale $\frac{U_*}{R_0}$ for the vorticity ω. Note that equations (5.3.7) and (5.3.9) do not change their forms in the dimensionless variables. Equation (5.3.12) now reads

$$\epsilon_1\left(\frac{\partial \omega}{\partial t} + \epsilon\left(u_r\frac{\partial \omega}{\partial r} + \frac{u_\theta}{r}\frac{\partial \omega}{\partial \theta}\right)\right) = \frac{1}{r^2}\frac{\partial}{\partial r}\left(r^2\frac{\partial \omega}{\partial r}\right) + \frac{1}{r^2\sin\theta}\frac{\partial}{\partial \theta}\left(\sin\theta\frac{\partial \omega}{\partial \theta}\right). \tag{5.4.7}$$

The boundary conditions (5.3.16) and (5.3.17) keep their forms in the dimensionless variables. The condition at infinity (5.2.11) suggests the relative velocity between the flow and the wax particle in the form

$$U^*\hat{u}_d(t) = U - U^*\hat{u_p}(\hat{t}) \tag{5.4.8}$$

and then

$$\hat{\vec{u}} \to (\hat{u}_d(\hat{t}), 0, 0) \qquad (\hat{r} \to \infty). \tag{5.4.9}$$

Note that the pressure $P(r, \theta, t)$ is needed in the calculations of hydrodynamic force, see equation (5.3.18) and (5.3.19). The pressure can be obtained from the equations (5.2.9) and (5.2.10), which have the following forms in the dimensionless variables (hats are dropped):

$$\epsilon_1 \left(\frac{\partial \vec{u}}{\partial t} + \epsilon(\vec{u} \cdot \nabla)\vec{u} \right) = -\nabla P + \nabla^2 \vec{u} - \epsilon_1 \frac{d\vec{u_p}}{dt} \tag{5.4.10}$$

$$\nabla \cdot \vec{u} = 0 \tag{5.4.11}$$

Note that $\epsilon \cdot \epsilon_1 = \frac{U_* R_0}{\nu} = Re$. Therefore the case under consideration corresponds to the slow motion of the wax particle with respect to the flow.
Equations (5.2.12) and (5.3.18) of the particle motion, equation (5.3.28) for the mass of the particle and equation (5.4.8) provide

$$T = \frac{\mu U_*}{R_0}\hat{T}, \qquad F_x = \mu U_* R_0 \hat{F}_x, \qquad m = \rho_{ws} R_0^3 \hat{m}(\hat{t}),$$

$$\frac{D}{R_0^2}\frac{d}{d\hat{t}}\left[\rho_{ws} R_0^3 \hat{m}(\hat{t})(U - U_* \hat{u_d})\right] = \rho \nu U_* R_0 \hat{F}_x(\hat{t}),$$

and

$$\frac{\rho_{ws}}{\rho}\frac{U}{U_*}\epsilon_1 \frac{d}{d\hat{t}}\left[\hat{m}(\hat{t})\left(1 - \frac{U_*}{U}\hat{u_d}\right)\right] = \hat{F}_x(\hat{t}). \tag{5.4.12}$$

The derived equation is non-trivial as $\epsilon_1 \to 0$ only if the velocity scale U_* is small compared to the velocity of the fluid flow U,

$$U_* = \epsilon_1 U \frac{\rho_{ws}}{\rho} \cdot \gamma, \tag{5.4.13}$$

where $\gamma = O(1)$. Then equation of the particle motion (5.4.12) yields (hats are dropped)

$$\frac{1}{\gamma}\frac{dm}{dt} - \epsilon_1 \frac{\rho_{ws}}{\rho}\frac{d}{dt}\left(m(t)u_d(t)\right) = F_x(t) \qquad (t > 0), \tag{5.4.14}$$

$$u_d(0) = 1. \tag{5.4.15}$$

The hydrodynamic force equation (5.3.18) keeps its form in the dimensionless variables.

5.5 Asymptotic analysis of the flow around the growing particle

In order to perform asymptotic analyses of the problem formulated in the previous section, we assume that the velocity of the flow with respect to the moving wax particle is much smaller than the velocity of the flow U in the global coordinate system, see (5.4.13). Then the growth of the wax particle is governed by the diffusion in the leading order with the convective terms being responsible for deviation of the wax particle shape from a spherical one. We are concerned with the leading order of this deviation under the assumption $\epsilon_1 = \alpha\epsilon$, $\alpha = O(1)$. We write the asymptotic expansion for the shape of the particle surface, $r = R(\theta, t)$, in terms of ϵ as:

$$R(\theta, t) = R^{(0)}(t) + \epsilon R^{(1)}(\theta, t) + O(\epsilon^2), \tag{5.5.1}$$

where $R^{(0)}(t)$, and $R^{(1)}(\theta, t)$ are of order O(1) as $\epsilon \longrightarrow 0$. Here ϵ is a small parameter which is responsible for small deviation of the wax particle shape from spherical. Then, (5.3.1) provides

$$S = r - R^{(0)}(t) - \epsilon R^{(1)}(\theta, t) + O(\epsilon^2). \tag{5.5.2}$$

The unit normal vector $\vec{n}$ given by (5.3.3) and appeared in the boundary condition (5.3.17) can be approximated for small ϵ as

$$\vec{n} = \frac{\nabla S}{|\nabla S|} = \vec{i}_r - \epsilon \left(\vec{i}_\theta \frac{1}{R^{(0)}(1+\epsilon\frac{R^{(1)}}{R^{(0)}})} \frac{\partial R^{(1)}}{\partial \theta} \right) + O(\epsilon^2) \tag{5.5.3}$$

$$= \vec{i}_r - \epsilon \left(\vec{i}_\theta \frac{1}{R^{(0)}} \left(1 - \epsilon \frac{R^{(1)}}{R^{(0)}} + \dots \right) \frac{\partial R^{(1)}}{\partial \theta} \right) + O(\epsilon^2) \tag{5.5.4}$$

where $|\nabla S| = \sqrt{1+O(\epsilon^2)} = 1 + O(\epsilon^2)$.

Hence,

$$\vec{n} = \vec{i}_r - \epsilon \frac{1}{R^{(0)}} \frac{\partial R^{(1)}}{\partial \theta} \vec{i}_\theta + O(\epsilon^2). \tag{5.5.5}$$

The stream function is sought in the form

$$\psi(r,\theta,t) = \psi_0(r,\theta,t) + \epsilon\psi_1(r,\theta,t) + O(\epsilon^2). \tag{5.5.6}$$

The boundary conditions (5.3.16) and (5.3.17) with Taylor expansion at $r = R^{(0)}$ provide

$$\begin{aligned}
&\psi[R^{(0)}(t) + \epsilon R^{(1)}(\theta,t) + O(\epsilon^2), \theta, t] \\
&\quad = \psi(R^{(0)}(t),\theta,t) + \frac{\partial \psi}{\partial r}(R^{(0)}(t),\theta,t) \cdot \epsilon R^{(1)}(\theta,t) + O(\epsilon^2) = \psi_0(R^{(0)}(t),\theta,t) \\
&\quad + \epsilon \left[\psi_1(R^{(0)}(t),\theta,t) + \frac{\partial \psi_0}{\partial r}(R^{(0)}(t),\theta,t) R^{(1)}(\theta,t) \right] + O(\epsilon^2) = 0.
\end{aligned} \tag{5.5.7}$$

and

$$\begin{aligned}
&\frac{\partial \psi}{\partial n}[R^{(0)}(t) + \epsilon R^{(1)}(\theta,t) + O(\epsilon^2), \theta, t] = \\
&\quad \nabla\psi \cdot \vec{n} = \frac{\partial \psi}{\partial r} - \frac{1}{R^2}\frac{\partial R}{\partial \theta}\frac{\partial \psi}{\partial \theta} + O(\epsilon^2) = \frac{\partial \psi}{\partial r}(R^{(0)}(t),\theta,t) \\
&\qquad + \frac{\partial^2 \psi}{\partial r^2}(R^{(0)}(t),\theta,t)\epsilon R^{(1)}(\theta,t) - \frac{1}{(R^{(0)})^2}\epsilon\frac{\partial R^{(1)}}{\partial \theta}\frac{\partial \psi}{\partial \theta} + O(\epsilon^2) \\
&\qquad = \frac{\partial \psi_0}{\partial r}(R^{(0)}(t),\theta,t) + \epsilon \left[\frac{\partial^2 \psi_0}{\partial r^2}(R^{(0)}(t),\theta,t) R^{(1)}(\theta,t) \right. \\
&\qquad \left. - \frac{1}{(R^{(0)})^2}\frac{\partial R^{(1)}}{\partial \theta}\frac{\partial \psi_0}{\partial \theta}(R^{(0)}(t),\theta,t) + \frac{\partial \psi_1}{\partial r}[R^{(0)}(t),\theta,t] \right] + O(\epsilon^2) = 0.
\end{aligned} \tag{5.5.8}$$

Equating the terms of the same order in ϵ in equation (5.5.7) and (5.5.8), we find

$$\psi_0 = 0, \qquad \frac{\partial \psi_0}{\partial r} = 0 \qquad (r = R^{(0)}(t)), \tag{5.5.9}$$

$$\psi_1 = 0, \qquad \frac{\partial \psi_1}{\partial r} = -\frac{\partial^2 \psi_0}{\partial r^2}[R^{(0)}(t), \theta, t]R^{(1)}(\theta, t) \qquad (r = R^{(0)}(t)). \tag{5.5.10}$$

The asymptotic expansion (5.5.6), equations (5.3.7), (5.3.9), (5.4.8), and (5.4.10) provide

$$\begin{aligned} u_r(r,\theta,t) &= u_r^{(0)}(r,\theta,t) + \epsilon u_r^{(1)}(r,\theta,t) + O(\epsilon^2), \\ u_\theta(r,\theta,t) &= u_\theta^{(0)}(r,\theta,t) + \epsilon u_\theta^{(1)}(r,\theta,t) + O(\epsilon^2), \\ \omega(r,\theta,t) &= \omega^{(0)}(r,\theta,t) + \epsilon \omega^{(1)}(r,\theta,t) + O(\epsilon^2), \\ P(r,\theta,t) &= P^{(0)}(r,\theta,t) + \epsilon P^{(1)}(r,\theta,t) + O(\epsilon^2), \\ u_d(t) &= u_d^{(0)}(t) + \epsilon u_d^{(1)}(t) + O(\epsilon^2). \end{aligned} \tag{5.5.11}$$

The Navier-Stokes equations (5.4.10) and (5.4.11) give

$$-\nabla P^{(0)} + \nabla^2 \vec{u}^{(0)} = 0, \qquad \nabla \cdot \vec{u}^{(0)} = 0, \tag{5.5.12}$$

$$-\nabla P^{(1)} + \nabla^2 \vec{u}^{(1)} = -\alpha \frac{d\vec{u_p}^{(0)}}{dt} + \alpha \frac{\partial \vec{u}^{(0)}}{\partial t}, \qquad \nabla \cdot \vec{u}^{(1)} = 0. \tag{5.5.13}$$

In order to derive the equation for the stream function $\psi_0(r, \theta, t)$ from the Navier-Stokes equations (5.5.12), we use the vector identity

$\nabla^2 \vec{u} = \nabla(\nabla \cdot \vec{u}) - \nabla \times (\nabla \times \vec{u})$. Then equation (5.5.12) and the definition of the vorticity, see section 5.3, provide

$$\nabla P^{(0)} = \nabla^2 \vec{u}^{(0)} = \nabla(\nabla \cdot \vec{u}^{(0)}) - \nabla \times (\nabla \times \vec{u}^{(0)}) = -\nabla \times \vec{\omega}^{(0)},$$

where $\vec{\omega}^{(0)} = \omega^{(0)}(r, \theta, t)\vec{i}_\phi$ and ω is related to the stream function by equation (5.3.9) which following [2] is written here in the form

$$\omega^{(0)} = -\frac{1}{r\sin\theta}E^2\psi_0, \qquad E^2\psi_0 = \frac{\partial^2\psi_0}{\partial r^2} + \frac{\sin\theta}{r^2}\frac{\partial}{\partial\theta}\left(\frac{1}{\sin\theta}\frac{\partial\psi_0}{\partial\theta}\right).$$

By algebra,

$$-\nabla\times\vec{\omega}^{(0)} = -\nabla\times(\omega^{(0)}\vec{i}_\phi) = -\frac{1}{r\sin\theta}\frac{\partial}{\partial\theta}(\sin\theta\omega^{(0)})\vec{i}_r + \frac{1}{r}\frac{\partial}{\partial r}(r\omega^{(0)})\vec{i}_\theta$$

and then

$$\nabla P^{(0)} = \frac{1}{r^2\sin\theta}\frac{\partial}{\partial\theta}(E^2\psi_0)\vec{i}_r - \frac{1}{r\sin\theta}\frac{\partial}{\partial r}(E^2\psi_0)\vec{i}_\theta. \tag{5.5.14}$$

The gradient of the leading-order pressure in (5.5.14) is given by

$$\nabla P^{(0)} = \frac{\partial P^{(0)}}{\partial r}\vec{i}_r + \frac{1}{r}\frac{\partial P^{(0)}}{\partial\theta}\vec{i}_\theta. \tag{5.5.15}$$

By taking the components in the direction $\vec{i}_r$ and $\vec{i}_\theta$ in equations (5.5.14) and (5.5.15) and equating them we find

$$\begin{aligned}\frac{\partial P^{(0)}}{\partial r} &= \frac{1}{r^2\sin\theta}\frac{\partial}{\partial\theta}(E^2\psi_0),\\ \frac{\partial P^{(0)}}{\partial\theta} &= -\frac{1}{\sin\theta}\frac{\partial}{\partial r}(E^2\psi_0).\end{aligned} \tag{5.5.16}$$

Eliminating finally the pressure in (5.5.16) by cross-differentiation, we obtain

$$E^2(E^2\psi_0) = 0. \tag{5.5.17}$$

Substituting the definition of the differential operator E^2 into (5.5.17), we arrive at a partial differential equation for the stream function

$$\left[\frac{\partial^2}{\partial r^2} + \frac{\sin\theta}{r^2}\frac{\partial}{\partial\theta}\left(\frac{1}{\sin\theta}\frac{\partial}{\partial\theta}\right)\right]^2\psi_0 = 0. \tag{5.5.18}$$

The boundary conditions (5.5.9) provide the velocity components on the surface of the wax particle at the leading order,

$$u_r^{(0)}{=}0, \qquad u_\theta^{(0)} = 0 \qquad \left(r = R^{(0)}(t)\right). \tag{5.5.19}$$

The far-field condition (5.4.9) gives (hats are dropped)

$$u_r^{(0)} \sim u_d^{(0)}(t)\cos\theta, \qquad u_\theta^{(0)} \sim -u_d^{(0)}(t)\sin\theta, \qquad (r \to \infty). \tag{5.5.20}$$

Conditions (5.5.20) and the formula (5.3.7) for the velocity components in the far-field provide

$$\frac{1}{r^2\sin\theta}\frac{\partial\psi_0}{\partial\theta} \sim u_d^{(0)}(t)\cos\theta \Rightarrow \psi_0 = \frac{1}{2}u_d^{(0)}(t)r^2\sin^2\theta + f(r),$$
$$-\frac{1}{r\sin\theta}\frac{\partial\psi_0}{\partial r} \sim -u_d^{(0)}(t)\sin\theta \Rightarrow \psi_0 = \frac{1}{2}u_d^{(0)}(t)r^2\sin^2\theta + g(\theta),$$

and the far-field condition for stream function reads

$$\psi_0 \sim \frac{1}{2}u_d^{(0)}(t)r^2\sin^2\theta \qquad \text{as} \qquad r \to \infty. \tag{5.5.21}$$

This condition suggests the solution of equation (5.5.18) in the form, see [2],

$$\psi_0 = f(r,t)\sin^2\theta. \tag{5.5.22}$$

This gives

$$\left(\frac{\partial^2}{\partial r^2} - \frac{2}{r^2}\right)^2 f(r,t) = 0.$$

The solution of this equation, which also satisfies the conditions on the surface of the particle (5.5.9) and the far-field condition (5.5.21), is obtained in [2],

$$\psi_0 = \frac{u_d^{(0)}(t)}{4}\left[2r^2 + \frac{[R^{(0)}(t)]^3}{r} - 3rR^{(0)}(t)\right]\sin^2\theta. \tag{5.5.23}$$

The flow velocity components are

$$u_r^{(0)} = u_d^{(0)}(t)\left[1 - \frac{3}{2}\frac{R^{(0)}(t)}{r} + \frac{1}{2}\left(\frac{R^{(0)}(t)}{r}\right)^3\right]\cos\theta,$$

$$u_\theta^{(0)} = -u_d^{(0)}(t)\left[1 - \frac{3}{4}\frac{R^{(0)}(t)}{r} - \frac{1}{4}\left(\frac{R^{(0)}(t)}{r}\right)^3\right]\sin\theta.$$

In order to calculate the hydrodynamic force acting on the wax particle, we need to determine the pressure. Substituting $E^2\psi_0 = \frac{3u_d^{(0)}R^{(0)}(t)}{2r}\sin^2\theta$ into (5.5.16) we then integrate it with respect to r from r to ∞. We find

$$P^{(0)} = P_\infty - \frac{3}{2}\frac{u_d^{(0)}(t)R^{(0)}}{r^2}\cos\theta, \tag{5.5.24}$$

where P_∞ is the uniform pressure in the flow far from the wax particle.

The elements of the stress tensor (5.3.19) are estimated on the surface of the wax particle (5.5.1) in the non-dimensional variables as $\epsilon \longrightarrow 0$ using the boundary conditions (5.5.9) and (5.5.10), see Appendix B,

$$\frac{\partial u_\theta}{\partial\theta} = O(\epsilon), \qquad \frac{\partial u_r}{\partial\theta} = O(\epsilon^2), \qquad u_\theta = O(\epsilon^2),$$

$$\frac{\partial u_r}{\partial r} = -\epsilon\frac{\frac{\partial R^{(1)}}{\partial\theta}}{(R^{(0)})^2\sin\theta}\frac{\partial^2\psi_0}{\partial r^2}(R^{(0)}(t),\theta,t)+O(\epsilon^2), \qquad \hat{T}_{\theta\theta} = -P^{(0)}(R^{(0)},\theta,t)+O(\epsilon),$$

$$\hat{T}_{rr} = -P^{(0)}(R^{(0)},\theta,t) - \epsilon\left[P^{(1)} + \frac{\partial P^{(0)}}{\partial r}R^{(1)} + 2\frac{\frac{\partial R^{(1)}}{\partial\theta}}{(R^{(0)})^2\sin\theta}\frac{\partial^2\psi_0}{\partial r^2}\right] + O(\epsilon^2),$$

$$\hat{T}_{r\theta} = \frac{\partial u_\theta}{\partial r} + O(\epsilon^2),$$

$$\frac{\partial u_\theta}{\partial r} = -\frac{1}{R^{(0)}\sin\theta}\frac{\partial^2\psi_0}{\partial r^2}+\epsilon\left[\frac{R^{(1)}}{(R^{(0)})^2\sin\theta}\frac{\partial^2\psi_0}{\partial r^2} - \frac{1}{R^{(0)}\sin\theta}\left[\frac{\partial^2\psi_1}{\partial r^2} + \frac{\partial^3\psi_0}{\partial r^3}R^{(1)}\right]\right]+O(\epsilon^2).$$

The equation (5.3.21) provides at the leading order

$$\vec{i_x}\cdot\vec{T}\cdot\vec{n} = -P^{(0)}\cos\theta + \frac{1}{R^{(0)}}\frac{\partial^2\psi_0}{\partial r^2} + O(\epsilon). \tag{5.5.25}$$

Substituting (5.5.5) and (5.5.24) into (5.5.25), and using (5.3.18) the dimensionless force $F_x^{(0)}$ reads

$$
\begin{aligned}
F_x^{(0)}(t) =& 2\pi \int_0^{\pi} (R^{(0)})^2 \left(\frac{1}{R^{(0)}} \frac{\partial^2 \psi_0}{\partial r^2}(R^{(0)}, \theta, t) - P^{(0)} \cos\theta \right) \sin\theta d\theta \\
=& 2\pi \int_0^{\pi} \left(-P_\infty \cos\theta + \frac{3}{2} \frac{u_d^{(0)}(t)}{R^{(0)}(t)} \left[\cos^2\theta + \sin^2\theta \right] \right) R^{(0)2} \sin\theta d\theta \\
=& 6\pi u_d^{(0)}(t) R^{(0)}(t),
\end{aligned}
\tag{5.5.26}
$$

which is the force acting on a spherical wax particle of radius $R^{(0)}(t)$ see [42]. Note that $F_x^{(0)}$ is independent of the speed of the particle growth. The force $F_x^{(0)}$ is equal to the force acting on the solid wax particle of radius $R^{(0)}(t)$ in a viscous fluid with speed $u_d^{(0)}(t)$.

The velocity of the particle $u_p^{(0)}(t)$ follows from the equation (5.4.14), which yields at leading order

$$
\frac{1}{\gamma} \frac{d}{dt} \left(\frac{4}{3} \pi R^{(0)3}(t) \right) = 6\pi u_d^{(0)}(t) R^{(0)}(t),
$$

and then

$$
u_d^{(0)}(t) = \frac{2}{3\gamma} R^{(0)}(t) \frac{dR^{(0)}}{dt}. \tag{5.5.27}
$$

The physical dimensional velocity of the wax particle (5.4.8) is

$$
\frac{u_p^{(0)}(t)}{U} = 1 - \frac{2}{3} \epsilon_1 \frac{\rho_{ws}}{\rho} R^{(0)}(t) \frac{dR^{(0)}(t)}{dt}. \tag{5.5.28}
$$

Therefore the particle velocity $u_p^{(0)}(t)$ is just slightly different from the velocity of the flow and decays in time with increasing the radius of the wax particle. A large growing wax particle moves slower than the flow.

5.6 The first-order correction to the wax particle shape

We seek the concentration $C(r,\theta,t)$ around a single wax particle moving at speed (5.5.28) in the form

$$C(r,\theta,t) = C^{(0)}(r,t) + \epsilon C^{(1)}(r,\theta,t) + O(\epsilon^2). \tag{5.6.1}$$

where $\epsilon << 1$. Note that the leading order solution $C^{(0)}(r,t)$ was studied in chapter 4.

The expansions (5.6.1) and (5.5.11) are substituted into (5.4.1) giving

$$\frac{\partial C^{(0)}}{\partial t} + \epsilon \frac{\partial C^{(1)}}{\partial t} + \epsilon u_r^{(0)}(r,\theta,t) \frac{\partial C^{(0)}}{\partial r} = \frac{1}{r^2}\frac{\partial}{\partial r}\left(r^2\left[\frac{\partial C^{(0)}}{\partial r} + \epsilon \frac{\partial C^{(1)}}{\partial r}\right]\right) + \frac{1}{r^2\sin\theta}\frac{\partial}{\partial \theta}\left(\epsilon \sin\theta \frac{\partial C^{(1)}}{\partial \theta}\right) + O(\epsilon^2). \tag{5.6.2}$$

At the leading order we have $C^{(0)}(r,t)$ which is the spherically symmetric solution independent of θ, see chapter 4. At order ϵ we have:

$$\frac{\partial C^{(1)}}{\partial t} + u_r^{(0)}(r,\theta,t) \frac{\partial C^{(0)}}{\partial r} = \frac{1}{r^2}\frac{\partial}{\partial r}\left(r^2 \frac{\partial C^{(1)}}{\partial r}\right) + \frac{1}{r^2\sin\theta}\frac{\partial}{\partial \theta}\left(\sin\theta \frac{\partial C^{(1)}}{\partial \theta}\right), \tag{5.6.3}$$

where the second term on the left-hand side of equation (5.6.3) plays a role of a forcing term.

In the boundary condition (5.4.4) and the equation of the particle's shape (5.4.5), and using the asymptotic expansion (5.6.1) and (5.5.1) we find that

$$\frac{1}{R^2}\frac{\partial R}{\partial \theta}\frac{\partial C}{\partial \theta} = -\frac{\epsilon^2}{(R^{(0)})^2}\frac{\partial R^{(1)}}{\partial \theta}\frac{\partial C^{(1)}}{\partial \theta} + O(\epsilon^3), \tag{5.6.4}$$

$$\frac{\partial C}{\partial r}\left(R(t),\theta,t\right) = \frac{\partial C}{\partial r}(R^{(0)}(t),\theta,t) + \frac{\partial^2 C}{\partial r^2}(R^{(0)}(t),\theta,t)\epsilon R^{(1)}(\theta,t) + O(\epsilon^2)$$
$$= \frac{\partial C^{(0)}}{\partial r} + \epsilon\left(\frac{\partial C^{(1)}}{\partial r} + R^{(1)}(\theta,t)\frac{\partial^2 C^{(0)}}{\partial r^2}\right) + O(\epsilon^2). \tag{5.6.5}$$

The right-hand side of (5.4.4) reads

$$\hat{k_r}(C\left(R(t),\theta,t\right)+1)\sqrt{1+\frac{1}{R^2}\left(\frac{\partial R}{\partial\theta}\right)^2} = \hat{k_r}(C^{(0)} + \epsilon(C^{(1)} + \frac{\partial C^{(0)}}{\partial r}R^{(1)}) + O(\epsilon^2) \tag{5.6.6}$$

Then the boundary condition (5.4.4) has the form at the leading order

$$\frac{\partial C^{(0)}}{\partial r} = \hat{k_r}\left(C^{(0)}(r,t)+1\right) \qquad \text{on} \qquad r = R^{(0)}(t), \tag{5.6.7}$$

and at the first order,

$$\frac{\partial C^{(1)}}{\partial r} - \hat{k_r}C^{(1)}(r,\theta,t) = R^{(1)}\left(\hat{k_r}\frac{\partial C^{(0)}}{\partial r} - \frac{\partial^2 C^{(0)}}{\partial r^2}\right) \qquad \text{on } r = R^{(0)}(t). \tag{5.6.8}$$

The boundary condition for the particle shape (5.4.5) becomes

$$\frac{\partial R^{(0)}}{\partial t} + \epsilon\frac{\partial R^{(1)}}{\partial t} = (C_0 - C_*)\left[\frac{\partial C^{(0)}}{\partial r} + \epsilon\frac{\partial C^{(1)}}{\partial r} + \epsilon R^{(1)}\frac{\partial^2 C^{(0)}}{\partial r^2}\right] + O(\epsilon^2)$$
$$\text{on } r = R^{(0)}(t). \tag{5.6.9}$$

At the leading order we have

$$\frac{\partial R^{(0)}}{\partial t} = (C_0 - C_*)\frac{\partial C^{(0)}}{\partial r} \qquad \text{on } r = R^{(0)}(t). \tag{5.6.10}$$

At the first order equation (5.6.9) implies

$$\frac{\partial R^{(1)}}{\partial t} = (C_0 - C_*)\left[\frac{\partial C^{(1)}}{\partial r} + R^{(1)}\frac{\partial^2 C^{(0)}}{\partial r^2}\right] \qquad \text{on } r = R^{(0)}(t). \tag{5.6.11}$$

The velocity component u_r at the leading order which is required for equation (5.6.3) was obtained in the previous section,

$$u_r^{(0)} = u_d^{(0)}(t)\left[1 - \frac{3}{2}\frac{R^{(0)}(t)}{r} + \frac{1}{2}\left(\frac{R^{(0)}(t)}{r}\right)^3\right]\cos\theta. \tag{5.6.12}$$

Substituting (5.6.12) into (5.6.3) gives

$$\begin{aligned}\frac{\partial C^{(1)}}{\partial t} + u_d^{(0)}(t)\left[1 - \frac{3}{2}\frac{R^{(0)}(t)}{r} + \frac{1}{2}\left(\frac{R^{(0)}(t)}{r}\right)^3\right]\cos\theta\frac{\partial C^{(0)}}{\partial r} = \\ \frac{1}{r^2}\frac{\partial}{\partial r}\left(r^2\frac{\partial C^{(1)}}{\partial r}\right) + \frac{1}{r^2\sin\theta}\frac{\partial}{\partial\theta}\left(\sin\theta\frac{\partial C^{(1)}}{\partial\theta}\right).\end{aligned} \tag{5.6.13}$$

The concentration of the wax molecules around the wax particle is independent of the angular coordinate θ at the leading order as $\epsilon \longrightarrow 0$ and is described by the equation

$$\frac{\partial C^{(0)}}{\partial t} = \frac{1}{r^2}\frac{\partial}{\partial r}\left(r^2\frac{\partial C^{(0)}}{\partial r}\right) \qquad (r > R^{(0)}(t)) \tag{5.6.14}$$

with the boundary condition (5.6.7), the far-field condition (5.4.3) and the initial condition (5.4.2). The radius of the wax particle, $R^{(0)}(t)$, is obtained by integration of the equation (5.6.10) with the initial condition $R^{(0)}(0) = 1$. This problem was solved in chapter 4.

In the following, we assume that the solution of the leading order problem, $C^{(0)}(r,t)$ and $R^{(0)}(t)$, is known together with the leading order velocity field of the flow around the particle. To find the correction to the shape of the wax particle caused by its time-dependent motion with respect to the flow, we need to find the solution to the non-homogeneous equation (5.6.13), where $u_d^{(0)}(t)$, $R^{(0)}(t)$ and $C^{(0)}(r,t)$ are given, subject to the boundary condition (5.6.8), the far-field condition $C^{(1)}(r,\theta,t) \longrightarrow 0$ as $r \longrightarrow \infty$, and the initial condition $C^{(1)}(r,\theta,0) = 0$. The equation (5.6.13) is to be solved in the known region, $r > R^{(0)}(t)$, in contrast to the leading order problem for $C^{(0)}(r,t)$, where the solution should be determined together with the radius of the wax particle. The boundary condition (5.6.7) is imposed on the known surface, $r = R^{(0)}(t)$.

However, this condition should be satisfied together with the equation of the particle shape (5.6.11). These properties of the first-order problem make it a non-trivial task for analysis.

The forcing term in equation (5.6.13) suggests the solution in the form

$$C^{(1)}(r,\theta,t) = W(r,t)\cos\theta, \qquad R^{(1)}(\theta,t) = H(t)\cos\theta. \tag{5.6.15}$$

Substituting (5.6.15) into equations (5.6.13), (5.6.8), and (5.6.11), we arrive at the following problem for the new unknown functions $W(r,t)$ and $H(t)$:

$$\frac{\partial W}{\partial t} - \frac{1}{r^2}\frac{\partial}{\partial r}\left(r^2\frac{\partial W}{\partial r}\right) - \frac{2}{r^2}W = -u_d^{(0)}(t)\left[1 - \frac{3}{2}\frac{R^{(0)}(t)}{r} + \frac{1}{2}\left(\frac{R^{(0)}(t)}{r}\right)^3\right]\frac{\partial C^{(0)}}{\partial r} \qquad r \geq R^{(0)}, \tag{5.6.16}$$

$$W(r,0) = 0 \qquad (t=0), \tag{5.6.17}$$

$$W(r,t) \longrightarrow 0 \qquad (r \longrightarrow \infty), \tag{5.6.18}$$

$$\frac{\partial W}{\partial r} - \hat{k_r}W(r,t) = H(t)\left(\hat{k_r}\frac{\partial C^{(0)}}{\partial r} - \frac{\partial^2 C^{(0)}}{\partial r^2}\right) \qquad \text{on } r = R^{(0)}(t), \tag{5.6.19}$$

$$\frac{dH}{dt} = (C_0 - C_*)\left[\frac{\partial W}{\partial r} + H(t)\frac{\partial^2 C^{(0)}}{\partial r^2}\right] \qquad \text{on } r = R^{(0)}(t). \tag{5.6.20}$$

We simplify the problem above by introducing a new unknown function $g(r,t) = rW(r,t)$, then the problem becomes

$$\frac{\partial g}{\partial t} - \frac{\partial^2 g}{\partial r^2} + \frac{2}{r^2}g = -u_d^{(0)}(t)\left[r - \frac{3}{2}R^{(0)}(t) + \frac{\left(R^{(0)}(t)\right)^3}{2r^2}\right]\frac{\partial C^{(0)}}{\partial r} \qquad r \geq R^{(0)}, \tag{5.6.21}$$

$$g(r,0) = 0 \qquad (t=0), \tag{5.6.22}$$

$$g(r,t) \longrightarrow 0 \qquad (r \longrightarrow \infty), \tag{5.6.23}$$

$$\frac{1}{r}\frac{\partial g}{\partial r} - \frac{g(r,t)}{r^2} - \hat{k_r}\frac{g(r,t)}{r} = H(t)\left(\hat{k_r}\frac{\partial C^{(0)}}{\partial r} - \frac{\partial^2 C^{(0)}}{\partial r^2}\right) \qquad \text{on } r = R^{(0)}(t), \tag{5.6.24}$$

$$\frac{dH}{dt} = (C_0 - C_*)\left[\frac{1}{r}\frac{\partial g}{\partial r} - \frac{g(r,t)}{r^2} + H(t)\frac{\partial^2 C^{(0)}}{\partial r^2}\right] \qquad \text{on } r = R^{(0)}(t). \tag{5.6.25}$$

The derived problem (5.6.21)-(5.6.25) can be solved numerically together with the non-linear boundary problem for the leading order solution. However, even without the solution in the first order, we may conclude that the effect of particle velocity on its shape is described by the equation (5.5.1),

$$r = R^{(0)}(t) + \epsilon H(t)\cos\theta + O(\epsilon^2). \tag{5.6.26}$$

Here r is the radial coordinate of the particle surface in the coordinate system moving together with the wax particle. For the wax particle which changes its shape in time, the position of its centre of mass and the position of the origin of moving system do not necessarily coincide one with another. Equation (5.6.26) approximately describes the sphere of radius $R^{(0)}(t)$ shifted along the x-axis in the direction of the flow by $\epsilon H(t)$. Therefore, within the first order approximation, where the terms of order $O(\epsilon)$ are taken into account, the wax particle is still spherical. The first-order correction due to time-dependent motion of the wax particle affects the particle displacement with respect to the flow.

Note that equation (5.2.12) of the particle motion is written with respect to the speed $u_p(t)$ of the centre of mass of the particle. The equation predicts that the speed $u_p(t)$ changes if either the force, $F_x(t)$, or the particle mass, $m(t)$, change. However if the particle grows differently in different directions without disturbing the flow around, then the resulting displacement of the centre of mass is not described by the equation (5.2.12). To explain this drawback of

our model, let us consider a particle in an initially non-uniform concentration field $C(r, \theta, \phi, 0)$ without any flow around the particle, $\vec{u}(\vec{x}, 0) = 0$, $u_p(0) = 0$. Then the growth of particle is described by the three-dimensional diffusion problem without convection. The boundary conditions (5.2.7) and (5.2.8) on the surface of the particle assume that a flow is not generated by the growth of the particle. Under these circumstances the hydrodynamic force $F_x(t)$ in (5.2.12) is zero for $t > 0$ and $u_p(t) = 0$ as well. However, the centre of the mass of the particle is displaced in the non-uniform concentration field around the particle. The model of this chapter should be developed further to account for the displacement of the particle centre of mass due to diffusion as well.

Chapter 6

Conclusions and future work

The results and conclusions obtained in this thesis are summarized in this chapter. Some recommendations for future work are also discussed, in section 6.2.

6.1 Conclusions

In chapter 1 we started with the physical motivation and description of the problem. We discussed the most relevant observations of wax deposition in pipes reported in the literature, and discussed the objectives of this study.

Chapter 2 started with a description of the problem. The problem is formulated for a horizontal subsea pipe of circular cross-section. We have a straight pipe of length L and radius a. Part of the pipe is beneath the sea bottom with 60°C oil temperature and part of the pipe is surrounded by sea water at 10°C. The oil flows in a positive x direction. The radial flow velocity distribution was found, the maximum velocity is achieved at the centreline of the

pipe. We used the energy equation, with steady constant oil properties, to find the temperature distribution in the pipe. First, we considered the solution of the energy equation far from the entrance, with constant wall temperature along the whole pipe. We neglected the axial diffusion term because it is small compared with the radial diffusion term. This solution described the temperature distribution in Poiseuille flow with constant temperature maintained at the wall, where $r = a$. The obtained temperature increases with increasing distance from the wall of the pipe and the maximum temperature is achieved at the centreline axis of the pipe. We found that the viscous heating term in the energy equation does not affect the temperature distribution and can be neglected at the leading order. Then, we introduced the non-dimensional variables for the energy equation without viscous heating term. The axial diffusion term was neglected because the parameter $\epsilon = \frac{1}{P_e{}^2}$ is very small, where P_e is the Peclet number [27]. Thus, the axial diffusion term in the energy equation can be neglected relative to the radial diffusion. The temperature distribution satisfies a Graetz problem, which consists of a partial differential equation solved using the separation of variables method. We found the temperature variation along the pipe. It was shown that, as x increases, the temperature decreases, the temperature distribution becomes more uniform, and the oil cools down toward the temperature of the pipe wall. We found that for a pipe of length $1km$, the wax appearance temperature is observed close to the wall.

In Chapter 3 we modelled the growth of a single spherical wax particle. We introduced a small spherical wax particle of initial radius R_0 which is moving together with the flow. At the beginning the wax particle does not increase its radius because the temperature at the entrance of the pipe is too high

for the waxes to precipitate out of solution. Thus, the wax particle grows only if the temperature at the location of the wax particle is below the wax appearance temperature. The growth of a wax particle is caused by the flux of wax molecules coming out of solution and changing phase from liquid and forming a solid state.

The spherical wax particle was assumed to move with the flow and without any relative motion between the wax particle and the oil. Correspondingly we neglected the convective terms in the diffusion equation. There are two boundary conditions on the unknown surface of the wax particle, the first condition is for the mass flux. Dawson et al. [24] introduced a boundary condition on the surface of a salt crystal in terms of the mass flux of solute out of a salt solution into the solid crystal, where the mass transfer coefficient k_r was constant. In our model we generalized this condition by assuming that the mass transfer coefficient is a given function of temperature. The temperature at the location of the wax particle is a function of time, see chapter 2. We decompose the mass transfer coefficient as $k_r(t) = Dk_1\zeta(t)$, where k_1 is a non-dimensional factor. The second boundary condition describes the rate of increase of the radius of the wax particle. The problem derived is a free boundary value problem. We solved the problem numerically and analytically. The analytical self-similar solution exists only if $\zeta(t) = \frac{1}{\sqrt{t}}$. The radius of the spherical wax particle grows as $R(t) = \lambda\sqrt{Dt}$, where λ is an important coefficient which has been determined. We also found the concentration distribution in the fluid outside the wax particle. The concentration at the surface of the wax particle is lower than the concentration in the far-field.

In Chapter 4 we studied the initial boundary value problem numerically. We studied the problem derived in chapter 3, with the mass transfer coefficient

$k_r(t)$ being a function of time. The problem was written in non-dimensional variables and solved by using a Green's function. This helped us to derive a nonlinear boundary integral equation with respect to the wax concentration on the surface of the wax particle. We discretized the boundary integral equation for the wax concentration and the differential equation for the radius of the wax particle by using a time-stepping numerical method. We found numerical results for the concentration on the surface of the wax particle, the concentration distribution in the fluid, and the evolution of the particle radius. These numerical results were compared with the self-similar solution of chapter 3. We found the results were indistinguishable when the size of the time step was made sufficiently small, and there were only small differences in the results for large time step. Then we investigated the initial-boundary value problem when the mass transfer coefficient k_r is made constant.

In Chapter 5 we formulated the coupled diffusion/ flow problem in the spherical coordinate system. First, the three-dimensional problem of wax particle growth in a viscous flow was formulated. Then we restricted ourselves to the axisymmetric case. We non-dimensionalized the diffusion and flow problem by using dimensionless variables. We asymptotically expanded the velocity field and the concentration field around the growing particle with respect to a small parameter ϵ. The growth and the concentration at the leading order, without account for flow around the wax particle was shown in chapter 4. At the first order correction we assumed the shape of the particle to be non-spherical. However, the wax particle was spherical initially. We found that at first-order the correction due to a small difference between the local velocity of the flow and the velocity of the particle does not change the shape of the particle but predicts the particle displacement in the direction of the flow.

6.2 Future work

Many open problems have been identified after the present study on wax deposition in oil pipelines.

In chapter 2, we studied only the temperature distribution far from the entrance and also far from the wall of the pipe. So, we neglected the axial diffusion term and our solution corresponds to the temperature distribution in the main part of the pipe. For relatively short pipes which are only a few hundred meters long, it is important to find the temperature distribution near the entrance to the pipe and close to the wall. For example, if the temperature at the entrance of the pipe is 60°C and the temperature at the wall is 10°C, then these two conditions do not match each other at the pipe entrance. So we need to account for both the axial and radial diffusion terms and solve the corresponding two dimensional problem for temperature.

For particles moving close to the wall of the pipe, the flow velocity is not uniform due to the viscous shear. It is important to account for the shear of the flow in places with smaller velocity of the flow and lower temperature near the wall of the pipe.

The non-dimensional mass transfer coefficient $\hat{k_r}$ introduced in chapter 4, is the ratio between two time scales, $\frac{\text{Diffusion time scale}}{\text{Particle growth time scale}}$, $\hat{k_r} = \frac{R_0^2/D}{R_0/k_r} = \frac{k_r R_0}{D}$. If $\hat{k_r}$ is small, then the diffusion time is much smaller than the growth time. Then the diffusion quickly makes the concentration uniform and equal to the concentration in the far field, C_0. In chapter 4, we showed that the concentration is different from the far-field concentration only close to the wax particle surface. This gives us an idea that the method of matched asymptotic expan-

sions can be used in further studies of the problem with a one-dimensional inner layer on the surface of the particle. At the leading order we expect that everything important is happening near the particle surface. For large $\hat{k_r}$, the particle grows much quicker than the diffusion occurs. Then $C = C_0$ on the particle surface at leading order as $\hat{k_r} \to \infty$, see equation $(4.8.2)_4$. The wax particle growing so fast that the surface always moves towards fresh material.

The presence of a second wax particle has some influence, to be determined, on the first wax particle. From the results of chapter 4 we suspect that if the second particle is closer than 6 radii from the first particle then this influence on the wax concentration gradient is significant. Then the particles can not be treated as isolated. It is seen in figure 4.8.3 that at $t = 0.3$ s the concentration is visibly decreased on the surface of the wax particle. At this time the particle radius is 0.3 mm. We can see at $t = 0.3$ s the concentration is visibly decreased over a distance of about 6 particle radii from the particle surface. At the distance $r = 1.8$ mm any neighbouring particles would start to disturb each other from this time onward, because the concentration gradient would be noticeable by a wax particle of similar radius.

The correction to the wax particle shape in chapter 5 could be further continued to higher order approximations finding the non-spherical correction to the wax particle shape due to its motion with non-constant speed. In addition, non-spherical initial data are important to consider when a particle starts to grow from a non-spherical shape.

Interaction between two identical spherical wax particles can be studied as explained below. Consider two identical wax particles as shown in figure 6.2.1, of radius R, moving in the same line with the flow. The particles are small and their velocities are equal to the velocity of the flow. The particles

are close to each other and each particle is affected by the presence of another particle. For example, in figure 6.2.1 the first particle, on the left of the image, is spherically symmetric in the absence of the second particle on the right of the image. However, this particle will be non spherically symmetric in the precent of the other particle. We have two coordinate systems, (r, θ) for the particle on the left and (ρ, ω) for the particle on the right. The interaction between these two particles is weak if they are not very close to each other. Then we can take into account the interaction between these two particles by using perturbation analysis.

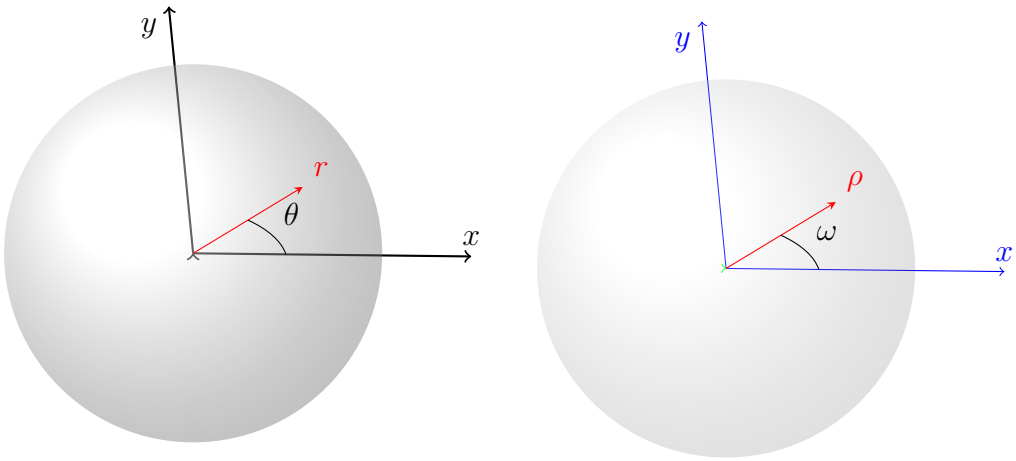

Figure 6.2.1: Sketch of the two symmetric particles. The ranges of the angles are $0 \leqslant \theta \leqslant \pi$ and $0 \leqslant \omega \leqslant \pi$, and the radial coordinates are such that $r > 0$, $\rho > 0$.

Let $C^{(0)}(r, t)$ be the concentration around the first particle, and let $C^{(1)}(\rho, t)$ be the concentration around the second particle at the leading order without account for another particle. The results for the spherical wax particle from chapter 4 can be used to determine $C^{(0)}$ and $C^{(1)}$. Note that $C^{(1)}$ depends on the coordinate ρ, and ρ depends on r and θ, see Figure 6.2.1.

The concentration $C(r,\theta,t)$ due to the two wax particles can be expressed as an asymptotic expansion in powers of a formal small parameter ϵ. The parameter ϵ quantifies that the interaction between the two wax particles is week. In chapter 4, we found this interaction to be of order 10^{-7} as shown in figure 4.8.3. We seek the concentration in the form:

$$C(r,\theta,t) = C^{(0)}(r,t) + C^{(1)}(\rho(r,\theta),t) - C_0 + \epsilon C^{(2)}(r,\theta,t) + O(\epsilon^2), \quad (6.2.1)$$

and the radius of the particle as

$$R(\theta,t) = R^{(0)}(t) + \epsilon R^{(1)}(\theta,t) + O(\epsilon^2). \quad (6.2.2)$$

Note that we must subtract C_0 in (6.2.1), which is the concentration in the far-field to avoid including it twice from the addition of the two concentration fields $C^{(0)}$ and $C^{(1)}$. The boundary value problem for the corrections to spherically symmetric solution, $C^{(2)}(r,\theta,t)$ and , $R^{(2)}(\theta,t)$, is obtained from equations (5.2.15)-(5.2.18), (5.2.21) and (5.2.24) by using (6.2.1), (6.2.2), and collecting terms of order ϵ. The resulting problem is linear but with non-constant coefficients in the boundary conditions on $r = R^{(0)}(t)$. The region where $C^{(2)}(r,\theta,t)$ should be determined is $r > R^{(0)}(t)$. Note that the second particle enters the boundary value problem for $C^{(2)}(r,\theta,t)$ and $R^{(2)}(\theta,t)$ only through the small perturbation of the concentration field described by $C^{(1)}(\rho(r,\theta),t) - C_0$ in (6.2.1).

The two bodies problem could be posed in another coordinate system, like bispherical coordinates, see [60], this is alternative way treating the problem.

Appendix A

Orthogonality of $f_n(r)$

Consider two solutions of (2.2.32), (2.2.33), $f_n(r)$ and $f_m(r)$, corresponding to β_n and β_m, where $\beta_n \neq \beta_m$. These two functions satisfy the equations

$$f_n'' + \frac{1}{r} f_n' + \beta_n^2 (1 - r^2) f_n = 0 \tag{A.0.1}$$

and

$$f_m'' + \frac{1}{r} f_m' + \beta_m^2 (1 - r^2) f_m = 0. \tag{A.0.2}$$

Multiply (A.0.1) by f_m, (A.0.2) by f_n, and subtract (A.0.2) from (A.0.1). The result is

$$f_m f_n'' - f_n f_m'' + \frac{1}{r}(f_m f_n' - f_n f_m') + (\beta_n^2 - \beta_m^2)(1 - r^2) f_n f_m = 0. \tag{A.0.3}$$

Multiply (A.0.3) by r and integrate in r from 0 to 1,

$$\begin{aligned} \int_0^1 r(f_m f_n'' - f_n f_m'')dr + \int_0^1 (f_m f_n' - f_n f_m')dr \\ + (\beta_n^2 - \beta_m^2) \int_0^1 r(1 - r^2) f_n f_m dr = 0 \end{aligned} \tag{A.0.4}$$

Integrate the first term in the left-hand side of equation (A.0.4) by parts,

$$\int_0^1 r(f_m f_n^{''} - f_n f_m^{''})dr = r f_m f_n'|_0^1 - \int_0^1 f_m f_n' dr - \int_0^1 r f_m' f_n' dr \\ - r f_n f_m'|_0^1 + \int_0^1 f_m' f_n dr + \int_0^1 r f_m' f_n' dr, \tag{A.0.5}$$

term cancels and using the condition $f_m(1) = f_n(1) = 0$, then (A.0.5) becomes

$$\int_0^1 r(f_m f_n^{''} - f_n f_m^{''})dr = -\int_0^1 (f_m f_n' - f_m' f_n)dr. \tag{A.0.6}$$

Substituting (A.0.6) into (A.0.4), we obtain

$$(\beta_n^2 - \beta_m^2)\int_0^1 r(1-r^2) f_n f_m dr = 0. \tag{A.0.7}$$

So, if $\beta_n \neq \beta_m$ and $m \neq n$, then f_n and f_m are orthogonal on $[0,1]$ with the wighting $r(1-r^2)$, this gives equation (2.2.43).

Appendix B

Dimensionless stress tensor's components

Using the boundary conditions (5.5.9) and (5.5.10), and the velocity components (5.3.7) and (5.5.11), we expand the dimensionless stress tensors components, $\hat{T_{rr}}$, $\hat{T_{r\theta}}$, and $\hat{T_{\theta\theta}}$ at $r = R^{(0)}(t) + \epsilon R^{(1)}(\theta, t) + O(\epsilon^2)$ as

$$\begin{aligned}\hat{T_{r\theta}}(R^{(0)} + \epsilon R^{(1)} + O(\epsilon^2), \theta, t) = \frac{1}{R^{(0)}}\left(\frac{\partial u_r^{(0)}}{\partial \theta} - u_\theta^{(0)}\right) + \frac{\partial u_\theta^{(0)}}{\partial r} + \\ \epsilon\Bigg[\frac{1}{R^{(0)}}\left(\frac{\partial u_r^{(1)}}{\partial \theta} + R^{(1)}\frac{\partial^2 u_r^{(0)}}{\partial \theta \partial r} - u_\theta^{(1)} - R^{(1)}\frac{\partial u_\theta^{(0)}}{\partial r} - \frac{R^{(1)}}{R^{(0)}}\left[\frac{\partial u_r^{(0)}}{\partial \theta} - u_\theta^{(0)}\right]\right) \\ + \frac{\partial u_\theta^{(1)}}{\partial r} + R^{(1)}\frac{\partial^2 u_\theta^{(0)}}{\partial r^2}\Bigg] + O(\epsilon^2).\end{aligned} \tag{B.0.1}$$

From equation (5.5.9), we have $\psi_0|_{r=R^{(0)}} = 0$ and $\frac{\partial \psi_0}{\partial r}|_{r=R^{(0)}} = 0$ and then $u_r^{(0)} = 0$, and $u_\theta^{(0)} = 0$.

Equation (5.3.7) gives in the fluid:

$$\frac{\partial u_\theta}{\partial \theta} = \frac{\cos\theta}{r\sin^2\theta}\frac{\partial \psi}{\partial r} - \frac{1}{r\sin\theta}\frac{\partial^2 \psi}{\partial r \partial \theta}. \tag{B.0.2}$$

Expanding equation (B.0.2) at $r = R^{(0)} + \epsilon R^{(1)} + O(\epsilon^2)$, we have

$$\begin{aligned}\frac{\partial u_\theta}{\partial \theta}(R^{(0)} + \epsilon R^{(1)} + O(\epsilon^2), \theta, t) &= \frac{\cos\theta}{\sin^2\theta}\frac{1}{R^{(0)} + \epsilon R^{(1)}}\left(\frac{\partial \psi}{\partial r} + \frac{\partial^2 \psi}{\partial r^2}\epsilon R^{(1)}\right) \\ &- \frac{1}{\sin\theta}\frac{1}{R^{(0)} + \epsilon R^{(1)}}\left(\frac{\partial^2 \psi}{\partial r \partial \theta} + \frac{\partial^3 \psi}{\partial r^2 \partial \theta}\epsilon R^{(1)}\right) + O(\epsilon^2) \\ &= \frac{\cos\theta}{\sin^2\theta}\frac{1}{R^{(0)}}\left(1 - \epsilon\frac{R^{(1)}}{R^{(0)}}\right)\left(\frac{\partial \psi_0}{\partial r} + \epsilon\frac{\partial \psi_1}{\partial r} + \epsilon R^{(1)}\frac{\partial^2 \psi_0}{\partial r^2}\right) \\ &- \frac{1}{\sin\theta}\frac{1}{R^{(0)}}\left(1 - \epsilon\frac{R^{(1)}}{R^{(0)}}\right)\left(\frac{\partial^2 \psi_0}{\partial r \partial \theta} + \epsilon\frac{\partial^2 \psi_1}{\partial r \partial \theta} + \epsilon R^{(1)}\frac{\partial^3 \psi_0}{\partial r^2 \partial \theta}\right) \\ &+ O(\epsilon^2),\end{aligned} \tag{B.0.3}$$

where $\frac{\partial \psi_0}{\partial r} = 0$ and $\frac{\partial^2 \psi_0}{\partial r \partial \theta} = 0$, then equation (B.0.3) becomes

$$\frac{\partial u_\theta}{\partial \theta} = O(\epsilon).$$

Equation (5.3.7) gives

$$\frac{\partial u_\theta}{\partial r} = \frac{1}{r^2 \sin\theta}\frac{\partial \psi}{\partial r} - \frac{1}{r\sin\theta}\frac{\partial^2 \psi}{\partial r^2}. \tag{B.0.4}$$

Expanding equation (B.0.4) at $r = R^{(0)} + \epsilon R^{(1)} + O(\epsilon^2)$, gives

$$\begin{aligned}\frac{\partial u_\theta}{\partial r}(R^{(0)} + \epsilon R^{(1)} + O(\epsilon^2), \theta, t) &= \frac{1}{[R^{(0)}(1 + \epsilon\frac{R^{(1)}}{R^{(0)}})]^2 \sin\theta}\left(\frac{\partial \psi}{\partial r} + \frac{\partial^2 \psi}{\partial r^2}\epsilon R^{(1)}\right) \\ &- \frac{1}{R^{(0)}(1 + \epsilon\frac{R^{(1)}}{R^{(0)}})\sin\theta}\left(\frac{\partial^2 \psi}{\partial r^2} + \frac{\partial^3 \psi}{\partial r^3}\epsilon R^{(1)}\right) + O(\epsilon^2) \\ &= \frac{1}{[R^{(0)}]^2 \sin\theta}\left(1 - 2\epsilon\frac{R^{(1)}}{R^{(0)}}\right)\left(\frac{\partial \psi_0}{\partial r} + \frac{\partial \psi_1}{\partial r}\epsilon + \frac{\partial^2 \psi_0}{\partial r^2}\epsilon R^{(1)}\right) \\ &- \frac{1}{R^{(0)}\sin\theta}\left(1 - \epsilon\frac{R^{(1)}}{R^{(0)}}\right)\left(\frac{\partial^2 \psi_0}{\partial r^2} + \epsilon\frac{\partial^2 \psi_1}{\partial r^2} + \epsilon R^{(1)}\frac{\partial^3 \psi_0}{\partial r^3}\right) \\ &+ O(\epsilon^2),\end{aligned} \tag{B.0.5}$$

where $\frac{\partial \psi_0}{\partial r} = 0$ and $\frac{\partial \psi_1}{\partial r} + \frac{\partial^2 \psi_0}{\partial r^2}R^{(1)} = -\frac{\partial^2 \psi_0}{\partial r^2}R^{(1)} + \frac{\partial^2 \psi_0}{\partial r^2}R^{(1)} = 0$, then (B.0.5) becomes

$$\frac{\partial u_\theta}{\partial r}(R^{(0)}+\epsilon R^{(1)}+O(\epsilon^2),\theta,t)=-\frac{1}{R^{(0)}\sin\theta}\left(1-\epsilon\frac{R^{(1)}}{R^{(0)}}\right)\left(\frac{\partial^2\psi_0}{\partial r^2}\right.$$
$$\left.+\epsilon\left[\frac{\partial^2\psi_1}{\partial r^2}+R^{(1)}\frac{\partial^3\psi_0}{\partial r^3}\right]\right)+O(\epsilon^2)$$
$$=-\frac{1}{R^{(0)}\sin\theta}\frac{\partial^2\psi_0}{\partial r^2}(R^{(0)},\theta,t)+\epsilon\left[-\frac{1}{R^{(0)}\sin\theta}\left(\frac{\partial^2\psi_1}{\partial r^2}\right.\right.$$
$$\left.\left.+R^{(1)}\frac{\partial^3\psi_0}{\partial r^3}\right)+\frac{R^{(1)}(\theta,t)}{R^{(0)2}\sin\theta}\frac{\partial^2\psi_0}{\partial r^2}\right]+O(\epsilon^2). \tag{B.0.6}$$

Equation (5.3.7) gives

$$\frac{\partial u_r}{\partial\theta}=-\frac{\cos\theta}{r^2\sin^2\theta}\frac{\partial\psi}{\partial\theta}+\frac{1}{r^2\sin\theta}\frac{\partial^2\psi}{\partial\theta^2} \tag{B.0.7}$$

and

$$\frac{\partial u_r}{\partial r}=-\frac{2}{r^3\sin\theta}\frac{\partial\psi}{\partial\theta}+\frac{1}{r^2\sin\theta}\frac{\partial^2\psi}{\partial r\partial\theta}. \tag{B.0.8}$$

Expanding equation (B.0.7) at $r=R^{(0)}+\epsilon R^{(1)}+O(\epsilon^2)$, gives

$$\frac{\partial u_r}{\partial\theta}(R^{(0)}+\epsilon R^{(1)}+O(\epsilon^2),\theta,t)=O(\epsilon^2) \tag{B.0.9}$$

and also expanding (B.0.8) gives

$$\frac{\partial u_r}{\partial r}(R^{(0)}+\epsilon R^{(1)}+O(\epsilon^2),\theta,t)=-\frac{2}{R^{(0)3}\sin^3\theta}\left(1-3\epsilon\frac{R^{(1)}}{R^{(0)}}\right)\left(\frac{\partial\psi_0}{\partial\theta}\right.$$
$$\left.+\epsilon\frac{\partial\psi_1}{\partial\theta}+\epsilon R^{(1)}\frac{\partial^2\psi_0}{\partial r\partial\theta}\right)+\frac{1}{R^{(0)2}\sin^2\theta}\left(1-2\epsilon\frac{R^{(1)}}{R^{(0)}}\right)$$
$$\left(\frac{\partial^2\psi_0}{\partial r\partial\theta}+\epsilon\frac{\partial^2\psi_1}{\partial r\partial\theta}+\epsilon R^{(1)}\frac{\partial^3\psi_0}{\partial r^2\partial\theta}\right)+O(\epsilon^2), \tag{B.0.10}$$

where $\frac{\partial\psi_0}{\partial\theta}=0$, $\frac{\partial\psi_1}{\partial\theta}=0$, and $\frac{\partial}{\partial\theta}(\frac{\partial\psi_1}{\partial r})=-\frac{\partial^3\psi_0}{\partial r^2\partial\theta}R^{(1)}-\frac{\partial^2\psi_0}{\partial r^2}\frac{\partial R^{(1)}}{\partial\theta}$, then (B.0.10) becomes

$$\frac{\partial u_r}{\partial r}(R^{(0)}+\epsilon R^{(1)}+O(\epsilon^2),\theta,t)=-\epsilon\frac{\frac{\partial R^{(1)}}{\partial\theta}}{R^{(0)2}\sin\theta}\frac{\partial^2\psi_0}{\partial r^2}(R^{(0)},\theta,t)+O(\epsilon^2). \tag{B.0.11}$$

Expanding the velocity component u_θ at $r = R^{(0)} + \epsilon R^{(1)} + O(\epsilon^2)$ gives

$$\begin{aligned} u_\theta(R^{(0)} + \epsilon R^{(1)} + O(\epsilon^2), \theta, t) = &- \frac{1}{(R^{(0)} + \epsilon R^{(1)}) \sin\theta} \Bigg(\frac{\partial \psi_0}{\partial r} + \epsilon R^{(1)} \frac{\partial \psi_1}{\partial r} \\ &+ \epsilon R^{(1)} \frac{\partial^2 \psi_0}{\partial r^2} \Bigg) + O(\epsilon^2) \\ = &- \frac{\epsilon}{R^{(0)} \sin\theta} \Bigg(\frac{\partial \psi_1}{\partial r} + R^{(1)} \frac{\partial^2 \psi_0}{\partial r^2} \Bigg) + O(\epsilon^2), \end{aligned} \tag{B.0.12}$$

where $\frac{\partial \psi_1}{\partial r} + R^{(1)} \frac{\partial^2 \psi_0}{\partial r^2} = 0$, then equation (B.0.12) gives

$$u_\theta = O(\epsilon^2). \tag{B.0.13}$$

Finally, the dimensionless stress tensor components can be written as:

$$\hat{T}_{r\theta}(R^{(0)} + \epsilon R^{(1)} + O(\epsilon^2), \theta, t) = \frac{\partial u_\theta}{\partial r} + O(\epsilon^2). \tag{B.0.14}$$

$$\begin{aligned} \hat{T}_{\theta\theta}(R^{(0)} + \epsilon R^{(1)} + O(\epsilon^2), \theta, t) = -P - \epsilon R^{(1)} \frac{\partial P}{\partial r} + O(\epsilon) = -P^{(0)}(R^{(0)}, \theta, t) \\ + O(\epsilon). \end{aligned} \tag{B.0.15}$$

$$\begin{aligned} \hat{T}_{rr}(R^{(0)} + \epsilon R^{(1)} + O(\epsilon^2), \theta, t) = &-P^{(0)} - \epsilon P^{(1)} - \epsilon R^{(1)} \frac{\partial P^{(0)}}{\partial r} \\ &- 2\epsilon \frac{\frac{\partial R^{(1)}}{\partial \theta}}{R^{(0)2} \sin\theta} \frac{\partial^2 \psi_0}{\partial r^2} + O(\epsilon^2). \end{aligned} \tag{B.0.16}$$

Bibliography

[1] M. Abramowitz and I. A. Stegun. *Handbook of mathematical functions: with formulas, graphs, and mathematical tables*. Number 55. Courier Corporation, 1964.

[2] D. J. Acheson. *Elementary fluid dynamics*. Oxford University Press, 1990.

[3] A. Aiyejina, D. P. Chakrabarti, A. Pilgrim, and M. Sastry. Wax formation in oil pipelines: A critical review. *International journal of multiphase flow*, 37(7):671–694, 2011.

[4] K. Atkinson, W. Han, and D. E. Stewart. *Numerical solution of ordinary differential equations*, volume 108. John Wiley & Sons, 2011.

[5] R. Bagatin, C. Carniani, S. Correra, M. Margarone, C. Busto, et al. Wax modeling: There is need for alternatives. In *SPE Russian oil and gas technical conference and exhibition*. Society of Petroleum Engineers, 2008.

[6] R. Banki, H. Hoteit, and A. Firoozabadi. Mathematical formulation and numerical modeling of wax deposition in pipelines from enthalpy–porosity approach and irreversible thermodynamics. *International Journal of Heat and Mass Transfer*, 51(13):3387–3398, 2008.

[7] A. Barletta and E. Zanchini. Forced convection in the thermal entrance region of a circular duct with slug flow and viscous dissipation. *International journal of heat and mass transfer*, 40(5):1181–1190, 1997.

[8] G. Barton. *Elements of Green's functions and propagation: potentials, diffusion, and waves*. Oxford University Press, 1989.

[9] D.-F. Bautista-Parada, D.-A. Fuentes-Díaz, P. Gauthier-Maradei, and A. Chaves-Guerrero. Application of a wax deposition model in oil production pipelines. *CT&F-Ciencia, Tecnología y Futuro*, 6(1):29–42, 2015.

[10] P. A. Bern, V. R. Withers, R. J. Cairns, et al. Wax deposition in crude oil pipelines. In *European offshore technology conference and exhibition*. Society of Petroleum Engineers, 1980.

[11] T. Brown, V. Niesen, D. Erickson, et al. Measurement and prediction of the kinetics of paraffin deposition. In *SPE annual technical conference and exhibition*. Society of Petroleum Engineers, 1993.

[12] E. Burger, T. Perkins, J. Striegler, et al. Studies of wax deposition in the trans alaska pipeline. *Journal of Petroleum Technology*, 33(06):1–075, 1981.

[13] J. L. P. Cabanillas, A. T. Leiroz, and L. F. A. Azevedo. Paraffin deposition in laminar channel flow, in the presence of suspended crystals. In *Proceedings of the 19th International Congress of Mechanical Engineering*, pages 5–9, 2007.

[14] H. S. Carslaw and J. C. Jaeger. Conduction of heat in solids. *Oxford: Clarendon Press, 1959, 2nd ed.*, 1, 1959.

[15] H. S. Carslaw and J. C. Jaeger. *Conduction of heat in solids*. Clarendon Press, 1960.

[16] X. Chen, T. Butler, M. Volk, J. Brill, et al. Techniques for measuring wax thickness during single and multiphase flow. In *SPE Annual Technical Conference and Exhibition*. Society of Petroleum Engineers, 1997.

[17] K. D. Cole, J. V. Beck, A. Haji-Sheikh, and B. Litkouhi. *Heat conduction using Green's functions*. Taylor & Francis, 2010.

[18] A. Cordoba and C. Schall. Application of a heat transfer method to determine wax deposition in a hydrocarbon binary mixture. *Fuel*, 80(9):1285–1291, 2001.

[19] S. Correra, A. Fasano, L. Fusi, and D. Merino-Garcia. Calculating deposit formation in the pipelining of waxy crude oils. *Meccanica*, 42(2):149–165, 2007.

[20] S. Correra, A. Fasano, L. Fusi, M. Primicerio, and F. Rosso. Wax diffusivity under given thermal gradient: a mathematical model. *ZAMM-Journal of Applied Mathematics and Mechanics/Zeitschrift für Angewandte Mathematik und Mechanik*, 87(1):24–36, 2007.

[21] J. Crank et al. *The mathematics of diffusion*, volume 2. Clarendon press Oxford, 1975.

[22] J. Creek, H. J. Lund, J. P. Brill, and M. Volk. Wax deposition in single phase flow. *Fluid Phase Equilibria*, 158:801–811, 1999.

[23] J. Creek, A. Matzain, M. Apte, J. Brill, M. Volk, E. Delle Case, and H. Lund. Mechanisms for wax deposition. In *AIChE, National Spring Meeting, Houston, TX*, 1999.

[24] M. Dawson, D. Borman, R. Hammond, D. Lesnic, and D. Rhodes. Modelling the morphology of crystalline deposits evolving from impinging droplets of salt solution. In *Proceedings of the 9th South African Conference on Computational and Applied Mechanics*. Leeds, 2014.

[25] M. Dawson, D. Borman, R. B. Hammond, D. Lesnic, and D. Rhodes. Moving boundary models for the growth of crystalline deposits from undetected leakages of industrial process liquors. *Computers & Chemical Engineering*, 71:331–346, 2014.

[26] J. B. Dobbs. A unique method of paraffin control in production operations. In *SPE Rocky Mountain regional meeting*, pages 487–492, 1999.

[27] O. Duru. *Reservoir analysis and parameter estimation constrained to temperature, pressure and flow rate histories*. Stanford University, 2011.

[28] P. Eaton and G. Weeter. Paraffin deposition in flow lines. In *Proceedings of the 16th National Heat Transfer Conference*, 1976.

[29] M. Ebadian and H. Zhang. An exact solution of extended graetz problem with axial heat conduction. *International Journal of Heat and Mass Transfer*, 32(9):1709–1717, 1989.

[30] G. Elphingstone, K. Greenhill, and J. Hsu. Modeling of multiphase wax deposition. *Journal of energy resources technology*, 121(2):81–85, 1999.

[31] A. Fasano, L. Fusi, S. Correra, and M. Margarone. A survey on mathematical modelling of deposition in waxy crude oils. *Mathematical Modelling of Natural Phenomena*, 6(5):157–183, 2011.

[32] A. Fasano, L. Fusi, J. Ockendon, and M. Primicerio. Gelification and mass transport in a static non-isothermal waxy solution. *Eur. J. Appl. Math*, 20:93, 2009.

[33] A. Fasano and M. Primicerio. Heat and mass transport in non-isothermal partially saturated oil-wax solutions. In *New Trends In Mathematical Physics: In Honour of the Salvatore Rionero 70th Birthday*, pages 34–44. World Scientific, 2004.

[34] A. Fasano and M. Primicerio. Temperature driven mass transport in concentrated saturated solutions. *Trends in Partial Differential Equations of Mathematical Physics*, pages 91–108, 2005.

[35] J. Q. Feng. Diffusion-controlled quasi-stationary mass transfer for an isolated spherical particle in an unbounded medium. *Chemical Engineering Communications*, 200(1):65–76, 2013.

[36] G. Fichtenholz. Differential and integral calculus. *Fizmatlit, Moscow*, 2001.

[37] H. Fogler and R. Venkatesan. Comments on analogies for correlated heat and mass transfer in turbulent flow (r&d note). *AIChE journal*, (7):1623, 2004.

[38] M. Griebel, W. Merz, and T. Neunhoeffer. Mathematical modeling and numerical simulation of freezing processes of a supercooled melt under

consideration of density changes. *Computing and Visualization in Science*, 1(4):201–219, 1999.

[39] V. Gunnerud and B. Foss. Oil production optimization a piecewise linear model, solved with two decomposition strategies. *Computers & Chemical Engineering*, 34(11):1803–1812, 2010.

[40] A. Hamouda, S. Davidsen, et al. An approach for simulation of paraffin deposition in pipelines as a function of flow characteristics with a reference to teesside oil pipeline. In *SPE International Symposium on Oilfield Chemistry*. Society of Petroleum Engineers, 1995.

[41] A. D. Handal. Analysis of some wax deposition experiments in a crude oil carrying pipe. 2008.

[42] J. Happel and H. Brenner. *Low Reynolds number hydrodynamics: with special applications to particulate media*, volume 1. Springer Science & Business Media, 2012.

[43] S. I. Hayek. *Advanced mathematical methods in science and engineering*. CRC Press, 2010.

[44] R. Hoffmann and L. Amundsen. Single-phase wax deposition experiments. *Energy & Fuels*, 24(2):1069–1080, 2009.

[45] R. F. Hoskins. *Delta functions: Introduction to generalised functions*. Elsevier, 2009.

[46] Z. Huang, H. S. Lee, M. Senra, and H. Scott Fogler. A fundamental model of wax deposition in subsea oil pipelines. *AIChE Journal*, 57(11):2955–2964, 2011.

[47] E. B. Hunt Jr et al. Laboratory study of paraffin deposition. *Journal of Petroleum Technology*, 14(11):1–259, 1962.

[48] P. R. Johnston. Axial conduction and the graetz problem for a bingham plastic in laminar tube flow. *International journal of heat and mass transfer*, 34(4-5):1209–1217, 1991.

[49] S. Kakac, Y. Yener, and A. Pramuanjaroenkij. *Convective heat transfer*. CRC press, 2013.

[50] I. A. Karimi and R. Srinivasan. *11th International Symposium on Process Systems Engineering-PSE2012*. Elsevier, 2012.

[51] H.-C. Ku and D. Hatziavramidis. Chebyshev expansion methods for the solution of the extended graetz problem. *Journal of Computational Physics*, 56(3):495–512, 1984.

[52] K. Kumar. *Engineering fluid mechanics*. S. Chand Publishing, 2008.

[53] C. Laohakul, C. Chan, K. Look, and C. Tan. On approximate solutions of the graetz problem with axial conduction. *International journal of heat and mass transfer*, 28(3):541–545, 1985.

[54] L. G. Leal. *Advanced transport phenomena: fluid mechanics and convective transport processes*. Cambridge University Press, 2007.

[55] A. Majeed, B. Bringedal, and S. Overa. Model calculates wax deposition for north-sea oils. *Oil & Gas Journal*, 88(25):63–69, 1990.

[56] J. L. Martin and S. C. McCutcheon. *Hydrodynamics and transport for water quality modeling*. CRC Press, 1998.

[57] H. Mehrer. *Diffusion in solids: fundamentals, methods, materials, diffusion-controlled processes*, volume 155. Springer Science & Business Media, 2007.

[58] M. Michelsen and J. Villadsen. The graetz problem with axial heat conduction. *International Journal of Heat and Mass Transfer*, 17(11):1391–1402, 1974.

[59] T. Min, J. Y. Yoo, and H. Choi. Laminar convective heat transfer of a bingham plastic in a circular pipe. analytical approach thermally fully developed flow and thermally developing flow (the graetz problem extended). *International journal of heat and mass transfer*, 40(13):3025–3037, 1997.

[60] P. Moon and D. E. Spencer. *Field theory handbook: including coordinate systems, differential equations and their solutions*. Springer, 2012.

[61] R. Najjar and C. Laohakul. An approximate solution to the graetz problem with axial conduction and prescribed wall heat flux. *International communications in heat and mass transfer*, 13(3):315–324, 1986.

[62] S. Olek. Heat transfer in duct flow of non-newtonian fluids with axial conduction. *International communications in heat and mass transfer*, 25(7):929–938, 1998.

[63] J.-W. Ou and K. Cheng. Viscous dissipation effects on thermal entrance heat transfer in laminar and turbulent pipe flows with uniform wall temperature. In *AIAA/ASME 1974 Thermophysics and Heat Transfer Conference*, 1974.

[64] A. D. Polyanin, A. Kutepov, D. Kazenin, and A. Vyazmin. *Hydrodynamics, mass and heat transfer in chemical engineering*, volume 14. CRC Press, 2001.

[65] E. Ramirez-Jaramillo, C. Lira-Galeana, and O. Manero. Modeling wax deposition in pipelines. *Petroleum science and technology*, 22(7-8):821–861, 2004.

[66] D. Readey and A. Copper. Molecular diffusion with a moving boundary and spherical symmetry. *Chemical Engineering Science*, 21(10):917–922, 1966.

[67] F. S. Ribeiro, P. R. S. Mendes, and S. L. Braga. Obstruction of pipelines due to paraffin deposition during the flow of crude oils. *International journal of heat and mass transfer*, 40(18):4319–4328, 1997.

[68] R. K. Shah and A. L. London. *Laminar flow forced convection in ducts: a source book for compact heat exchanger analytical data*. Academic press, 2014.

[69] A. Sharma and S. Chakraborty. Semi-analytical solution of the extended graetz problem for combined electroosmotically and pressure-driven microchannel flows with step-change in wall temperature. *International Journal of Heat and Mass Transfer*, 51(19):4875–4885, 2008.

[70] P. Singh, R. Venkatesan, H. S. Fogler, and N. Nagarajan. Formation and aging of incipient thin film wax-oil gels. *AIChE Journal*, 46(5):1059–1074, 2000.

[71] P. Singh, R. Venkatesan, H. S. Fogler, and N. Nagarajan. Morphological evolution of thick wax deposits during aging. *AIChE Journal*, 47(1):6–18, 2001.

[72] A. Stevenson and M. Waite. *Concise Oxford English Dictionary: Book & CD-ROM Set*. Oxford University Press, 2011.

[73] R. S. Subramanian and R. Balasubramaniam. *The motion of bubbles and drops in reduced gravity*. Cambridge University Press, 2001.

[74] J. A. Svendsen. Mathematical modeling of wax deposition in oil pipeline systems. *AIChE Journal*, 39(8):1377–1388, 1993.

[75] A. P. Szilas. *Production and transport of oil and gas*, volume 3. Elsevier, 2010.

[76] K.-T. Tang. *Mathematical methods for engineers and scientists*, volume 1. Springer, 2007.

[77] J. F. Tinsley and R. K. Prud'homme. Deposition apparatus to study the effects of polymers and asphaltenes upon wax deposition. *Journal of Petroleum Science and Engineering*, 72(1):166–174, 2010.

[78] B. Vick and M. Özişik. An exact analysis of low peclet number heat transfer in laminar flow with axial conduction. *Letters in Heat and Mass Transfer*, 8(1):1–10, 1981.

[79] B. Vick, M. Özişik, and D. Ullrich. Effects of axial conduction in laminar tube flow with convective boundaries. *Journal of the Franklin Institute*, 316(2):159–173, 1983.

[80] L. Wardhaugh and D. Boger. Flow characteristics of waxy crude oils: application to pipeline design. *AIChE Journal*, 37(6):871–885, 1991.

[81] F. M. White and I. Corfield. *Viscous fluid flow*, volume 3. McGraw-Hill Higher Education Boston, 2006.

[82] Z. Zapryanov and S. Tabakova. *Dynamics of bubbles, drops and rigid particles*, volume 50. Springer Science & Business Media, 2013.

[83] D. Zill, W. S. Wright, and M. R. Cullen. *Advanced engineering mathematics*. Jones & Bartlett Learning, 2011.